uOttawa

L'Université canadienne
Canada's university

FACULTÉ DES ÉTUDES SUPÉRIEURES ET POSTOCTORALES

uOttawa

L'Université canadienne
Canada's university

FACULTY OF GRADUATE AND POSDOCTORAL STUDIES

Taijiro Sato

AUTEUR DE LA THÈSE / AUTHOR OF THESIS

Ph.D. (Civil Engineering)

GRADE / DEGREE

Department of Civil Engineering

FACULTÉ, ÉCOLE, DÉPARTEMENT / FACULTY, SCHOOL, DEPARTMENT

Applications of Nanotechnology for the Sustainable Development of Cement-based Materials

TITRE DE LA THÈSE / TITLE OF THESIS

Jim Beaudoin

DIRECTEUR (DIRECTRICE) DE LA THÈSE / THESIS SUPERVISOR

CO-DIRECTEUR (CO-DIRECTRICE) DE LA THÈSE / THESIS CO-SUPERVISOR

EXAMINATEURS (EXAMINATRICES) DE LA THÈSE / THESIS EXAMINERS

Burkan Isgor

Jason Weiss (teleconference)

Beatriz Martin-Perez

Dan Palermo

Gary W. Slater

Le Doyen de la Faculté des études supérieures et postdoctorales / Dean of the Faculty of Graduate and Postdoctoral Studies

Applications of Nanotechnology for the Sustainable Development of Cement-based Materials

by

Taijiro Sato

A thesis
submitted under the supervision of
Dr. J.J. Beaudoin

in partial fulfilment of the
requirements of the degree of
Doctorate in Philosophy
Civil Engineering

Department of Civil Engineering
University of Ottawa
Ottawa, Canada
K1N 6N5

October 2006

Your file Votre référence
ISBN: 978-0-494-25893-4
Our file Notre référence
ISBN: 978-0-494-25893-4

This thesis is dedicated to my beloved parents.

ACKNOWLEDGEMENTS

My special gratitude is deeply expressed to my supervisor, Dr. J.J. Beaudoin, Research Emeritus, at the Institute for Research in Construction, National Research Council Canada and Adjunct Professor at the Department of Civil Engineering, University of Ottawa, for his continuous advice and support on all aspects of this research.

The author would also like to thank Messrs. Gordon Chan and Jim Margeson, at the Institute for Research in Construction, National Research Council Canada, for their technical supports with the laboratory work and analysis.

ABSTRACT

Nanotechnology is a revolutionary discipline in the area of applied science and technology and is expected to have a considerable impact on society. The field of construction materials is no exception. The intrinsically conservative nature of the construction industry might have slowed down the implementation of nanotechnology. It was soon realized however that nanotechnology could facilitate the development of new monitoring systems, new repair methods and even new construction materials.

It is undeniable that more sources of energy will be required worldwide to satisfy a growing population. It is therefore recognized that all the industries are responsible for implementing policies for sustainable development – the ability to meet the needs of the present without depleting the resources for the future.

Three themes were chosen for this thesis based on the application and potential of nanotechnology to enhance the use of the cement-based construction materials for sustainable development.

Theme 1 focuses on the effect of a nano-sized calcium carbonate ($CaCO_3$) as an accelerating additive for the hydration of cement paste containing high volumes of supplementary cementing materials (SCMs). The conduction calorimetry results showed that the delayed early hydration of ordinary Portland cement (OPC) paste containing high volumes of SCMs was significantly counteracted by the addition of nano-sized $CaCO_3$.

Theme 2 focuses on the synthesis of a highly reactive nano-sized β-C_2S at low temperatures by a novel technique, referred to as the Sucrose method, used for the first time in the field of civil engineering. The highly reactive nano-sized β-C_2S was successfully synthesized at 600°C and its hydration was significantly faster than that of the commercial β-C_2S. It was also demonstrated that the mechanical property of the hydrated highly reactive nano-sized β-C_2S was improved.

Theme 3 focuses on the synthesis of a nano-sized calcium hydroxide ($Ca(OH)_2$) by two methods, the planetary-mill grinding method and the vacuum calcination method in order to tailor the pozzolanic reaction between the nano-sized $Ca(OH)_2$ and metakaolinite. The efficacy of the use of the nano-sized $Ca(OH)_2$ to enhance the pozzolanic reaction with metakaolinite was confirmed.

TABLE OF CONTENTS

LIST OF TABLES

LIST OF FIGURES

GLOSSARY

a	distance between the support and the point of loading
A_{CS}	cross sectional area of nitrogen gas molecule
b_E	a constant for a slope of log modulus of elasticity versus porosity
b_H	a constant for a slope of log microhardness versus porosity
C	a constant related to heat of adsorption
d	distance between the atomic planes
d_i	mean diagonal of the indentation
E	modulus of elasticity
E_o	modulus of elasticity at zero porosity
h	thickness of the specimen
H	microhardness
H_o	microhardness at zero porosity
m	an integer
M	molecular weight of nitrogen gas
n	moles of gas occupying V_c at P_a
n_1	moles of gas occupying $(V_c - V_p)$ at P_a
n_2	moles of gas occupying $(V_c - V_p)$ at P_2
n_o	the number of moles of gas in a system
n_a	moles of gas occupying V_A at P_a
N	Avogadro's number
P	partial pressure of nitrogen gas
P_2	pressure above atmosphere
P_o	saturated vapour pressure of nitrogen gas
P_a	atmospheric pressure
P_r	porosity
P_A	an applied load for microhardness
P_L	an applied load for modulus of elasticity
R	universal gas constant
S	specific surface area of the specimen
S_t	total surface area of the specimen
T_a	ambient temperature
V_{ads}	measured volume of nitrogen gas molecules adsorbed on the surface
V_A	additional volume
V_{Bulk}	bulk volume of the specimen
V_c	volume of sample chamber
V_p	volume of specimen
w_o	deflection at the centre of the circular plate
W	mass of nitrogen gas molecules adsorbed on the surface at a given relative pressure, P/P_o
W_m	mass of nitrogen gas molecules at a coverage of one monolayer
W_S	mass of the specimen
λ	wavelength of x-rays
θ	angle of incidence
θ_d	angle between faces of diamond (136°)
υ	Poisson's Ratio

Abbreviations

ACI	American Concrete Institute
CANMET	Canadian Centre for Mineral and Energy Technology
CNT	Carbon Nanotube
C-S-H	Calcium Silicate Hydrate
DSC	Differential Scanning Calorimetry
EDS	Evaporative Decomposition of Solution
FHWA	Federal Highway Administration
GGBFS	Ground Granulated Blast-furnace Slag
GU	General Use
HVFA	High-Volume Fly Ash
IRC	Institute for Research in Construction
NMR	Nuclear Magnetic Resonance Spectroscopy
NNI	National Nanotechnology Initiative
OPC	Ordinary Portland Cement
PVA	Aqueous Polyvinyl Acetate
RH	Relative Humidity
SCMs	Supplementary Cementing Materials
SEM	Scanning Electron Microscopy
TGA	Thermogravimetric Analysis
UHP	Ultra High Purity
XRD	X-ray Diffractometry

C	CaO / Calcium Oxide (Lime)
A	Al_2O_3 / Aluminum Oxide (Alumina)
S	SiO_2 / Silicon Dioxide (Silica)
F	Fe_2O_3 / Iron Oxide (III)
M	MgO / Magnesium Oxide
H	H_2O / Hydrogen Oxide (Water)
N	Na_2O / Sodium Monoxide
K	K_2O / Potassium Monoxide

CHAPTER 1

INTRODUCTION AND OBJECTIVES

1.1 Introduction

Nanotechnology is a revolutionary discipline in the field of science and technology and is expected to have a considerable impact on society (Péro, 2003). It has already been used for a number of industrial applications, such as electronics, sensors and batteries. The extension of nanotechnology to the applications in material science has demonstrated its potential in the area of construction materials including traditional materials such as polymers, structural steel and concrete. Nanotechnology in civil engineering can be defined in the context of materials and structures as the synthesis, design and modification of materials with dimensions in the range of 1 to 100 nm. The various components of cement and concrete materials at the various scales are shown in Fig. 1.1. Calcium-silicate-hydrate (C-S-H), a key product of hydrated cement paste, has particle sizes in the range of 1 nm to 100 nm. Understanding a structure of C-S-H at nano-scale would help improving the performance of the material. This new technology has a potential to significantly modify the intricate hydration mechanism of the cement-based materials and the properties of hardened concrete. It should be possible to more precisely control and modify the mechanical behaviour of existing systems or to tailor the performance of novel construction materials.

It is now recognized that all the industries are responsible for implementing policies for sustainable development – the ability to meet the needs of the present without depleting the resources for the future. The construction industry, one of the most energy-intensive and resource-consuming industries, is no exception and it is the time to seek more environmentally friendly and sustainable ways of using the cement-based materials in construction. Three themes

were chosen for this thesis based on the application and potential of nanotechnology to enhance the use of the cement-based construction materials and optimize the gains made toward sustainable development.

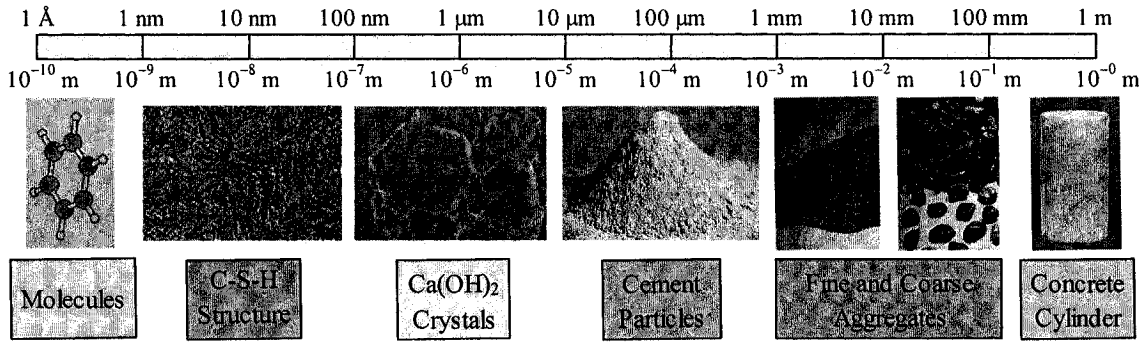

Fig. 1.1 Various components of cement and concrete materials at the various scales

Theme 1 focuses on an investigation of the effect of a nano-sized calcium carbonate ($CaCO_3$) addition as an accelerating additive for cement paste containing high volumes of supplementary cementing materials (SCMs) such as fly ash and ground granulated blast-furnace slag. The use of SCMs in the concrete mixes as a partial replacement of ordinary Portland cement (OPC) is currently one of the most common practices that contribute to sustainable development. It, however, generally delays the initial setting and the rate of the hydration and decreases the rate of early strength development. The accelerating effect of the nano-sized $CaCO_3$ addition, as opposed to a reagent grade micro-sized $CaCO_3$ addition, should compensate for the delayed hydration process caused by the high volume of SCMs and take a full advantage of the use of SCMs from the environmental point of view.

Theme 2 focuses on the synthesis of a highly reactive nano-sized β-C_2S by a novel technique referred to as the Sucrose method. OPC contains about 50% of tricalcium silicate (C_3S) and 20% of dicalcium silicate (C_2S). C_3S reacts with water more rapidly and contributes to the early strength development, whereas C_2S reacts more slowly and contributes to the late strength development. C_3S, however, can be formed in a cement kiln only at high temperatures, generally above 1450°C, whereas C_2S can be formed at relatively lower temperatures, generally around 900°C. Manufacturing cement at high temperatures can produce a high level of CO_2 emissions and is considered to be one of the main CO_2 producers among different industries. The highly reactive β-C_2S is one specific form of C_2S and its nano-sized particles can be synthesized at

temperatures as low as 600°C. A potential replacement of C_3S with less energy-intensive and more reactive β-C_2S is a promising practice from the sustainable development point of view.

Theme 3 focuses on the use of nano-sized calcium hydroxide ($Ca(OH)_2$) and to employ it for sustainable development purposes. $Ca(OH)_2$ is not just a by-product of the cement hydration, but also a reactant which, if judiciously used, could result in improvement of the properties of cement paste and concrete. Metakaolinite, one of the most common SCMs, is a pozzolanic material, which in itself possesses little or no cementitious property, but chemically reacts with $Ca(OH)_2$ to form compounds possessing cementitious properties. The nano-sized $Ca(OH)_2$, as opposed to a reagent grade micro-sized $Ca(OH)_2$, could accelerate the pozzolanic reaction with metakaolinite and form even higher quality products. A technique based on the Hedvall effect can be applied to compare the relative reactivity of both micro- and nano-sized $Ca(OH)_2$. An understanding of the thermal decomposition characteristics of different types of $Ca(OH)_2$ is also essential to tailor the use of the nano-sized $Ca(OH)_2$.

1.2 Three Themes of the Thesis

The following sections provide a detailed description of the objectives and experimental outlines for each of the three themes of the thesis. The three themes based on the applications of nanotechnology for the sustainable development of cement-based materials, are;

Theme 1: The use of nano-sized $CaCO_3$ addition to cement paste containing high volumes of supplementary cementing materials.

Theme 2: The synthesis and characterization of the highly reactive nano-sized β-C_2S by the Sucrose method.

Theme 3: The synthesis of the nano-sized $Ca(OH)_2$ and its effect on the pozzolanic reaction with metakaolinite.

1.3 Theme 1: The Use of Nano-sized $CaCO_3$ Addition to Cement Paste Containing High Volumes of Supplementary Cementing Materials

1.3.1 Objectives

The use of SCMs in the concrete mixes has become a common practice and is beneficial for sustainable development in the concrete industry. SCMs replacement levels as high as 50% of the cement content have been reported (Gillies, 2001). One of the major disadvantages of concrete containing high volumes of SCMs, however, is often the slower initial setting and rate of early strength development especially in cold weather. The ground limestone ($CaCO_3$) has also been used to replace a certain portion of OPC in the concrete mixes. The replacement has led to reduced raw materials use, reduced energy consumption and reduced CO_2 emissions, essential for sustainable development. In Canada, the use of up to 5% ground limestone has been permitted since the early 1980's. The relevant quote in the CSA standard is; "a maximum of 5% addition of limestone is permitted for Normal Portland cement, Type 10, and for High-early-strength Portland cement, Type 30." In Europe, the British / European Standard, BS EN 197-1 specifies "Portland limestone cement" which contains 6% to 35% of the ground limestone. In the US, the ASTM is in the process of accepting the use of up to 5% ground limestone in OPC (ASTM C150). The addition of $CaCO_3$ was first considered as a simple replacement of a more valuable material (OPC) by a less valuable material (limestone). A number of studies, however, have indicated positive effects of the $CaCO_3$ addition on the hydration of cement and strength development of hardened concrete, especially its accelerating effect on the rate of the hydration. Several calorimetry results have shown that the rate of the cement hydration was accelerated when the finely ground $CaCO_3$ was added. The slower rate of the hydration of cement paste containing high volumes of SCMs might be counteracted by the finely ground $CaCO_3$ addition. It is suggested here that the rate of the hydration should be even greater by using the nano-sized $CaCO_3$ as an accelerating additive as opposed to the conventional reagent grade micro-sized $CaCO_3$. An improvement of the mechanical properties of hydrated cement paste would also be expected by the addition of nano-sized $CaCO_3$. The effects of the micro- and nano-sized $CaCO_3$ additions on the hydration of cement paste containing high volumes of SCMs were investigated under Theme 1 of the thesis. Specifically, the processes involved in overcoming the slower initial

setting and rate of early strength development were studied. The specific objectives of Theme 1 are as follows;

1. To understand the hydration mechanism of cement paste containing high volumes of SCMs.
2. To characterize the micro-sized $CaCO_3$ and the nano-sized $CaCO_3$.
3. To investigate the hydration mechanism of cement paste with additions of the micro- and the nano-sized $CaCO_3$.
4. To study the effect of the additions of the micro- and the nano-sized $CaCO_3$ on the delayed early hydration of cement paste containing high volumes of SCMs.
5. To investigate the mechanical properties of the cement paste containing high volumes of SCMs to establish the link between cement chemistry and civil engineering properties.

1.3.2 Experimental Outline

The experiments were designed and conducted in a methodical way so that the specific objectives stated above could be achieved. The flowchart of the experimental outline is shown in Fig. 1.2. In Stage 1, the hydration mechanism of cement paste containing high volumes of fly ash was investigated by studying its rate of hydration and hydration products. In Stage 2, OPC was hydrated with the separate addition of reagent grade micro-sized $CaCO_3$ and nano-sized $CaCO_3$ and their accelerating effects were examined. In this stage, the degree of hydration was also estimated by determining the amount of $Ca(OH)_2$ in the hydration products for various periods of hydration. In Stage 3, the effects of the additions of micro- and nano-sized $CaCO_3$ on the delayed initial setting and the rate of early strength development of OPC paste containing high volumes of fly ash were determined. In addition to the characterization of hydration products and the determination of the rate of hydration, the mechanical properties of OPC containing high volumes of fly ash with the additions of micro- and nano-sized $CaCO_3$ were also investigated. The investigations of mechanical properties were considered extremely important and essential for linking the cement chemistry and civil engineering. In Stage 4, some of experiments were repeated for OPC containing high volumes of ground granulated blast-furnace slag (GGBFS) to assess and confirm the similar occurrence of an accelerating effect of the nano-sized $CaCO_3$ addition in the system. The objective was to confirm that the addition of nano-sized $CaCO_3$ can

compensate for the slower rate of hydration of OPC containing high volumes of not only fly ash but also GGBFS, which is gaining wider use.

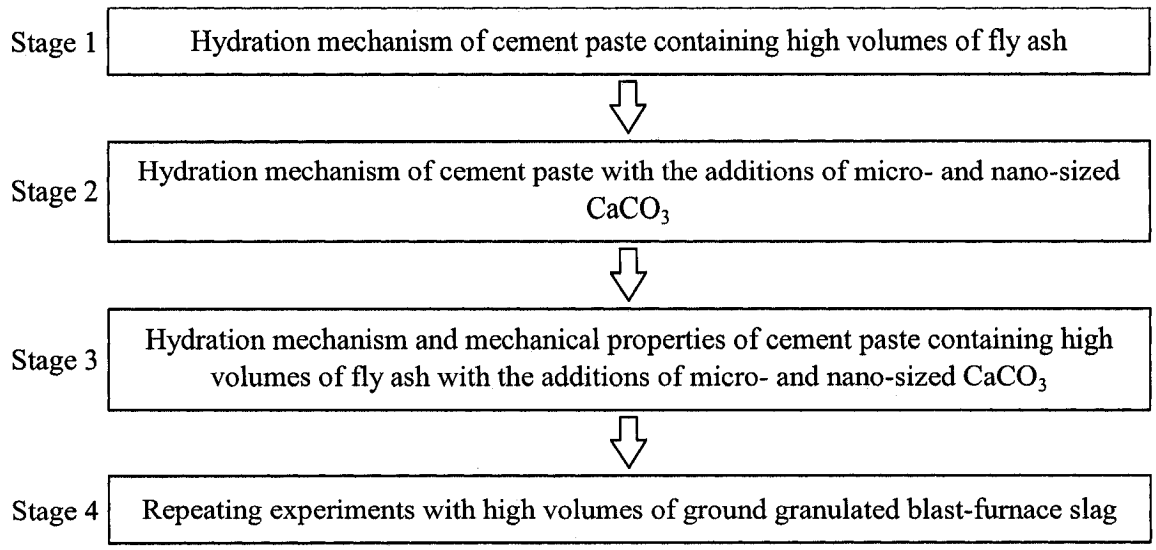

Fig. 1.2 Flowchart of experimental outline for Theme 1

1.4 Theme 2: The Synthesis and Characterization of the Highly Reactive Nano-sized β-C_2S by the Sucrose Method

1.4.1 Objectives

Portland cement is a core material in the concrete-making process. It is the most widely used construction material. A significant amount of CO_2, however, is emitted in the course of cement manufacture. Some reports attribute 7% of the total CO_2 emissions in the world (Mehta, 1999) to cement manufacture. One of the primary reasons for the large amount of CO_2 emissions is the fuel combustion for the operation of the cement kiln at high temperatures. C_3S, a main compound in OPC, can only form at high temperatures, generally above 1450°C, whereas C_2S, another main compound in OPC, can form at lower temperatures. C_3S reacts with water more rapidly and contributes to the early strength development, whereas C_2S reacts more slowly and contributes to the late strength development. Approximately 70% of C_3S reacts in the first 28 days while only

30% of C_2S reacts in the same period (Taylor, 1964). The C_3S content in OPC is critical especially as high performance concrete becomes more commonly used. A replacement of energy intensive C_3S by a highly reactive nano-sized β-C_2S synthesized at lower temperatures, however, can significantly reduce the CO_2 emissions in cement manufacture and make a tremendous contribution to sustainable development. The advent of nanotechnology in many fields of science and technology has produced more studies involving the synthesis of nano-sized materials. Das (2001) introduced a solution-based chemical synthesis method referred to as the Sucrose method for the preparation of fine oxide ceramic powders. The synthesis of the highly reactive nano-sized β-C_2S by the Sucrose method for the first attempt in the field of civil engineering was studied under Theme 2 of the thesis. The chemical and engineering properties of both control and hydrated materials were examined. The specific objectives of Theme 2 are as follows;

1. To synthesize the highly reactive nano-sized β-C_2S by applying the Sucrose method for the first time in the field of civil engineering.
2. To characterize the synthesized highly reactive nano-sized β-C_2S and compare it with the commercially available micro-sized β-C_2S.
3. To study the chemical and mechanical properties of hydrated nano-sized β-C_2S synthesized by the Sucrose method.

1.4.2 Experimental Outline

The flowchart of the experimental outline is shown in Fig. 1.3. In Stage 1, the synthesis and characterization of the highly reactive nano-sized β-C_2S by the Sucrose method were conducted. In Stage 2, the synthesized β-C_2S was mixed with water and its reactivity and hydration characteristics were studied. The determination of microhardness, a mechanical property, was also performed on the synthesized β-C_2S hydrated for 3, 7, 14 and 28 days. The properties of the synthesized nano-sized β-C_2S were compared with those of the commercially available micro-sized β-C_2S. In Stage 3, the amounts of the ingredients were slightly modified according to the observations in Stages 1 and 2 to produce an even finer β-C_2S. Characterization of this product was carried out.

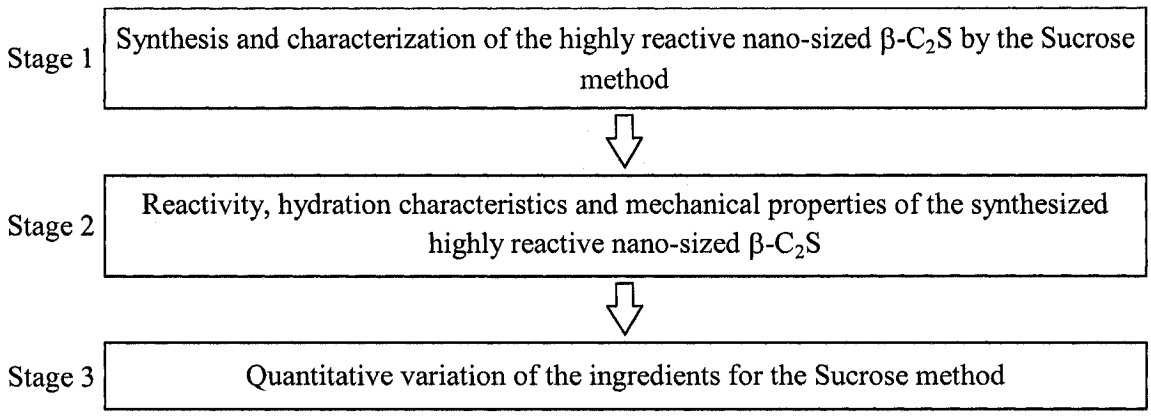

Fig. 1.3 Flowchart of experimental outline for Theme 2

1.5 Theme 3: The Synthesis of the Nano-sized $Ca(OH)_2$ and its Effect on the Pozzolanic Reaction with Metakaolinite

1.5.1 Objectives

$Ca(OH)_2$ is not only one of the hydration products, but also a reactant in many reactions that affect the properties of hardened cement paste and concrete. The alkali-aggregate reactions and carbonation of concrete, for example, are largely impacted by $Ca(OH)_2$. $Ca(OH)_2$ can also play an important role in the pozzolanic reaction, which is the reaction between $Ca(OH)_2$ and SCMs. Metakaolinite, one of the most common SCMs, is a calcined clay produced by the low-temperature calcination of the high purity kaolin clay. Many studies have been conducted to investigate the reaction between metakaolinite and $Ca(OH)_2$. Chemical processes, such as the Sucrose method, or physical processes, or even combined chemical and physical processes (often referred to as physico-chemical processes) can be used to synthesize nano-sized materials. Under this theme, the physical process, a planetary-mill grinding method and the physico-chemical process, a vacuum-calcination method, were applied to synthesize the nano-sized $Ca(OH)_2$. The fundamental aspects of the effect of the nano-sized $Ca(OH)_2$ on the pozzolanic reaction with metakaolinite were investigated under Theme 3 of the thesis. In addition, the Hedvall effect, a novel method developed at the Institute for Research in Construction (IRC), National Research Council Canada, was applied to examine the relative reactivity of the nano-sized $Ca(OH)_2$ as

opposed to a reagent grade micro-sized $Ca(OH)_2$. The thermal decomposition of nano-sized $Ca(OH)_2$ was also investigated in order to elucidate the nature of different types of $Ca(OH)_2$ that exists in a cement paste. The specific objectives of Theme 3 are as follows;

1. To synthesize and characterize the nano-sized $Ca(OH)_2$ by the planetary-mill grinding and the vacuum-calcination methods.
2. To apply the Hedvall effect to examine the relative reactivity of the nano-sized $Ca(OH)_2$.
3. To investigate the effect of the nano-sized $Ca(OH)_2$ on the pozzolanic reaction with metakaolinite.
4. To study the thermal decomposition of nano-sized $Ca(OH)_2$.

1.5.2 Experimental Outline

The flowchart of the experimental outline is shown in Fig. 1.4. In Stage 1, the synthesis of the nano-sized $Ca(OH)_2$ was attempted by the planetary-mill grinding and the vacuum-calcination methods. Characterization of synthesized nano-sized $Ca(OH)_2$ was also conducted in Stage 1. In Stage 2, the Hedvall effect was applied to determine the relative reactivity of the reagent grade micro-sized $Ca(OH)_2$ and the nano-sized $Ca(OH)_2$ synthesized by both planetary-mill grinding and vacuum-calcination methods. In Stage 3, the synthesized $Ca(OH)_2$ was reacted with metakaolinite and its pozzolanic reaction was studied by the conduction calorimetry. In Stage 4, the characteristics of thermal decomposition of nano-sized $Ca(OH)_2$ were studied.

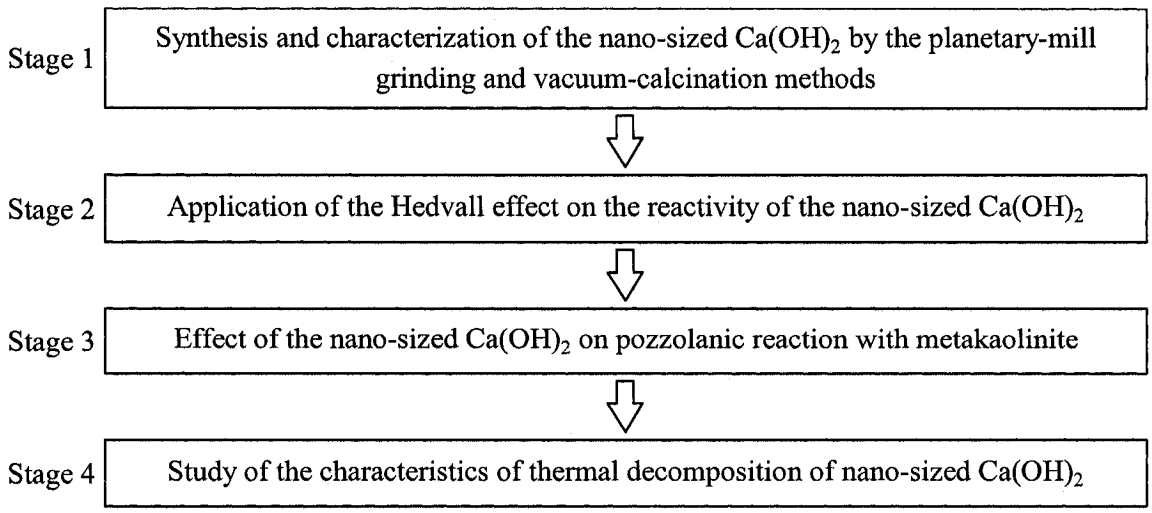

Fig. 1.4 Flowchart of experimental outline for Theme 3

CHAPTER 2

LITERATURE REVIEW AND THEORY

2.1 Applications of Nanotechnology in Construction Materials

2.1.1 General Trends

Nanotechnology has been applied to many different fields of science and technology for more than a decade. It is only in the last few years, however, that the possibility of using nanotechnology to enhance the performance of construction materials has been discussed. The cost efficiency and intrinsically conservative nature of the construction industry might have decelerated the exponentially increasing trend of the application of nanotechnology. It was, however, soon realized that the revolutionary approach of nanotechnology could facilitate the development of new monitoring systems, new repair methods and even new construction materials. The 1st International Symposium on Nanotechnology in Construction was held in UK in June 2003 where the importance of a long-term vision for the application of nanotechnology in construction was clearly indicated. The 2nd International Symposium on Nanotechnology in Construction was held in Spain in November 2005 where more detailed results from early studies for the application of nanotechnology in construction were presented. In the US, the research projects on several topics related to construction, such as polymer intercalated cement products, nano-composites and nano-sensing, have been funded since 2000 by the National Nanotechnology Initiative (NNI) to investigate the potential for the application of nanotechnology. The Federal Highway Administration's (FHWA) Advanced Infrastructure Research program is also leading research in the application of nanotechnology. One of the FHWA-funded research projects is a nano-scale study on the interaction between fly ash and the Portland cement gel structure, which has a large influence on the

strength and durability of concrete. In Canada, a multi-researcher project was initiated at the Institute for Research in Construction (IRC), National Research Council Canada to develop new approaches based on nanotechnology for the construction industry with an emphasis on cements, cement-based materials, admixtures and concretes. The University of Toronto Joint Centre for Bioethics has also suggested that the use of nanotechnology in construction is one of the top ten directives for changing the world with respect to energy production and conservation. The following sections will review previous studies relevant to the application of nanotechnology in construction materials, focusing on cementitious materials.

2.1.2 Understanding Nano-scale Phenomena of Materials

Understanding phenomena at the nano-scale to improve the performance of the existing materials is a major part of the application of nanotechnology in construction materials. It includes theoretical modelling of C-S-H nano-structure, nano-characterization techniques and instrumentation. An investigation at the nano-scale provides a better understating on various issues associated with construction materials. De Miguel (2004) modelled the silicate formation of C-S-H gel and its chain growth mechanisms at the nano-scale by ^{29}Si Nuclear Magnetic Resonance Spectroscopy (NMR). Skibsted et al. (2005) also characterized the nano-structure of the poorly crystalline C-S-H phase by both ^{29}Si and ^{27}Al NMR. Pignat (2003) studied the water permeability of cement paste by simulation of the multiscale pore distribution including the sub-nanometre level. Research conducted by Garboczi and Neumann (2003) combined the existing software developed at the Virtual Cement and Concrete Testing Laboratory (simulating the micrometre to millimetre size range of concrete) with molecular dynamics simulations of the C-S-H to understand the critical nano-scale structure and dynamics of the C-S-H. Bernard et al. (2003) used a multistep micromechanics approach developed from the nano-level of the C-S-H matrix. Kirkpatrick (2005) examined the structuring of water on solid surfaces and in pores with dimensions of the order of nanometres to understand the cement hydration at the molecular scale.

Several new techniques have been suggested, as well, in order to understand the phenomena at the nano-scale. Juenger et al. (2003) applied a technique, soft x-ray transmission microscopy, initially introduced by Kurtis et al. (1998), to the systems of the cementitious material to observe the nano-scale formation of C-S-H. Hughes and Trtik (2003) applied a depth sensing nano-indentation technique in combination with quantitative elemental analysis to study compositional

relationships with the mechanical properties of cement paste. Ultrasonic force microscopy, an atomic force microscopy-based technique, was proposed by Cuberes (2005) to determine the dynamic mechanical properties of materials at the nano-scale. Livingston (2005) applied neutron scattering methods to characterize the microscopic properties of Portland cement concrete at the nano-scale. The use of transmission electron microscopy and electron energy loss spectroscopy was suggested by Scrivener et al. (2003) to investigate the phases of the hydrated calcium aluminate cement intermixed at the nano-scale. Transmission electron microscopy was also applied by Richardson et al. (2005) combined with NMR spectroscopy to model the nano-structure of C-S-H.

2.1.3 Development of Cement-based Nano-materials

Further to understanding the nano-scale phenomena in cementitious materials, several studies have been conducted with the objective of modifying the existing materials at the nano-scale, tailoring nano-sized materials for the specific applications or blending nano-sized materials with the existing cementitious materials. Raki (2004) developed new nanocomposites by intercalating admixtures into layered double hydroxides to control the release rate of the chemicals. Mitchell et al. (2003) synthesized nanoparticulate calcium aluminate using a highly acidic sucrose method and examined the mechanical properties of the product by the application of the microhardness test. Raki and Mojumdar (2005) prepared a series of the C-S-H – polymer nanocomposites by incorporating organic polymers into the nano-layers of C-S-H and characterized these products by a number of techniques including X-ray fluorescence and atomic force microscopy. Makar (2004 and 2005) examined the effect of the carbon nanotube (CNT) addition into a cement paste matrix as a reinforcement and demonstrated the resultant improvement in the tensile strength of the cement paste by CNT crack bridging. The CNT crack bridging effect in the hydrated cement paste was observed by the scanning electron microscopy (SEM) and is shown in Fig. 2.1 (Makar, 2004). Wansom et al. (2006) investigated the fibre-reinforced cement composites with multi-walled carbon nanotubes using the AC impedance spectroscopy. Campillo et al. (2003), who also worked on the use of CNT with cement paste, investigated the effect of the nano-sized silica addition into the cement paste on the mechanical behaviour.

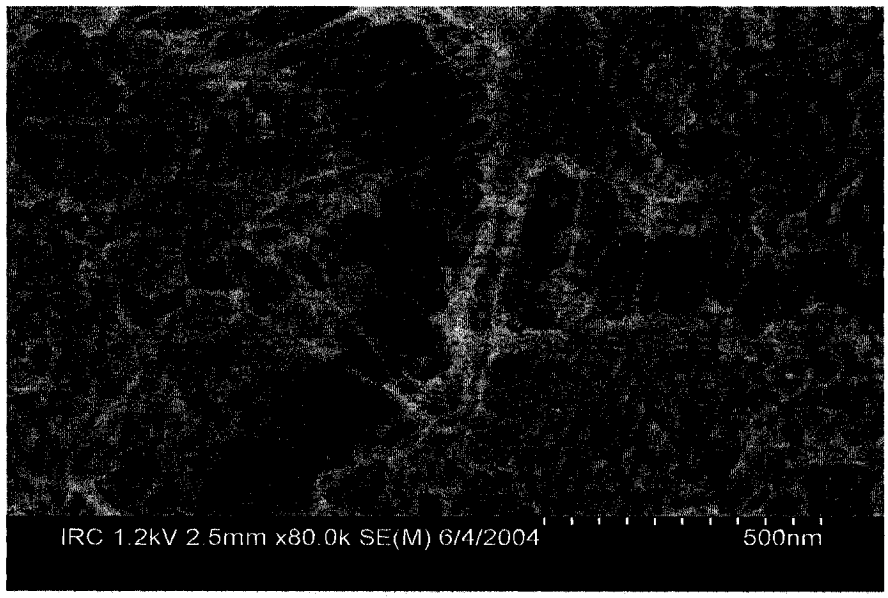

Fig. 2.1 CNT crack bridging in hydrated cement paste observed by scanning electron microscopy (SEM)

2.2 Sustainable Development in the Construction Industry

2.2.1 Introduction

It is undeniable that more clean water, more infrastructure, more landfills and most importantly more sources of energy will be required worldwide with the growing population. The concept of sustainable development was first introduced in the 1970's, discussed intensively through the 1980's and defined ultimately at the 1992 UN Conference on Environment and Development, in Rio de Janeiro, as "Development that meets the needs of the present without compromising the ability of future generations to meet their own needs." Sustainable development has been one of the most investigated topics since then.

Concrete is the most popular and widely used construction material and yet one of the most energy-intensive materials from the perspective of sustainable development. Cement manufacture is an extremely resource-consuming industry where it requires about 1.5 tonne of raw materials and releases about 1 tonne of CO_2 per tonne of cement produced. It was inevitable for the cement

manufacture to be considered as a primary target for contributions to sustainable development. Since 1998, seminars, symposia, workshops and conferences have been organized by the Canadian Centre for Mineral and Energy Technology, CANMET, and American Concrete Institute, ACI, to determine the importance and role of the cement and concrete industries in reducing greenhouse gases and conserving energy and resources. In 2003, a series of conferences was held in Dundee, Scotland for cement science and concrete in sustainable development. ASTM introduced, in 2005, a term "green building" which represents the concept of sustainable development in the construction industry and defined it as "a building that provides the specified building performance requirements while minimizing disturbance to and improving the functioning of local, regional and global ecosystems both during and after its construction and specified service life." It should be emphasized that sustainable development can only be accomplished when all the economic, social and environmental factors are taken into account in a practical manner. It is not an easy task to pursue such an innovative change due to the intrinsically conservative nature of the construction industry where a structure is expected to be built as soon and as cheaply as possible. The aim of sustainable development, however, will be achieved with foresight and firm 'concrete' plans.

2.2.2 Current Eco-strategies in the Cement and Concrete Industries

There are many ongoing efforts in the construction industry to contribute to sustainable development, for example, reducing CO_2 emissions and conserving energy. This section will focus on those efforts in the cement and concrete industries and to explain how they relate to the concept of sustainable development.

2.2.2.1 Use of Supplementary Cementing Materials

The idea of a partial replacement of cement content in the concrete mixes by other less energy-intensive materials is well known and widely recognized. The supplementary cementing materials (SCMs) are the industrial by-products, or natural minerals, which can be added to the concrete mixes as the partial replacement of OPC. The primary purpose is to reduce the total amount of cement used in the mixes and therefore to conserve the energy and maintain the properties and behaviour of hardened concrete at the same or even improved level. The use of SCMs is covered under CSA A23.5-86, Supplementary Cementing Materials, and partially under CSA A362-98, Blended Hydraulic Cement. As mentioned above, cement manufacture releases approximately 1

tonne of CO_2 per tonne of cement produced. The amount of cement replaced by the SCMs would therefore be the amount of CO_2 saved. The common SCMs are fly ash, ground granulated blast-furnace slag (GGBFS), silica fume and metakaolinite. Fly ash is the most commonly used SCM in Canada followed by GGBFS and silica fume. Bouzoubaâ and Fournier (2003) report that, in Canada, approximately 524,000, 347,000 and 37,000 tonnes of fly ash, GGBFS and silica fume, respectively, were used in the cement and concrete applications in 2001. The amount of SCMs used in the cement and concrete applications is increasing each year.

A number of studies aimed at utilizing more SCMs to conserve more energy have been conducted. Natural Resources Canada, CANMET, has been working intensively on High-Volume Fly Ash (HVFA) concrete, which is concrete containing approximately 50% of fly ash. The SCMs can be used not only for replacing OPC but also for other applications, such as grout and masonry cement. A report by Mehta (1999), however, states that the total of 500 million tonnes of fly ash produced today, only about 8% of this is used by the cement and concrete industries, the rest is being disposed, mainly in landfills. The Government of Canada recently decided to invest $1.1 million over five years to promote the increased use of the SCMs to replace OPC in concrete and other such materials (National Resources Canada, 2002). It was considered essential to study the use of SCMs to keep the increasing demand of energy consumption under control. The SCMs will be described more in detail in Section 2.3.3.

2.2.2.2. Use of Belite Cement and Highly Reactive β-C_2S

One of the major drawbacks of cement manufacture is the significant amount of CO_2 emissions. This originates mainly from two events; one is from chemical process of calcining limestone into lime in a cement kiln and the other from combustion of fuel to operate the cement kiln itself at high temperatures. As the cement kiln is heated up to about 700°C, the calcination of limestone starts with the following reaction:

$$CaCO_3 \text{ (limestone)} + \text{Heat} \rightarrow CaO + CO_2 \qquad (2.1)$$

This chemical reaction produces approximately 40% of the total CO_2 emissions in cement manufacture. The other 60% is from the fuel combustion for the operation of the cement kiln at high temperatures. Wilson (1993) summarized the amount of CO_2 emissions from the cement and concrete productions as shown in Table 2.1. Raw materials, such as clay, chalk and limestone, are heated in the cement kiln up to approximately 1450°C to produce OPC clinker. A high tempera-

ture is required in the cement kiln because C_3S, the main compound in OPC, can only be formed at high temperatures, generally above 1250°C. The content of C_3S is very important in OPC and it contributes to the early strength development. C_2S, another main compound in OPC, can be formed at lower temperatures, but its much slower hydration reaction only contributes to the late strength development. Belite cement (the word "belite" is defined as β-C_2S plus impurities such as oxides in the cement clinker) became a subject of many studies, because of its low temperature of formation in the manufacturing process. At the same time, synthesis of highly reactive β-C_2S itself became a subject of many studies. A replacement of energy intensive C_3S by highly reactive β-C_2S synthesized at low temperatures can save a significant amount of CO_2 emissions from cement manufacture and make a tremendous contribution to sustainable development. A review of a number of studies on highly reactive β-C_2S will be covered in Section 2.4.2.

Table 2.1 Summary of CO_2 emissions from the cement and concrete productions

	lbs CO_2 Per Tonne of Cement	lbs CO_2 Per cu. Yd. of Concrete	Percent of Total CO_2
CO_2 Emissions from Calcining Limestone	997	250	40
CO_2 Emissions from Cement Kiln Operation	1,410	381	60
Total CO_2 Emissions	2,410	631	100

2.2.2.3. Use of Recycled Concrete

Although the reduction of CO_2 emissions from cement manufacture is important in sustainable development, studies on recycling solid waste have been intensively conducted as well. Aggregates, which account for about 70% of the concrete volume, can be obtained by mining, processing and transporting naturally occurring rocks and minerals. Recently, concrete buildings and structures, which have reached their service lives, have been recycled as a source of aggregates in several projects. Meyer (2002) reported that construction debris and demolition waste constitute about 23% to 33% of the municipal solid waste and the demolished concrete contributes the largest share of the waste material. Therefore, the use of old concrete, which otherwise goes to landfills, as a source of aggregates represents potentially a substantial contribution to sustainable development. In practice, it is used in cases such as concrete retaining walls or highway dividers. It has been reported that durability of new concrete made from recycled concrete aggregate is generally the same or even better than concrete with conventional aggregates (Portland Cement

Association, 2002). The economics of recycled concrete depends on a number of different factors. The procedure of recycling concrete involves breaking up and crushing a concrete structure, removing reinforcing steel and other foreign materials, grading and washing and finally storing in a proper environment. Also, the transportation cost of the recycled concrete has to be compared with that of conventional aggregate. Under the right conditions, however, recycling the old concrete structure as a source of aggregates will help the environment and contribute to sustainable development. Investigations of the possibility of lengthening the service life of structures itself and the use of less energy and resources in the long-term for the price of a relatively marginal capital cost increase are being pursued world-wide as well.

2.3 Theme 1: The Use of Nano-sized $CaCO_3$ Addition to Cement Paste Containing High Volumes of Supplementary Cementing Materials

2.3.1 Introduction

The main objective of Theme 1 is to investigate the effect of the nano-sized $CaCO_3$ addition on the hydration and engineering performance of cement paste containing high volumes of SCMs. A significant accelerating effect owing to the nano-sized $CaCO_3$ addition on the delayed initial setting and rate of early strength development of the cement paste containing high volumes of SCMs is expected. It is also expected that the addition of the nano-sized $CaCO_3$ will significantly improve the mechanical properties of hydrated cement paste. In the following sections, the hydration mechanism and setting process of OPC cement paste with the $CaCO_3$ addition will first be discussed, including nucleation phenomena and the accelerating effect of finely ground $CaCO_3$ addition on the hydration of cementitious materials observed in the previous studies. Then, the physical and chemical properties of fly ash and ground granulated blast-furnace slag (GGBFS) will be described. Finally, the previous studies on the high-volume fly ash (HVFA) concrete will be briefly discussed.

2.3.2 Cement Paste with the $CaCO_3$ Addition

2.3.2.1 The Hydration Mechanism and Setting Process

The finely ground $CaCO_3$, as mentioned earlier, has been used as a partial replacement of OPC to reduce the total amount of OPC in the concrete mixes. The first area to investigate in association with the effect of $CaCO_3$ addition on the hydration of cement is the hydration reactions. Characterized in detail by Carlson and Berman (1960), tricalcium aluminate, C_3A, one of the four major constituents in cement, reacts with $CaCO_3$ to form calcium carboaluminate hydrate. It forms both high- and low- carbonate forms of calcium aluminate hydrate in a similar manner as C_3A reacts with calcium sulphate (gypsum), $CaSO_4 \cdot 2H_2O$, to form both high- and low- sulphate forms of calcium aluminate hydrate. The high- and low- carbonate forms of calcium aluminate hydrate appear respectively as $3CaO \cdot Al_2O_3 \cdot 3CaCO_3 \cdot 32H_2O$ and $3CaO \cdot Al_2O_3 \cdot CaCO_3 \cdot 12H_2O$, which are very similar to the high- and low- sulphate forms of calcium aluminate hydrate, $3CaO \cdot Al_2O_3 \cdot 3CaSO_4 \cdot 32H_2O$ and $3CaO \cdot Al_2O_3 \cdot CaSO_4 \cdot 12H_2O$. Feldman et al. (1965) investigated the effect of the $CaCO_3$ addition on the hydration of 90% pure C_3A and found that the hydration reactions were suppressed by the $CaCO_3$ addition because of the formation of the low form of calcium carboaluminate hydrate on the surface of the C_3A grains. Also the reaction of tetracalcium aluminoferrite, C_4AF with $CaCO_3$ to form calcium carboaluminoferrite was suggested by Lea (1970). When ground cement clinker without gypsum was hydrated with the addition of $CaCO_3$, the calcium carboaluminate hydrate would rapidly form. The question arises as to what would happen if both $CaCO_3$ and gypsum were present in the hydrating cement paste. The x-ray diffractometry studies by Ingram et al. (1990) illustrated that $CaCO_3$ reacts with the clinker C_3A to form a calcium carboaluminate hydrate in a 2% gypsum, 6% limestone and 92% clinker system. Bensted (1980) investigated the effect of calcium carbonate substitution of gypsum in OPC and concluded that some substitution of gypsum by limestone was possible without negatively affecting the setting behaviour and compressive strength from three days to one year. Klemm and Adams (1990) investigated the reaction of 5% and 15% of both reagent $CaCO_3$ and interground limestone with Type II cement. They determined that the formation of calcium carboaluminate hydrate was much slower than that of ettringite and 80-90% of $CaCO_3$ remained unreacted after 129 days of the hydration. Ramachandran and Zhang (1986) studied the influence of finely ground $CaCO_3$ addition on the hydration of tricalcium silicate, C_3S. The amounts of $CaCO_3$ in the hydrated C_3S were determined at various hydration periods by the thermal analysis and it was revealed that the amount of added $CaCO_3$ decreased as hydration took place, indicating that the

added $CaCO_3$ was chemically reacting. It was suggested that the missing carbonates may be chemisorbed or even enter the interlayer region of C-S-H.

2.3.2.2 Nucleation Phenomena and the Accelerating Effect

It is important to note that even if a material is not highly chemically reactive, it can have a significant impact on the hydration. Some studies found that the finely ground limestone particles, when added to cement, act as nucleation sites to accelerate the cement hydration process. Soroka and Stern (1976) studied the effect of two calcareous fillers, ground limestone and reagent grade $CaCO_3$ on the compressive strength of OPC. They argued the possibility that calcareous fillers act as nucleation sites to explain the acceleration effect on the early strength development. It was also concluded that the observed formation of calcium carboaluminate hydrate did not necessarily affect the compressive strength. Soroka and Setter (1977) investigated the effects of the ground limestone filler with the different contents and fineness on the hydration of cement mortars and concluded that the compressive strength essentially increased with both filler content and fineness. The conduction calorimetry results, by Ramachandran and Zhang (1986) mentioned above, for the hydration of C_3S containing different amounts of $CaCO_3$ are shown in Fig. 2.2. The C_3S hydration containing $CaCO_3$ is accelerated and the greater the $CaCO_3$ content, the earlier the hydration takes place. The rate of the heat development, as evidenced by the peak height, is also higher for the higher contents of $CaCO_3$. Péra et al. (1999) also studied the influence of the finely ground limestone on the cement hydration and concluded that the hydration of OPC with the limestone addition had higher heat development than that without limestone.

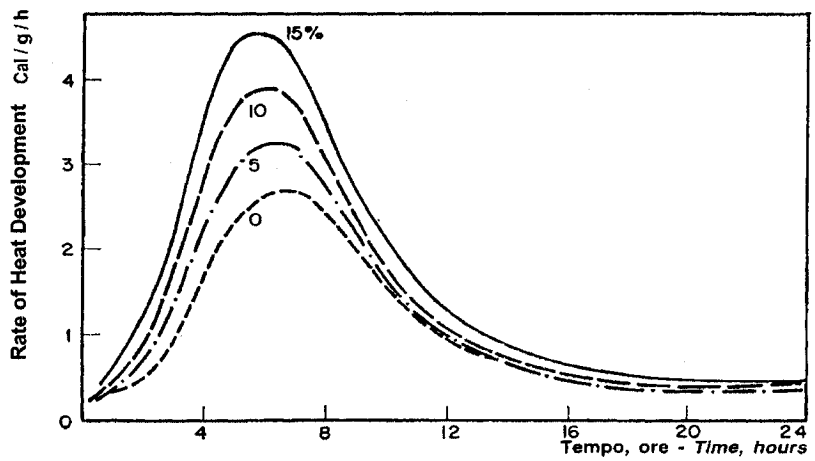

Fig. 2.2 Conduction calorimetry results for the hydration of C_3S containing different amounts of $CaCO_3$

2.3.3 Significance of SCMs in the Field of Cement and Concrete

The use of SCMs from the aspect of sustainable development and how it contributes to saving energy and natural resources were discussed in Section 2.2.2.1. The SCMs, such as fly ash, GGBFS, silica fume and metakaolinite, are materials that, when used in conjunction with Portland or blended cement, contribute to the properties of the hardened concrete through hydraulic or pozzolanic activity or both (Portland Cement Association, 2002). A pozzolan is a siliceous or aluminosiliceous material, that chemically reacts in the presence of moisture with calcium hydroxide produced by the OPC hydration to form calcium silicate hydrate, C-S-H, and other cementing compounds. The reaction between the pozzolans and $Ca(OH)_2$ is known as a pozzolanic reaction. Both the OPC hydration and the pozzolanic reaction are relevant. The detailed mechanism of the pozzolanic reaction associated with cement hydration will be discussed in Section 4.3.1.1. In the following sections, the physical and chemical properties of each individual SCM will be introduced first and the study on high-volume fly ash concrete will then be discussed.

2.3.3.1 Fly Ash

Fly ash, the most widely used SCM, is a by-product of the combustion of pulverized coal in the electric power generating plants. It contains silica, alumina, calcium and iron with minor constituents such as magnesium, sulphur, sodium, potassium and carbon. The typical ranges for the chemical composition of fly ash are shown in Table 2.2. Two major classes of fly ash are specified by CSA A23.5 based on their chemical compositions. Class F fly ash is the one with the low calcium content (less than 8% CaO) and is generally produced from burning anthracite or bituminous coal. Class C fly ash is the one with the high calcium content (8% to 20%) and is generally produced from the burning of subbituminous coal and lignite. A replacement level for Class F fly ash is generally 15% to 25% and for Class C fly ash is generally 15% to 40% by mass of cementing material. Most of the fly ash particles are solid spheres, but they can also be hollow spheres or hollow spheres containing small spheres. An SEM image of the typical Class F fly ash particles is shown in Fig. 2.3. The particle size can vary from less than 1 μm to more than 100 μm. The BET surface area is typically in the range of 0.3 to 0.5 m^2/g, but some fly ashes can have surface area values as low as 0.2 m^2/g and as high as 0.7 m^2/g. The chemical composition and physical properties of fly ash can vary widely depending on how it was processed. Therefore a careful quality control of fly ash is essential when it is to be used in the concrete mixes.

Table 2.2 Typical chemical composition of fly ash (wt. %)

SiO_2	Al_2O_3	CaO	Fe_2O_3	MgO	SO_3	Na_2O	K_2O	C
35 ~ 52	15 ~ 23	5 ~ 20	6 ~ 30	1.0 ~ 2.0	0.8 ~ 4.1	0 ~ 5.8	0 ~ 2.0	0 ~ 5.0

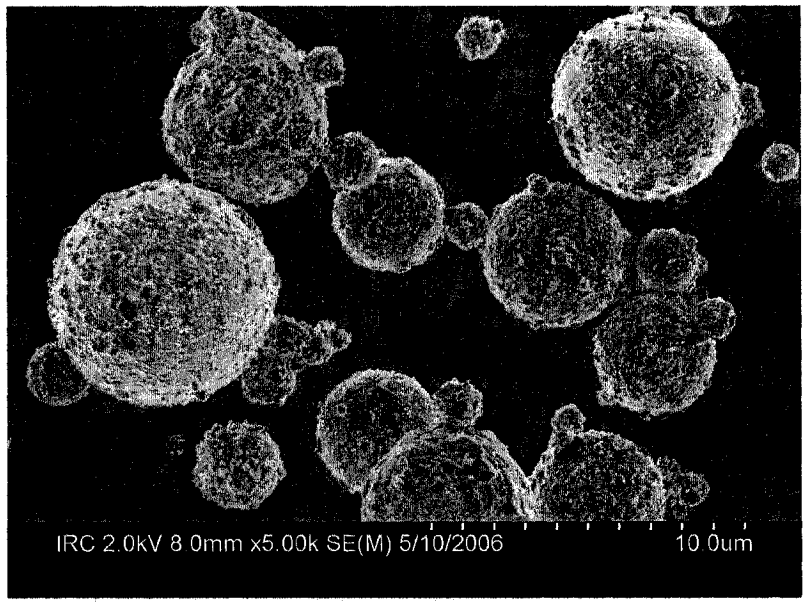

Fig. 2.3 High resolution SEM image of the typical Class F fly ash particles

2.3.3.2 Ground Granulated Blast-furnace Slag

Ground granulated blast-furnace slag (GGBFS) is a by-product of molten iron production in a blast furnace. It consists essentially of silicates and aluminosilicates of calcium developed in a molten condition with iron in the blast furnace. Table 2.3 shows the typical chemical composition ranges of GGBFS. A replacement level for GGBFS is generally 30% to 45% of the cementing material in the mix. The use of GGBFS needs to meet the requirements specified in CSA A23.5. The BET surface area is typically in the range of 0.4 to 0.6 m^2/g.

Table 2.3 Typical chemical composition of GGBFS (wt. %)

SiO_2	Al_2O_3	CaO	Fe_2O_3	MgO	SO_3	Na_2O	K_2O
30 ~ 41	5 ~ 20	35 ~ 40	0.3 ~ 1.5	3 ~ 15	0.6 ~ 4.0	0 ~ 0.3	0 ~ 0.4

2.3.3.3 High-Volume Fly Ash Concrete

The high-volume fly ash (HVFA) concrete is one specific type of fly ash concrete which contains a significantly higher volume of fly ash than normal. This serves to produce an even more envi-

ronmentally friendly and sustainable concrete by replacing a higher amount of cement in the concrete mixes. The HVFA concrete, defined as a concrete containing approximately 50% of fly ash, was developed at CANMET, Natural Resources Canada. It has been a subject of extensive study for more than 15 years at CANMET. Gillies (2001) reported that some of the physical and mechanical properties, such as workability and long-term compressive strength, were improved by the HVFA. It is recommended for the HVFA concrete mixes to have relatively low water/cementitious solid (w/c) ratios, typically below 0.35 accompanied by the use of superplasticizer for workability. The Canadian Standards Association is in the process of including an annex in the CSA Standards for the use of concrete containing high volumes of supplementary cementing materials. It will include the required specification for fly ash replacement levels for the use of the HVFA in practice. However, one of the biggest challenges associated with the use of the HVFA, along with the scaling issue, is the slower initial setting and rate of early strength development especially in cold weather. A period for concrete form stripping can be critical when a tight schedule of construction is demanded in the competitive industry. EcoSmart is a 'not-for-profit' organization guided by a National Advisory Committee on which CANMET is one of the representatives. EcoSmart has recently reported a series of studies on the use of HVFA concrete mixes for high-rise construction. Gerry and Seabrook (2000) reported on the compressive strength of the HVFA concrete cured at 23°C and 5°C, simulating summer and winter conditions, respectively. The test results are summarized in Table 2.4. Three mixes were cured at 23°C and two at 5°C. The w/c ratios were kept relatively high and no superplasticizer was used. The contents of fly ash are 20% and 45% and a set accelerating admixture was used for those containing 45% fly ash content. The greater the fly ash content, the lower is the compressive strength at any hydration period for curing at both 5 and 23°C, even though the accelerating admixture was used for the higher fly ash contents. The values of compressive strength for the 45% fly ash content are much lower than those for 20%, especially at 1 day hydration. The differences become smaller, as the hydration proceeds. The values of setting time are in accordance with the values of the compressive strength shown.

2.3.4 Summary of Theme 1

Under Theme 1, the properties and the hydration characteristics of the OPC cement paste containing high volumes of SCMs (fly ash and GGBFS) will be examined with the additions of both nano-sized and conventional micro-sized reagent grade $CaCO_3$. The use of high volumes of

SCMs is essential from the aspect of sustainable development. The major disadvantage of the use of concrete mixes containing high volumes of SCMs is however the slower initial setting and rate of early strength development. It has been recognized that the addition of the finely ground $CaCO_3$ has an accelerating effect on the hydration of cement. The effect of the nano-sized $CaCO_3$ addition on the delayed hydration of OPC containing high volumes of SCMs will be studied for the first time.

Table 2.4 High-Volume Fly Ash (HVFA) concrete mixes test results

Mix No.		1	2	3	4	5
Curing Temperature, °C		23	23	23	5	5
Water/Cement Ratio		0.50	0.43	0.45	0.50	0.45
Fly Ash, % by Total Mass		20	45	45	20	45
Accelerator*		None	Low	High	None	High
Compressive Strength, MPa	1d	11.0	7.5	6.8	6.5	4.2
	2d	17.0	12.4	11.3	10.9	8.5
	3d	20.4	14.7	12.6	13.1	10.6
	7d	25.7	18.7	16.7	23.1	17.2
	56d	37.1	32.2	28.1	34.7	30.9
Time of Setting, Hours	Initial	5.5	6.75	6.25	10	13
	Final	6.5	8.5	8	12	15

*Note Accelerator: PolarSet from GRACE

2.4 Theme 2: The Synthesis and Characterization of the Highly Reactive Nano-sized β-C_2S by the Sucrose Method

2.4.1 Introduction

The main objectives of Theme 2 are to synthesize the highly reactive nano-sized β-C_2S by the Sucrose method and to examine the chemical and mechanical properties of both control and hydrated materials. In the following sections, the synthesis of highly reactive β-C_2S conducted in the previous studies will first be discussed including the general information on C_2S phases in a

cement clinker. Then the Sucrose method, used to synthesize the highly reactive nano-sized β-C_2S, will be described.

2.4.2 Highly Reactive β-C_2S

2.4.2.1 The C_2S Phase in OPC

C_2S accounts for approximately 20% of the Type GU (formerly known as Type 10) OPC. There is, however, more than one form of C_2S in terms of its crystal structure and it is essential to distinguish them when C_2S is synthesized. The crystal structure of C_2S has been studied intensively since Bredig (1950) suggested its hexagonal structure. The five different polymorphic transitions were reported by Niesel (1972) and are summarized in Fig. 2.4. The phase transitions of C_2S between α-α'$_H$-α'$_L$-β are reversible with temperature. The transition from β- to γ-C_2S is known as dusting owing to a large increase in volume. γ-C_2S is a stable form at room temperature and is barely hydraulic. β-C_2S is rather unstable at room temperature, however it is relatively hydraulic. Stabilizing β-C_2S at room temperature can be achieved by introducing stabilizers. The presence of the small amounts of oxides such as B_2O_3 and Cr_2O_3 as stabilizers is effective in stabilizing β-C_2S (Lea, 1970). β-C_2S is a general form of C_2S in OPC where impurities included in the raw materials function as stabilizers for β-C_2S in the cement kiln for manufacturing OPC. The effects of the calcining temperature and cooling rate of C_2S on its crystal structures and phase transition were also examined by Niesel (1972) and Gawlicki and Nocun-Wczelik (1980). In the studies of highly reactive C_2S, its phase is generally β-C_2S, unless otherwise stated.

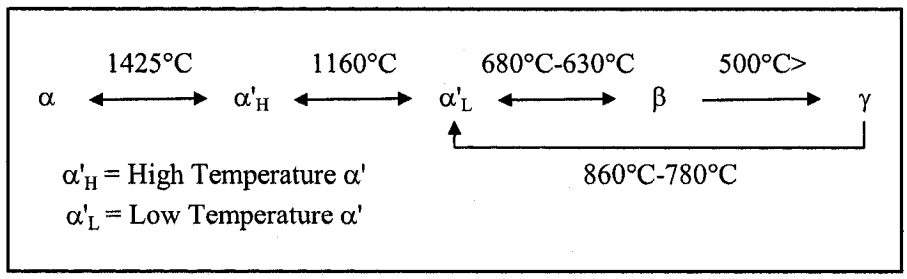

Fig. 2.4 Different polymorphic transitions of C_2S

2.4.2.2. Synthesis of β-C_2S

Belite cement has been a subject of intensive study since the concept of sustainable development and reduction of CO_2 emissions started gaining the attention. Belite cement is known as a low-

heat cement because the cement kiln is not heated as high as for OPC. The amount of lime as a raw material required for manufacturing belite cement is lower than that for OPC, because the amount of belite, in belite cement, is greater than that of alite (C_3S + impurities in clinker) resulting in saving natural resources. The amount of $Ca(OH)_2$, one of the hydration products, is less in the hydrated belite cement than in the hydrated OPC. The only disadvantage is its lower reactivity and therefore the slower rate of initial strength development. Many studies have been conducted to increase the reactivity of the belite cement including introduction of the stabilizing agents and change of the particle size. At the same time, synthesis of β-C_2S itself becomes a subject of intensive study as well. The background of studies on the belite cement and the highly reactive β-C_2S from the aspect of sustainable development and how they contribute to the reduction of the CO_2 emissions were discussed in Section 2.2.2.2. This section will focus on the details of those studies of highly reactive β-C_2S synthesized at relatively lower temperature than the solid-state reaction and their chemical and physical properties. The earliest chemical synthesis of highly reactive β-C_2S with a specific surface area of 7.43 ~ 12.94 m^2/g was performed by both gel and spray-drying techniques with a solution of $Ca(NO_3)_2 \cdot 4H_2O$ and colloidal SiO_2 in hot air at 750-1050°C (Roy and Oyefesobi, 1977). The compressive strength of the hydrated synthesized β-C_2S was found to be slightly higher than that of the commercial β-C_2S. Roy et al. (1978) also used the Evaporative Decomposition of Solution (EDS) technique to produce more reactive β-C_2S. Yang and Zhong (1982) synthesized a reactive β-C_2S by mixing CaO and amorphous silica subjected to hydrothermal treatment at 100°C and ignition at no higher than 850°C without stabilizers. It was observed that the hydration rate of the synthesized β-C_2S was more rapid than that of the ordinary β-C_2S. A similar study was conducted by Kralj et al. (1986) where amorphous silica was mixed with $CaC_2O_4 \cdot H_2O$ or $CaCO_3$ in the temperature range between 760°C and 970°C to produce β-C_2S. Ishida et al. (1992) have successfully produced β-C_2S that has a higher reactivity than a conventional β-C_2S. Hillebrandite ($Ca_2SiO_3(OH)_2$) was hydrothermally synthesized using CaO and quartz at 250°C, then it was heated at 600°C for 1 hour to obtain β-C_2S with a specific surface area of approximately 7 m^2/g. The hydration rate of β-C_2S with fibrous crystals was extremely rapid and the hydration was completed in 14 days for a w/c ratio of 1.0. Nettleship et al. (1993) developed a process to produce high surface area C_2S powder using colloidal silica for the silicon precursor. The desired silicate was developed between 500°C and 700°C, using $CaCO_3$ as an intermediate compound. Most recently, Hong and Young (1999) synthesized the reactive C_2S by the Pechini process, which formed an intermediate amorphous solid that was subsequently

decomposed and thermally reacted to form oxide phases. The BET specific surface area ranged from 1 to 40 m^2/g that largely affected the rate of hydration.

2.4.3 The Sucrose Method

The advent of nanotechnology and its application in many fields of science and technology has resulted in the synthesis of various nano-sized materials. Das (2001) introduced the Sucrose method, which is a solution-based chemical synthesis process at low processing temperatures for the preparation of fine oxide ceramic powders. This process was used to prepare the multi-component oxides, such as lead zirconate titanate and spinel ferrites. The stoichiometrically proper amounts of the metal nitrates were mixed with water to form a mixed metal ionic solution. The pH of the solution was kept at 1 by adding nitric acid. A 10% aqueous polyvinyl acetate (PVA) solution and the aqueous solution of sucrose were mixed together with stirring. The resulting solution was evaporated at 200°C leading to the liberation of brown fumes of NO_2 and the formation of a highly viscous liquid. Further heating of the liquid caused it to decompose into a voluminous, organic-based, black mass, which was ground to a fine powder to form a precursor material. Calcination of the precursor at the proper temperature resulted in the desired nano-crystalline oxides. The experimental process of the Sucrose method will be described in detail in Section 5.2.3.

2.4.4 Summary of Theme 2

Under Theme 2, the Sucrose method will be applied for the first time in the field of civil engineering to synthesize the highly reactive nano-sized β-C_2S. The synthesized highly reactive β-C_2S will be characterized with a number of techniques and will be hydrated for further examination of the chemical, physical and engineering properties. The significant amount of CO_2 emissions can be produced in cement manufacture because of the operation of the cement kiln at high temperatures. The cement production at lower temperatures has a significant potential for contributing to sustainable development. The application of nanotechnology permits the synthesis of the highly reactive nano-sized β-C_2S produced at a relatively lower temperature than the conventional cement produced in the cement kiln.

2.5 Theme 3: The Synthesis of the Nano-sized $Ca(OH)_2$ and its Effect on the Pozzolanic Reaction with Metakaolinite

2.5.1 Introduction

The main objective of Theme 3 is to investigate the effect of the nano-sized $Ca(OH)_2$ on the pozzolanic reaction with metakaolinite. In addition, the Hedvall effect was applied to examine the relative reactivity of the nano-sized $Ca(OH)_2$ as opposed to the conventional reagent grade micro-sized $Ca(OH)_2$. In the following sections, the physical and chemical properties of metakaolinite will be described first. Then two methods of synthesizing the nano-sized $Ca(OH)_2$, planetary-mill grinding and high-temperature calcination methods are described. An application of the Hedvall effect to investigate the relative reactivity of $Ca(OH)_2$ will also be explained. Finally, the previous studies of the thermal decomposition characteristics of $Ca(OH)_2$, especially the doublet characteristics, will be described.

2.5.2 Metakaolinite

A volcanic ash, (origin of the term "pozzolan"), has been used with calcined clay as a hydraulic material for millennia. Many of the Roman pozzolan-based structures can still be seen, indicating these high durability. The use of natural pozzolans in a concrete mix dates to the early 20^{th} century in the US where they were used to avoid rapid temperature rise in mass concrete. Metakaolinite is one of the most common natural pozzolans (SCMs obtained mainly by processing natural minerals). It is produced by the calcination of pure or refined kaolin clay at the temperature of between 650 and 850°C, followed by grinding to an average particle size of about 1 to 2 μm. Metakaolinite itself is not cementitious, however, it reacts with $Ca(OH)_2$ to form C-S-H when added to a cement mix. Metakaolinite is used especially when very low permeability or very high strength is required. Ramachandran et al. (1998) studied the compressive strength of Portland cement paste with the addition of metakaolinite and found that the strength was improved when 10% metakaolinite was added to the system. The typical ranges for the chemical composition of metakaolinite are shown in Table 2.5. Natural pozzolans are classified by CSA A23.5 as Type N pozzolans.

Table 2.5 Typical chemical composition of metakaolinite (wt. %)

SiO_2	Al_2O_3	CaO	Fe_2O_3	MgO	SO_3	Na_2O	K_2O
52 ~ 53	42 ~ 43	0.02 ~ 0.1	0.5 ~ 1.0	0 ~ 1.0	0 ~ 0.1	0 ~ 0.05	0.4 ~ 1.5

2.5.3 Synthesis of the Nano-sized $Ca(OH)_2$

Many studies, as described in Section 2.4.2.2, have been conducted to chemically synthesize nano-sized materials. The physical or combined physical and chemical (physico-chemical) synthesis of the nano-sized materials is however as effective as the chemical synthesis. The planetary-mill grinding method and the vacuum-calcination method are described in the following sections.

2.5.3.1 Planetary-mill Grinding Method

Grinding is one of the most classic physical methods to produce finer materials and yet there is no absolute method established. The planetary-mill grinding is based on in-solution grinding whereas a process known as a micronizing is based on dry grinding. The resulting fineness of materials depends on many factors such as grinding duration, type of grinding solution and the mass ratio of the material to the solution.

2.5.3.2 Vacuum-calcination Method

One of the methods to synthesize a nano-sized $Ca(OH)_2$ is to prepare a nano-sized CaO by calcining a conventional reagent grade $Ca(OH)_2$ and re-hydrating it to form the nano-sized $Ca(OH)_2$. Decomposition of $Ca(OH)_2$ typically starts at around 350°C, peaks out at 450°C and ends at 500°C. Therefore, the calcination of $Ca(OH)_2$ is generally conducted between 450 to 500°C. The higher the calcination temperature, the larger are the resulting particles of CaO because of the agglomeration. Glasson (1956) calcined $Ca(OH)_2$ at temperatures from 350°C to 500°C under vacuum. The vacuum helps the decomposition of $Ca(OH)_2$ occur at lower temperatures. It was observed that the surface area of $Ca(OH)_2$ calcined at lower temperatures is much higher than that calcined at higher temperatures. The BET surface area of the $Ca(OH)_2$ calcined at 350°C for 16 hours under vacuum was reported to be 100 m^2/g.

2.5.4 *An Application of the Hedvall Effect*

A change in the rate of chemical reaction of a solid during and as a consequence of a crystalline transformation is known as the Hedvall effect. Ramachandran and Sereda (1971) applied the theory of this effect in cement chemistry and used it as one of the techniques to determine the relative reactivity of several calcium compounds. CaO, $Ca(OH)_2$, C_3S, and C_2S were mixed with the known amount of $AgNO_3$ and heated to 250°C. It was found that the reactions of $AgNO_3$ with CaO and $Ca(OH)_2$ were stoichiometric with respect to Ca, but only 27% of the Ca present in C_3S and 6% of the Ca in C_2S reacted with $AgNO_3$. This correlates with the hydration reactivity of C_3S and C_2S. The experimental process of the application of the Hedvall effect will be described in detail in Section 6.3.2.

2.5.5 *Thermal Decomposition Characteristics of $Ca(OH)_2$*

The decomposition of the reagent grade micro-sized $Ca(OH)_2$ typically starts at around 350°C, peaks out at 450°C and ends at 500°C. These thermal decomposition characteristics of $Ca(OH)_2$, however, may change depending on the effects of particle size, surface area, morphology and crystallinity of $Ca(OH)_2$. It would be expected, that two distinctively different types of $Ca(OH)_2$ in one system would result in decomposition peaks that have a doublet characteristic. Greene (1960) observed the doublet associated with the decomposition of $Ca(OH)_2$ in hydrated Portland cement in the vicinity of 500°C. It was suggested that the smaller endothermic peak indicates chemisorbed water held on the surface of free lime particles, whereas the second larger peak is attributed to the more coarsely crystalline $Ca(OH)_2$. Herrick et al. (1992) reported the presence of two differential thermal analysis (DTA) endothermic peaks during the decomposition of $Ca(OH)_2$ formed during the hydration of expansive clinker pastes. The lower decomposition peak was attributed to the metastable cubic $Ca(OH)_2$ pseudomorphs. The slow conversion to the hexagonal form of $Ca(OH)_2$ accounted for the second decomposition peak at a higher temperature.

2.5.6 *Summary of Theme 3*

Under Theme 3, the effect of the nano-sized $Ca(OH)_2$ on the pozzolanic reaction with metakaolinite will be determined in detail. The use of metakaolinite, one of the most widely used SCMs,

is an important part of the ongoing effort in the construction industry to make a contribution to sustainable development. Metakaolinite reacts with $Ca(OH)_2$ to form cementing compounds. The planetary-mill grinding and the vacuum-calcination methods will be applied in an attempt to synthesize the nano-sized $Ca(OH)_2$. The Hedvall effect will be applied to determine the relative reactivity of those two synthesized $Ca(OH)_2$. Metakaolinite will be hydrated with the nano-sized $Ca(OH)_2$ and to determine the effect of the nano-sized $Ca(OH)_2$, as opposed to the micro-sized $Ca(OH)_2$. Also the thermal decomposition characteristics of the nano-sized $Ca(OH)_2$ will be investigated.

CHAPTER 3

EXPERIMENTAL TECHNIQUES

3.1 Introduction

The experimental techniques used in the investigations are an essential part of this thesis. These experimental techniques were frequently used in each of the three themes of the thesis. They are commonly known techniques in the field of science and engineering, especially in materials. Some techniques were used to characterize the materials and to conduct the elemental analysis, while others were used to investigate the mechanical properties of the materials. In this chapter, each experimental technique will be described with its general description and experimental description. In the general description, a brief background theory and capability of the technique will be illustrated. The main purpose of this section is to provide a general idea of the techniques and instruments themselves especially for the ones which are not often used in the field of civil engineering. Further information on the background theory can be found in a reference indicated in each section. In the experimental description, the actual experimental setup and procedure used in the thesis will be illustrated including the apparatus and analytical software. The experimental setup and procedure remain the same throughout the thesis, unless otherwise stated. The experiments unique to each theme of the thesis, such as the Sucrose method, planetary-mill grinding method, vacuum calcination method and the application of the Hedvall effect will be described in the corresponding chapters in detail. The materials and specimen preparation will also be described in the corresponding chapter for each theme.

3.2 Conduction Calorimetry

3.2.1 General Description of Conduction Calorimetry

Conduction calorimetry is one of the most common techniques to investigate the hydration reaction of cementitious materials. It measures the amount of heat released from hydration of cementitious materials as a function of time. A number of factors including the chemical composition and physical properties of materials have a significant impact on heat development associated with the hydration. Conduction calorimetry provides valuable information on the mechanism of hydration, effects of additives and reactivity of materials. One unit of the calorimeter generally consists of two cells; a sample cell which holds a specimen to be tested and a reference cell which is left empty, as shown in Fig. 3.1. Heat produced by any chemical reaction or physical event in the sample cell is detected by a heat flow sensor imbedded underneath the cell as a voltage signal proportional to the heat flow. The unit consisting of both sample and reference cells allows the recorded heat flow from the sample cell to be compared directly to that from the reference cell. Instead of measuring heat flow directly from the sample cell, it improves the stability of the results and reduces the noise within the system, by determining the difference between sample and reference cells.

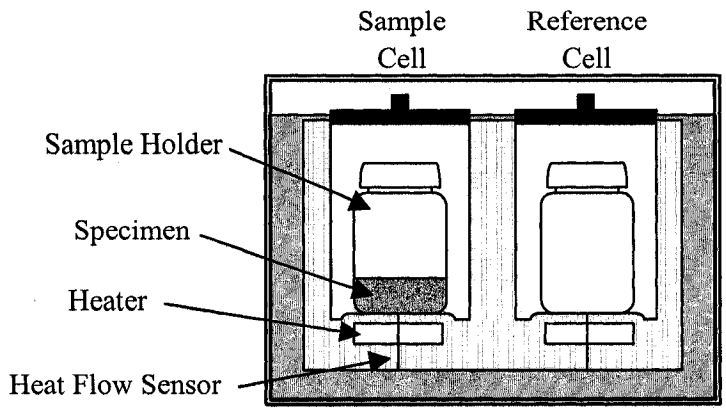

Fig. 3.1 A schematic of a calorimetry unit consisting of sample and reference cells

A typical conduction calorimetry result for the hydration of OPC is illustrated in Fig. 3.2. The rate of heat development is plotted on the y-axis against time on the x-axis. A dormant period starts within a couple of hours after the very early contact of cement particles with water. Then the acceleration of hydration initiates, mainly the hydration of C_3S. Following this peak, the rate

of hydration slows down over a long period. A detailed explanation of the calorimetry curve associated with cement hydration would be beyond the scope of this thesis and will not be discussed here. Generally, a measurement of heat flow is taken up to 3 to 7 days where the heat flow signal becomes too small to distinguish from its background. One common challenge with conduction calorimetry is to capture the heat flow from very early hydration, typically, 0 ~ 5 minutes. For some research, the capture of very early hydration is critical, however, the difficulty exists due to the nature of experimental procedure. The specimen in a sample holder needs to be mixed with water and the holder has to be capped and inserted into an instrument. These processes may take approximately 5 minutes. There exists a special sample holder that can be inserted into the instrument first, then the material is mixed with water, so that the calorimeter can capture the heat flow from very nearly 0 minutes. Further information on conductive calorimetry can be found in Ramachandran et al. (2003).

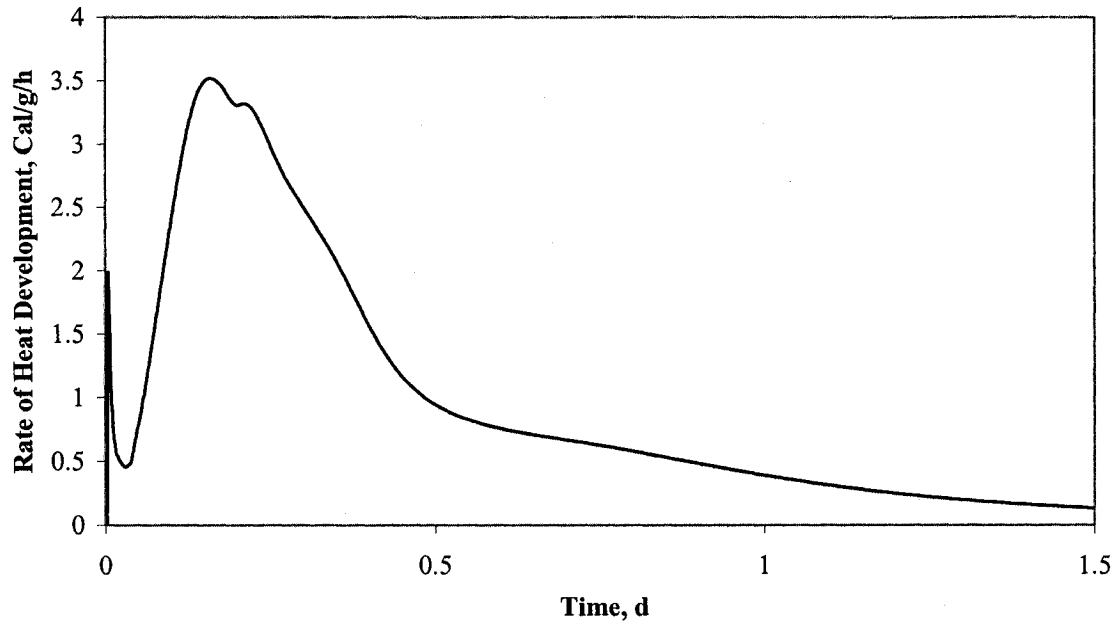

Fig. 3.2 A typical conduction calorimetry result for OPC with w/c 0.50

3.2.2 Experimental Description of Conduction Calorimetry

The conduction calorimetry was performed using the Thermometric TAM Air Isothermal Calorimeter, 3114/3236, shown in Fig. 3.3 (a). The instrument is connected to a data logging computer where a calorimetric result can be monitored simultaneously. The instrument is capable of testing 8 different specimens at the same time, therefore there are 16 cells (8 sample and 8 reference

cells) in total. A calibration was performed four times a year in addition to any change in the experimental setup, such as sample size and performance temperature of the instrument. The calibration was conducted by determining the calibration constant for each individual unit with a known amount of heat flow applied to the system. The instrument has been calibrated for specimens of 10 g. The instrument was set at 24°C as the performance temperature and located in a laboratory which was also set at 24°C. A sample holder is shown in Fig. 3.3 (b) with a specimen inside. A container of deaerated mixing water was kept in the laboratory, so that the temperature of the mixing water would be the same as the performance temperature of the instrument. The mixing water was poured into the sample holder by a micropipette for a desired amount immediately after the measurement of the heat flow was initiated on the data logger. This is to set the beginning of the mixing as 0 minutes. As soon as the mixing water was poured in, the mixing was conducted by a small spatula, then the sample holder with the mixed paste was capped and inserted to the instrument. These processes usually take about 5 minutes and are the reason for unavailability of calorimetry results for the first 5 minutes as described in the previous section. The measurement of heat flow was taken every 2 seconds and usually continued for 3 to 7 days. The resulting data can be converted to any type of graphing software, such as Excel.

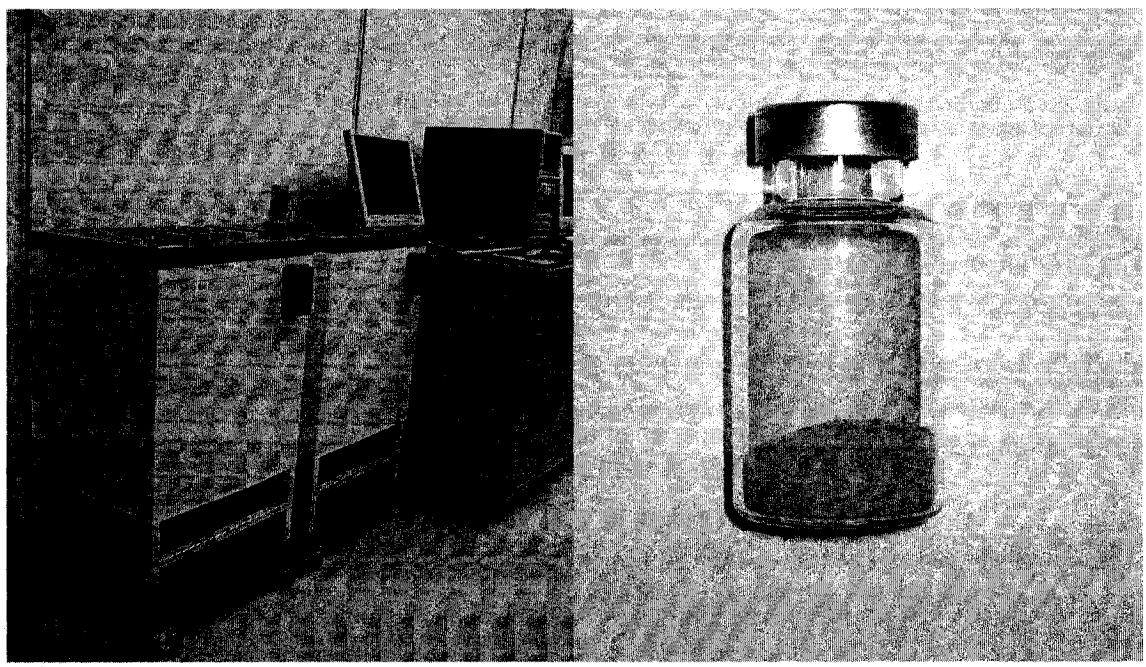

(a) (b)

Fig. 3.3 (a) The Thermometric TAM Air Isothermal Calorimeter, 3114/3236 and (b) A sample holder

3.3 Thermogravimetric Analysis and Differential Scanning Calorimetry

3.3.1 General Description of Thermogravimetric Analysis

Thermogravimetric Analysis (TGA) is an often used technique in the thermal analysis field. The technique involves monitoring the change in mass of a material as a function of temperature and time. TGA provides critical information required for the determination of properties of hydrated cement, such as degree of hydration, water content of specimen and degree of carbonation. TGA generally consists of a sensitive microbalance and a high temperature furnace as shown in Fig. 3.4. A specimen is in an aluminum cup which is loaded onto a balance beam. The beam is installed to the sensitive microbalance where the data acquisition system monitors the change in mass of the specimen. A thermocouple is imbedded in the balance beam. The aluminum cup with the specimen is inside a furnace tube which is installed in the high temperature furnace. A cooling apparatus is embedded around the tube, so that the specimen can be subjected to desired heating rates. A gas flow inlet is attached to the furnace tube so that the test can be conducted under desired gases, which are usually air or nitrogen. The other end of the furnace tube is connected to an exhaust vent for decomposed substances from the specimen to be ventilated during the test. The TGA is typically capable of heating the specimen up to 1500°C.

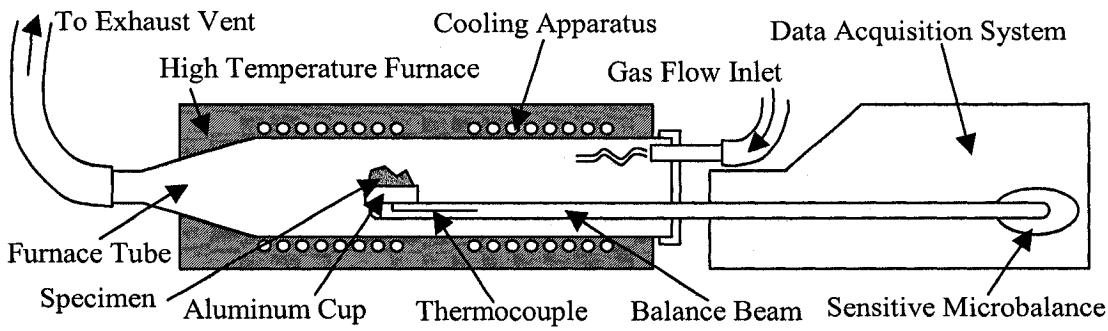

Fig. 3.4 A schematic of a TGA

A typical TGA result and its derivative curve for anhydrous OPC ignited up to 1050°C are illustrated in Fig. 3.5. A weight loss at around 90°C ~ 140°C is a decomposition of gypsum. A large drop in weight at around 575°C ~ 725°C is a decomposition of $CaCO_3$ indicating that the cement

had been carbonated remarkably during storage. A small weight loss at around 400°C is a decomposition of $Ca(OH)_2$ also indicating that the cement had been exposed to the moisture in the air during storage. The usefulness of TGA was greatly increased by introducing the derivative curve of weight change. Dehydration and decomposition of materials can be illustrated as a peak on the derivative curve and the area under the peak represents the amount of weight loss within a particular event. Further information on TGA can be found in Ramachandran et al. (2003).

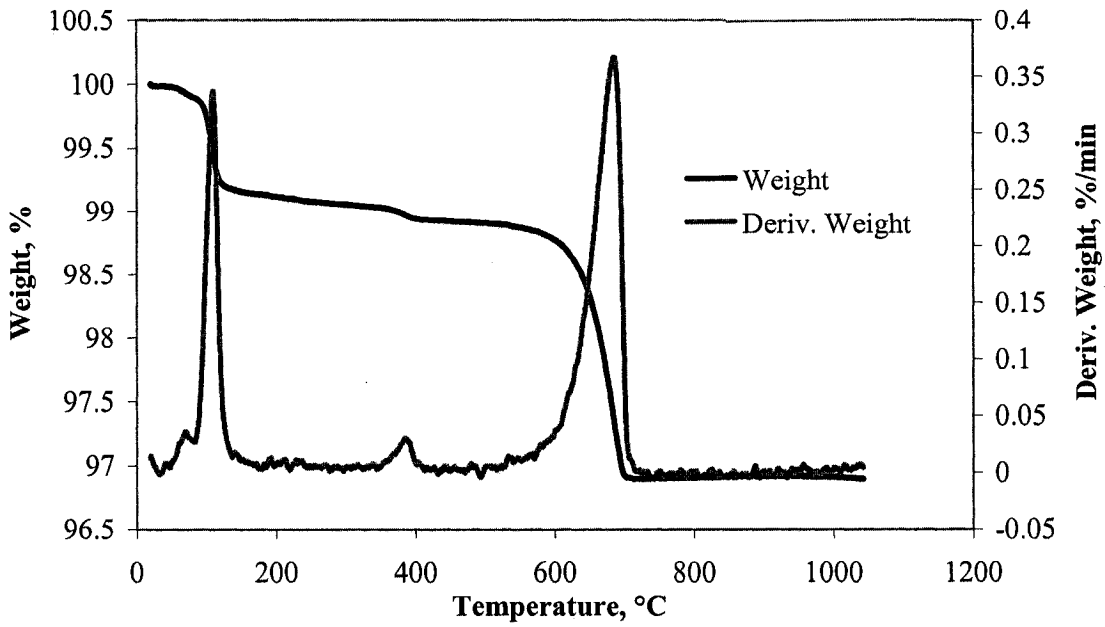

Fig. 3.5 A typical TGA result and its derivative curve for anhydrous OPC

3.3.2 General Description of Differential Scanning Calorimetry

Differential Scanning Calorimetry (DSC) is also one of the most powerful techniques in the thermal analysis field. The theory of DSC is very similar to that of conduction calorimetry. The main difference is that the DSC measures the heat flow from a material subjected to temperature changes whereas the conduction calorimetry measures the heat flow at the constant temperature (conduction calorimetry is often referred to as isothermal conduction calorimetry for this reason). The heat flow which can be measured by the DSC is the heat flow generated by the decomposition and/or phase transition of the material as a function of temperature. As mentioned above, the setup of the DSC is very similar to that of conduction calorimetry as shown in Fig. 3.1 which consists of a sample cell and reference cell. Instead of keeping the cells at the constant tempera-

ture, the DSC is typically capable of changing the temperature anywhere from –200°C to 1500°C. Further information on DSC can be found in Ramachandran et al. (2003).

3.3.3 *Experimental Description of Thermogravimetric Analysis and Differential Scanning Calorimetry*

The TGA and DSC experiments were conducted using TA Instruments, Q600, shown in Fig. 3.6 (a), which performs the TGA and DSC simultaneously. There are both sample and reference cells for the DSC component and the sample cell is attached to the balance beam for the TGA component as shown in Fig. 3.6 (b). The Ultra High Purity (UHP) Grade 5.0 nitrogen gas cylinder was provided by the BOC. A calibration was performed approximately once in every two months. The calibrations for the TGA and DSC components were conducted using the aluminum and indium calibration specimens, respectively. Prior to the testing, a specimen was immersed in isopropyl alcohol for 1 day to stop hydration at a desired hydration period and it was then dried under vacuum for 1 day to remove the isopropyl alcohol from the system. The specimen was broken down to small pieces. An aluminum sample cup was once tared on the balance beam of the instrument and taken to a desktop balance to weigh about 20 mg of the specimen. Then it was placed back onto the balance beam. The temperature was ramped from room temperature to 1050°C at 10°C/min with a 100 ml/min nitrogen gas flow. The analysis was conducted by the software, the TA Instruments, Universal Analysis 2000.

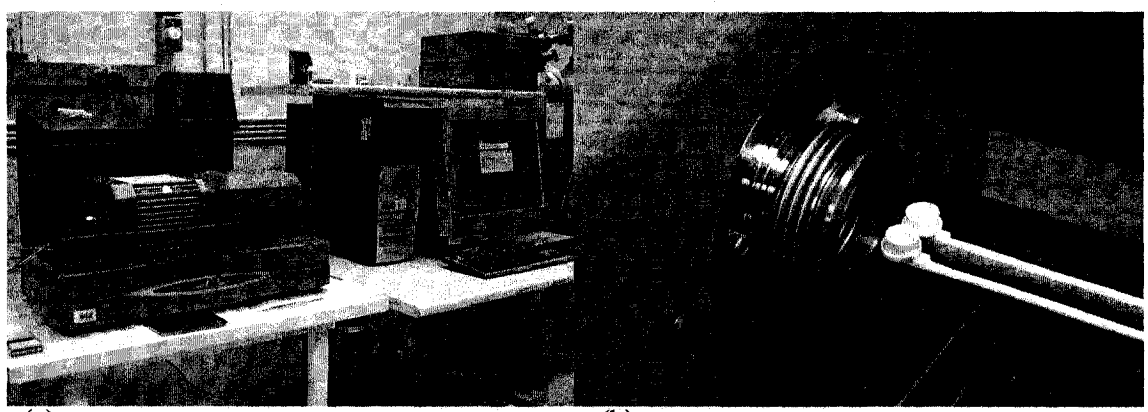

(a) (b)

Fig. 3.6 (a) The TA Instruments, Q600 and (b) Sample cell and reference cell

3.4 X-ray Diffractometry

3.4.1 General Description of X-ray Diffractometry

One of the most important techniques to characterize cementitious materials is X-ray diffractometry (XRD). XRD can be used to identify and characterize the crystalline component of a material. It provides valuable information on phases, preferred crystal orientations and other structural parameters such as a grain size, crystallinity, strain and crystal defects. A quantitative analysis can also be conducted if a proper experimental procedure is taken. The theory of XRD is based on the diffraction of x-rays on various structures of atoms in a crystal at certain angles of incidence as shown in Fig. 3.7 and can be expressed by the Bragg's law as follows:

$$m\lambda = 2d \sin\theta \tag{3.1}$$

where m = an integer

λ = wavelength of x-rays

d = distance between the atomic planes

θ = angle of incidence

A wave reflecting from the second atomic plain has to travel a distance 2d sin θ farther than the wave reflecting from the top plain, which is equal to λ (m = 1). All the wave reflecting from the plains below the top plain are retarded with respect to the wave reflecting from the top plain by m λ (m = 1, 2, 3...). This phenomenon is known as diffraction.

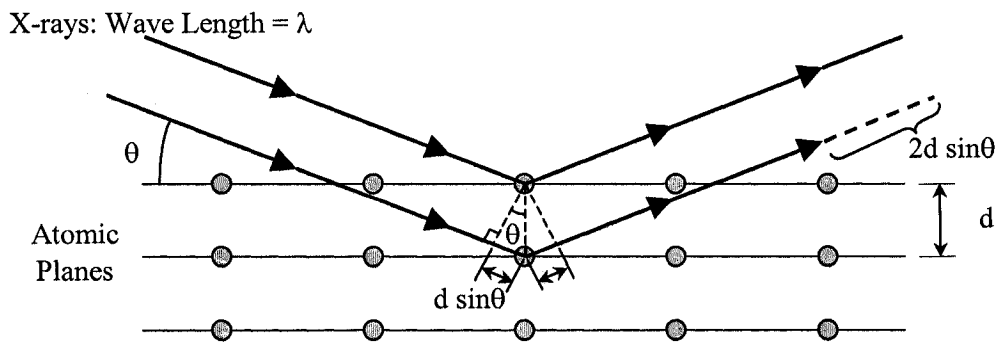

Fig. 3.7 Diffraction of x-rays on the atomic planes in a crystal

A schematic of an XRD is shown in Fig. 3.8. An XRD system can be slightly varied depending on the diffractometer geometry that an instrument is based on. A system shown in Fig. 3.8 is based on the Bragg-Brentano geometry, whereas other geometries such as parallel beam geometry are also available. The x-rays are emitted from an x-ray tube, travel through a divergence slit which collimates the x-rays and impinge on a specimen. The x-rays scatter from the specimen and the diffracted beams travel through a receiving slit to a detector. The unit of both x-ray tube and detector rotate about the specimen, so that the x-rays emit onto the specimen at various angles. The detector measures the x-ray intensity as a function of angle 2θ. Measurement of the x-ray intensity appears as intensity peaks and the intensity peaks for all the common substances are stored in database.

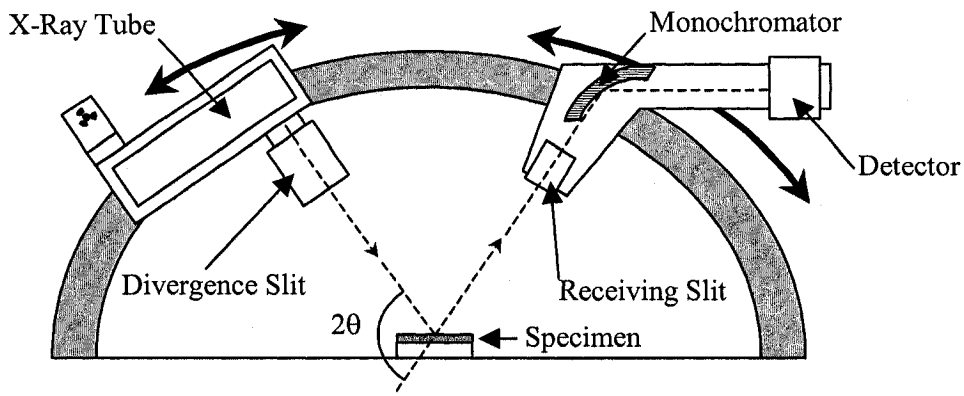

Fig. 3.8 A schematic of an XRD

A typical XRD result on reagent grade $Ca(OH)_2$ and the database intensity peaks for $Ca(OH)_2$ are illustrated in Fig. 3.9. If the tested specimen is an unknown material, the substance can readily be identified by searching the database, especially with the recent development of well-designed software and powerful computers. XRD can also be used, for example, to determine the degree of hydration of cement, by analysing the change in the intensity peaks of $Ca(OH)_2$, which grow as hydration takes place. It is generally possible to detect the presence of an element if there is more than 5% abundance in a specimen. The use of XRD is however limited for amorphous materials, as opposed to crystalline materials, because of the nature of the principle behind this technique. The combination of XRD with other techniques is therefore often necessary to characterize the amorphous materials and amorphous contents in a specimen. Further information on XRD can be found in Jenkins and Snyder (1996).

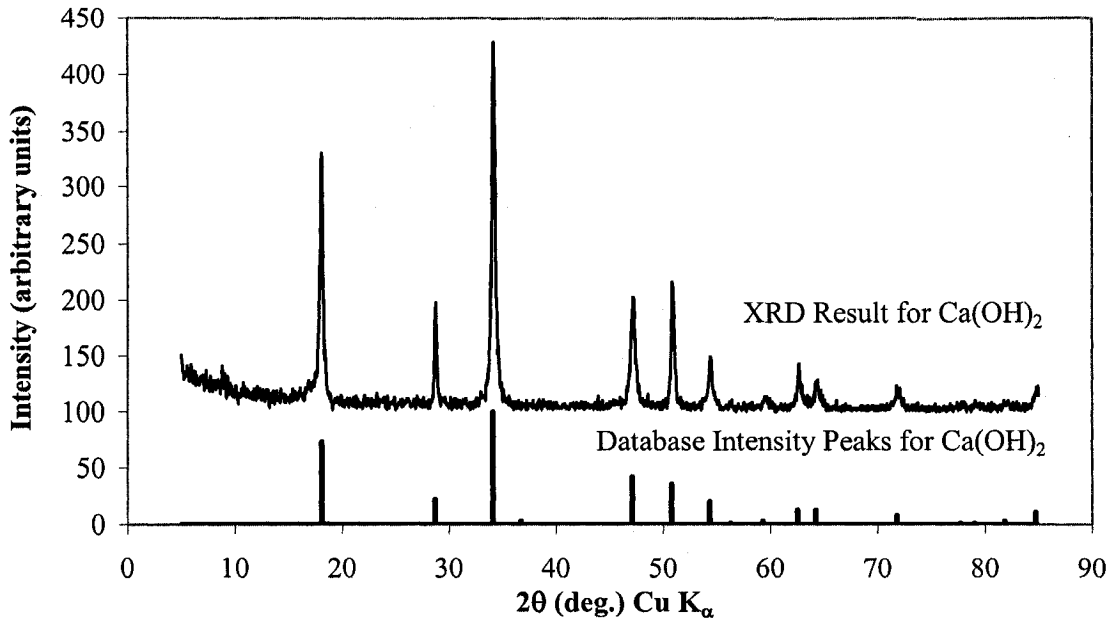

Fig. 3.9 A typical XRD result and the database intensity peaks for $Ca(OH)_2$

3.4.2 *Experimental Description of X-ray Diffractometry*

The Scintag, XDS 2000, shown in Fig. 3.10 (a), was used for the XRD. A cover door with an x-ray shielding window has a safety system where the x-rays would immediately be shut off if the door was accidentally opened during the test. The laboratory is also monitored by a dosimeter provided by Health Canada. The cooling unit is located near the instrument to cool the x-ray tube. The calibration was performed approximately twice a year, using a silicon metal as a standard calibration material. The specimen for the XRD was preconditioned prior to the testing in the same way as the TGA. It was immersed in isopropyl alcohol for 1 day and dried under vacuum for 1 day. The specimen was then ground by a mortar and pestle and sieved using a 275 μm^2 micro-sieve. The ground powder specimen was leveled onto an XRD sample holder as shown in Fig. 3.10 (b). The sample holder was then mounted into the XRD instrument. The XRD measurement was taken at every 0.05° for 2 minutes from 5° to 85° (2θ). The analysis was conducted using a software, JADE, provided by the Materials Data Inc., Livermore, USA.

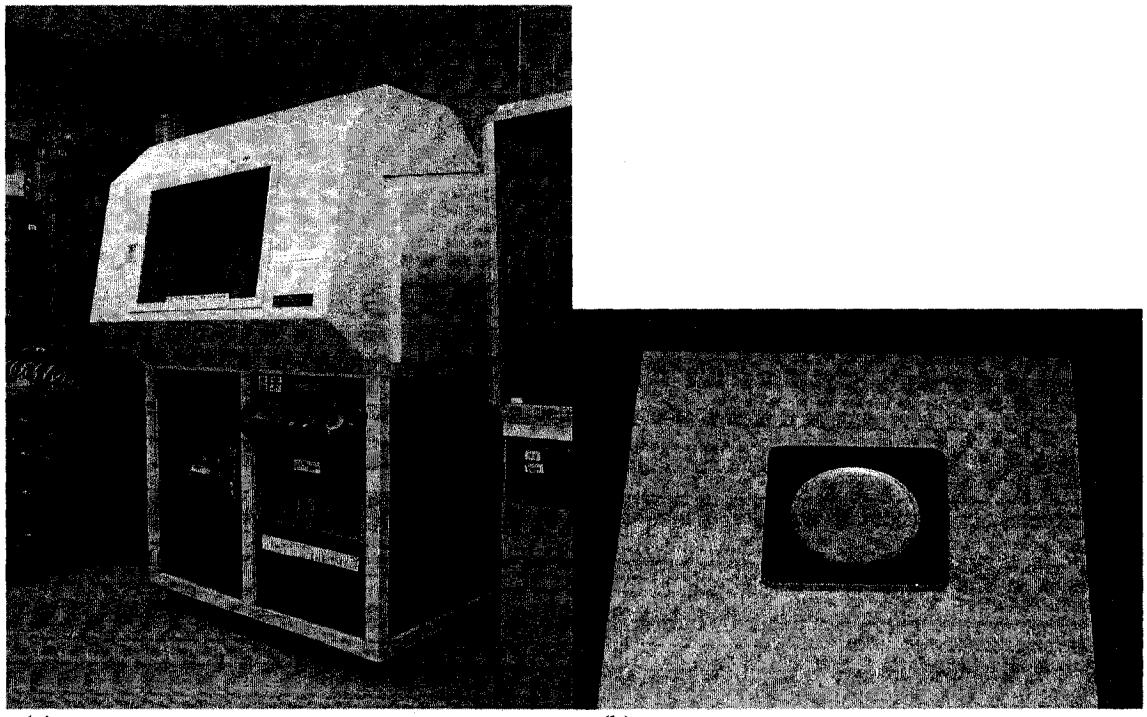

(a) (b)

Fig. 3.10 (a) The Scintag, XDS 2000 and (b) A sample holder

3.5 Nuclear Magnetic Resonance Spectroscopy

3.5.1 General Description of Nuclear Magnetic Resonance Spectroscopy

Nuclear magnetic resonance (NMR) spectroscopy has been one of the most powerful tools to characterize materials in the field of material science ("NMR" often refers to the technique itself using the theory of the nuclear magnetic resonance). A direct application of NMR spectroscopy to the cement and concrete studies has become intensive in the recent years. The NMR spectroscopy observes the behaviour of atomic nucleus through a property called nuclear spin that only certain atoms, such as hydrogen, aluminum and silicon, possess. An atom behaves like a small magnet and aligns itself when an external magnetic field is applied to a system as shown in Fig. 3.11. There are two spin states depending on the external magnetic field strength. It is referred to as low energy state when the alignment is N-S-N-S and high energy state when N-N-S-S. The difference in energy between two spin states depends on the external magnetic field strength and

the difference increases when the magnetic field increases as well. Since this difference at a certain magnetic field strength is unique to the molecule structure of a material, it can be used to identify the materials and to determine the different phases of the materials.

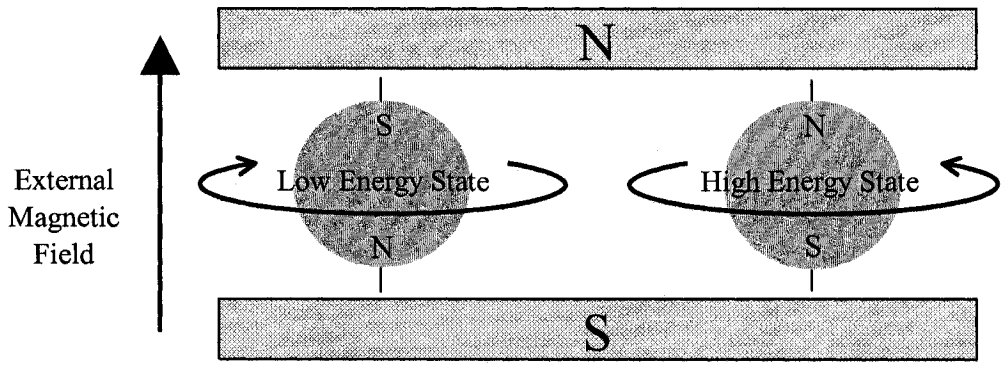

Fig. 3.11 Nuclear spin of atoms subjected to an external magnetic field

The process of NMR spectrum measurement is illustrated in Fig. 3.12. A specimen tube is subjected to the external magnetic field and excited by a radio frequency input. When the radio frequency input becomes exactly the same as the energy difference between two states, the resonance occurs, which is known as a nuclear magnetic resonance. Then the radio frequency output will produce a spectrum where the resonance is indicated by a peak. A typical NMR spectrum for commercially available β-C_2S is shown in Fig. 3.13. One of the major advantages associated with the use of NMR is that this technique is effective for amorphous materials as well as crystalline materials, whereas the XRD can only be used for crystalline materials. Further information on NMR can be found in Bensted and Barnes (2002).

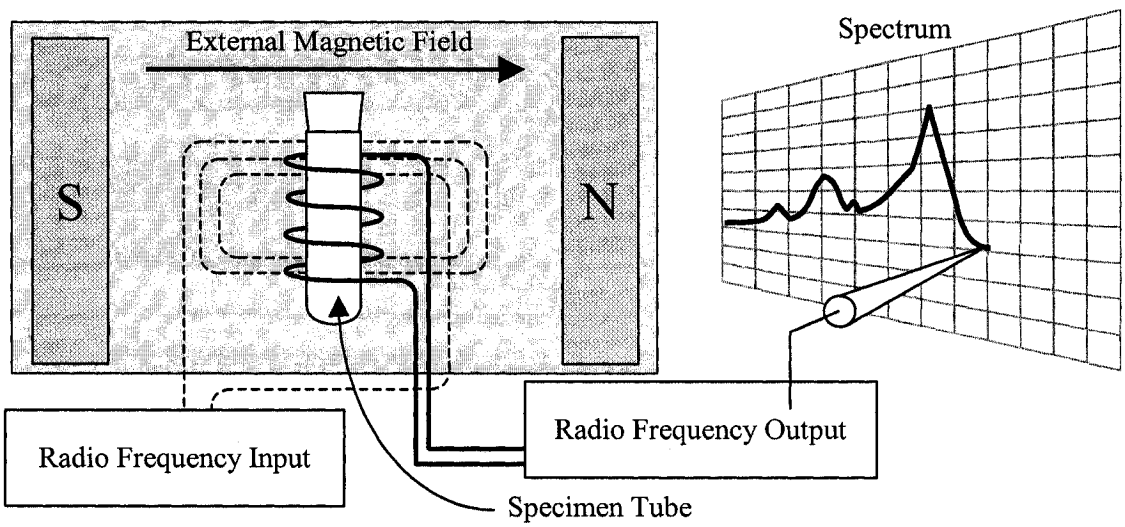

Fig. 3.12 A schematic of an NMR

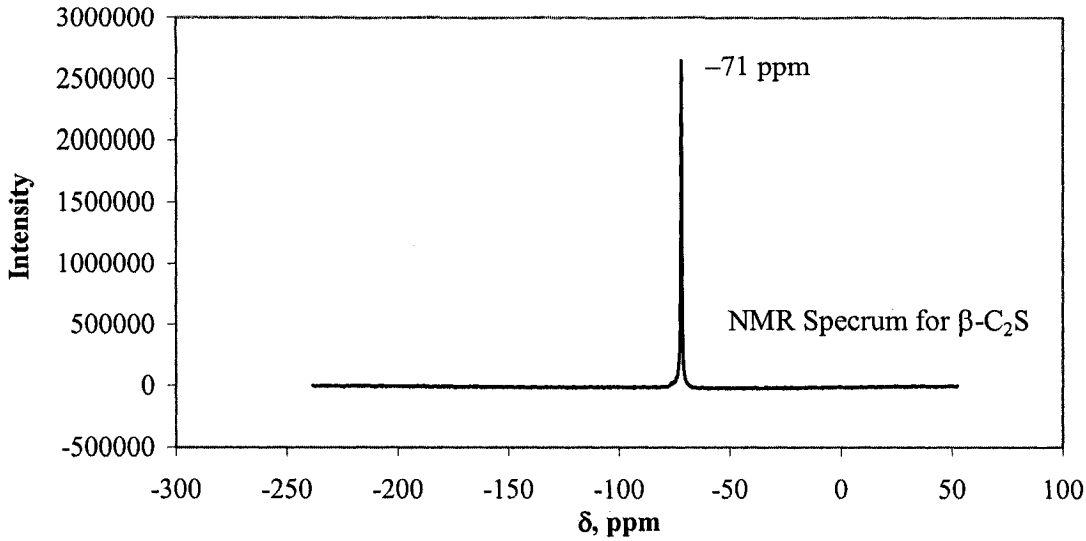

Fig. 3.13 A typical NMR spectrum for β-C_2S

3.5.2 Experimental Description of Nuclear Magnetic Resonance Spectroscopy

The NMR was conducted using the ^{29}Si MAS NMR spectra recorded at 39.7 MHz, on either a TecMag Apollo spectrometer using a 7 mm Doty probe, or a Bruker Avance spectrometer with a 7 mm Chemmagnetics probe. Samples were spun in 7 mm zirconia rotors at 4 kHz and a 7 micro-seconds 90° pulse was used, on both spectrometers. The relaxation delay varied from 30 to 120 seconds, depending on how long it was needed to produce constant relative intensities for each sample. Proton decoupling was not applied.

3.6 Scanning Electron Microscopy

3.6.1 General Description of Scanning Electron Microscopy

High resolution microscopes have been used more frequently as the studies of materials at the smaller scale became more common. Among other high resolution microscopes, a scanning electron microscopy (SEM) has been a leading tool to reveal and analyze the surface characteriza-

tion of materials at the nano-scale. Typically, the resolution of SEM can be as high as 10 to 5 nm depending on several factors such as types and surface conditions of the specimens. A schematic of a SEM is illustrated in Fig. 3.14. A beam of electrons is generated and emitted from a field emission gun located at the top. The beam travels through a series of lenses and apertures to be focused into a very fine focal point on a specimen. When the beam strikes the surface of the specimen, various reactions, commonly known as a surface interaction, occur. Secondary and backscattered electrons are collected by detectors and converted into an image of the surface. X-rays, which are also produced from the surface interaction, can be detected by the SEM equipped with an energy dispersive X-ray spectroscopy. The sample chamber is under vacuum so that the electrons can be emitted and detected without an interference by any gas molecules. Further information on SEM can be found in Goldstein et al. (1992).

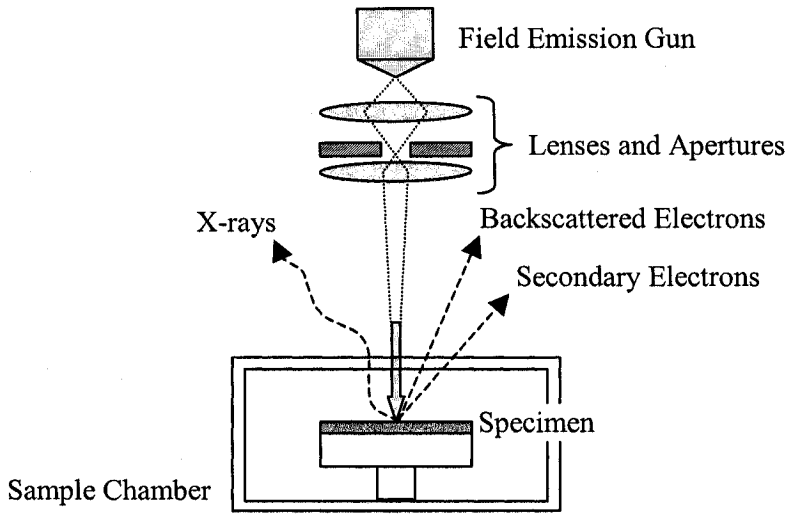

Fig. 3.14 A schematic of an SEM

3.6.2 Experimental Description of Scanning Electron Microscopy

The SEM analysis was conducted using the Hitachi S-4800 Field Emission Scanning Electron Microscope, shown in Fig. 3.15 (a). A liquid nitrogen tank is located on the upper part of the column. The liquid nitrogen is used to cool the x-ray detector. The vacuum pump, located behind the SEM, ensures the high quality vacuum in the sample chamber. A specimen can be either a solid or in powder form. The specimen was mounted on an aluminum stab using a carbon tape as shown in Fig. 3.15 (b). Any powder loosely stuck on the carbon tape was removed by blowing compressed air to avoid contaminating the sample chamber under the vacuum. If the specimen

has little conductivity, the specimen can be sputter coated with a conductive layer of gold to obtain a better SEM image, since the electrons tend to be charged up on a non-conductive material, resulting in a white streaking noise on the image. The operation of the SEM is facilitated by associated software. The accelerating voltage and the emission current, which are the important parameters for the field emission gun, were set at 2.0 kV and 10 μA, respectively. The magnification of the Hitachi S-4800 can be as high as 800,000 times.

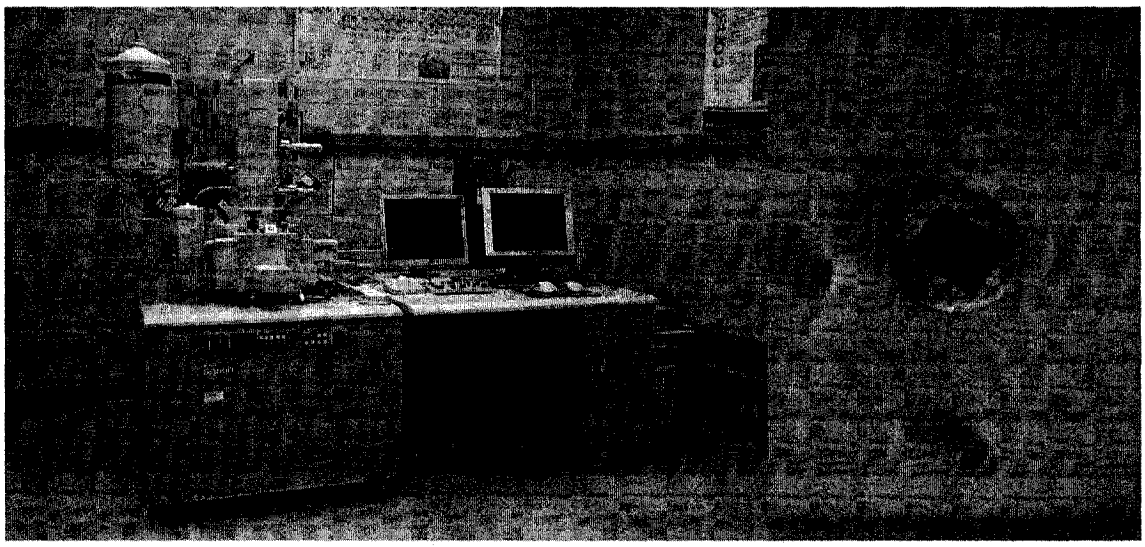

(a) (b)

Fig. 3.15 (a) The Hitachi S-4800 Field Emission Scanning Electron Microscope and (b) An aluminum stab with a carbon tape

3.7 Helium Pycnometry

3.7.1 General Description of Helium Pycnometry

Porosity is one of the most fundamental properties of a material as well as surface area and particle size. A helium pycnometer is an instrument used to determine the solid density of a material, as opposed to a bulk density. It uses helium gas to determine the solid volume of the sample. The helium gas is used since its small atomic dimension is suitable for penetrating into micro- and nano-sized pores of the material. It is also non-adsorbing. Porosity of the material can then be

calculated from the values of sample solid volume and bulk volume. A schematic of a helium pycnometer is illustrated in Fig. 3.16.

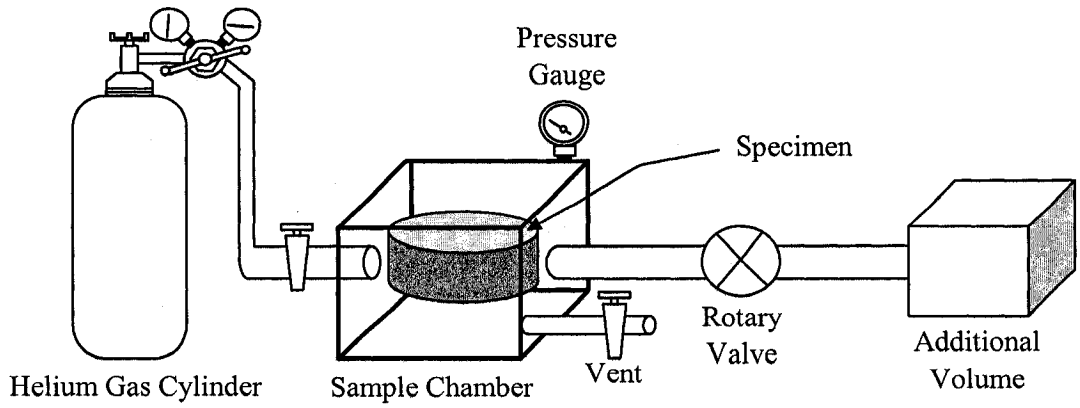

Fig. 3.16 A schematic of a helium pycnometer

When a sample chamber is empty, a rotary valve is closed and a vent is open without a gas inflow, the ideal gas law can be written as following:

$$P_a V_c = n R T_a \tag{3.2}$$

where P_a = atmospheric pressure

V_c = volume of sample chamber

n = moles of gas occupying V_c at P_a

R = universal gas constant

T_a = temperature

When a specimen is placed in the sample chamber:

$$P_a (V_c - V_p) = n_1 R T_a \tag{3.3}$$

where V_p = volume of specimen

n_1 = moles of gas occupying $(V_c - V_p)$ at P_a

By closing the vent and letting the helium gas into the sample chamber, the pressure would increase:

$$P_2 (V_c - V_p) = n_2 R T_a \tag{3.4}$$

where P_2 = pressure above atmosphere

n_2 = moles of gas occupying $(V_c - V_p)$ at P_2

Then a rotary valve is opened and the additional volume V_A comes into the system:

$$P_3 (V_c - V_p + V_A) = n_2 R T_a + n_a R T_a \quad (3.5)$$

where V_A = additional volume

n_a = moles of gas occupying V_A at P_a

Since $n_a R T_a = P_a V_a$, Eq. (2.5) becomes:

$$P_3 (V_c - V_p + V_A) = n_2 R T_a + P_a V_a \quad (3.6)$$

Substituting $n_2 R T_a = P_2 (V_c - V_p)$ from Eq. (2.4), Eq. (2.6) changes to:

$$P_3 (V_c - V_p + V_A) = P_2 (V_c - V_p) + P_a V_a \quad (3.7)$$

Then, Eq. (2.7) can be written as:

$$V_p = V_c + \frac{V_A}{1 - \left(\frac{P_2 - P_a}{P_3 - P_a}\right)} \quad (3.8)$$

Since all the pressure measurements are relative to P_a which was zeroed prior to helium gas inflow, $P_a = 0$. Eq. (2.8) becomes:

$$V_p = V_c + \frac{V_A}{1 - \left(\frac{P_2}{P_3}\right)} \quad (3.9)$$

Now the porosity of the specimen can be calculated as follows:

$$P_r = \frac{V_{Bulk} - V_p}{V_{Bulk}} \times 100 \quad (3.10)$$

where P_r = porosity

V_{Bulk} = bulk volume of the specimen

Further information on helium pycnometry can be found in Ramachandran et al. (1981).

3.7.2 Experimental Description of Helium Pycnometry

The helium pycnometry was conducted by the Quantachrome Corporation, Stereopycnometer, shown in Fig. 3.17. The UHP Grade 5.0 helium gas cylinder was provided by the BOC. A calibration was performed approximately once a year. A chrome calibration cylinder was provided by the Quantachrome Corporation for the calibration. A specimen was sliced into a circular plate, approximately 31.5 mm in diameter and 1.0 mm in thickness. It was then preconditioned prior to the testing in the same way as the TGA and XRD. The specimen was immersed in isopropyl alcohol for 1 day and dried under vacuum for 1 day. The specimen was weighed and its dimensions were determined before the testing in order to calculate the bulk volume of the specimen. The pressure of the helium gas was kept approximately 18 mmHg through the testing. The data acquisition was a manual process and the data were used for the porosity calculation and summarized on a spread sheet.

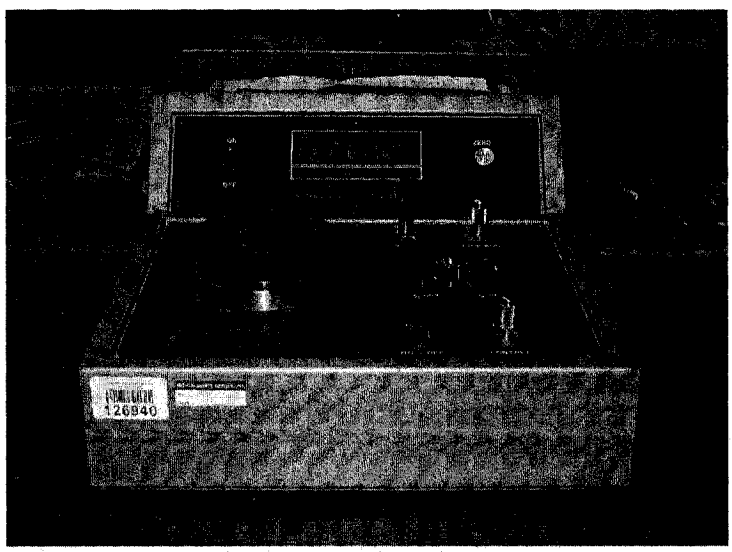

Fig. 3.17 The Quantachrome Corporation, Stereopycnometer

3.8 BET Surface Area Determination

3.8.1 General Description of BET Surface Area Determination

Surface area is one of the most fundamental properties of a material. Determination of surface area is essential especially when the hydration and properties of hardened concrete are often attributed to the surface reaction of cement with water. Among the several methods to determine the surface area of the material, the BET surface area determination, based on the BET theory, is the most widely known and often used as a standard value (BET stands for Brunauer, Emmett and Teller who suggested the BET theory). The BET theory is an extension of the Langmuir theory which is a theory of physical adsorption of adsorbate gas molecules (generally nitrogen) on a solid surface. It is based on the following equation often referred to as the BET equation (Brunauer, Emmett and Teller, 1938):

$$\frac{1}{W\left(\frac{P}{P_o}-1\right)} = \frac{1}{W_m C} + \frac{(C-1)}{W_m C}\frac{P}{P_o} \tag{3.11}$$

where W = mass of nitrogen gas molecules adsorbed on the surface at a given relative pressure, P/P_o

P = partial pressure of nitrogen gas

P_o = saturated vapour pressure of nitrogen gas

W_m = mass of nitrogen gas molecules for a coverage of one monolayer

C = a constant related to heat of adsorption

For a single-point method, Eq. (2.11) can be simplified as:

$$\frac{1}{W\left(\frac{P}{P_o}-1\right)} = \frac{1}{W_m}\frac{P}{P_o} \tag{3.12}$$

or

$$W_m = W\left(1-\frac{P}{P_o}\right) \tag{3.13}$$

A schematic of a BET surface area determination is illustrated in Fig. 3.18. A specimen is first conditioned in a U-shape glassware with nitrogen gas flow. Generally this gas flow is a mixture of 30% nitrogen and 70% helium to achieve a monolayer of nitrogen gas adsorption on the surface of the specimen instead of a multilayer of gas adsorption. Then the glassware is immersed in a coolant (generally liquid nitrogen when a mixture of nitrogen and helium is used) where the nitrogen gas molecules begin adsorbing on the surface of the specimen, which is referred to as a physisorption (physical adsorption). The glassware is then removed from the coolant and the desorption of gas molecules begins.

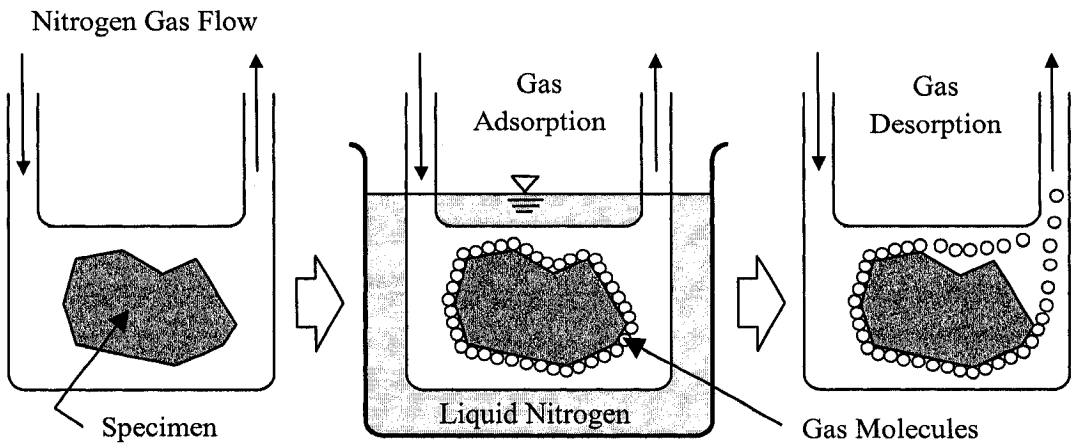

Fig. 3.18 A schematic of a BET surface area determination

An instrument is capable of measuring the difference in the concentration of an outflow gas and to calculate the volume of nitrogen gas adsorbed on the surface of the material, V_{ads}. A mass of nitrogen gas molecules adsorbed on the surface can be calculated as follows:

$$W = M\, n_o \tag{3.14}$$

where M = molecular weight of nitrogen gas

n_o = the number of moles of gas in a system

Since $n_o = \frac{PV}{RT}$ from the ideal gas law, Eq. (2.14) becomes:

$$W = M \frac{P_a V_{ads}}{RT} \tag{3.15}$$

where V_{ads} = measured volume of nitrogen gas molecules adsorbed on the surface

Substituting Eq. (2.15) into Eq. (2.13), it gives:

$$W_m = M\frac{P_a V_{ads}}{RT}\left(1-\frac{P}{P_o}\right) \tag{3.16}$$

The total surface area can be calculated as follows:

$$S_t = \frac{W_m N A_{CS}}{M} \tag{3.17}$$

where S_t = total surface area of the specimen

N = Avogadro's number

A_{CS} = cross sectional area of nitrogen gas molecule

Now, the specific surface area can be determined as follows:

$$S = \frac{S_t}{W_S} \tag{3.18}$$

where S = specific surface area of the specimen

W_S = mass of the specimen

The typical values of BET surface area using a nitrogen gas for the selected materials are provided in Table 3.1. Further information on BET surface area determination can be found in Brunauer et al. (1938).

Table. 3.1 Typical values of BET surface area for selected materials

Materials	BET Surface Area*
Anhydrous OPC	2.24 m^2/g
Anhydrous C_3S	2.76 m^2/g
Anhydrous C_2S	2.35 m^2/g
$Ca(OH)_2$	16.6 m^2/g
$CaCO_3$	0.35 m^2/g

Note: Nitrogen Gas, Single Point, 10 minutes Pre-drying

3.8.2 Experimental Description of BET Surface Area Determination

The BET surface area determination was performed using the Quantachrome Corporation, Quantasorb Sorption System shown in Fig. 3.19 (a). All the necessary gas cylinders were provided by the BOC. The calibration of the instrument was performed approximately once a year, using a powder of zinc oxide which was provided by the Quantachrome Corporation. A powder specimen was inserted in a U-shape glassware shown in Fig. 3.19 (b), then dried in a heating mantle at 140°C for 10 minutes prior to the testing. The data acquisition was a manual process and the data were used for the surface area calculation and summarized on a spread sheet.

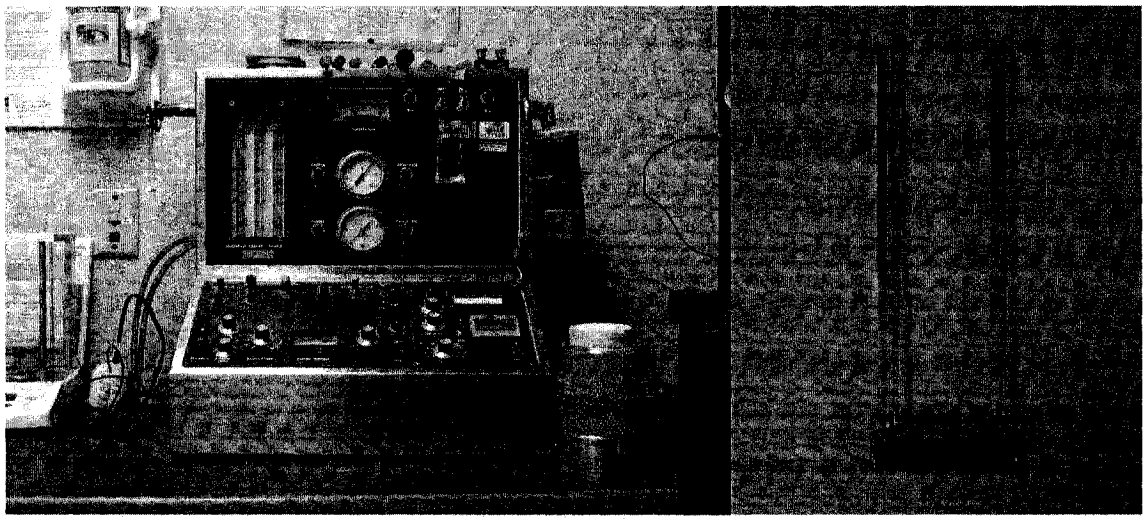

(a) (b)

Fig. 3.19 (a) The Quantachrome Corporation, Quantasorb Sorption System and (b) A sample holder

3.9 Microhardness Determination

3.9.1 General Description of Microhardness Determination

Hardness determination is widely used as a means of comparing the mechanical behaviour of a material. It is determined by the indentation on the surface of the material under a static loading.

Hardness determination can be classified into macro- and micro-hardness tests according to the applied force and size of indentation. Microhardness is determined by measuring the size of the indentation of either the Vickers diamond pyramid or the Knoop elongated diamond pyramid with loadings generally from 15 to 1000 gf. A detailed standard method for microhardness determination is described in ASTM E 384 – 89. A description of the Vickers diamond for microhardness is illustrated in Fig. 3.20 (Boyer and Gall, 1985). The indenter, made of diamond, has a square-based pyramid shape having an angle of 136° between faces. The Vickers hardness number (HV) is a ratio of the applied loading to the surface area of the indentation. The HV can be calculated as:

$$HV = 2P_A \sin\left(\frac{\theta_d}{2}\right)\frac{1}{d_i^2} \tag{3.19}$$

where P_A = an applied loading

θ_d = angle between faces of diamond (136°)

d_i = mean diagonal of the indentation

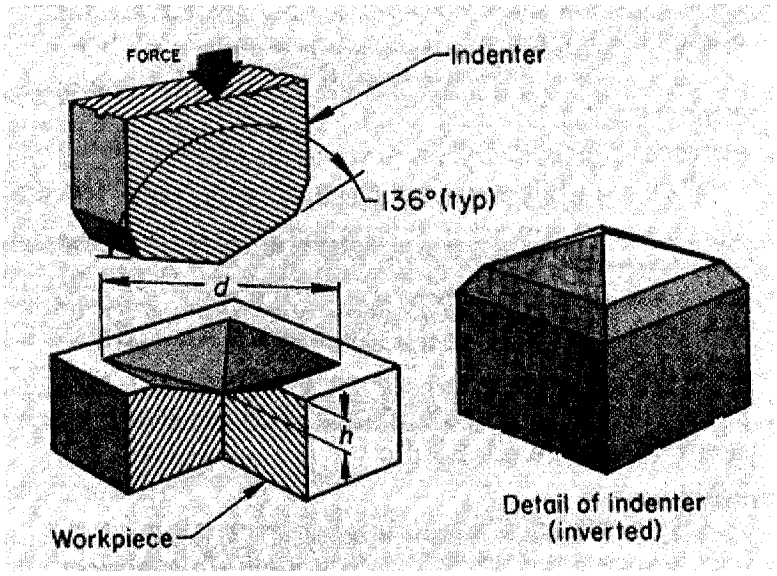

Fig. 3.20 A description of the Vickers diamond for microhardness

The hardness test was originally designed to determine a hardness of the surface of the metal, which is relatively homogeneous. A challenge lies when the hardness test is applied to a non-homogeneous material, such as a cement paste. Even on the surface of a well-mixed cement paste, there is a wide variation with the surface characterization, such as pores and clumps of anhydrous cement particles. The error tends to become large when the hardness test is used for cementitious

materials. Nevertheless the microhardness determination is an essential tool to investigate the surface characteristics of hydrated materials at the micro-scale. A correlation with compressive strength was demonstrated by Beaudoin and Feldman (1975). Further information on microhardness can be found in the same reference.

3.9.2 Experimental Description of Microhardness Determination

The microhardness determination was performed using the DURIMET, Small-hardness Tester shown in Fig. 3.21 (a). The Clemex light microscope, shown in Fig. 3.21 (b), was used to measure the dimension of indentation. A calibration was performed using an Aluminum 6061 T6. A specimen was sliced into a circular plate, about 31.5 mm in diameter and 1.0 mm in thickness. An extra care was taken for slicing the specimen with uniform thickness. The loading weights were 100, 200, 300, 500, 1000 and 2000 g and changed depending on the hardness of the specimen. The diamond was indented onto the surface of the specimen for 13 seconds and in total 49 indentations were made on each of three specimens. Indentations were at least 1275 μm away from each other as specified in the ASTM. The measurements of the indentations were used for the microhardness calculation and summarized on a spread sheet.

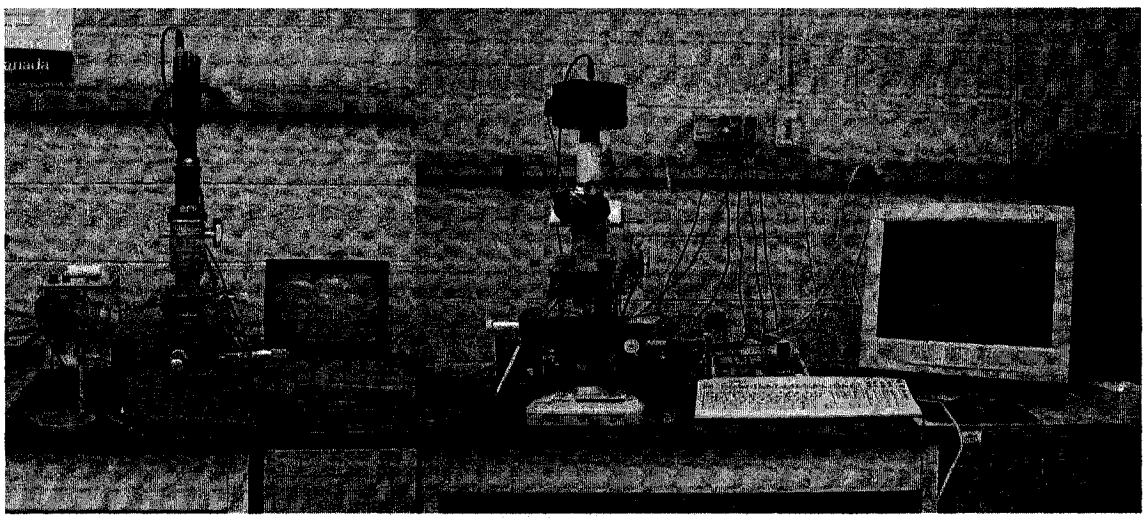

(a) (b)

Fig. 3.21 (a) The DURIMET, Small-hardness Tester and (b) The Clemex light microscope

3.10 Modulus of Elasticity Determination

3.10.1 General Description of Modulus of Elasticity Determination

Modulus of elasticity is one of the most fundamental mechanical properties of a material. An instrument used to determine the modulus of elasticity of a particularly smaller scale specimen was designed and fabricated at the Institute for Research in Construction, National Research Council Canada. A circular plate specimen with approximately 31.5 mm in diameter and 1.0 mm in thickness supported at 3 points was tested with centre point loading. The deflection at the centre point was recorded. A schematic of the testing instrument and the cross sectional view at loading and supporting are illustrated in Figs. 3.22 (a) and (b), respectively.

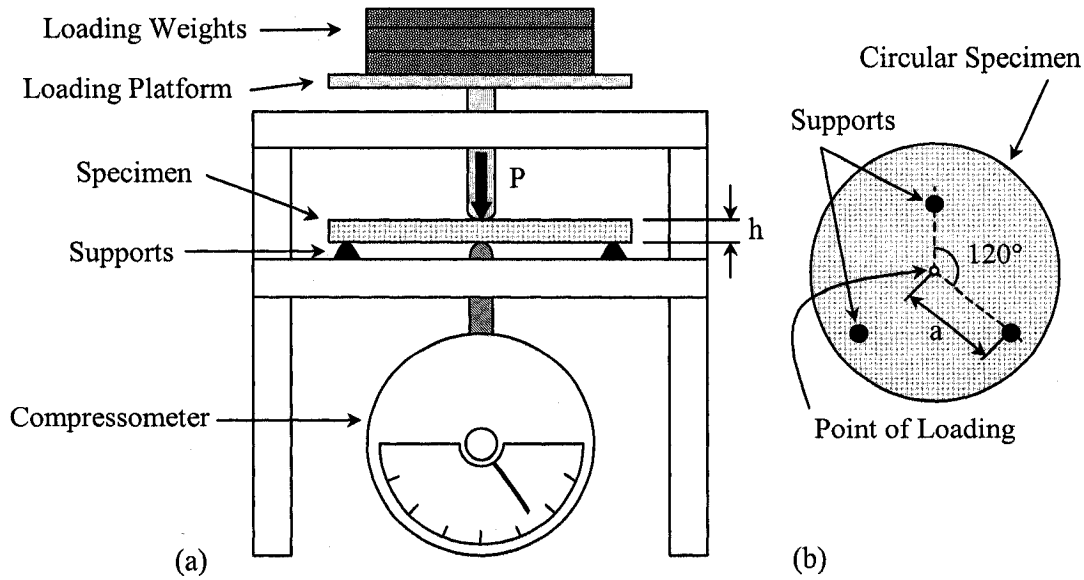

Fig. 3.22 (a) A schematic of the testing instrument for modulus of elasticity determination and (b) Cross sectional view at loading and supporting

Timoshenko and Woinowsky-Krieger (1959) have derived the equation for deflection at the centre of a circular plate when the circular plate is supported at three points 120° apart and is loaded at the centre:

$$w_o = 0.0670 \frac{P_L a^2}{D} \tag{3.20}$$

where w_o = deflection at the centre of the circular plate

P_L = an applied load

a = distance between the support and the point of loading, shown in Fig. 3.22 (b)

$$D = \frac{E h^3}{12(1-\upsilon^2)}$$

where E = modulus of elasticity

h = thickness of the specimen

υ = Poisson's Ratio (0.25 for cement paste taken from Sereda, 1966 and Anson, 1964)

Then, Eq. (2.20) can be rewritten as:

$$E = \frac{0.804(1-\upsilon^2) P_L a^2}{w_o h^3} \tag{3.21}$$

Further information on this particular technique for determining modulus of elasticity can be found in Sereda et al. (1966).

3.10.2 Experimental Description of Modulus of Elasticity Determination

An instrument, designed and fabricated at the Institute for Research in Construction, National Research Council Canada, is shown in Fig. 3.23. A calibration was performed using the Aluminum 6061 T6 circular plates prior to a series of specimens for modulus of elasticity determination. A specimen was prepared in the same way as the microhardness test. It was sliced into a circular plate and an extra care was taken for slicing the specimen with uniform thickness. The specimen was placed on the supports, a height of a compressometer was then adjusted so that it could be tared where a tip of the compressometer contacted the specimen. The loading weights were either a set of 10 of 10 g weights or a set of 10 of 25 g weights, depending on the specimen. A deflection was measured every time each weight was placed on the loading platform shown in Fig. 3.22. When a weight was applied, the instrument was tapped a few times by a small spatula to remove any slack. The measurements of the deflections were used for the modulus of elasticity calculation and summarized on a spread sheet.

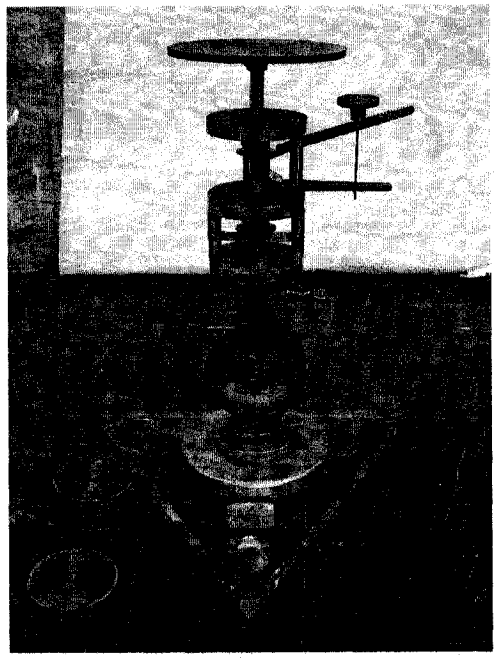

Fig. 3.23 The instrument for modulus of elasticity determination

CHAPTER 4

THEME 1: THE USE OF NANO-SIZED $CaCO_3$ ADDITION TO CEMENT PASTE CONTAINING HIGH VOLUMES OF SUPPLEMENTARY CEMENTING MATERIALS

4.1 Introduction

Theme 1 of this thesis: The Use of Nano-sized $CaCO_3$ Addition to Cement Paste Containing High Volumes of Supplementary Cementing Materials, is described in Chapter 4 including the experimental and analytical approaches, materials, specimen preparation, results and discussion. In the first section, the detailed experimental and analytical approaches are presented as well as the materials and specimen preparation used under Theme 1. In the following section, the results and discussion are presented. All the experimental techniques used to obtain the results are described in Chapter 3, unless otherwise stated.

4.2 Experimental

4.2.1 Experimental and Analytical Approaches

Theme 1, as indicated in Chapter 1, was divided into four stages. Each stage was further subdivided into two stages, early hydration (0 ~ 3 days hydration) and late hydration (3 ~ 28 days

hydration). One of the main objectives under Theme 1 was to investigate the efficacy of the accelerating effect of the nano-sized $CaCO_3$ addition on counteracting the delayed initial setting and rate of early strength development of cement paste containing high volumes of SCMs. This is achieved by examining the early hydration. Another objective was to investigate the effect of the nano-sized $CaCO_3$ addition on the long-term strength development of cement paste containing high volumes of SCMs and to observe the influence of the accelerated early hydration on the late strength development. This needs to be conducted on a well hydrated cement paste, that is, up to 28 days hydration. The detailed experimental and analytical approaches are summarized in Table. 4.1. The results and discussion are presented in the same chronological manner as shown in the table.

In Stage 1 - early hydration, difference in the rates of heat development between OPC paste and those containing high volumes of fly ash was studied by the conduction calorimetry. The hydration of OPC paste is expected to be significantly delayed by the high volumes of fly ash. Then the hydration products at 1 and 3 days hydration were analyzed using XRD to understand the mechanisms of hydration and pozzolanic reaction. The amount of $Ca(OH)_2$ produced by the hydration of OPC was also observed using TGA to examine the effect of the pozzolanic reaction on the amount of $Ca(OH)_2$. Difference in mechanical properties between OPC and that containing high volumes of fly ash was studied by determining microhardness and modulus of elasticity to observe the effect of high volumes of fly ash on the strength development at early hydration. In Stage 1 - late hydration, the hydration products and the amount of $Ca(OH)_2$ at 3, 7, 14 and 28 days hydration were determined by XRD and TGA, respectively for the same purpose as the early hydration analysis. The mechanical properties were also studied to observe the effect of delayed hydration of OPC containing high volumes of fly ash on the strength development up to 28 days.

In Stage 2 - early hydration, conduction calorimetry was applied to observe the accelerating effect of both micro- and nano-sized $CaCO_3$ additions on the control OPC without high volumes of fly ash. The amount of $CaCO_3$ was estimated by TGA to determine whether the added $CaCO_3$ was inert or chemically reacting in the hydration of OPC. The XRD would then be applied to study the reaction mechanism if $CaCO_3$ was found to be chemically reacting with the hydration of OPC. In Stage 2 - late hydration, the amount of $CaCO_3$ was estimated by TGA in the course of hydration up to 28 days to determine whether $CaCO_3$ reacts with the hydration of OPC as hydration takes place for a long-term period. In the case that $CaCO_3$ was reacting with the hydration of OPC, the XRD would then be applied to reveal the hydration products.

Table. 4.1 The experimental and analytical approaches for Theme 1

	Early Hydration (0 ~ 3 days)	Late Hydration (3 ~ 28 days)
Stage 1	Hydration mechanism of cement paste containing high volumes of fly ash	
	▪ Rate of heat development by conduction calorimetry ▪ Hydration products by XRD ▪ Amount of $Ca(OH)_2$ by TGA ▪ Mechanical properties by microhardness and modulus of elasticity	▪ Hydration products by XRD ▪ Amount of $Ca(OH)_2$ by TGA ▪ Mechanical properties by microhardness and modulus of elasticity
Stage 2	Hydration mechanism of cement paste with the additions of micro- and nano-sized $CaCO_3$	
	▪ Rate of heat development by conduction calorimetry ▪ Amounts of $Ca(OH)_2$ and $CaCO_3$ by TGA ▪ Hydration products by XRD	▪ Amounts of $Ca(OH)_2$ and $CaCO_3$ by TGA ▪ Hydration products by XRD
Stage 3	Hydration mechanism of cement paste containing high volumes of fly ash with the additions of micro- and nano-sized $CaCO_3$ hydrated at 23°C and 5°C	
	▪ Rate of heat development by conduction calorimetry ▪ Amounts of $Ca(OH)_2$ and $CaCO_3$ by TGA ▪ Mechanical properties by microhardness and modulus of elasticity	▪ Amounts of $Ca(OH)_2$ and $CaCO_3$ by TGA ▪ Mechanical properties by microhardness, modulus of elasticity and porosity
Stage 4	Repeating experiments with high volumes of ground granulated blast-furnace slag	
	▪ Rate of heat development by conduction calorimetry ▪ Mechanical properties by microhardness and modulus of elasticity	▪ Mechanical properties by microhardness, modulus of elasticity and porosity

In Stage 3, the micro- and nano-sized $CaCO_3$ were added to OPC containing high volumes of fly ash. In Stage 3 - early hydration, the accelerating effect of nano-sized $CaCO_3$ addition on the delayed hydration of OPC paste containing high volumes of fly ash was investigated by conduction calorimetry to see whether the nano-sized $CaCO_3$ addition would compensate for the delayed hydration. The results from TGA would indicate whether the hydration mechanism, when the $CaCO_3$ was added to OPC containing fly ash, would be similar with those observed in Stages 1 and 2. The determinations of microhardness and modulus of elasticity would also indicate whether or not the nano-sized $CaCO_3$ addition could compensate for the delayed hydration in terms of strength development. OPC cement pastes containing high volumes of fly ash with the additions of both micro- and nano-$CaCO_3$ were also hydrated at 5°C, as opposed to 23°C to observe the effect of a low temperature curing condition. In Stage 3 - late hydration, the investigation on the mechanical properties focused on the determinations of microhardness, modulus of elasticity and porosity. Determination of porosity by helium pycnometry provided the opportunity to rationalize the results independent of hydration time. The results from TGA were also analyzed to determine the hydration characteristics up to 28 days when the $CaCO_3$ was added to OPC containing fly ash.

In Stage 4 - early hydration, the rate of heat development was investigated by the conduction calorimetry for OPC containing high volumes of ground granulated blast-furnace slag (GGBFS) instead of fly ash to assess and confirm the similar occurrence of an accelerating effect of the nano-sized $CaCO_3$ addition. In Stage 4 - late hydration, mechanical properties of hydrated OPC containing high volumes of GGBFS were determined for assessment of the long-term strength development.

4.2.2 Materials

Type GU CSA cement (ASTM Type I) was supplied by Lafarge North America, Herndon, Virginia, USA. Its chemical composition is shown in Table 4.2. Class "F" fly ash was supplied by Shaw Resources, Milford, Nova Scotia, Canada. Its chemical composition is shown in Table 4.3. The GGBFS was supplied by the Standard Slag Cement Co., Fruitland, Ontario, Canada. Its chemical composition is shown in Table 4.4. Reagent grade micro-sized $CaCO_3$ was supplied by Anachemia Canada Inc., Montreal, Quebec, Canada. Its purity was higher than 99%. The BET surface area value for the reagent grade $CaCO_3$ was 0.35 m^2/g. A nano-sized $CaCO_3$ was supplied

by READE, Riverside, Rhode Island, USA. Its purity was higher than 98%. The BET surface area value for the nano-sized $CaCO_3$ was 20.50 m^2/g. The SEM images of the reagent grade micro-sized $CaCO_3$ and nano-sized $CaCO_3$ are shown in Figs. 4.1 (a) and (b), with magnifications of ×5,000 and ×50,000, respectively. The average particle size of the micro-sized $CaCO_3$ is approximately 5 to 20 μm, whereas that of nano-sized $CaCO_3$ is about 50 to 120 nm.

Table. 4.2 Chemical composition of OPC (wt, %)

SiO_2	Al_2O_3	Fe_2O_3	CaO	MgO	SO_3
20.80	4.40	2.90	62.3	2.70	3.14

Table. 4.3 Chemical composition of fly ash (wt, %)

SiO_2	Al_2O_3	Fe_2O_3	CaO	MgO	SO_3
38.22	17.29	29.66	7.58	1.22	1.55

Table. 4.4 Chemical composition of GGBFS (wt, %)

SiO_2	Al_2O_3	Fe_2O_3	CaO	MgO	SO_3	Na_2O	K_2O
39.67	6.90	1.48	35.68	12.93	3.23	0.18	0.29

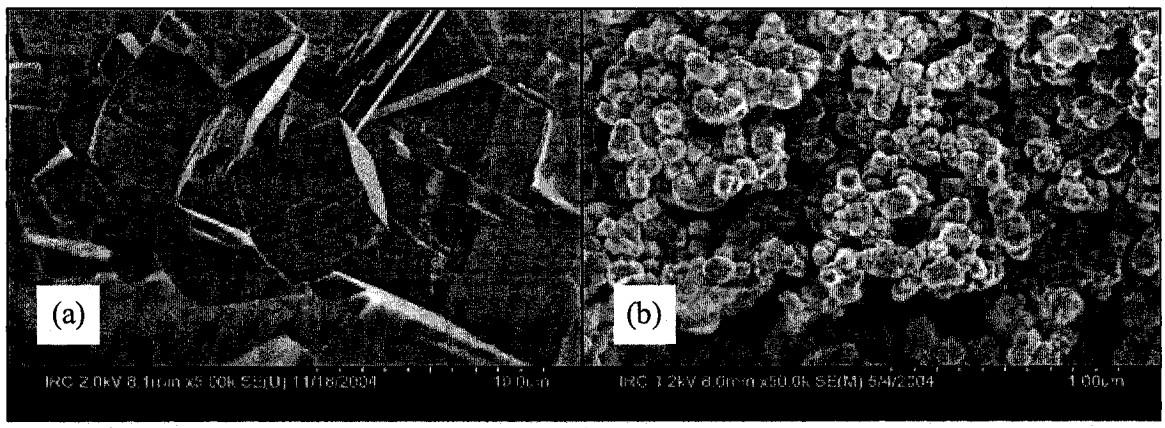

Fig. 4.1 SEM images of (a) reagent grade micro-sized $CaCO_3$ and (b) nano-sized $CaCO_3$

4.2.3 *Specimen Preparation (Mixing of Cement Paste)*

A basic description of the mixing of cement paste is illustrated in this section. A water / cementitious solid (w/c) ratio was designed to be 0.50. In a case of the mixing cement, SCMs and $CaCO_3$, the amount of water was calculated based on the total mass of cement and SCMs excluding that of $CaCO_3$. The mixing water was deaerated prior to the mixing. Mixing was conducted using the Hobart Mixer. The cement powder was first placed into a mixing bowl. The additives, such as SCMs and $CaCO_3$, were added into the mixing bowl as well if required. A small amount of the mixing water was poured in first. The mixing was then conducted for 1 minute to remove lumps in the cement powder. The rest of the mixing water was then poured into the bowl and the mixing was continued for 2 minutes. A schematic of the cylindrical plastic mould used for casting the cement paste is shown with dimensions in Fig. 4.2 (a).

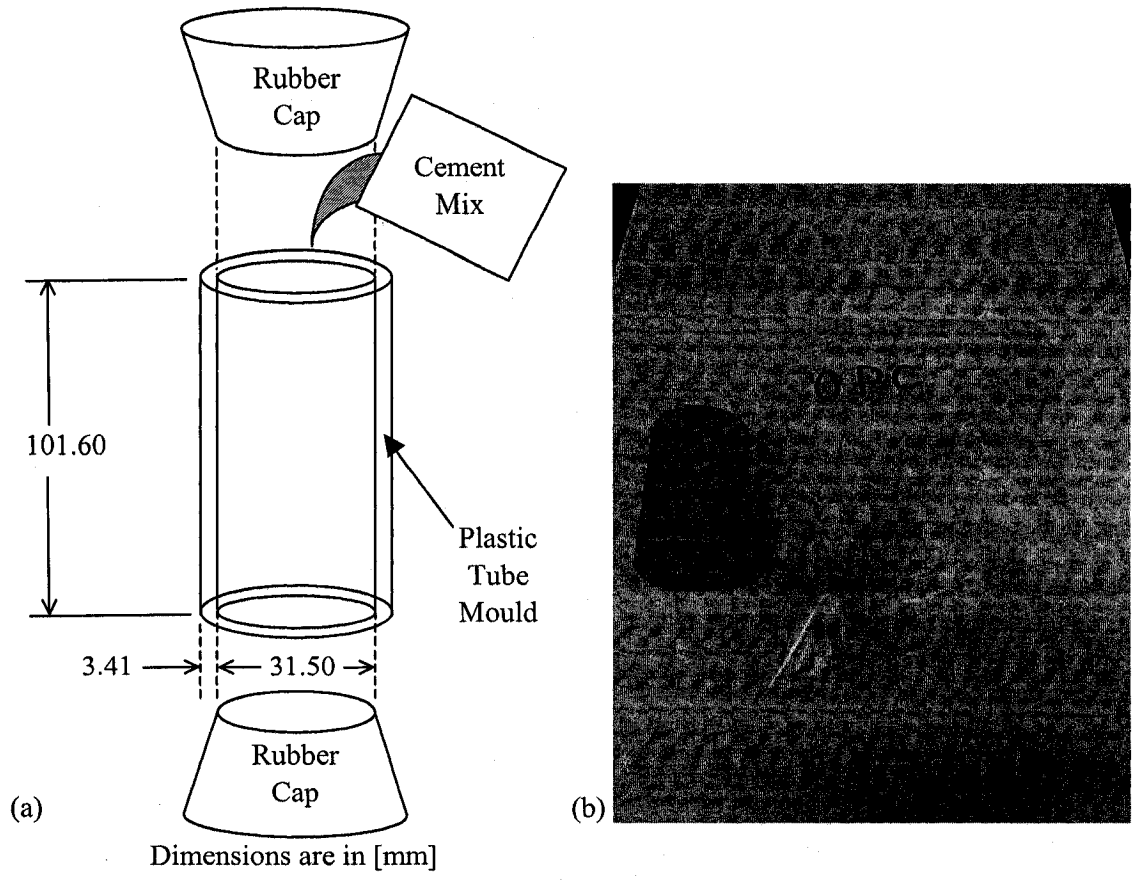

Fig. 4.2 *(a) A schematic of the plastic cylindrical mould used for casting the cement paste and (b) Cement paste specimen and the plastic bag used for curing with lime water*

The cement paste was poured from the bowl into the cylindrical plastic mould, with the bottom cap on, to one third of the height, and then vibration was applied for 30 seconds to remove any air bubbles. Those processes were repeated for three times to fill the mould. The mould was then capped by the rubber cap and placed on a roller to avoid segregation. The specimen was de-moulded the day following the casting and placed in a sealed plastic bag with a small amount of lime water to avoid leaching of $Ca(OH)_2$ from the cement paste system. The specimen in the plastic bag was cured at 23°C for a desired period of hydration as shown in Fig. 4.2 (b). The further specimen preparation for each experimental technique was described in Chapter 3. For example, a specimen for the TGA was immersed in isopropyl alcohol for 1 day and dried under vacuum for 1 day. If the TGA was to be conducted at 28 days hydration, the specimen was cured in a plastic bag with lime water at 23°C, as described above, for 28 days. A small piece of the specimen was then immersed in isopropyl alcohol for 1 day and dried under vacuum for 1 day. If the helium pycnometry was to be conducted at the 28 days hydration, the specimen was cured for 28 days, then sliced into circular plates, approximately 31.5 mm in diameter and 1.0 mm in thickness before immersing in isopropyl alcohol for 1 day and drying under vacuum for 1 day.

4.3 Results and Discussion

4.3.1 Stage 1: Hydration Mechanism of Cement Paste Containing High Volumes of Fly Ash

4.3.1.1 Early Hydration (0 ~ 3 Days)

The hydration of cement paste containing high volumes of fly ash is significantly different from that without fly ash in terms of the hydration rates, processes and products. It is widely known that the rate of hydration of cement paste is significantly delayed especially when the high volumes of SCMs are added. Both the hydration of cement paste and the pozzolanic reaction are relevant. The conduction calorimetry results of OPC and that with 50% fly ash by the total mass of solids for w/c 0.50 are shown in Fig. 4.3. The rate of heat development was calculated in calories per total mass of cementitious materials (OPC and fly ash) per hour. The hydration of OPC paste containing 50% fly ash is much more delayed than OPC itself, owing mainly to the delayed hydration of C_3S in OPC by the addition of fly ash. The delay of the C-S-H formation in

presence of fly ash is a result of the time lag for the production of $Ca(OH)_2$ from the cement-water reaction. The following discussion focuses on the pozzolanic reaction with the C_3S hydration. A possible mechanism of the hydration of C_3S and the pozzolanic reaction is suggested in Fig. 4.4 (the C_3S part was taken from Skalny and Young, 1980). In Stage I, calcium ions, Ca^{2+} and hydroxide ions, OH^- are released when the C_3S grain contacts with water. As a pozzolan grain contacts with water, the alkalis such as Na^+ and K^+ begin to dissolve into the solution. In Stage II, as Ca^{2+} and OH^- preferentially leach into solution, a surface layer reaction product forms a Si rich amorphous layer, that can be considered as an assembly of silicate ions, such as H_3SiO^{4-} and $H_4Si_2O_7^{2-}$. A release of alkalis from the pozzolan grain results in SiO_4^{4-} and AlO_2^- rich amorphous film on its surface. Calcium ions released from the C_3S grain are adsorbed onto the surface of the pozzolan grain. Between Stage II and III, the surface layer of the C_3S grain formed in Stage II continues to develop, and Ca^{2+} and OH^- ions continue to pass through the surface layer to leach into solution. The process is however slow because the ions must pass through the relatively thick surface layer (this is considered to be a dormant period). In Stage III, the ionic concentrations in the solution become large enough for the nuclei to grow. Some $Ca(OH)_2$ crystals begin to form. Calcium ions are, however, still consumed by the pozzolan grain, decelerating the process of nucleation (this might be a reason for the delayed hydration of OPC cement paste containing pozzolanic materials as shown in Fig. 4.3). In Stage IV, the solution becomes supersaturated and the C-S-H starts forming on the surface. Growth of $Ca(OH)_2$ may occur initially at the surface, but some crystals also form in the pores away from the grains. The C-S-H also starts forming on the surface of the pozzolan grain. In addition to the C-S-H, other types of hydrates, such as C_4AH_{13} and C_2ASH_8 may be formed depending on the chemical compositions of the pozzolanic materials. A similar theory was suggested by Takemoto and Uchiyama (1980).

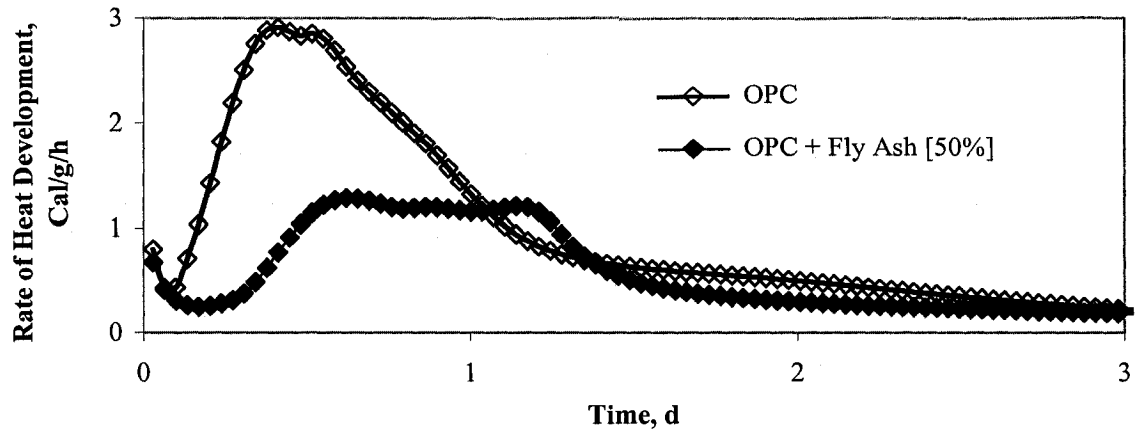

Fig. 4.3 Conduction calorimetry curves for OPC and OPC with 50% fly ash for w/c 0.50

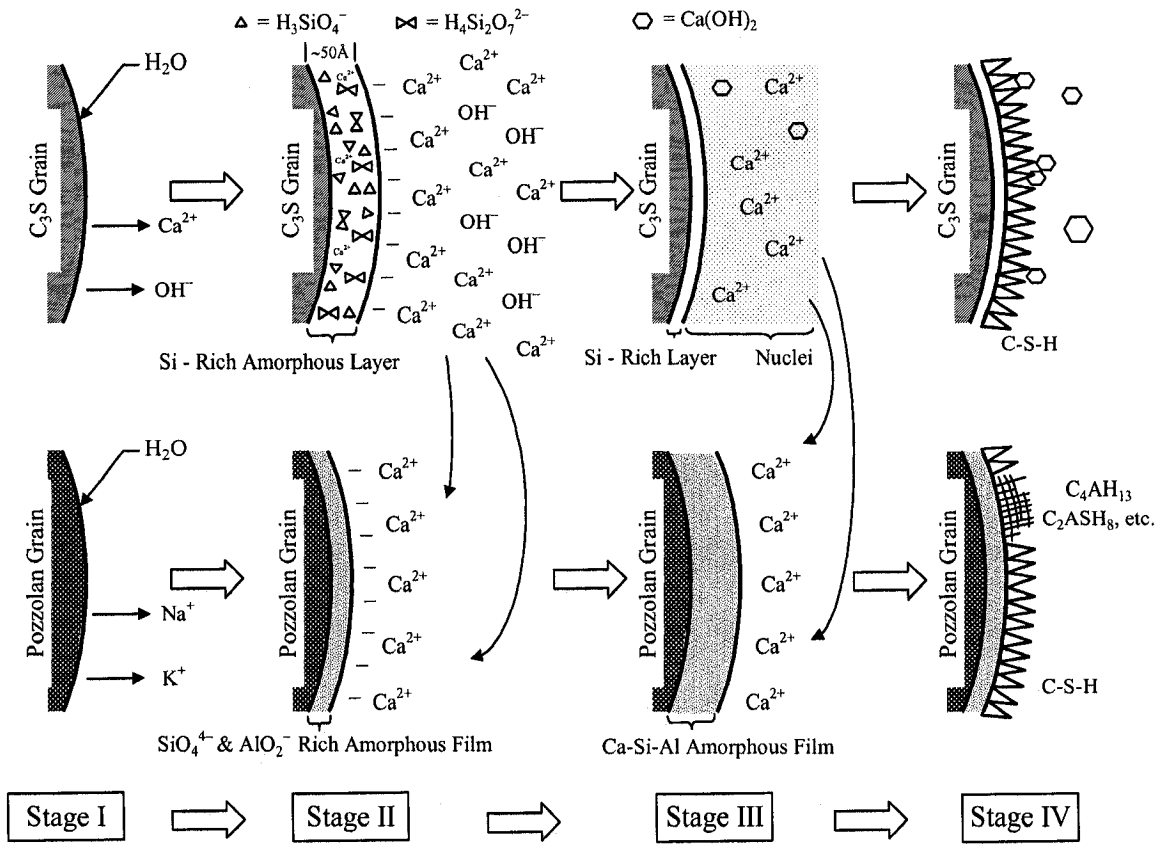

Fig. 4.4 A detailed description of the hydration of C_3S and the pozzolanic reaction

The XRD patterns for anhydrous OPC, OPC at 3 days hydration and OPC containing 50% fly ash at 3 days hydration for w/c 0.50 are shown in Fig. 4.5. The anhydrous OPC indicates mainly C_3S with smaller amounts of C_2S and C_4AF. The peaks for C_3A overlap the peaks for C_3S, C_2S and C_4AF and it is relatively difficult to observe. The peaks for gypsum and $CaCO_3$, which are common in the anhydrous cement, can also be observed. At 3 days hydration, OPC indicates the small amount of $Ca(OH)_2$, which is one of the main hydration products. The peaks for ettringite can also be detected. At 3 days hydration, the anhydrous components of OPC such as C_3S and C_2S can still be indicated. For the OPC containing 50% fly ash at 3 days hydration, the peaks for $Ca(OH)_2$ are lower than those for OPC at 3 days hydration. The height of $Ca(OH)_2$ peaks is often used as an indicator for the rate of hydration, since the amount of $Ca(OH)_2$, and therefore the height of $Ca(OH)_2$ peaks, increases with the hydration. In the case of cement paste containing high volumes of fly ash, however, the height of the $Ca(OH)_2$ peaks is affected not only by the rate of hydration but also by the pozzolanic reaction. The $Ca(OH)_2$ peaks would be higher as the OPC hydration takes place, at the same time, they would be lower as the pozzolanic reaction takes

place because of the consumption of $Ca(OH)_2$. This indicates that the delayed hydration of cement paste containing high volumes of fly ash observed by the conduction calorimetry is not observed by the XRD.

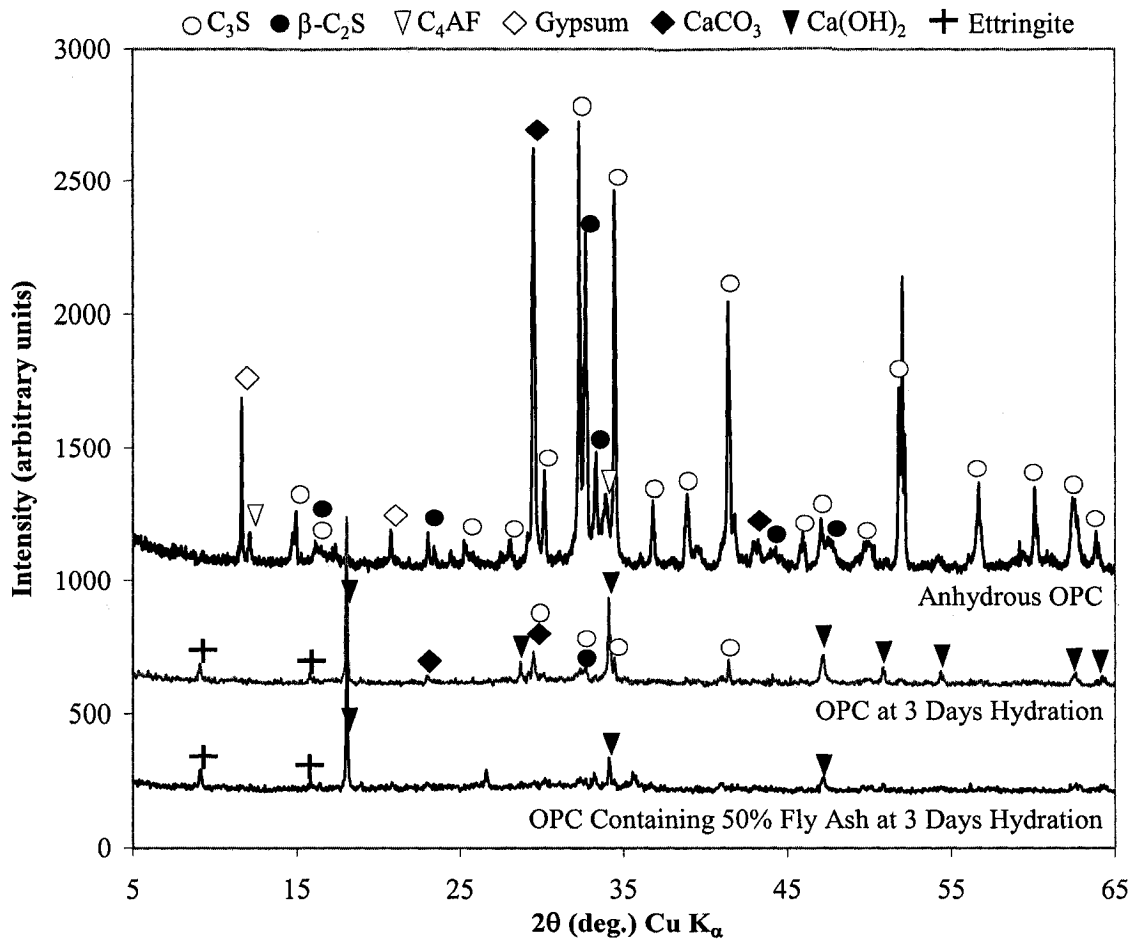

Fig. 4.5 The XRD patterns for anhydrous OPC, OPC at 3 days hydration and OPC containing 50% fly ash at 3 days hydration for w/c 0.50

The quantity of $Ca(OH)_2$ can also be determined by the TGA. The amount of $Ca(OH)_2$ in a specimen can be calculated from the amount of dehydrated H_2O from 300 to 500°C detected by TGA. The amount of dehydrated H_2O was calculated based on the total mass of cementitious materials (OPC and fly ash). The amounts of $Ca(OH)_2$ in the specimens for OPC and OPC containing 50% fly ash for w/c 0.50 at different periods of hydration were calculated and plotted in Fig. 4.6. The amounts of $Ca(OH)_2$ increase as hydration takes place from 1 day to 3 days for both OPC and OPC containing 50% fly ash, however, the amount of $Ca(OH)_2$ for OPC is significantly greater than that of OPC containing 50% fly ash due to the consumption of $Ca(OH)_2$ by the

pozzolanic reaction with fly ash. The TGA is a powerful tool to detect the amount of $Ca(OH)_2$ in a specimen and therefore can be used as an indicator for the rate of hydration. The greater the rate of hydration, the more is the amount of $Ca(OH)_2$ to be detected by the TGA. The delayed hydration of cement paste containing high volumes of fly ash observed by the conduction calorimetry, however, would not be observed by the TGA for the same reason mentioned for the XRD. The amount of $Ca(OH)_2$ is influenced not only by the rate of hydration but also by the pozzolanic reaction. The determination of the amount of $Ca(OH)_2$ in the hydrated cement paste containing high volumes of fly ash does not clearly indicate the delayed hydration because of the fly ash.

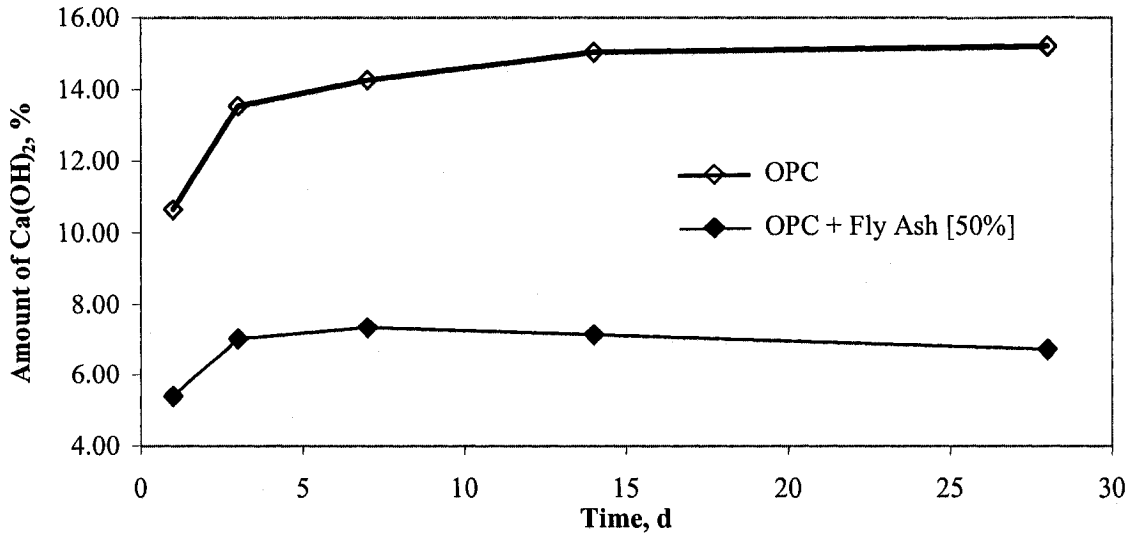

Fig. 4.6 The amounts of $Ca(OH)_2$ for OPC and OPC containing 50% fly ash for w/c 0.50 at different periods of hydration, determined by TGA

If it was possible to quantify the amount of C-S-H in the hydrated cement system, instead of the amount of $Ca(OH)_2$, by either XRD or TGA, it would have clearly indicated the rate of hydration, because the amount of C-S-H increases when either OPC hydration or pozzolanic reaction takes place or both. The amount of C-S-H cannot however be determined as straightforwardly as that of $Ca(OH)_2$ by either XRD or TGA. As mentioned in Section 3.4.1, the use of XRD is limited for amorphous materials, as opposed to crystalline materials, because of the principle on which it is based. The C-S-H has an amorphous structure, unlike $Ca(OH)_2$ with a very crystalline structure, and therefore it is relatively difficult to quantify the amount of C-S-H in a system by the XRD. Also there is no clearly defined separation between free water and the hydrates water associated with C-S-H in the hydrated cement paste. Both free water and the hydrates water of C-S-H tend to

be removed from the cement system as one event when the TGA is conducted, and therefore it is relatively difficult to quantify the amount of C-S-H by the TGA.

The determinations of mechanical properties will reflect the delayed hydration of cement paste containing high volumes of fly ash while both XRD and TGA were not suitable for that purpose. The microhardness values for OPC and OPC containing 50% fly ash for w/c 0.50 hydrated up to 3 days are plotted in Fig. 4.7. At 1 day hydration, the microhardness value of OPC is 56.3 MPa whereas that of OPC containing 50% fly ash is only 15.4 MPa. At 3 days hydration, the difference increases where the microhardness values of OPC and OPC containing fly ash are 102.4 MPa and 28.0 MPa, respectively. The results undoubtedly show that the early hydration of OPC paste was delayed by the addition of 50% fly ash. This is correlated with what was observed by the conduction calorimetry. The modulus of elasticity values for OPC and OPC containing 50% fly ash for w/c 0.50 hydrated up to 3 days are plotted in Fig. 4.8. The modulus of elasticity results are similar in character to the microhardness results. At 3 days hydration, the modulus of elasticity values of OPC and OPC with fly ash are 9.9 GPa and 2.5 GPa, respectively. It is clearly indicated that the addition of high volumes of fly ash delayed the rate of early development of mechanical properties of cement paste. Figures 4.7 and 4.8 are shown with an error bar for each value. The following figures of microhardness and modulus of elasticity in the thesis, however, will be shown without the error bars for the sake of clarity.

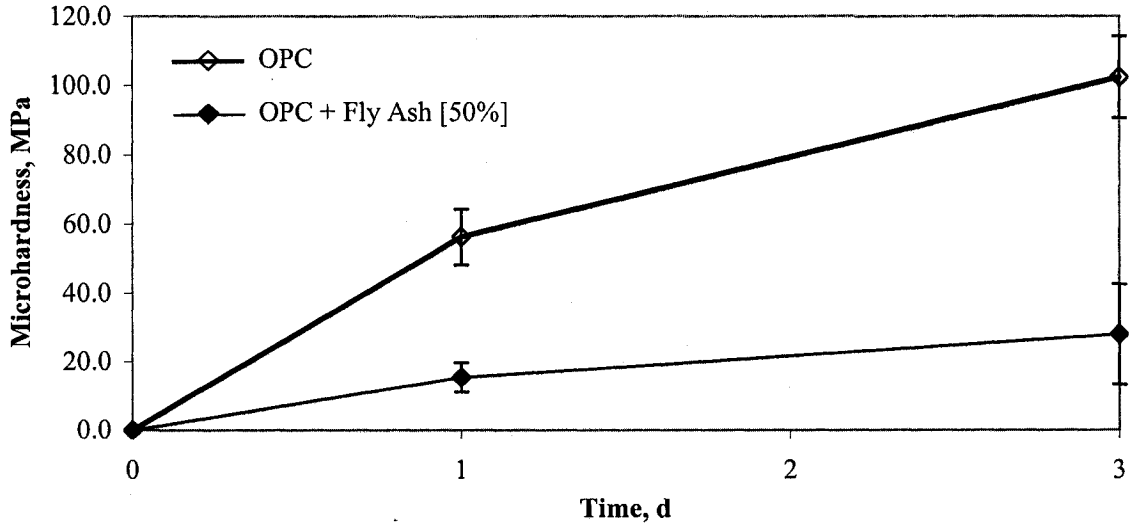

Fig. 4.7 Microhardness results for OPC and OPC containing 50% fly ash for w/c 0.50 hydrated up to 3 days

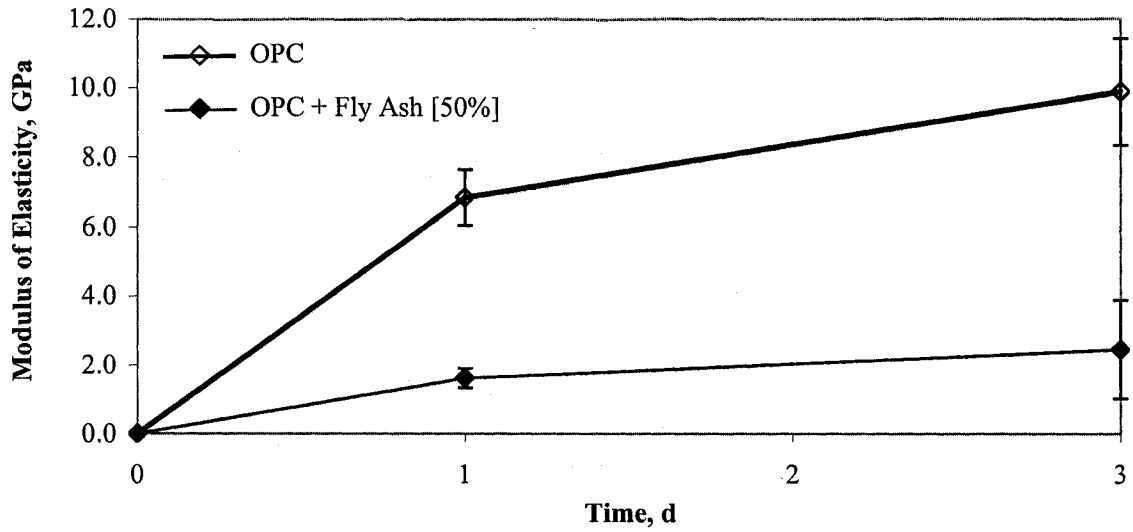

Fig. 4.8 Modulus of elasticity results for OPC and OPC containing 50% fly ash for w/c 0.50 hydrated up to 3 days

4.3.1.2 Late Hydration (3 ~ 28 Days)

In the previous section, the effect of the addition of high volumes of fly ash on the early hydration of OPC was observed. The delayed hydration was clearly indicated from the conduction calorimetry and determinations of mechanical properties. Especially at 1 day hydration, the hydration and strength development were significantly delayed when 50% fly ash was added to the mix. In this section, hydration progress and mechanical properties will be discussed for a longer period of hydration (3 ~ 28 days) to determine the effect of the addition of high volumes of fly ash on a long-term hydration.

The XRD patterns for OPC and OPC containing 50% fly ash for w/c 0.50 both at 28 days hydration are shown in Fig. 4.9. The pattern for OPC hydrated for 28 days indicates predominantly $Ca(OH)_2$ peaks along with small amounts of ettringite, gypsum and anhydrous C_2S. The C-S-H produced by the cement hydration has an amorphous structure, as mentioned earlier, and is relatively difficult to be detected on the XRD patterns. An amorphous material can however be detected in the XRD patterns through the presence of what is often referred to as amorphous humps. In the case of C-S-H produced by cement hydration (as opposed to a synthetic C-S-H which has a more crystalline structure and sharp intense peaks in the XRD patterns), there is an amorphous hump at 29.4°, 32.1° and 50.1° (2θ) as shown in the figure. Those amorphous humps are however too small to be used for an accurate analysis. As for the hydration of OPC containing 50% fly ash, it is still not very well understood because of the variations between different fly

ashes and between different particles within a fly ash (Roy, 1989). The XRD patterns for OPC containing 50% fly ash at 28 days hydration are also shown in this figure. The main peaks are $Ca(OH)_2$ produced from hydration and several Fe_2O_3 peaks, one of the original main constituents in control fly ash, can be observed as well. As mentioned above, it is rather difficult to conclusively identify the hydration products of OPC containing fly ash. A few reasonable suggestions, however, can possibly be made. Several peaks observed in the XRD pattern might be calcium aluminate hydrates and/or calcium carboaluminate hydrates as indicated in the figure.

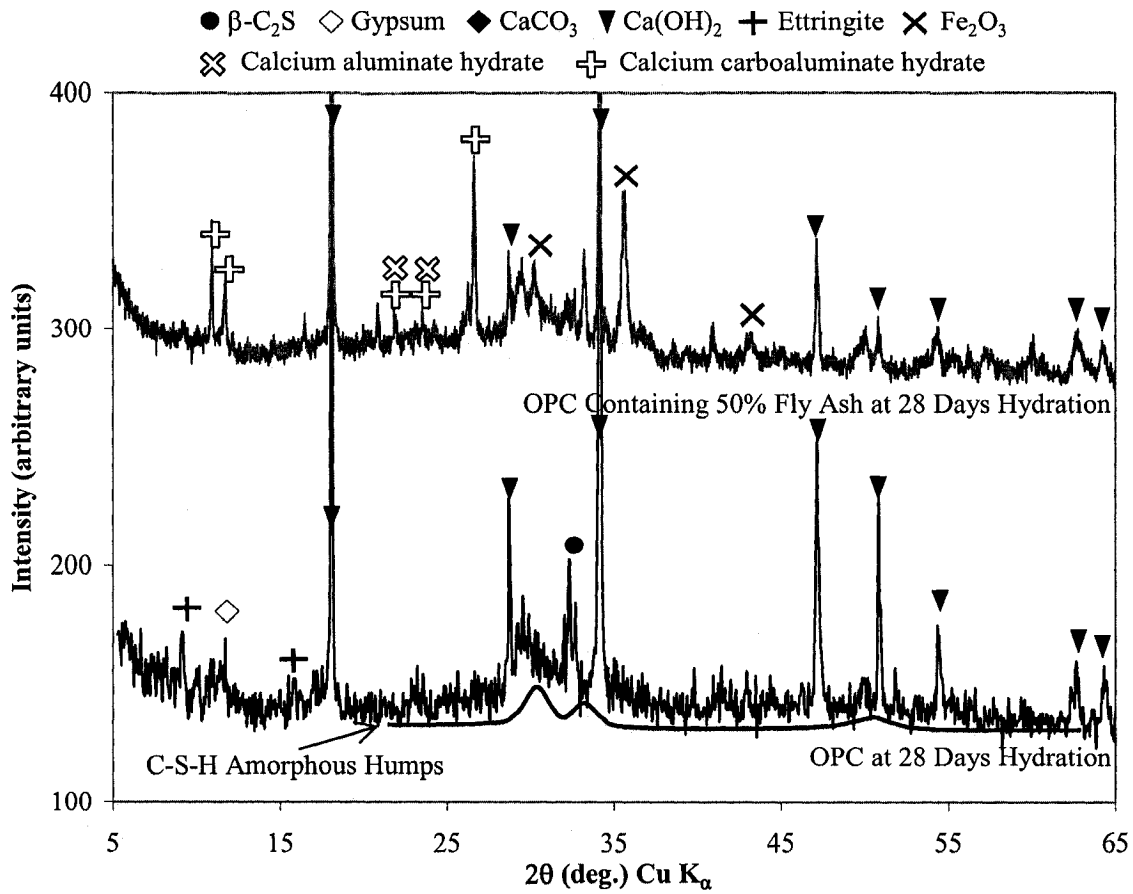

Fig. 4.9 The XRD patterns for OPC and OPC containing 50% fly ash for w/c 0.50 both at 28 days hydration

Figure 4.6, previously shown, provides an estimate of the amount of $Ca(OH)_2$ in the specimens of OPC and OPC containing 50% fly ash at different periods of hydration. The amount of $Ca(OH)_2$ in the hydrated OPC increases as hydration takes place from 3 days to 28 days. The amounts of $Ca(OH)_2$ in the hydrated OPC containing 50% fly ash at any time of the hydration are significantly lower than those in the OPC owing to the $Ca(OH)_2$ consumption by the pozzolanic reaction.

The amount of $Ca(OH)_2$ in the OPC containing 50% fly ash increases with hydration, however, it starts decreasing at 7 days. This indicates that the consumption of $Ca(OH)_2$ by the pozzolanic reaction becomes greater than the production of $Ca(OH)_2$ by the cement hydration at 7 days. The amount of $Ca(OH)_2$ continues to slightly decrease up to 28 days, implying that the pozzolanic reaction takes place much more slowly than the OPC hydration.

The microhardness results for OPC and OPC containing 50% fly ash for w/c 0.50 hydrated up to 28 days are shown in Fig. 4.10. The microhardness of OPC increases as hydration takes place, although the greater strength development between 14 days and 28 days hydration was expected. As it was shown in Fig. 4.7, the strength development of OPC paste containing 50% fly ash was significantly delayed compared to that of OPC up to 3 days hydration. Now it is clear in Fig. 4.10 that the hydration of OPC containing 50% fly ash was delayed up to 28 days hydration, where the microhardness value of OPC and that of OPC containing 50% fly ash are 163.9 MPa and 45.7 MPa, respectively. It is well known that the rate of strength development is generally greater towards the end of hydration when the hydration was delayed in the earlier stage of hydration. This is not the case, however, for the OPC containing 50% fly ash, as the microhardness at 28 days is much lower than that of OPC. The modulus of elasticity results for OPC and OPC containing 50% fly ash for w/c 0.50 hydrated up to 28 days are illustrated in Fig. 4.11. The modulus of elasticity of OPC increases as hydration takes place up to 28 days. Similarly, the modulus of elasticity of OPC containing 50% fly ash increases with hydration, but remains much lower than that of OPC at any time of the hydration. The late development of mechanical properties owing to the delayed early hydration is not indicative from the modulus of elasticity results either. It was indicated in Fig. 4.6 that, after 7 days hydration, the overall amount of $Ca(OH)_2$ in the system decreases because the consumption of $Ca(OH)_2$ by the pozzolanic reaction becomes greater than the production of $Ca(OH)_2$ by the cement hydration. Both values of microhardness and modulus of elasticity for the OPC containing 50% fly ash, however, increased even after 7 days hydration. This may indicate that the amount of $Ca(OH)_2$ in a hydrated cement system has only an indirect influence on strength development.

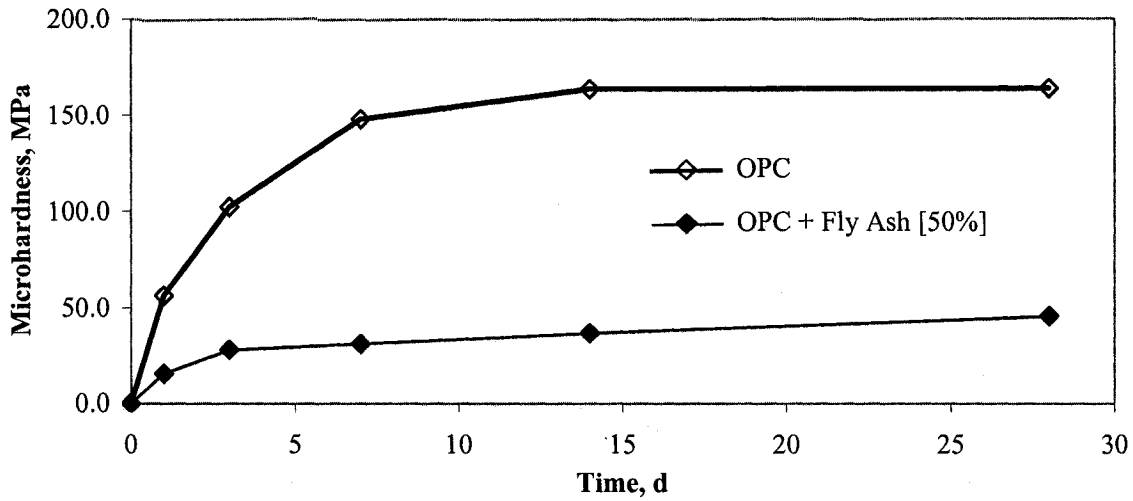

Fig. 4.10 Microhardness results for OPC and OPC containing 50% fly ash for w/c 0.50 hydrated up to 28 days

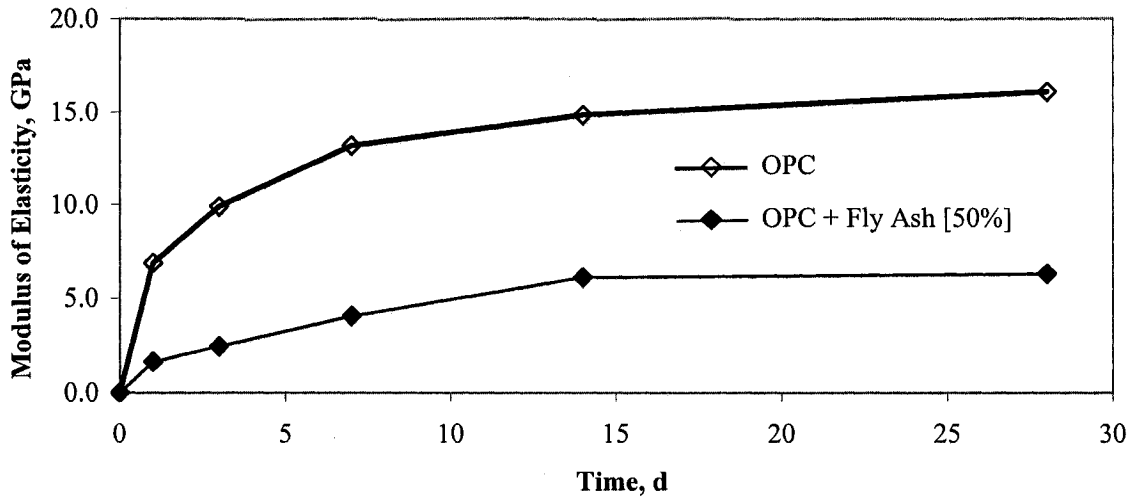

Fig. 4.11 Modulus of elasticity results for OPC and OPC containing 50% fly ash for w/c 0.50 hydrated up to 28 days

4.3.2 Stage 2: Hydration Mechanism of Cement Paste with the Additions of Micro- and Nano-sized $CaCO_3$

4.3.2.1 Early Hydration (0 ~ 3 Days)

The effect of micro- and nano-sized $CaCO_3$ additions on OPC hydration was studied in this section, and therefore no SCMs were added. The conduction calorimetry results for the control OPC and OPC containing 10% and 20% additions of reagent grade micro-sized $CaCO_3$ and nano-

sized $CaCO_3$ for w/c 0.50 are shown in Fig. 4.12. The rate of heat development was calculated in calories per mass of OPC (excluding that of $CaCO_3$) per hour. The content percentages of $CaCO_3$ are based on the mass of OPC. The curve for the control OPC and those for the OPC with the additions of 10% and 20% micro-sized $CaCO_3$ are almost overlapped, indicating that the additions of micro-sized $CaCO_3$ have little or almost no effect on the hydration of OPC in terms of the rate of heat development. It is clear, however, that both 10% and 20% additions of the nano-sized $CaCO_3$ significantly accelerate the early hydration of OPC. The first large peak of the main heat development curve for the control OPC and those for the OPC containing 10% and 20% nano-sized $CaCO_3$ additions occur at approximately 9.5, 5.8 and 4.8 hours, respectively. It is also evident that the greater the amount of $CaCO_3$ addition, the greater is the accelerating effect.

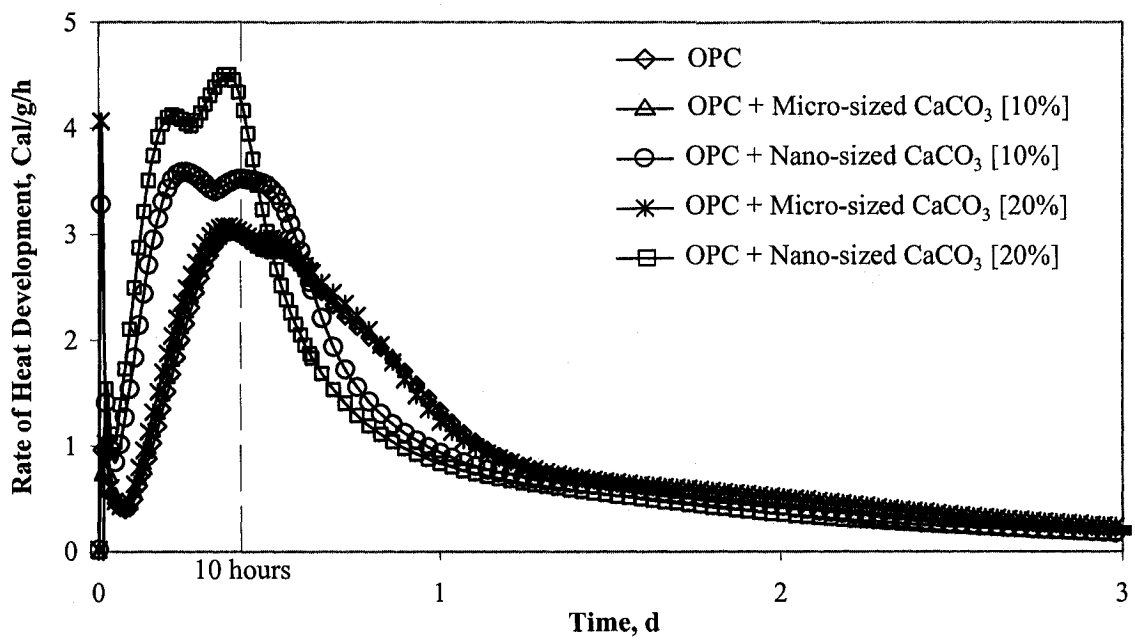

Fig. 4.12 Conduction calorimetry curves for OPC and OPC with the additions of micro- and nano-sized $CaCO_3$ for w/c 0.50

In addition to 1 day and 3 days hydration, the TGA and XRD were conducted at 10 hours as well. This is to observe the most prominent accelerating effect of $CaCO_3$ addition as shown in Fig. 4.12. The amounts of $Ca(OH)_2$ and $CaCO_3$ in the specimens for w/c 0.50 hydrated for 10 hours, 1 day and 3 days, are calculated from the TGA results and shown in Figs. 4.13 and 4.14, respectively. The amount of $Ca(OH)_2$ and $CaCO_3$ in a specimen was calculated from the amount of dehydrated H_2O and decomposed CO_2, based on the total mass of OPC and the total mass of OPC with $CaCO_3$, respectively. The amount of $Ca(OH)_2$, an indicator for the degree of hydration, demon-

strates a very similar characteristic to the calorimetry results. At 10 hours hydration, both 10% and 20% additions of micro-sized $CaCO_3$ increased the amount of $Ca(OH)_2$ produced only slightly greater than the OPC, whereas the additions of the nano-sized $CaCO_3$ significantly increased the amount of $Ca(OH)_2$ produced. This result correlates with that of calorimetry, although the amounts of $Ca(OH)_2$ observed in TGA was not significantly affected by a difference in the content percentages of added $CaCO_3$. At 1 day and 3 days hydration, the amount of $Ca(OH)_2$ produced in each specimen becomes similar within the range of 1%. This can also be observed by the amount of heat development, that is, the area under the calorimetry curves shown in Fig. 4.12. The amount of heat development at 10 hours hydration by the OPC with the additions of both 10% and 20% nano-sized $CaCO_3$ is considerably greater than those by the OPC and OPC with the additions of micro-sized $CaCO_3$. The amounts of heat development at 1 day and 3 days are however very similar with each other. This correlates with the similarity of the amount of $Ca(OH)_2$ in each specimen at 1 day and 3 days hydration.

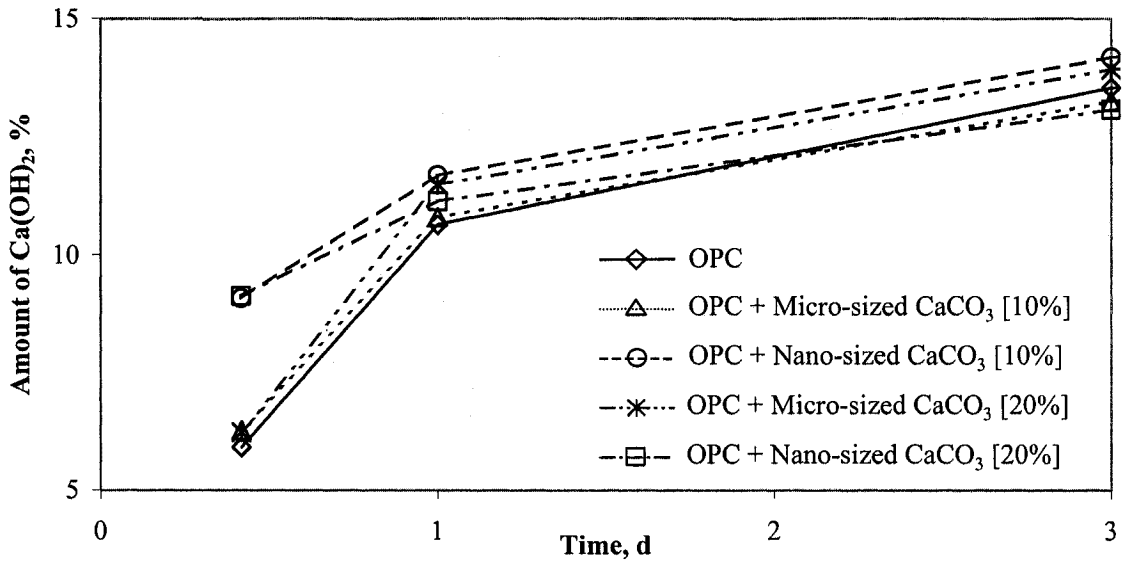

Fig. 4.13 The amounts of $Ca(OH)_2$ for OPC and OPC with the additions of micro- and nano-sized $CaCO_3$ for w/c 0.50 hydrated for 10 hours, 1 day and 3 days, determined by TGA

The amounts of $CaCO_3$ in the specimens hydrated for 10 hours, 1 day and 3 days are shown in Fig. 4.14. A certain amount of $CaCO_3$ is constantly observed for the control OPC, indicating that the anhydrous OPC powder might have been carbonated during the storage period. This was also observed by the XRD pattern of anhydrous OPC, shown in Fig. 4.5, indicating some peaks for $CaCO_3$. It is also possible that the mixing water contained a small amount of CO_2, although it was

deaerated prior to the mixing. It is important to note that the amount of $CaCO_3$ detected in each specimen is lower than the added amount and it decreases as hydration takes place. The OPC with 10% micro-sized $CaCO_3$ addition had 10.45% $CaCO_3$ at 10 hours hydration. Since the control OPC had 2.14% $CaCO_3$ at 10 hours hydration, it is clear that the OPC with 10% micro-sized $CaCO_3$ had lost about 1.70% $CaCO_3$ after 10 hours. The OPC with 20% micro-sized $CaCO_3$ addition had lost about 4.64% $CaCO_3$ at 10 hours hydration. These phenomena become more remarkable for the nano-sized $CaCO_3$ addition. The OPC with the 10% and 20% nano-sized $CaCO_3$ additions had lost approximately 4.26% and 8.61% $CaCO_3$, respectively at 10 hours hydration. It is clear that some portion of added $CaCO_3$ was chemically reacted in the hydration process and/or was not detected by a means of TGA.

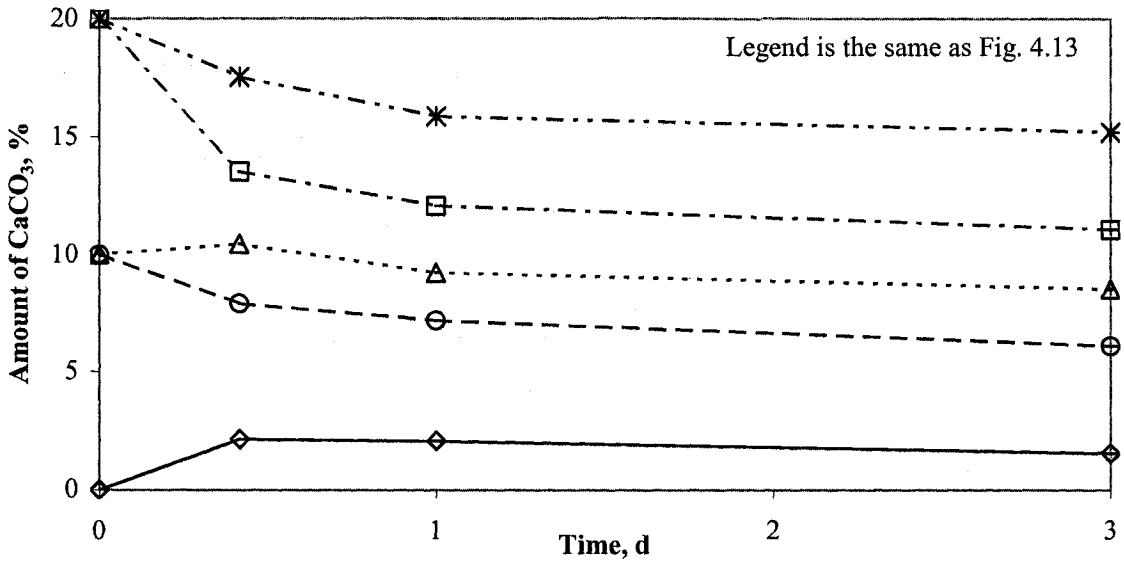

Fig. 4.14 The amounts of $CaCO_3$ for OPC and OPC with the additions of micro- and nano-sized $CaCO_3$ for w/c 0.50 hydrated for 10 hours, 1 day and 3 days, determined by TGA

It has been observed that the $CaCO_3$ chemically reacted with tricalcium aluminate, C_3A to form calcium carboaluminate hydrates (Carlson and Berman, 1960). It forms both high- and low-carbonate forms of calcium aluminate hydrate in a very similar manner as C_3A reacts with calcium sulphate (gypsum), $CaSO_4 \cdot 2H_2O$ to form both high- and low- sulphate forms of calcium aluminate hydrate. The high- and low- carbonate forms of calcium aluminate hydrate are respectively, $3CaO \cdot Al_2O_3 \cdot 3CaCO_3 \cdot 32H_2O$ and $3CaO \cdot Al_2O_3 \cdot CaCO_3 \cdot 11H_2O$. They are very similar to those of calcium sulphoaluminate hydrate, $3CaO \cdot Al_2O_3 \cdot 3CaSO_4 \cdot 32H_2O$ (ettringite) and $3CaO \cdot Al_2O_3 \cdot CaSO_4 \cdot 12H_2O$. The high-carbonate form, $3CaO \cdot Al_2O_3 \cdot 3CaCO_3 \cdot 32H_2O$ occurs as a

needle-like structure which is similar to that observed for ettringite (Lea, 1970). It is widely known that the conduction calorimetry curve of control OPC has a small shoulder right after the main peak of hydration, shown in Fig. 4.15. It has been suggested that this is related to the formation of ettringite (Pratt and Ghose, 1983). This small shoulder is significantly enhanced when 20% nano-sized $CaCO_3$ was added. The SEM images of the control OPC and the OPC containing 20% nano-sized $CaCO_3$ addition hydrated for 10 hours are shown in Figs. 4.16 (a) and (b), respectively. In the control OPC, no typical needle-like characteristics of ettringite can be observed, because the amount of ettringite formed at 10 hours hydration is not sufficient enough to be observed by SEM, although the formation of ettringite itself starts within a few hours after mixing with water. In the OPC with the 20% nano-sized $CaCO_3$ addition, however, the needle-like characteristics can be observed where the reaction peak has occurred before 10 hours due to the presence of the nano-sized $CaCO_3$. This could be a mixture of ettringite and $3CaO{\cdot}Al_2O_3{\cdot}3CaCO_3{\cdot}32H_2O$. The reaction between C_3A and gypsum could be accelerated by the nano-sized $CaCO_3$ addition and/or there could be a reaction between C_3A and the added nano-sized $CaCO_3$, itself. Nevertheless, the formation of $3CaO{\cdot}Al_2O_3{\cdot}3CaCO_3{\cdot}32H_2O$ was minimum. A previous study reported by Ramachandran and Zhang (1986) on the effect of the addition of finely ground limestone on the hydration of C_3S, concluded that some portion of the added $CaCO_3$ had been consumed during the hydration of C_3S. This indicates that the added $CaCO_3$ may be consumed also in the hydration of C_3S and the amount of the added $CaCO_3$ that may react with C_3A can be very small. This will be discussed more in the next section where the amount of $CaCO_3$ in the specimens will be determined up to 28 days hydration.

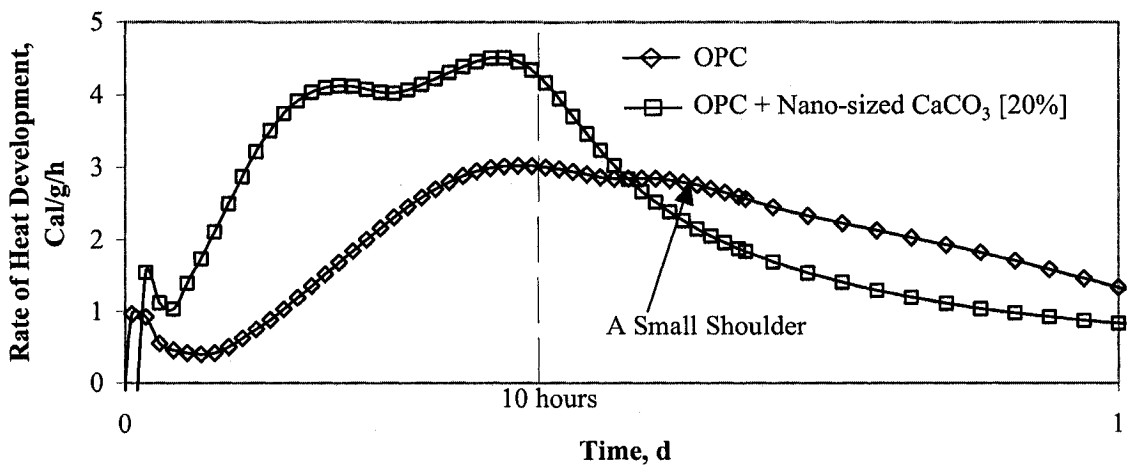

Fig. 4.15 Conduction calorimetry curves for OPC and OPC with the additions of 20% nano-sized $CaCO_3$ for w/c 0.50

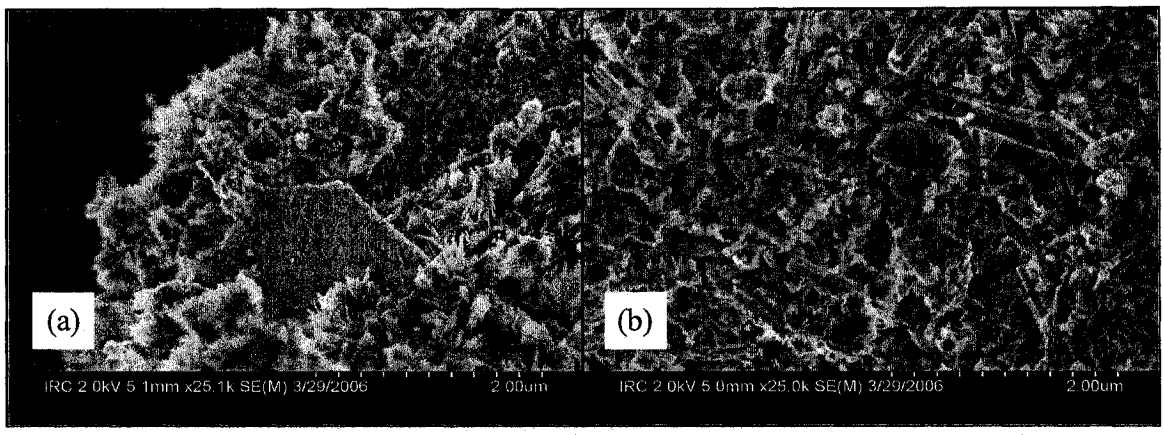

Fig. 4.16 SEM images of (a) control OPC and (b) OPC with the 20% nano-sized $CaCO_3$ addition hydrated for 10 hours

The XRD patterns of OPC and OPC with the 20% nano-sized $CaCO_3$ addition for w/c 0.50 at 10 hours hydration are shown in Fig. 4.17. For the OPC at 10 hours hydration, the peaks for anhydrous C_3S and C_2S are still dominating, although some $Ca(OH)_2$ peaks are already observed. It is obvious that the OPC with the 20% nano-sized $CaCO_3$ addition has several intense $CaCO_3$ peaks, though no peaks for calcium carboaluminate hydrate suggested above for the possible $CaCO_3$ reaction products can be observed, probably owing to the fact that the amount of calcium carboaluminate hydrate is less than 5%, which is generally the limit to be detected by the XRD. It is however indicated in Fig. 4.17 that the peaks for anhydrous C_3S detected in OPC are more intense than those in OPC with the 20% nano-sized $CaCO_3$ addition, indicting that the hydration was accelerated by the 20% nano-sized $CaCO_3$ addition.

4.3.2.2 Late Hydration (3 ~ 28 Days)

In the previous section, the accelerating effect of both micro- and nano-sized $CaCO_3$ additions on control OPC was studied especially for the early hydration (10 hours, 1 day and 3 days). In this section, the effect of that accelerating phenomenon in the early hydration on the late hydration (up to 28 days) will be discussed. The amounts of $Ca(OH)_2$ and $CaCO_3$ in the specimens for w/c 0.50 hydrated up to 28 days, are calculated from the TGA results and shown in Figs. 4.18 and 4.19, respectively. As previously shown in Fig. 4.6, the amount of $Ca(OH)_2$ for the hydration of control OPC increases as hydration takes place. The same is true in Fig. 4.18, although the data seem to be relatively scattered with the $CaCO_3$ additions. At 28 days, the amounts of $Ca(OH)_2$ for the OPC with both 10% and 20% nano-sized $CaCO_3$ additions are slightly lower than the rest. This could be related to their accelerating effect observed in the early hydration. It is well known

that the accelerated hydration in the earlier stage can cause delayed development in the later stage. The effect of accelerated hydration in the early stage on the strength development in the later stage will be discussed in the next section, since this section is intended only to explain the chemical and physical interactions between the control OPC and added $CaCO_3$. The amount of $CaCO_3$ in each specimen continues to decrease as hydration takes place hydrated up to 28 days, shown in Fig. 4.19. Ramachandran and Zhang (1986) calculated the CaO/SiO_2 (C/S) ratio of the C-S-H produced by the hydration of C_3S with finely ground $CaCO_3$ addition. The C/S ratio of the C-S-H for the C_3S specimen containing 0% $CaCO_3$ at 28 days hydration was 1.86, whereas that containing 15% $CaCO_3$ was 1.92. The amount of CaO in the C-S-H of the 28 days hydrated C_3S containing 15% added $CaCO_3$ was higher than that containing 0% added $CaCO_3$. This implies that some portion of added $CaCO_3$ chemically reacted in the hydration process. It was suggested that some $CaCO_3$ was chemisorbed or even incorporated into the interlayer region of C-S-H structure.

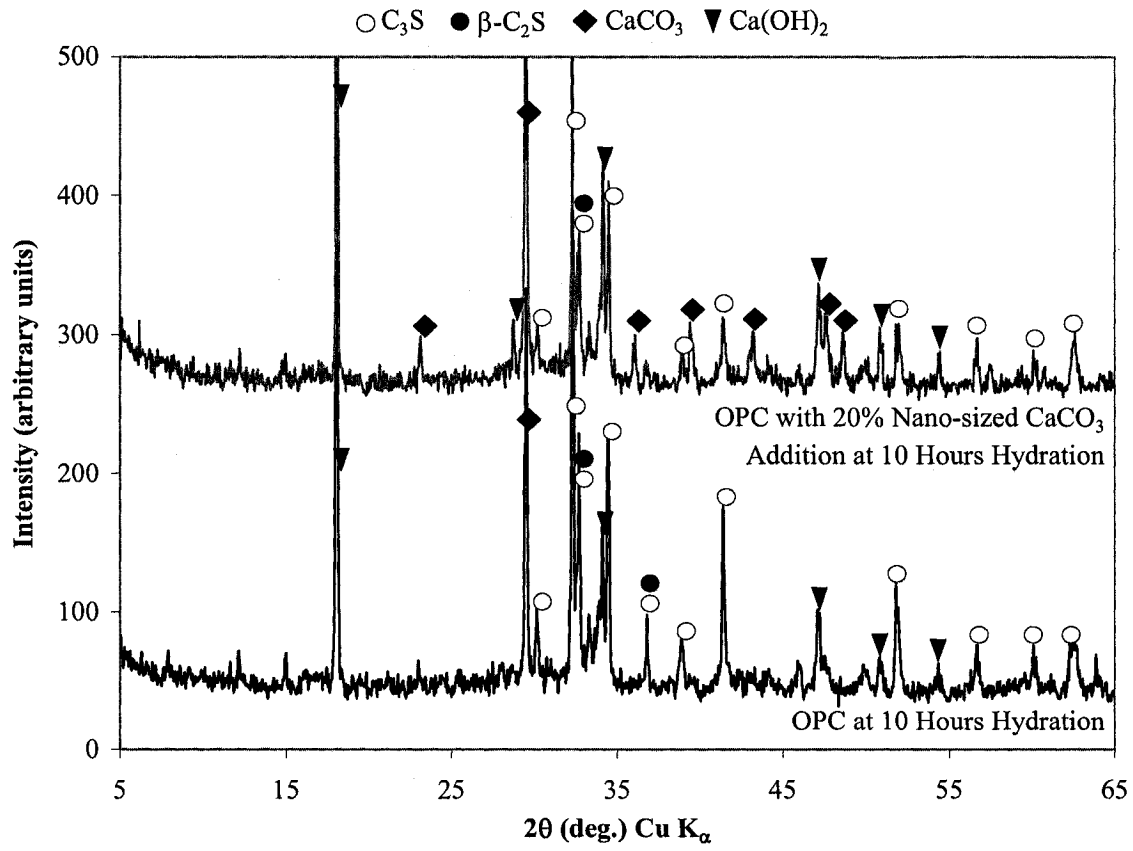

Fig. 4.17 The XRD patterns for OPC and OPC with 20% nano-sized $CaCO_3$ addition for w/c 0.50 both at 10 hours hydration

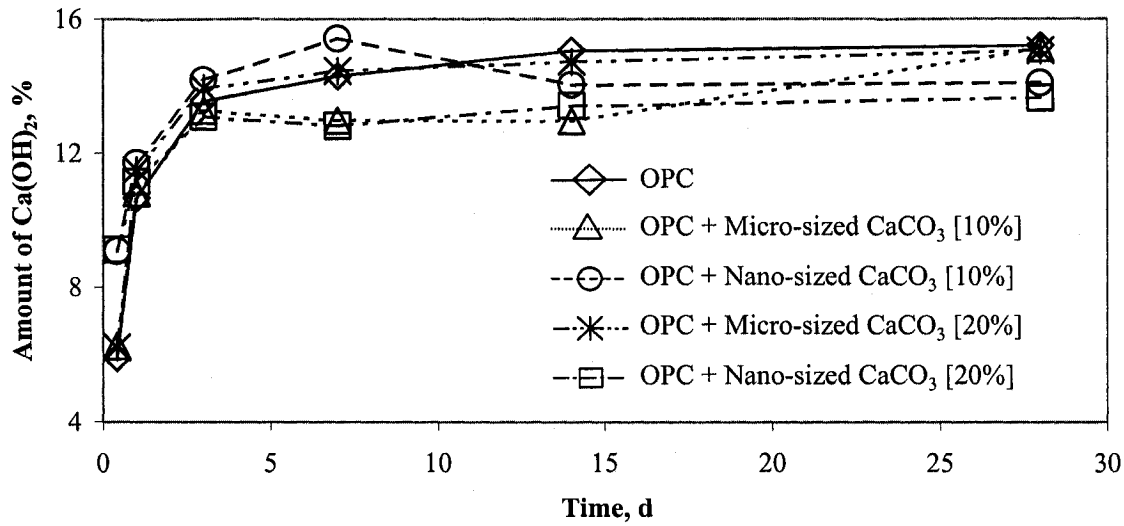

Fig. 4.18 The amounts of $Ca(OH)_2$ for OPC and OPC with the additions of micro- and nano-sized $CaCO_3$ for w/c 0.50 hydrated up to 28 days, determined by TGA

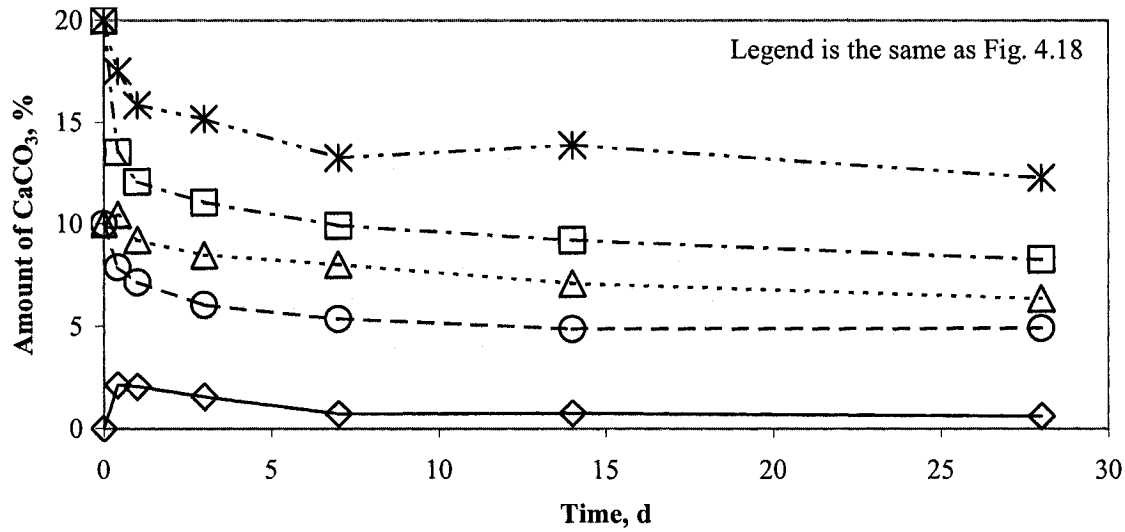

Fig. 4.19 The amounts of $CaCO_3$ for OPC and OPC with the additions of micro- and nano-sized $CaCO_3$ for w/c 0.50 hydrated up to 28 days, determined by TGA

The XRD pattern of OPC with 20% nano-sized $CaCO_3$ addition for w/c 0.50 at 28 days hydration is shown in Fig. 4.20. Most of main peaks observed are the $Ca(OH)_2$ and $CaCO_3$ peaks, except two peaks at 9.2° and 11.7° (2θ) that might be attributed to the calcium carboaluminate hydrate which is the possible reaction product caused by the addition of $CaCO_3$, considering that the ettringite, which has a very similar structure to the calcium carboaluminate hydrate, has a peak at 9.1° (2θ). A possible source for a peak at 56.6° (2θ) was not determined.

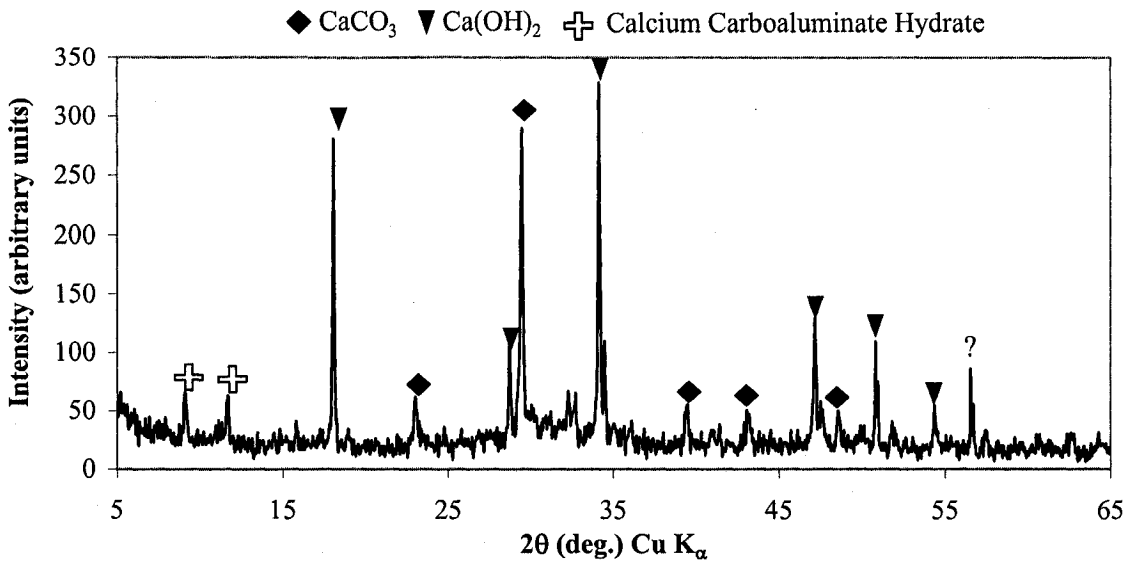

Fig. 4.20 The XRD pattern of OPC with the 20% nano-sized $CaCO_3$ addition for w/c 0.50 at 28 days hydration

4.3.3 Stage 3: Hydration Mechanism of Cement Paste Containing High Volumes of Fly Ash with the Additions of Micro- and Nano-sized $CaCO_3$ Hydrated at 23°C and 5°C

4.3.3.1 Early Hydration (0 ~ 3 Days)

In Section 4.3.1.1, the effect of the addition of high volumes of fly ash on the early hydration of control OPC was observed and the results of conduction calorimetry, TGA and determinations of mechanical properties have indicated that, when 50% fly ash was added to the mix, the early hydration of OPC was significantly delayed. In Section 4.3.2.1, the effect of the micro- and nano-sized $CaCO_3$ additions on the early hydration of control OPC was investigated and the calorimetry and TGA results have shown that the nano-sized $CaCO_3$ addition remarkably accelerated the OPC hydration. In this section, the micro- and nano-sized $CaCO_3$ were added to the OPC containing 50% fly ash to determine whether or not the delayed early hydration of OPC paste containing high volumes of fly ash would be counteracted by the accelerating effect of the nano-sized $CaCO_3$ addition. For the mechanical properties, the specimens were also cured at 5°C, as opposed to 23°C, to observe the effect of low temperature curing on the accelerating effect of the nano-sized $CaCO_3$ addition and the results will be shown later in the section.

The conduction calorimetry results for OPC, OPC containing 50% fly ash and OPC containing 50% fly ash with the additions of 10% and 20% micro- and nano-sized $CaCO_3$ for w/c 0.50 are shown in Fig. 4.21. The hydration of OPC paste containing 50% fly ash is significantly delayed compared to that of OPC as already shown in Fig. 4.3. The curves for the OPC containing 50% fly ash with the additions of 10% and 20% micro-sized $CaCO_3$ almost overlap the curve for the OPC containing 50% fly ash, implying very little or almost no accelerating effect on the delayed hydration. This was expected from the observation in Fig. 4.12 where the micro-sized $CaCO_3$ additions indicated no sign of accelerating effect on the hydration of control OPC. In Fig. 4.21, however, it is possible to observe a slight difference between the content percentages of 10% and 20% of the micro-sized $CaCO_3$ addition. The hydration with the 20% micro-sized $CaCO_3$ addition is slightly more accelerated than that with 10%. As for the nano-sized $CaCO_3$ additions, it is clearly indicated that the additions of nano-sized $CaCO_3$ accelerate and counteract the delayed early hydration of OPC paste containing high volumes of fly ash. The 10% nano-sized $CaCO_3$ addition significantly accelerates the delayed hydration caused by high volumes of fly ash. Furthermore, the OPC containing 50% fly ash with the 20% nano-sized $CaCO_3$ addition hydrates almost as fast as the control OPC, indicating the rate of early strength development of OPC containing 50% fly ash with the 20% nano-sized $CaCO_3$ addition may be as fast as the control OPC. This is very critical for a tight schedule of construction in the competitive industry.

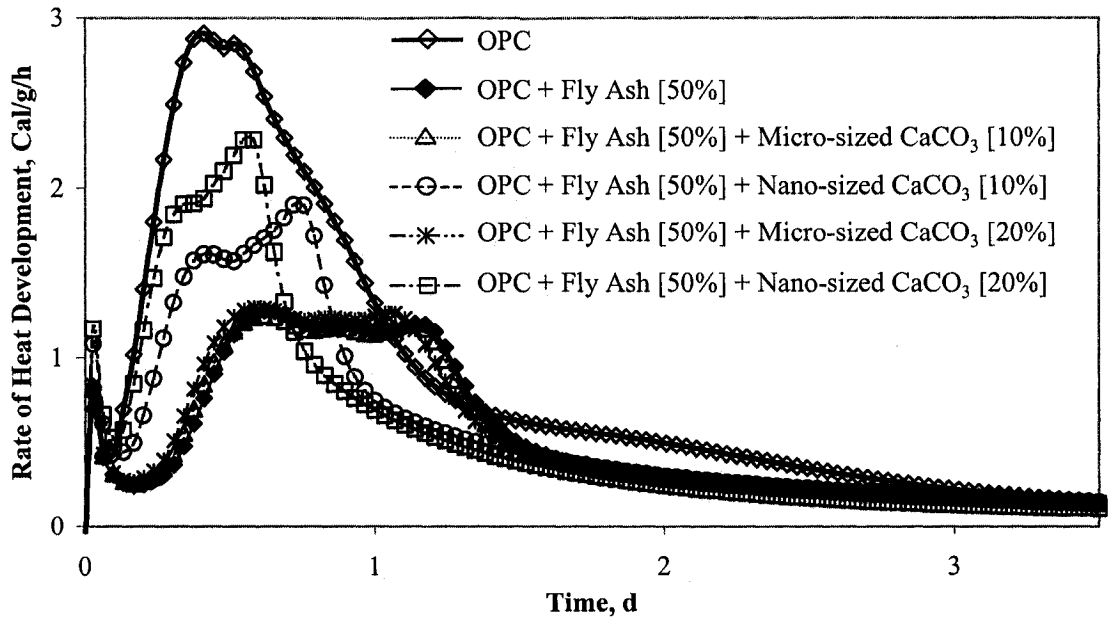

Fig. 4.21 Conduction calorimetry curves for OPC, OPC containing 50% fly ash and OPC containing 50% fly ash with the additions of micro- and nano-sized $CaCO_3$ for w/c 0.50

The amounts of $Ca(OH)_2$ and $CaCO_3$, determined by TGA, for OPC, OPC containing 50% fly ash and OPC containing 50% fly ash with the additions of micro- and nano-sized $CaCO_3$ for w/c 0.50 hydrated up to 3 days, are shown in Figs. 4.22 and 4.23, respectively. The additions of both micro- and nano-sized $CaCO_3$ apparently show very little effect on the amount of $Ca(OH)_2$ produced during the hydration. At 1 day hydration, the specimens for OPC containing fly ash with the additions of $CaCO_3$ have slightly more $Ca(OH)_2$ than that without the additions of $CaCO_3$, however, the difference is within the range of 1% which is relatively small compared with the amount of $Ca(OH)_2$ in the control OPC at 1 day hydration. The result shown in Fig. 4.23 is very similar to what was observed in Fig. 4.14, indicating that the existence of fly ash in the specimens has a very little effect on the reduced amounts of $CaCO_3$. The added $CaCO_3$ might be interacting with the hydration of the control OPC itself.

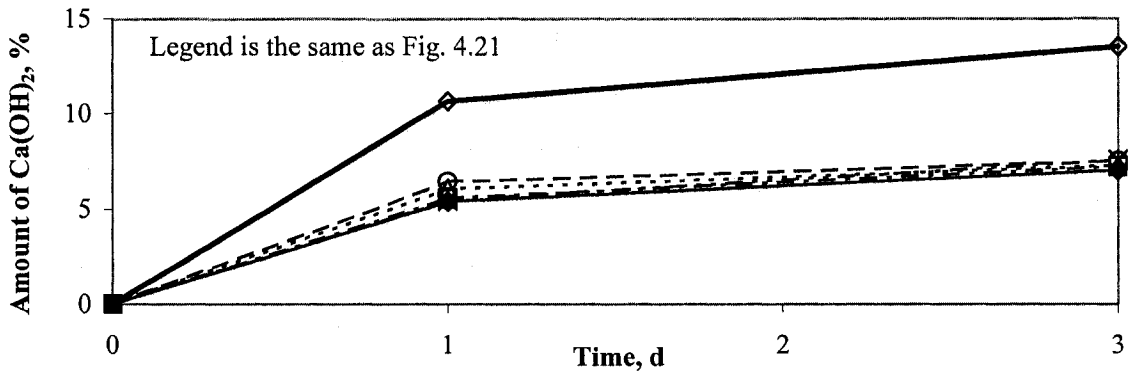

Fig. 4.22 The amounts of $Ca(OH)_2$ for OPC, OPC containing 50% fly ash and OPC containing 50% fly ash with the additions of micro- and nano-sized $CaCO_3$ for w/c 0.50 hydrated up to 3 days, determined by TGA

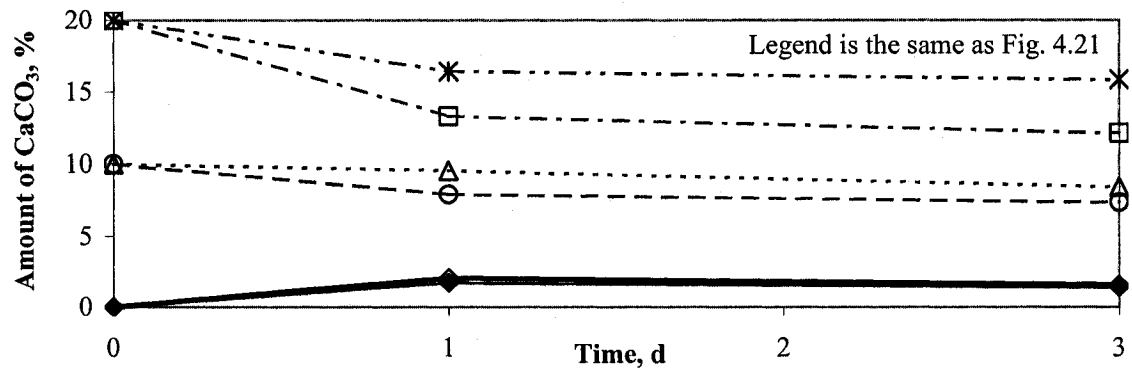

Fig. 4.23 The amounts of $CaCO_3$ for OPC, OPC containing 50% fly ash and OPC containing 50% fly ash with the additions of micro- and nano-sized $CaCO_3$ for w/c 0.50 hydrated up to 3 days, determined by TGA

The results of microhardness and modulus of elasticity for OPC, OPC containing 50% fly ash and OPC containing 50% fly ash with the additions of micro- and nano-sized $CaCO_3$ for w/c 0.50 hydrated up to 3 days, are shown in Figs. 4.24 and 4.25, respectively. It is evident that the additions of nano-sized $CaCO_3$ significantly improve the microhardness of the OPC containing 50% fly ash. At 1 day hydration, the microhardness value of OPC, 56.3 MPa, is reduced to 15.4 MPa when the 50% fly ash is added to the mix. It increases however to 34.6 MPa when 20% nano-sized $CaCO_3$ is added to the OPC containing 50% fly ash. At 3 days hydration, the values of microhardness for the OPC containing fly ash are increased by both 10% and 20% additions of nano-sized $CaCO_3$, however, those for the OPC containing fly ash with micro-sized $CaCO_3$ are as low as the OPC containing fly ash without $CaCO_3$. Similar behaviours can be observed in terms of modulus of elasticity as shown in Fig. 4.25. At 3 days hydration, the modulus of elasticity value of OPC, 9.9 GPa, is reduced to 2.5 GPa when the 50% fly ash is added. It increases however to 7.0 GPa when 20% nano-sized $CaCO_3$ is added. The determinations of microhardness and modulus of elasticity have evidently indicated that the rate of early development of mechanical properties of OPC paste containing 50% fly ash was greatly improved by the additions of nano-sized $CaCO_3$.

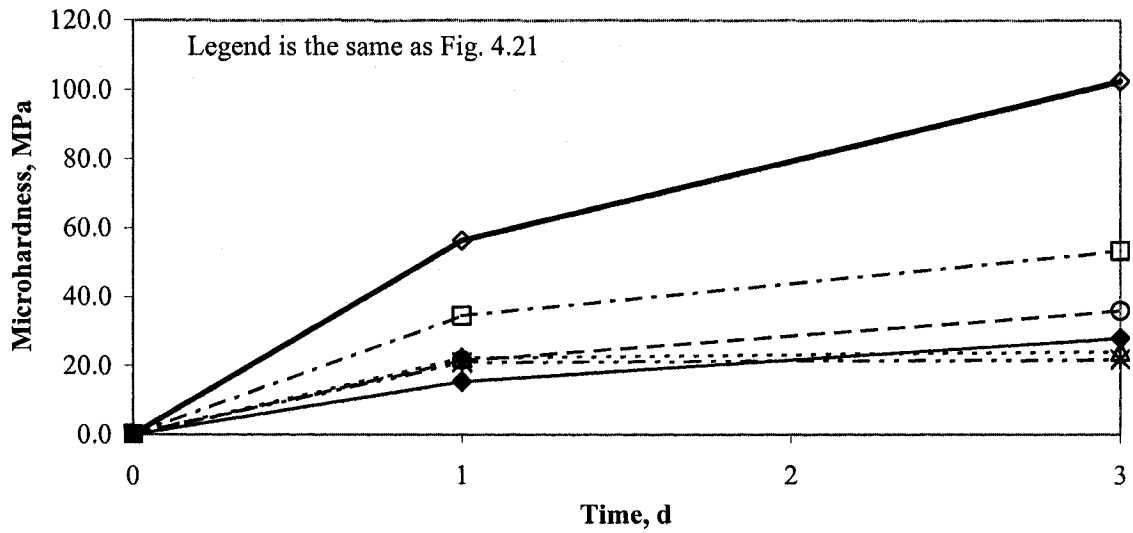

Fig. 4.24 Microhardness results for OPC, OPC containing 50% fly ash and OPC containing 50% fly ash with the additions of micro- and nano-sized $CaCO_3$ for w/c 0.50 hydrated up to 3 days

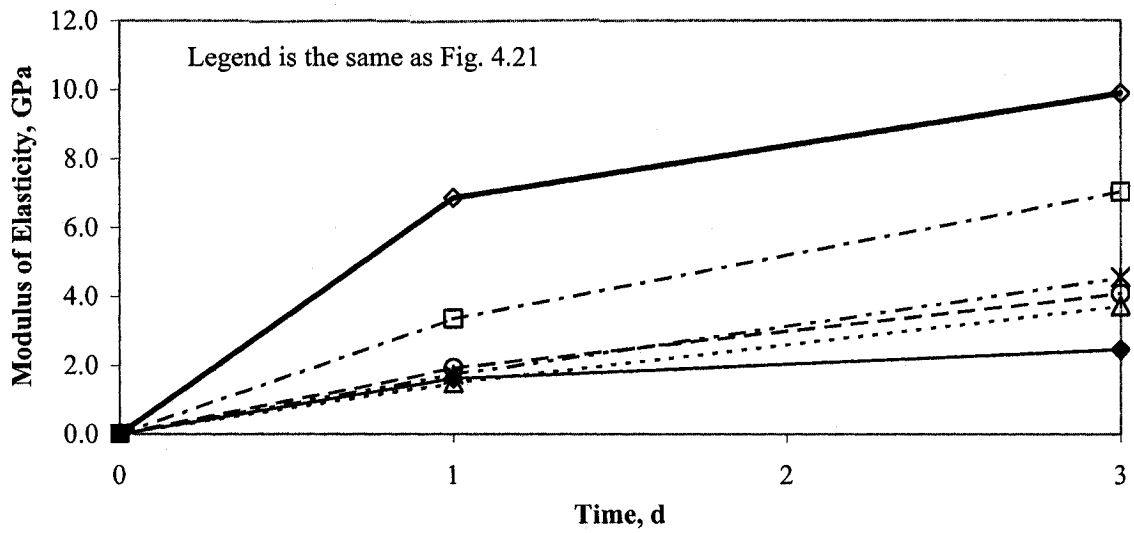

Fig. 4.25 Modulus of elasticity results for OPC, OPC containing 50% fly ash and OPC containing 50% fly ash with the additions of micro- and nano-sized $CaCO_3$ for w/c 0.50 hydrated up to 3 days

It was suggested previously that some portion of the added $CaCO_3$ reacts during the hydration of OPC to form calcium carboaluminate hydrates. The formation of calcium carboaluminate hydrates, however, is not solely responsible for the improved strength development with the additions of nano-sized $CaCO_3$. It may not even be relevant to the improvement of strength development. One of the reasons is that the high carbonate form of calcium aluminate hydrates, $3CaO{\cdot}Al_2O_3{\cdot}3CaCO_3{\cdot}32H_2O$, detected by the calorimetry in Fig. 4.15 and the SEM analysis in Fig. 4.16 (b) respectively, might not contribute significantly to the strength development. This argument assumes that its behaviour is analogous with ettringite, which would appear to have a small direct effect on the strength development. Another reason might be that, in addition to the small shoulder of the calorimetry curve, the main peak of the calorimetry curve was enhanced and accelerated by the additions of nano-sized $CaCO_3$ as shown in Fig. 4.15. This main peak is primarily attributed to the hydration of C_3S that is the key part of strength development. It is apparent that the accelerated hydration of C_3S in the OPC is responsible for this significant strength development. The study on the hydration of C_3S with the finely ground limestone addition mentioned earlier noted that the products formed between the hydrating C_3S and the added $CaCO_3$ could not be identified, as they were present in only small amounts (Ramachandran and Zhang, 1986). This suggests that there must be something else responsible for accelerating the C_3S hydration and for the significant strength development. One possibility is that the nano-sized $CaCO_3$

particles act as nucleation sites to accelerate the cement hydration process. The effect of two calcareous fillers, ground limestone and reagent grade $CaCO_3$ on the compressive strength of OPC was studied and it was argued that the calcareous fillers acted as nucleation sites responsible for the accelerating effect on the rate of early strength development (Soroka and Stern, 1976). The formation of C-S-H and/or $Ca(OH)_2$ may be accelerated by the nano-sized particles of $CaCO_3$. This could explain the lower efficacy of the micro-sized $CaCO_3$ addition, as opposed to the nano-sized $CaCO_3$ addition on the strength development. The micro-sized $CaCO_3$ would be too large to function as effective nucleation sites.

The specimens of OPC, OPC containing 50% fly ash and OPC containing 50% fly ash with the additions of micro- and nano-sized $CaCO_3$ for w/c 0.50 were cured in a 100% RH environment at 5°C, instead of 23°C, to observe the effect of low temperature curing condition. The results of microhardness and modulus of elasticity are shown in Figs. 4.26 and 4.27, respectively. The missing data in the figures are due to the insufficient strength of specimens to be tested because of the low temperature curing. At 1 day, the microhardness values for only OPC and OPC containing fly ash with 20% nano-sized $CaCO_3$ were measurable, indicating how effective the addition of the nano-sized $CaCO_3$ is to accelerate the hydration of OPC containing high volumes of fly ash and to gain a certain amount of strength at 1 day hydration even in the low temperature curing environment. At 2 days hydration, the microhardness values of both OPC containing 50% fly ash with 10% nano-sized $CaCO_3$ and 20% micro-sized $CaCO_3$ were measurable. At 3 days hydration, the OPC containing 50% fly ash and that with 10% micro-sized $CaCO_3$ were finally strong enough to be tested. As for the modulus of elasticity, it is more obvious that the specimens for OPC containing 50% fly ash and those with 10% and 20% micro-sized $CaCO_3$ gained basically no modulus of elasticity for the first 3 days when cured at 5°C. The addition of 20% nano-sized $CaCO_3$ to OPC containing 50% fly ash, however, made the measurements possible as well as those of the control OPC.

4.3.3.2 Late Hydration (3 ~ 28 Days)

In Section 4.3.3.1, the effect of the additions of both micro- and nano-sized $CaCO_3$ on the hydration of OPC containing 50% fly ash was investigated for the early hydration (0 ~ 3 days), and it was observed that the additions of 10% and 20% nano-sized $CaCO_3$ accelerated the hydration of OPC containing 50% fly ash and the mechanical properties were significantly improved, especially by the addition of 20% nano-sized $CaCO_3$. The mechanical properties were also effectively improved by the addition of 20% nano-sized $CaCO_3$ even for the specimens cured at 5°C which

simulated a typical construction environment in winter. In this section, the characteristics and properties of the OPC containing high volumes of fly ash with the micro- and nano-sized $CaCO_3$ additions were studied for late hydration (3 ~ 28 days) to examine how the accelerated early hydration of OPC containing 50% fly ash by the nano-sized $CaCO_3$ addition affects the late hydration. The porosity determinations were also performed along with those of microhardness and modulus of elasticity. The relation between the mechanical properties and porosity was investigated.

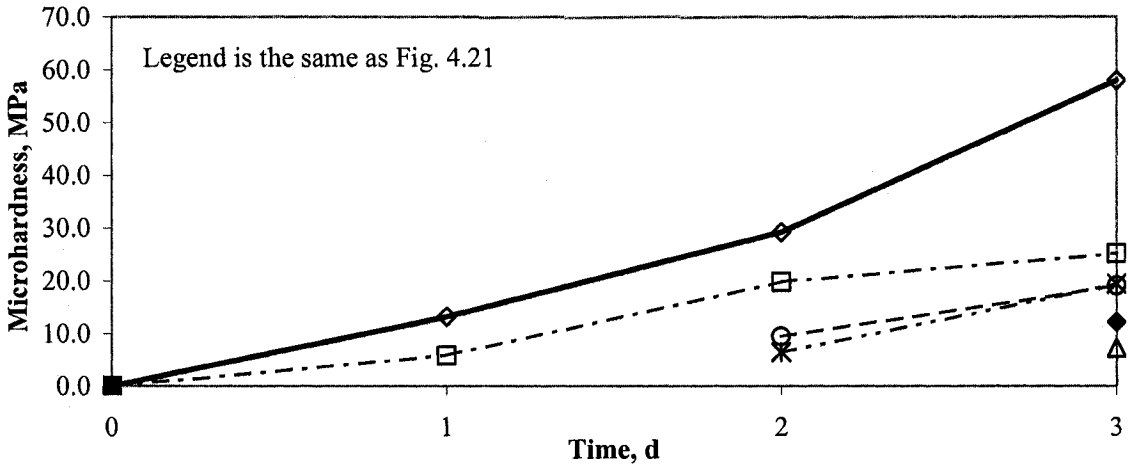

Fig. 4.26 Microhardness results for OPC, OPC containing 50% fly ash and OPC containing 50% fly ash with the additions of micro- and nano-sized $CaCO_3$ for w/c 0.50 cured at 5°C, hydrated up to 3 days

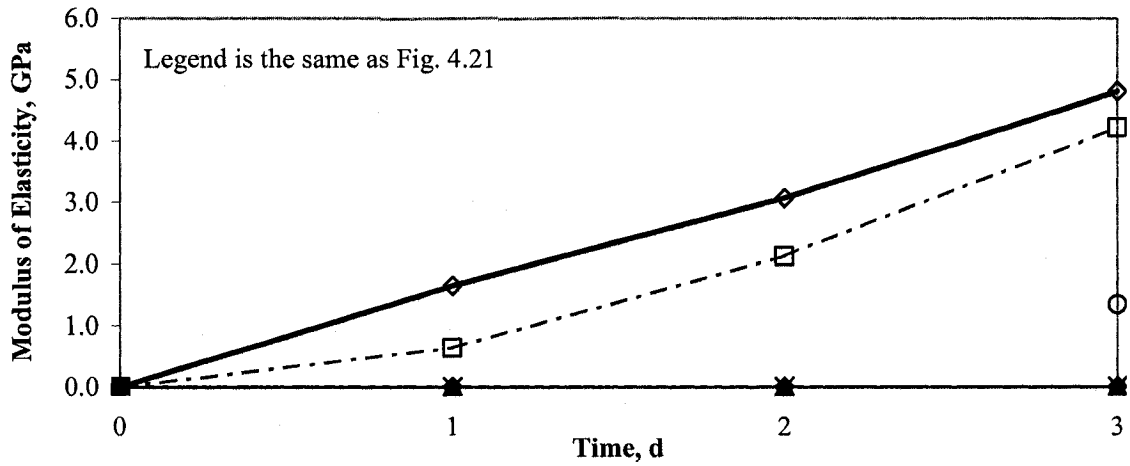

Fig. 4.27 Modulus of elasticity results for OPC, OPC containing 50% fly ash and OPC containing 50% fly ash with the additions of micro- and nano-sized $CaCO_3$ for w/c 0.50 cured at 5°C, hydrated up to 3 days

The amounts of $Ca(OH)_2$, determined by TGA, for OPC, OPC containing 50% fly ash and OPC containing 50% fly ash with the additions of micro- and nano-sized $CaCO_3$ for w/c ratio 0.50 hydrated up to 28 days, are shown in Fig. 4.28. All the specimens, except control OPC, produced relatively low amounts of $Ca(OH)_2$ through the 28 days hydration, indicating that a 50% fly ash has a significant influence on the amounts of $Ca(OH)_2$ produced with or without the accelerating effect of the nano-sized $CaCO_3$ addition. It can be suggested that the consumption of $Ca(OH)_2$ by the pozzolanic reaction is still greater at 28 days hydration than the production of $Ca(OH)_2$ by the accelerated hydration. At 7, 14 and 28 days hydration, the OPC containing fly ash with 20% nano-sized $CaCO_3$ has the least amount of $Ca(OH)_2$ in the specimen. This might be an evidence that the nano-sized $CaCO_3$ accelerates the pozzolanic reaction as well as the OPC hydration.

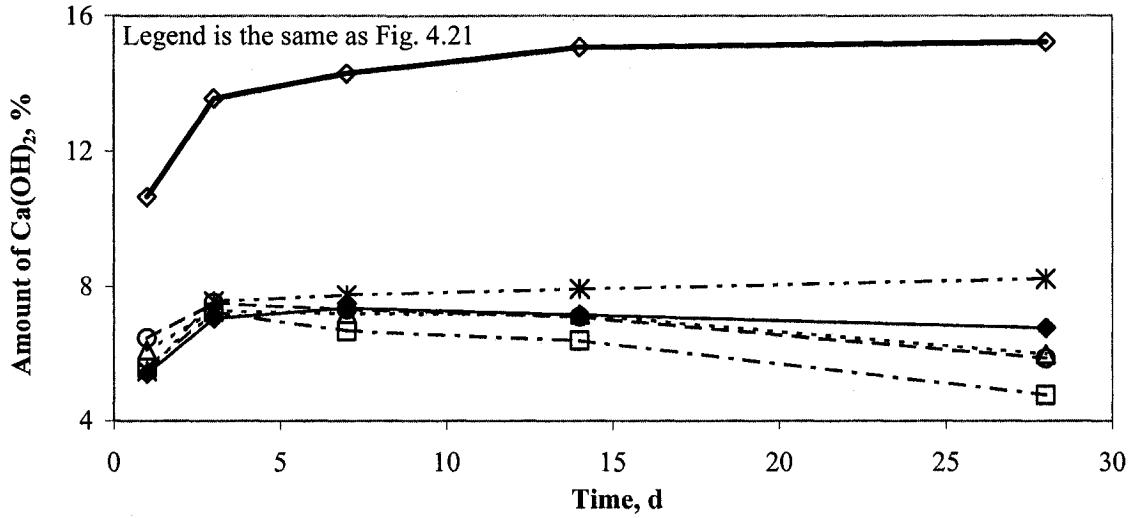

Fig. 4.28 The amounts of $Ca(OH)_2$ for OPC, OPC containing 50% fly ash and OPC containing 50% fly ash with the additions of micro- and nano-sized $CaCO_3$ for w/c 0.50 hydrated up to 28 days, determined by TGA

The results of microhardness and modulus of elasticity for OPC, OPC containing 50% fly ash, OPC containing 50% fly ash with the additions of micro- and nano-sized $CaCO_3$ for w/c 0.50 hydrated up to 28 days are shown in Figs. 4.29 and 4.30, respectively. As mentioned earlier, the accelerated reaction in the early hydration often decelerates the long-term strength development. The addition of 20% nano-sized $CaCO_3$ significantly accelerated the early hydration of OPC containing 50% fly ash, and therefore the decelerated strength development may be expected for a long-term hydration. It is however clearly illustrated in Fig. 4.29 that the addition of 20% nano-sized $CaCO_3$ contributes to the strength development even at 28 days hydration. The microhardness value for OPC at 28 days hydration is 163.9 MPa, whereas that for OPC containing 50% fly

ash and that for OPC containing 50% fly ash with 20% nano-sized $CaCO_3$ are 45.7 MPa and 94.4 MPa, respectively. The very similar results are shown in Fig. 4.30 where the additions of $CaCO_3$ significantly contribute to the development of modulus of elasticity at 28 days hydration. It can be observed in both Figs. 4.29 and 4.30 that the results of mechanical properties for the specimens with micro-sized $CaCO_3$, especially 20% content, are relatively scattered. This might be owing to the fact that the average size of micro-sized $CaCO_3$ crystals is much larger than that of nano-sized $CaCO_3$ crystals, as shown in Fig. 4.1. The nano-sized $CaCO_3$ would be dispersed throughout a specimen more uniformly than the micro-sized $CaCO_3$. Assuming the values of density of both types of $CaCO_3$ are similar, the specimen containing 20% micro-sized $CaCO_3$ would be less homogeneous than that containing 20% nano-sized $CaCO_3$, and therefore the results could be more scattered.

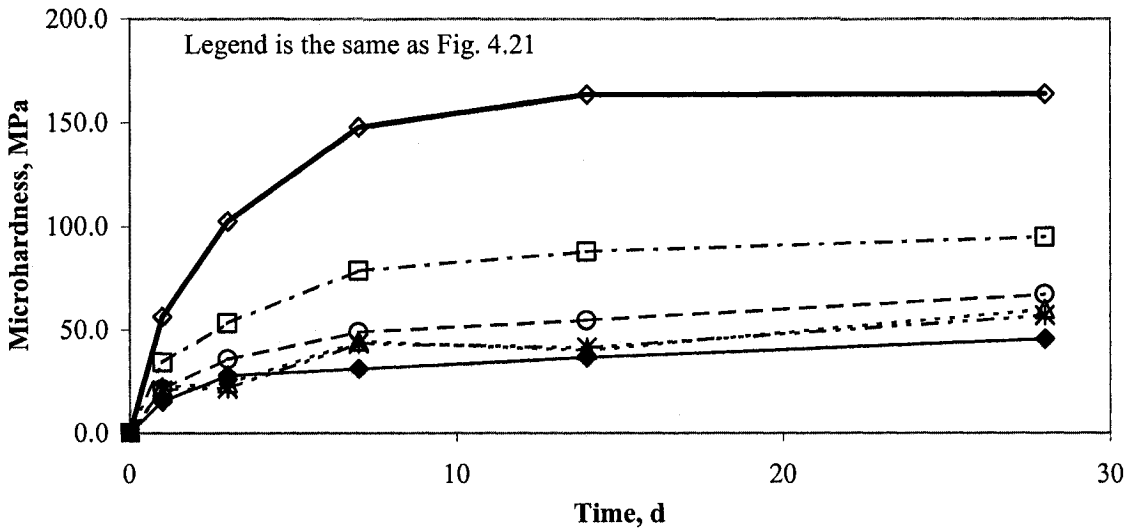

Fig. 4.29 Microhardness results for OPC, OPC containing 50% fly ash and OPC containing 50% fly ash with the additions of micro- and nano-sized $CaCO_3$ for w/c 0.50 hydrated up to 28 days

In addition to determinations of microhardness and modulus of elasticity, the determination of porosity was performed by the helium pycnometer. The porosity results for OPC, OPC containing 50% fly ash, OPC containing 50% fly ash with the additions of micro- and nano-sized $CaCO_3$ for w/c 0.50 hydrated up to 28 days are shown in Fig. 4.31. The porosity values decrease as the hydration takes place, although the curves are not necessarily in order as clearly as expected. The curves of OPC is at the bottom followed by the OPC containing 50% fly ash with the addition of 20% nano-sized $CaCO_3$, as expected. The rest of the curves are, however, rather scattered, especially the OPC containing 50% fly ash that was expected to have very high values of porosity, in

correlation with the very poor mechanical properties. In the following discussion, the mechanical properties, microhardness and modulus of elasticity will be examined in terms of porosity. The variable "Time (hydration period)" will be removed by plotting the mechanical properties versus porosity.

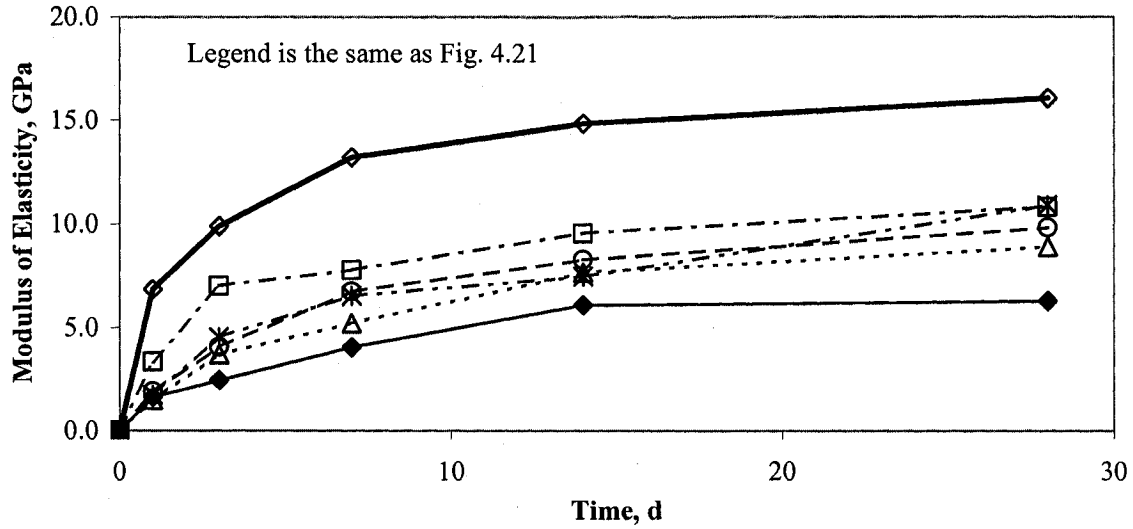

Fig. 4.30 Modulus of elasticity results for OPC, OPC containing 50% fly ash and OPC containing 50% fly ash with the additions of micro- and nano-sized $CaCO_3$ for w/c 0.50 hydrated up to 28 days

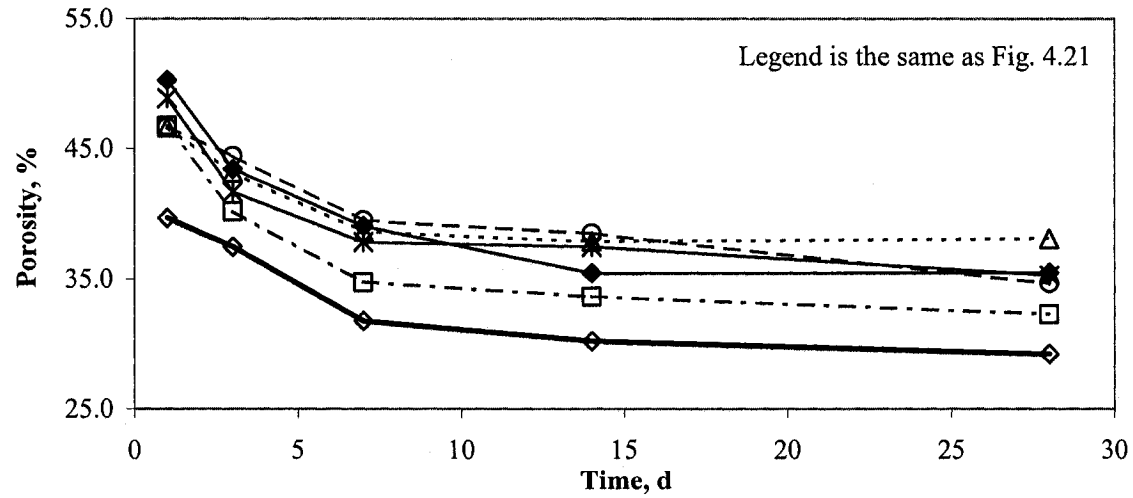

Fig. 4.31 Porosity results for OPC, OPC containing 50% fly ash and OPC containing 50% fly ash with the additions of micro- and nano-sized $CaCO_3$ for w/c 0.50 hydrated up to 28 days

A relationship between porosity and the mechanical properties such as compressive strength, microhardness and modulus of elasticity has been intensively studied. The total porosity has been shown to be one of the major parameters controlling the mechanical properties of porous bodies. Sereda (1972) studied the microhardness of porous and non-porous materials of halite (sodium chloride) and selenite (calcium sulphate) by determining the relationship between porosity and microhardness. Soroka and Sereda (1968) investigated the relation between hardness, modulus of elasticity and porosity of cement pastes to elucidate the interparticle bonding within the cement paste system. Furthermore, the relationship between porosity and the mechanical properties was studied for autoclaved calcium silicate systems (Beaudoin and Feldman, 1975), magnesium oxychloride (Beaudoin and Ramachandran, 1975) and cement paste containing finely divided sulphur (Feldman and Beaudoin, 1976). Feldman and Beaudoin (1976) suggested that an optimum balance between relatively denser, well-crystalline material and less dense, poorly crystalline material results in the highest strength at a specific porosity. Taylor (1977) and Crennan et al. (1977) applied the porosity versus mechanical properties approach to explain the effect of particle size and porosity on strength of C-S-H. Beaudoin (1983) later studied the dependence of the mechanical properties of compacted $Ca(OH)_2$ with porosity by changing the compaction pressure.

The logarithms of microhardness values versus porosity for OPC, OPC containing 50% fly ash and OPC containing 50% fly ash with the additions of micro- and nano-sized $CaCO_3$ for w/c 0.50 are shown in Fig. 4.32. The figure indicates that the OPC has the highest values of microhardness and OPC containing 50% fly ash the lowest. The microhardness values between those two specimens are in the following order, OPC containing 50% fly ash with 20% nano-sized $CaCO_3$ > 10% nano-sized $CaCO_3$ > 20% micro-sized $CaCO_3$ and 10% micro-sized $CaCO_3$. This trend was not clearly observed in the figure of porosity versus time as shown in Fig. 4.31. It is also illustrated in the figure that the lower the porosity, the higher is the microhardness for each specimen. An empirical relation between microhardness and porosity has been suggested by Sereda (1972) and many others as follows:

$$H = H_o \exp(-b_H P_r) \tag{4.1}$$

where H = microhardness

H_o = microhardness at zero porosity

b_H = empirical constant which is the slope of the respective log plot

P_r = porosity

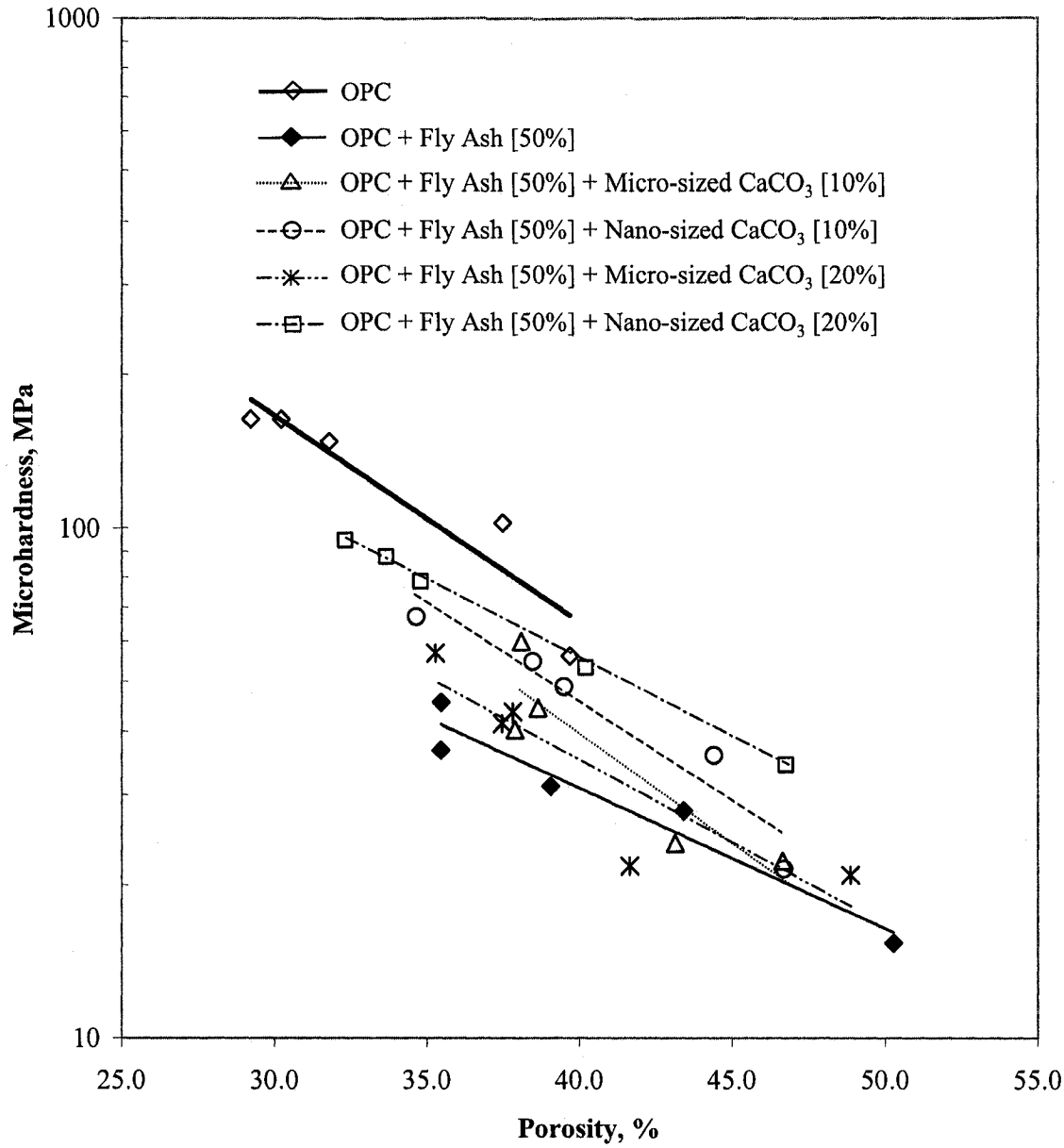

Fig. 4.32 The logarithms of microhardness values versus porosity for OPC, OPC containing 50% fly ash and OPC containing 50% fly ash with the additions of micro- and nano-sized $CaCO_3$ for w/c 0.50

Equation (4.1) was derived based on the assumptions; that one type of pore geometry and orientation of pores with respect to applied stress and that the equation does not hold for higher porosities (> 50%). The values of H_o and b_H for each specimen shown in Fig. 4.32 are tabulated in Table 4.5. The values of H_o, microhardness at zero porosity are indicative of "intrinsic strength"

(Feldman and Beaudoin, 1976) that essentially is the strength of the solid phase of cement paste with no pores. The intrinsic strength of OPC is significantly greater than that of OPC containing 50% fly ash. The value of b_H indicates how much the porosity affects the strength. The higher the b_H is, the greater is the change in strength associated with the change in porosity. The value of b_H for OPC is 0.0931 whereas that for OPC containing 50% fly ash is 0.0633 which indicates that the change in porosity affects that in strength for OPC more than that for OPC containing 50% fly ash.

Table. 4.5 The values of H_o and b_H responding to the curves in Fig. 4.32

	H_o, MPa	b_H
OPC	2718.4	0.0931
OPC containing 50% Fly Ash	390.2	0.0633
OPC containing 50% Fly Ash + 10% Micro-sized $CaCO_3$	2001.8	0.0985
OPC containing 50% Fly Ash + 10% Nano-sized $CaCO_3$	1576.0	0.0886
OPC containing 50% Fly Ash + 20% Micro-sized $CaCO_3$	680.5	0.0743
OPC containing 50% Fly Ash + 20% Nano-sized $CaCO_3$	930.7	0.0706

The microhardness – porosity results provide a valid comparison for the cement systems studied. The validity of the comparison however could be limited to the porosity range of the experimental data. The physical meaning of hardness values at zero-porosity, H_o, determined by the extrapolation, is complex. The order of these values is not necessarily similar to that obtained for the regression lines. Dense crystalline products, for example, can have hardness values lower or higher than normal OPC paste depending on the porosity range. The effect of grain boundaries and defects at low porosities can contribute to the non-linear behaviour in the microhardness – porosity plots.

The logarithms of modulus of elasticity values versus porosity for OPC, OPC containing 50% fly ash and OPC containing 50% fly ash with the additions of micro- and nano-sized $CaCO_3$ for w/c 0.50 are shown in Fig. 4.33 and the values of E_o and b_E are tabulated in Table 4.6 (E_o and b_E are modulus of elasticity at zero porosity and empirical constant which is the slope of the respective log plot, respectively). The results in Fig. 4.33 are similar in character to those in Fig. 4.32. The OPC has the highest values of the modulus of elasticity followed by the OPC containing fly ash with the addition of 20% nano-sized $CaCO_3$ whereas the OPC containing 50% fly ash generally has the lowest values. The difference from Fig. 4.32 is that the curve for OPC and that for OPC

containing 50% fly ash intersect at porosity of 7.0%. This indicates that when the porosity is higher than 7.0%, the modulus of elasticity for the OPC is greater than that for the OPC containing 50% fly ash and when the porosity is lower than 7.0%, the modulus of elasticity for OPC is lower than that for OPC containing 50% fly ash. This might be affected by many factors including its crystal structure, density and bonding condition.

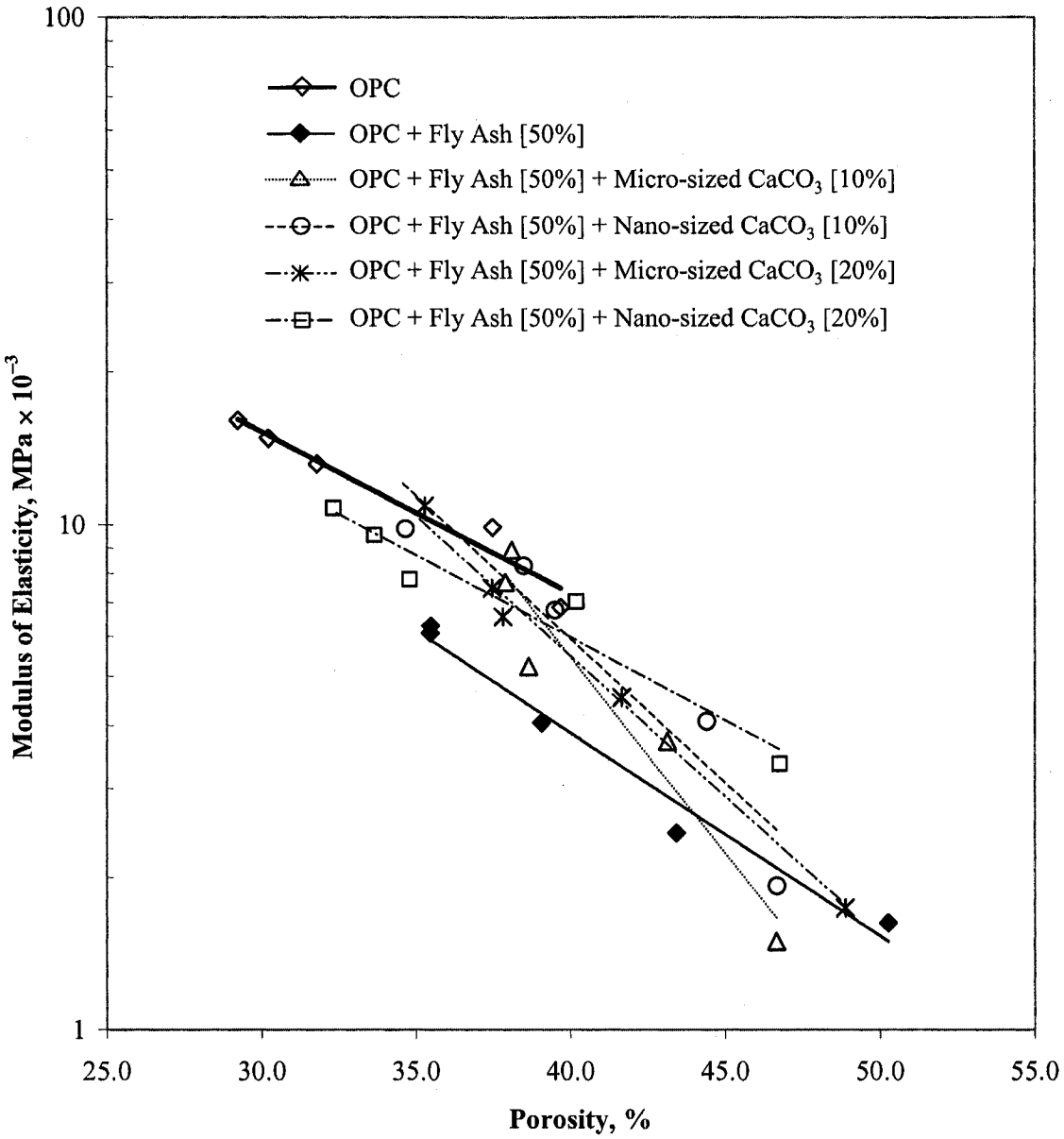

Fig. 4.33 The logarithms of modulus of elasticity values versus porosity for OPC, OPC containing 50% fly ash and OPC containing 50% fly ash with the additions of micro- and nano-sized $CaCO_3$ for w/c 0.50

Table. 4.6 The values of E_o and b_E responding to the curves in Fig. 4.33

	E_o, GPa	b_E
OPC	138.2	0.0735
OPC containing 50% Fly Ash	158.3	0.0928
OPC containing 50% Fly Ash + 10% Micro-sized $CaCO_3$	6262.8	0.1766
OPC containing 50% Fly Ash + 10% Nano-sized $CaCO_3$	1079.4	0.1303
OPC containing 50% Fly Ash + 20% Micro-sized $CaCO_3$	983.2	0.1298
OPC containing 50% Fly Ash + 20% Nano-sized $CaCO_3$	116.4	0.0742

4.3.4 Stage 4: Repeating Experiments with High Volumes of Ground Granulated Blast-furnace Slag

4.3.4.1 Early Hydration (0 ~ 3 Days)

In this section, the ground granulated blast-furnace slag (GGBFS) was used as an SCM instead of fly ash to determine the efficacy of the nano-sized $CaCO_3$ addition in counteracting the delayed hydration of OPC containing high volumes of SCMs other than fly ash. The reaction mechanism of GGBFS is slightly different from that of fly ash. Pozzolanic materials, such as fly ash, chemically react with $Ca(OH)_2$ to form C-S-H and other cementing compounds. With GGBFS, in contrast, $Ca(OH)_2$ functions as an activator, hence only a relatively small amount of $Ca(OH)_2$ is required. It is well known that the hydration is significantly delayed when a mix of OPC contains high volumes of fly ash, as shown in Fig. 4.3, and a similar behaviour with high volumes of GGBFS can be observed in Fig. 4.34. In terms of the peak positions, the OPC containing 50% GGBFS is not delayed as significantly as that containing high volumes of fly ash, however, the rate of heat development is remarkably decreased. This would result in the delay of the rate of early strength development. The values of microhardness and modulus of elasticity for the OPC and OPC containing 50% GGBFS for w/c 0.50 hydrated up to 3 days are shown in Figs. 4.35 and 4.36, respectively. The results are very similar to those for the OPC containing 50% fly ash shown in Figs. 4.7 and 4.8. The development of microhardness was clearly depressed by the high volumes of GGBFS. At 1 day hydration, the microhardness value of OPC is 48.2 MPa whereas that of OPC containing 50% GGBFS is only 12.0 MPa. At 3 days hydration, the difference in microhardness remarkably increases. The same is true for the modulus of elasticity, as shown in Fig. 4.36. The development of the mechanical properties of OPC paste are considerably delayed

at the early hydration, which is critical in terms of construction purposes, when 50% of its content is replaced by the GGBFS.

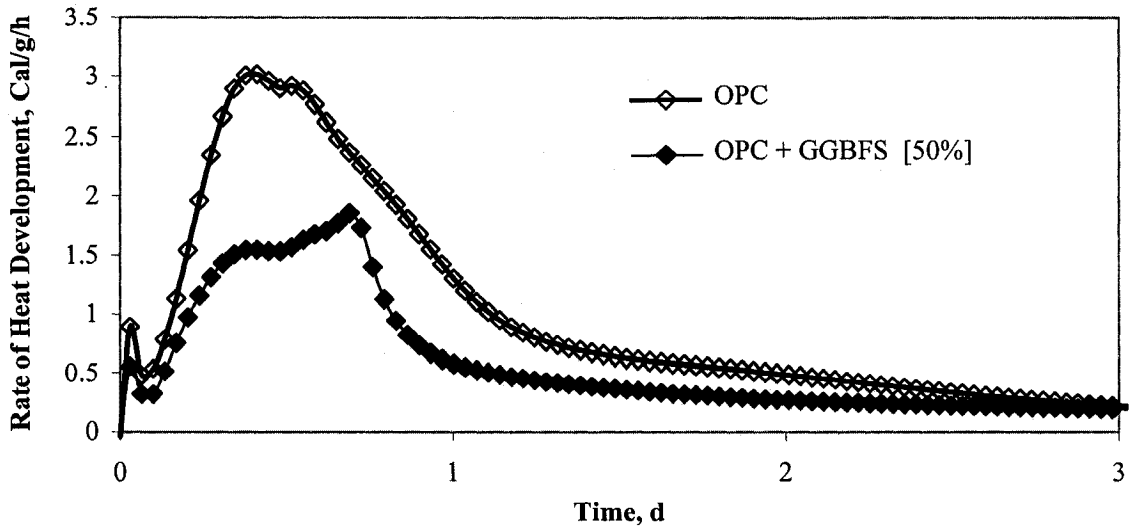

Fig. 4.34 Conduction calorimetry curves for OPC and OPC with 50% GGBFS for w/c 0.50

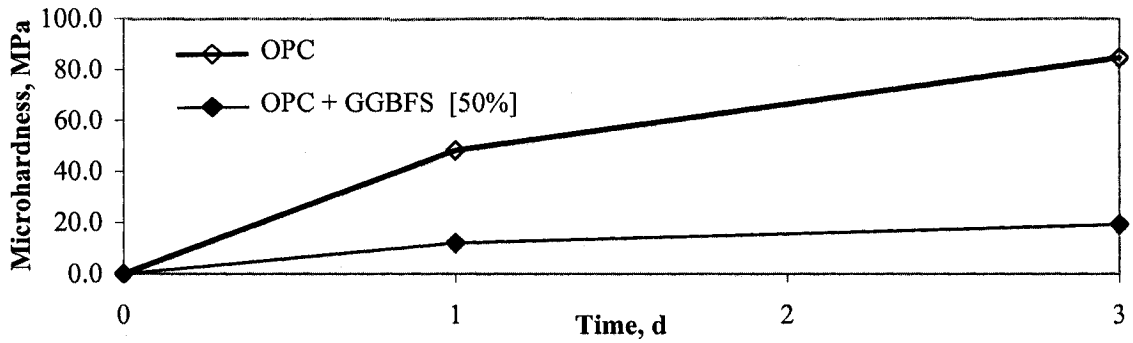

Fig. 4.35 Microhardness results of OPC and OPC containing 50% GGBFS for w/c 0.50 hydrated up to 3 days

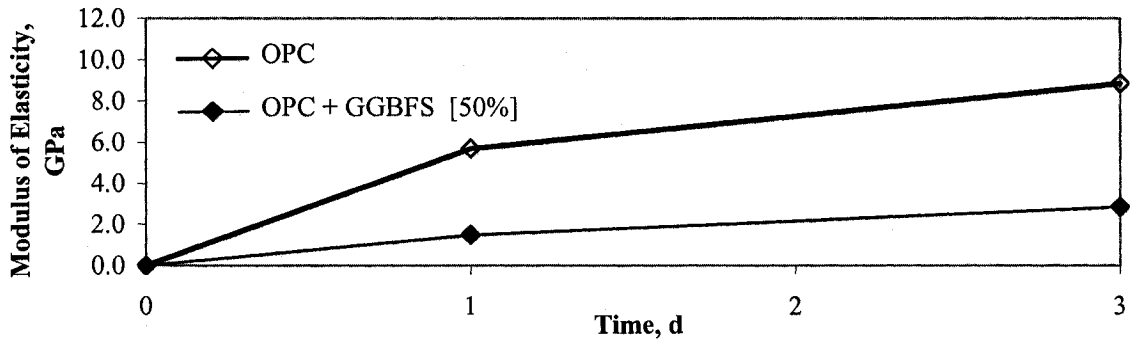

Fig. 4.36 Modulus of elasticity results of OPC and OPC containing 50% GGBFS for w/c 0.50 hydrated up to 3 days

The additions of the nano-sized $CaCO_3$, however, might counteract the delayed early hydration caused by the addition of GGBFS. The conduction calorimetry curves for OPC, OPC containing 50% GGBFS and OPC containing 50% GGBFS with the additions of micro- and nano-sized $CaCO_3$ for w/c 0.50 are shown in Fig. 4.37. The calorimetry curves for OPC containing 50% GGBFS with the additions of both 10% and 20% micro-sized $CaCO_3$ essentially overlap the curve for OPC containing 50% GGBFS, indicating that they have a little or no effect on the hydration of OPC. The rate of heat development is however much improved by the additions of the 10% and 20% nano-sized $CaCO_3$. The considerable improvement on the mechanical properties can be expected.

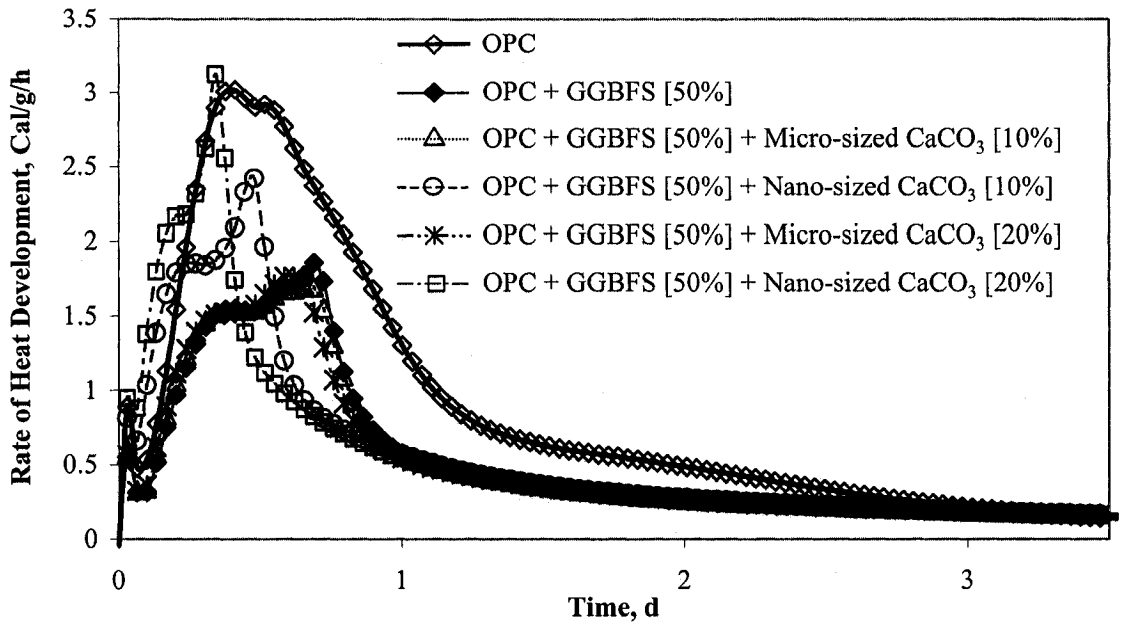

Fig. 4.37 Conduction calorimetry curves for OPC, OPC containing 50% GGBFS and OPC containing 50% GGBFS with the additions of micro- and nano-sized $CaCO_3$ for w/c 0.50

The results of microhardness and modulus of elasticity for the OPC, OPC containing 50% GGBFS and OPC containing 50% GGBFS with the additions of micro- and nano-sized $CaCO_3$ for w/c 0.50 hydrated up to 3 days are shown in Figs. 4.38 and 4.39. The microhardness is significantly improved when the $CaCO_3$ was added to the OPC containing high volumes of GGBFS. The microhardness value at 1 day hydration for the control OPC and that containing 50% GGBFS are 48.2 MPa and 12.0 MPa, respectively. The microhardness value, however, becomes 29.0 MPa when the 20% nano-sized $CaCO_3$ was added. The addition of 10% nano-sized $CaCO_3$ is as effective as that of 20% at 1 day hydration. At 3 days hydration, the effect of the $CaCO_3$ addition was

most significant when the 20% nano-sized $CaCO_3$ was added, followed in the expected order by the 10% nano-sized $CaCO_3$, 20% micro-sized $CaCO_3$ and 10% micro-sized $CaCO_3$. The similar behaviour can be observed for the modulus of elasticity. The modulus of elasticity values at 3 days hydration for OPC and OPC containing 50% GGBFS are 8.9 GPa and 2.8 GPa, respectively. The value for OPC containing GGBFS with 20% nano-sized $CaCO_3$ is however 7.7 GPa. The additions of micro-sized $CaCO_3$ resulted in only a modest effect on the rate of heat development shown in Fig. 4.37. The improvement of strength development by the additions of micro-sized $CaCO_3$, however, can be observed from the results of microhardness and modulus of elasticity. A small difference observed in terms of rate of heat development resulted in a large difference in terms of mechanical properties. Nevertheless, the delayed hydration of OPC paste containing 50% GGBFS was greatly compensated for by the additions of the nano-sized $CaCO_3$, including its mechanical properties for the early hydration.

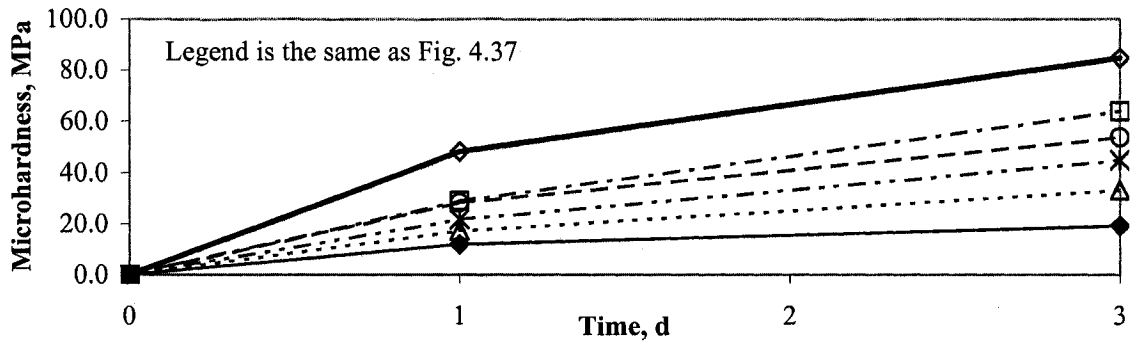

Fig. 4.38 Microhardness results for OPC, OPC containing 50% GGBFS and OPC containing 50% GGBFS with the additions of micro- and nano-sized $CaCO_3$ for w/c 0.50 hydrated up to 3 days

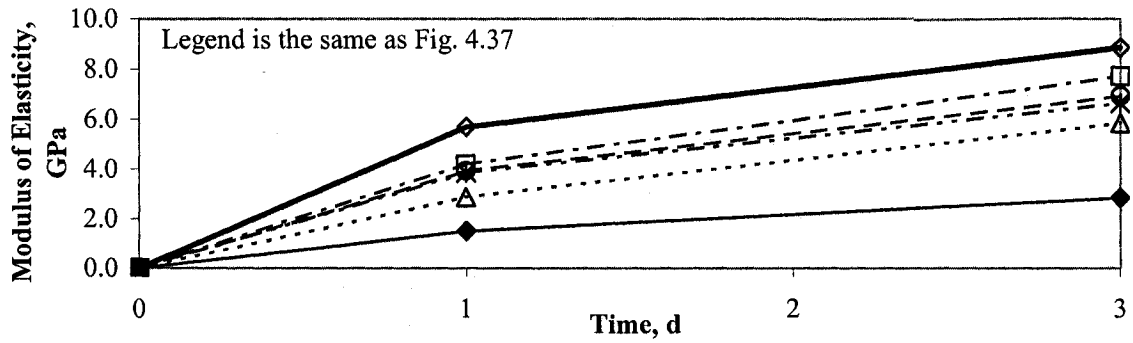

Fig. 4.39 Modulus of elasticity results for OPC, OPC containing 50% GGBFS and OPC containing 50% GGBFS with the additions of micro- and nano-sized $CaCO_3$ for w/c 0.50 hydrated up to 3 days

4.3.4.2 Late Hydration (3 ~ 28 Days)

In the previous section, it was indicated that the additions of the nano-sized $CaCO_3$ improve the mechanical properties of OPC containing 50% GGBFS in the early hydration. In this section, the effect of the additions of the nano-sized $CaCO_3$ on the long-term hydration was investigated. The results of microhardness and modulus of elasticity for the OPC and OPC containing 50% GGBFS with the additions of micro- and nano-sized $CaCO_3$ for w/c 0.50 hydrated up to 28 days are shown in Figs. 4.40 and 4.41, respectively.

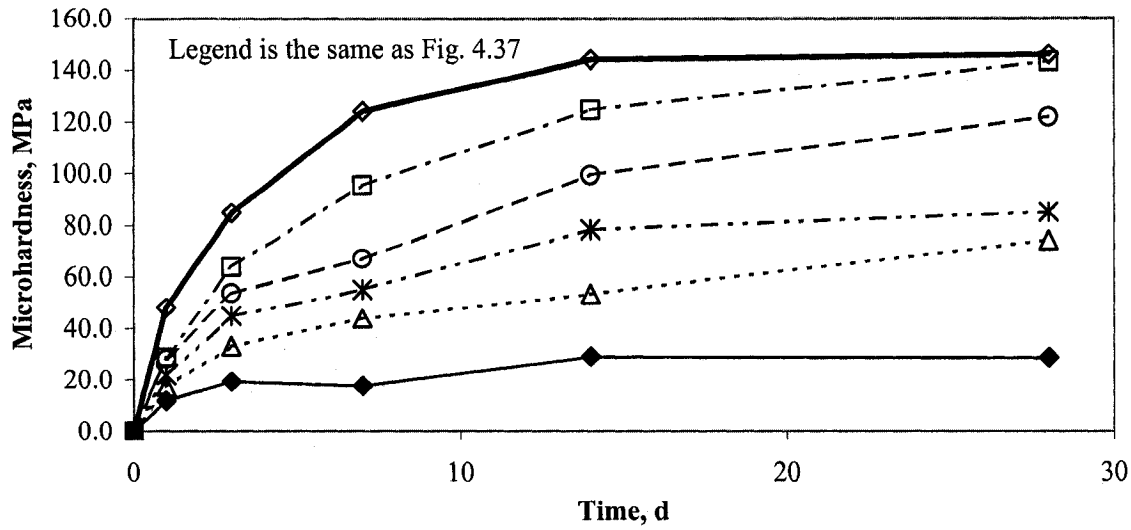

Fig. 4.40 Microhardness results for OPC, OPC containing 50% GGBFS and OPC containing 50% GGBFS with the additions of micro- and nano-sized $CaCO_3$ for w/c 0.50 hydrated up to 28 days

Throughout the hydration, the microhardness values for OPC containing 50% GGBFS are much lower than those for control OPC. At 28 days hydration, the microhardness value for control OPC is 145.7 MPa whereas that for OPC containing 50% GGBFS is 28.7 MPa. It is clear the high volumes of GGBFS in the specimen delayed the strength development in a long-term hydration. However, it is also clear that the additions of $CaCO_3$ have a significant effect on the hydration of OPC containing high volumes of GGBFS. The strength development is considerable not only in the early hydration but also in the late hydration. The accelerating effect in the early hydration generally depresses the strength development in a long-term hydration, however, in the case of the additions of nano-sized $CaCO_3$, the strength development continues up to 28 days. The addition of the 20% nano-sized $CaCO_3$ improves the microhardness development of OPC containing 50% GGBFS almost as high as the control OPC at 28 days hydration. As for the addition of the

micro-sized $CaCO_3$, a different behaviour from that with fly ash can be observed. As shown in Fig. 4.29, the additions of micro-sized $CaCO_3$ had a very little effect on the microhardness development of the OPC containing 50% fly ash. In the case of the OPC containing 50% GGBFS, however, even the additions of the micro-sized $CaCO_3$ seem to have a recognizable effect on the microhardness development. This might imply that the hydration products by the reaction between OPC containing fly ash and added $CaCO_3$ are slightly different from those by the reaction between OPC containing GGBFS and added $CaCO_3$ and result in a difference in strength development. The improvement of the modulus of elasticity is not as obvious as that of microhardness, but the positive effect of the nano-sized $CaCO_3$ addition on the modulus of elasticity development can definitely be observed as shown in Fig. 4.41. These results suggest that the accelerated early hydration does not slow down but contributes to the strength development in the long-term hydration.

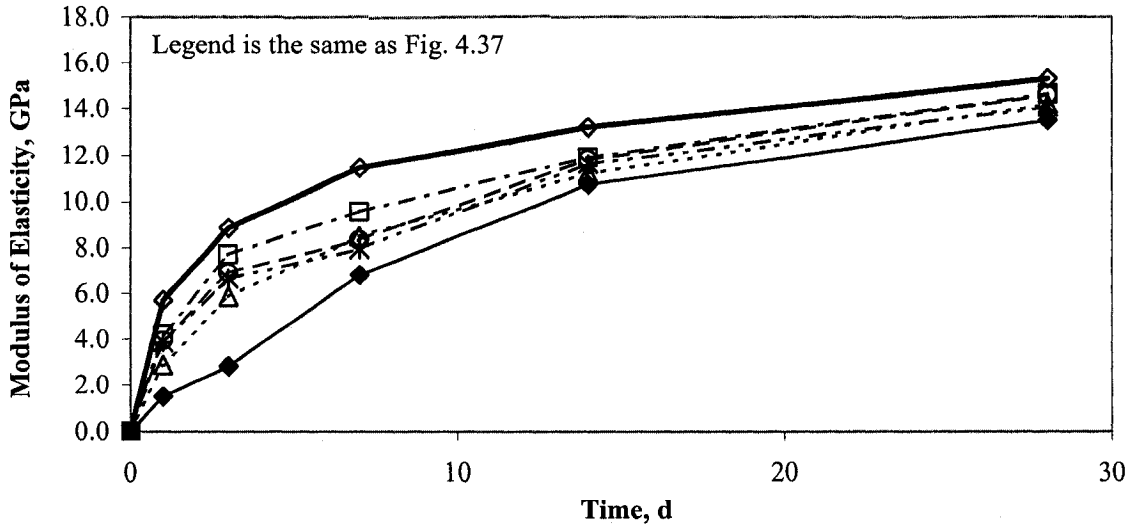

Fig. 4.41 Modulus of elasticity results for OPC, OPC containing 50% GGBFS and OPC containing 50% GGBFS with the additions of micro- and nano-sized $CaCO_3$ for w/c 0.50 hydrated up to 28 days

The logarithms of microhardness values versus porosity for OPC, OPC containing 50% GGBFS and OPC containing 50% GGBFS with the additions of micro- and nano-sized $CaCO_3$ for w/c 0.50 are shown in Fig. 4.42. The data points for OPC containing 50% GGBFS are located well below the data points for control OPC. The effect of the added $CaCO_3$ is in the expected order, depending on its content and size. The microhardness values of OPC containing GGBFS with 20% nano-sized $CaCO_3$ are even higher than those of control OPC when the porosity is lower

than 41%, where the two curves intersect. The values of H_o and b_H for each specimen shown in Fig. 4.42 are tabulated in Table 4.7. The value of intrinsic strength for the OPC containing 50% GGBFS is much lower than that for the control OPC. It is however significantly improved by the additions of both 10% and 20% nano-sized $CaCO_3$, as shown in the results obtained.

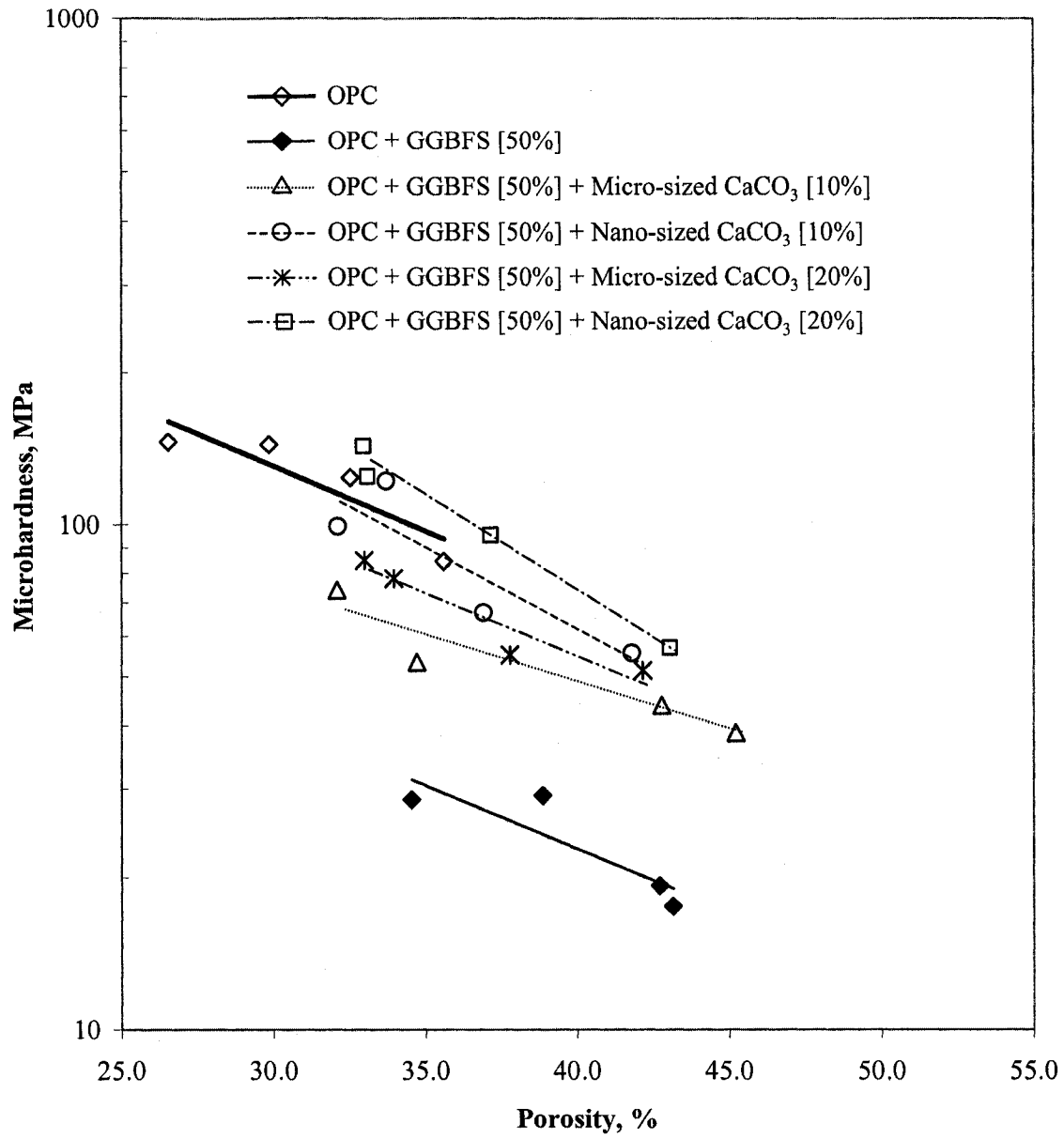

Fig. 4.42 The logarithms of microhardness values versus porosity for OPC, OPC containing 50% GGBFS and OPC containing 50% GGBFS with the additions of micro- and nano-sized $CaCO_3$ for w/c 0.50

Table. 4.7 The values of H_o and b_H responding to the curves in Fig. 4.42

	H_o, MPa	b_H
OPC	766.3	0.0590
OPC containing 50% GGBFS	231.1	0.0579
OPC containing 50% GGBFS + 10% Micro-sized $CaCO_3$	265.0	0.0425
OPC containing 50% GGBFS + 10% Nano-sized $CaCO_3$	1203.8	0.0743
OPC containing 50% GGBFS + 20% Micro-sized $CaCO_3$	526.1	0.0565
OPC containing 50% GGBFS + 20% Nano-sized $CaCO_3$	2179.4	0.0845

CHAPTER 5

THEME 2: THE SYNTHESIS AND CHARACTERIZATION OF THE HIGHLY REACTIVE NANO-SIZED β-C_2S BY THE SUCROSE METHOD

5.1 Introduction

Theme 2 of this thesis: The Synthesis and Characterization of the Highly Reactive Nano-sized β-C_2S by the Sucrose Method, is described in Chapter 5 including the experimental and analytical approaches, materials, specimen preparation, results and discussion. In the first section, the detailed experimental and analytical approaches are presented, followed by a description of the Sucrose method including materials and specimen preparation. In the following section, the results and discussion are presented. All the experimental techniques used to obtain the results are described in Chapter 3, unless otherwise stated.

5.2 Experimental

5.2.1 Experimental and Analytical Approaches

A key element of Theme 2 was to synthesize a highly reactive nano-sized β-C_2S by the Sucrose method. Also an attempt was made to link the chemical synthesis and its effect on engineering

properties. The synthesis process was designed to optimize the fineness of β-C_2S and maximize the mechanical behaviour of the hydrated products. The effect of the changes in the synthesis process was also investigated. The detailed experimental and analytical approaches are summarized in Table. 5.1. The results and discussion are presented in the same chronological manner as shown in the table. In Stage 1, the synthesis and characterization of the highly reactive nano-sized β-C_2S by the Sucrose method were conducted. The Sucrose method was applied for the first time in the field of civil engineering and therefore needed to be modified for the synthesis of a cementitious material. Characterization of the synthesized β-C_2S was conducted by a number of experimental techniques to confirm that the synthesized material was β-C_2S and to optimize its fineness. In Stage 2, the synthesized β-C_2S was mixed with water and its reactivity and hydration characteristics were studied. The conduction calorimetry was used to assess the effect of the difference in surface area on the reactivity. The XRD and TGA revealed the hydration characteristics of the synthesized β-C_2S. The determination of microhardness was performed for the synthesized β-C_2S hydrated for 3, 7, 14 and 28 days. In Stage 3, the amounts of the ingredients were slightly modified according to the observations in Stages 1 and 2 to produce an even finer β-C_2S. Characterization and conduction calorimetry were conducted for this synthesized material.

5.2.2 Materials

The materials used under this theme are sucrose, calcium nitrate, amorphous silica and nitric acid. Reagent grade sucrose was supplied by EMD Chemicals Inc., Gibbstown, New Jersey, USA. Reagent grade calcium nitrate tetrahydrate, $Ca(NO_3)_2{\cdot}4H_2O$, was supplied by Fisher Scientific, Fair Lawn, New Jersey, USA. Its purity was higher than 99%. The amorphous silica, CAB-O-SIL M5, was supplied by Cabot Corporation, Billerica, MA, USA. Its purity was higher than 99.8%. The BET surface area value for the amorphous silica was 200 m^2/g. Nitric acid was supplied by Fisher Scientific, Fair Lawn, New Jersey, USA. Commercially available β-C_2S and C_3S were supplied by Construction Technology Laboratories (CTL), Skokie, Illinois, USA. They were used to compare their hydration characteristics and mechanical properties with those of the synthesized β-C_2S.

Table. 5.1 · The experimental and analytical approaches for Theme 2

Stage 1	Synthesis and characterization of a highly reactive nano-sized β-C_2S by the Sucrose method
	▪ Fineness by BET surface area determination ▪ Material identification by TGA, XRD and NMR ▪ Particle characterization by SEM
Stage 2	Reactivity and hydration of the synthesized highly reactive nano-sized β-C_2S
	▪ Rate of heat development by conduction calorimetry ▪ Hydration products by XRD ▪ Amount of $Ca(OH)_2$ by TGA ▪ Mechanical property by microhardness determination
Stage 3	Quantitative variation of the ingredients for the Sucrose Method
	▪ Modified amount of ingredients ▪ Characterization by TGA, XRD, NMR BET and SEM ▪ Conduction calorimetry

5.2.3 Specimen Preparation (The Sucrose Method)

This section focuses on the experimental procedure of the Sucrose method. Preparation of a 4:1 molar ratio sucrose solution to synthesize C_2S (C_2S is an abbreviation of $2CaO{\cdot}SiO_2$ in cement chemistry) involves the use of the following ingredients: 100 mL of deaerated water, 119.16 g of sucrose, 13.71 g of $Ca(NO_3)_2{\cdot}4H_2O$ and 1.74 g of amorphous silica, SiO_2. The process for the calculation can be followed by the examination of Table. 5.2. The stoichiometry of C_2S requires 2 moles of CaO for 1 mole of SiO_2 (shown in the 3rd column). In order to prepare the 4:1 molar ratio sucrose solution, 12 moles of sucrose are required for 2 moles of CaO and 1 mole of SiO_2. Therefore the amount of each ingredient required to synthesize 1 mole of C_2S can be calculated (4th column). Then the amount of each ingredient required to synthesize 5 g of C_2S can be calculated (5th column). For example, for amorphous silica:

$$\frac{60.09\text{ g of } SiO_2}{1\text{ mol of } C_2S} \cdot \frac{5\text{ g of } C_2S}{172.25\text{ g/mol of } C_2S} = 1.74\text{ g of } SiO_2 \quad (5.1)$$

One hundred mL of deaerated water and 119.16 g of sucrose were placed in a stainless steel bowl and heated to boil on a hot plate. As soon as the solution started boiling, 13.71 g of $Ca(NO_3)_2{\cdot}4H_2O$ and 1.74 g of amorphous silica were added as shown in Fig. 5.1 (a). The pH of the solution was adjusted to 1 by adding the nitric acid. In the aqueous sucrose solution, there are Ca^{2+} ions, SiO_4^{4-} ions, OH^- ions and sucrose as shown in Fig. 5.1 (b). The temperature of the solution was kept approximately at 150°C. The ions are separated from each other in the solution. As soon as the water is evaporated and removed from the system, however, sucrose starts to bond together with Ca^{2+} and SiO_4^{4-} ions as shown in Fig. 5.1 (c). This is referred to as chelating and is enhanced by keeping the pH of solution low. Once all the water has been evaporated, the sucrose caramelizes and a highly viscous and porous liquid results as shown in Fig. 5.1 (d). The process of caramelization is very important for forming nano-sized particles, because the sucrose keeps the Ca^{2+} and SiO_4^{4-} ions separated instead of agglomerating into relatively larger particles. The bowl was placed in a 120°C oven for one day, after caramelizing for 30 minutes on the hot plate. This resulted in the dehydrated charred resin as shown in Fig. 5.1 (e). This charred mass was broken down and ground to smaller pieces and placed in aluminum dishes as shown in Fig. 5.1 (f). The calcination was conducted by placing those dishes into a muffle furnace at certain temperatures (600, 700, 800, 900 and 1000°C) for certain periods (6 and 9 hours) to burn off the sucrose. The Ca^{2+} and SiO_4^{4-} ions, which were held and kept separated by sucrose, finally bond together to form a nano-sized C_2S as shown in Fig. 5.1 (g). A water to cementitious solid (w/c) ratio of 2.0 was used when the synthesized nano-sized C_2S was mixed with water, owing to the extreme fineness of the synthesized material.

Table. 5.2 Calculation of quantities of the ingredients for the Sucrose method

	Molar Mass	Ratio of Moles Required	For 1 Mole of C_2S	For 5g of C_2S
C_2S [$2CaO{\cdot}SiO_2$]	172.25 g	-	-	-
Sucrose [$C_{12}H_{22}O_{11}$]	342.10 g	12	4105.20 g	119.16 g
$Ca(NO_3)_2{\cdot}4H_2O$	236.10 g	2	472.20 g	13.71 g
Amorphous Silica [SiO_2]	60.09 g	1	60.09 g	1.74 g

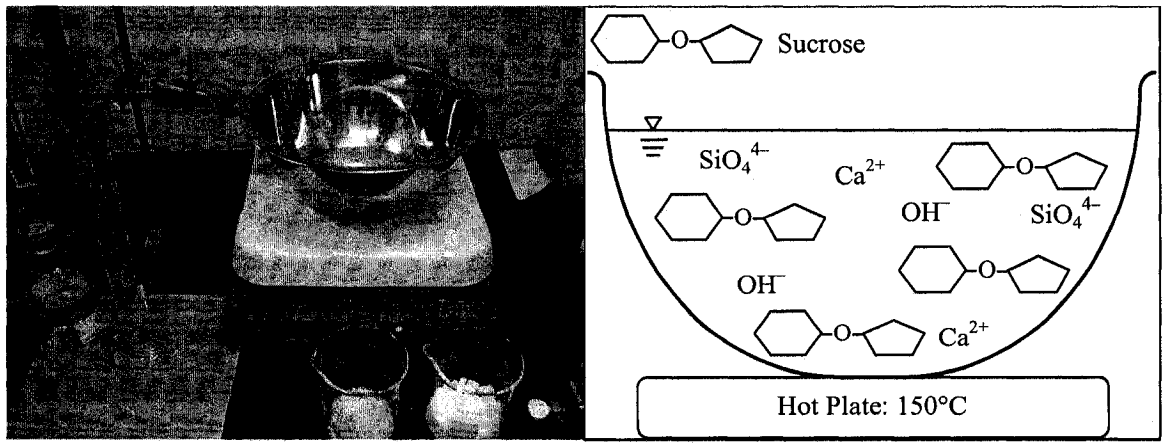

(a) (b)

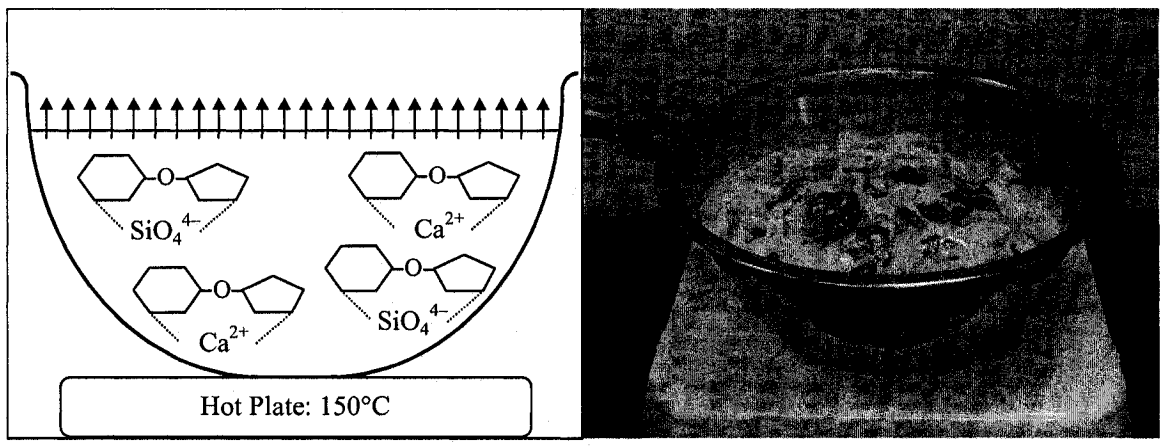

(c) (d)

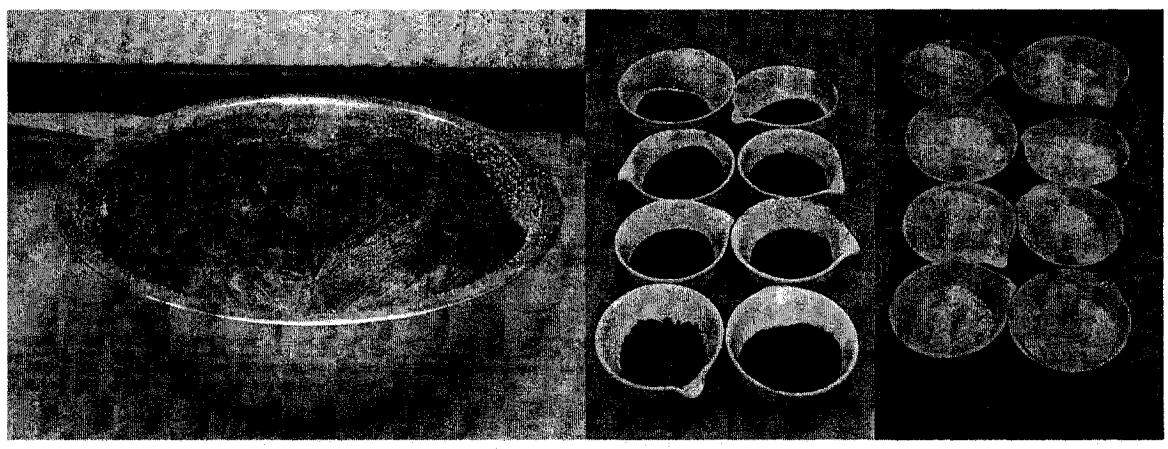

(e) (f) (g)

Fig. 5.1 A synthesis process of β-C_2S by the Sucrose Method

5.3 Results and Discussion

5.3.1 Stage 1: Synthesis and Characterization of the Highly Reactive Nano-sized β-C_2S by the Sucrose Method

As mentioned at the end of the previous section, the calcination was conducted at 600, 700, 800, 900 and 1000°C for 6 and 9 hours. The results of the BET surface area for the synthesized β-C_2S are shown in Fig. 5.2 which indicates that the lower the calcination temperature and the shorter the calcination duration, the higher are the values of the BET surface area of the synthesized β-C_2S. The BET surface area value of the β-C_2S calcined at 600°C for 6 hours is 47.3 m^2/g whereas that calcined at 1000°C for 6 hours is 2.9 m^2/g. The BET surface area value calcined at 1000°C is very close to that of the commercially available β-C_2S, which is 2.4 m^2/g. The shorter the calcination duration, the higher are the values of the BET surface area for the same calcination temperature. The BET surface area value of the β-C_2S calcined for 6 hours at 600°C is 47.3 m^2/g whereas that calcined for 9 hours at 600°C is 43.6 m^2/g. The difference in the resulting surface area values owing to the calcination duration is smaller than that owing to the calcination temperature. A specimen was however calcined at 600°C for 20 hours to observe the enhanced effect of calcination duration and the resulting surface area value was 37.8 m^2/g. The longer calcination duration definitely decreases the surface area of the synthesized β-C_2S. In order to optimize the surface area of the synthesized β-C_2S, a specimen was calcined at 500°C for 6 hours and at 600°C for 5 hours, respectively. The calcination process, however, was not completed by calcining at 500°C for 6 hours or at 600°C for 5 hours. The brown charred resin was still observed after the calcination. Also the BET surface area values for both specimens were lower than that for calcined at 600°C for 6 hours. This concluded that the BET surface area of the synthesized β-C_2S could be optimized when the specimen is calcined at 600°C for 6 hours.

The TGA was conducted for the synthesized β-C_2S calcined at 600°C for 6 hours and the result is shown in Fig. 5.3. A peak at 600°C ~ 800°C is a decomposition peak of $CaCO_3$ and it is suggested from the area under the decomposition peak that about 48% of the synthesized β-C_2S is $CaCO_3$. It could be owing to the decomposition of leftover sucrose that was not completely calcined at 600°C for 6 hours and the decomposition of $CaCO_3$ that was formed by Ca^{2+} ions. It is rather difficult to confirm the existence of β-C_2S in the specimen by the TGA technique. The

XRD patterns for the synthesized β-C_2S calcined at 600, 700, 800, 900 and 1000°C for 6 hours are shown in Fig. 5.4. The XRD pattern for the commercially available β-C_2S is also shown in the figure. When the specimen was calcined at 1000°C for 6 hours, the XRD pattern is almost identical to that for the commercial β-C_2S, except a small amount of wollastonite (calcium silicate) and CaO. It is a well known phenomenon that, when a specimen is calcined at higher temperatures, the particles tend to agglomerate to form larger particles and result in lower surface area. This explains the low surface area of commercial β-C_2S. In order to produce the commercial β-C_2S, similar to that in a cement clinker, it must be calcined at very high temperatures, generally above 1250°C. The β-C_2S peaks start to diminish as the calcination temperature decreases. At the calcination temperature of 700°C, most of the β-C_2S peaks have diminished and the $CaCO_3$ peaks start to appear instead. This is due to the fact that some portion of $CaCO_3$ was left uncalcined at lower calcination temperatures. When the specimen was calcined at 600°C for 6 hours, most of the β-C_2S peaks have diminished and only the $CaCO_3$ peaks can be observed. The β-C_2S peaks observed at the higher calcination temperatures become amorphous at lower calcination temperatures and therefore are not detected by the XRD. This confirms that 48% of the synthesized β-C_2S calcined at 600°C for 6 hours is the $CaCO_3$ as determined by the TGA. The remainder would be amorphous materials; it is suggested that it is β-C_2S.

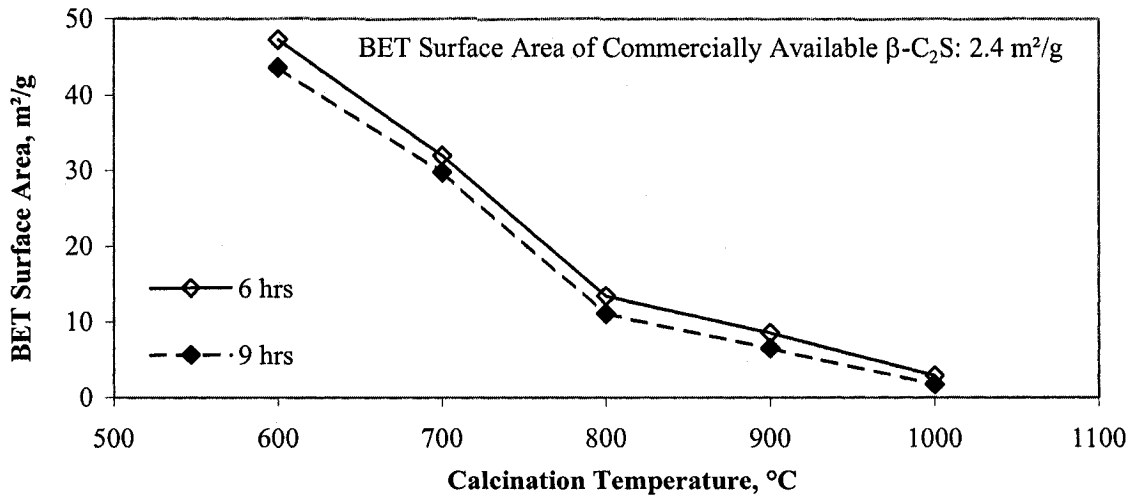

Fig. 5.2 The results of the BET surface area for the synthesized β-C_2S calcined at 600, 700, 800, 900 and 1000°C for 6 and 9 hours

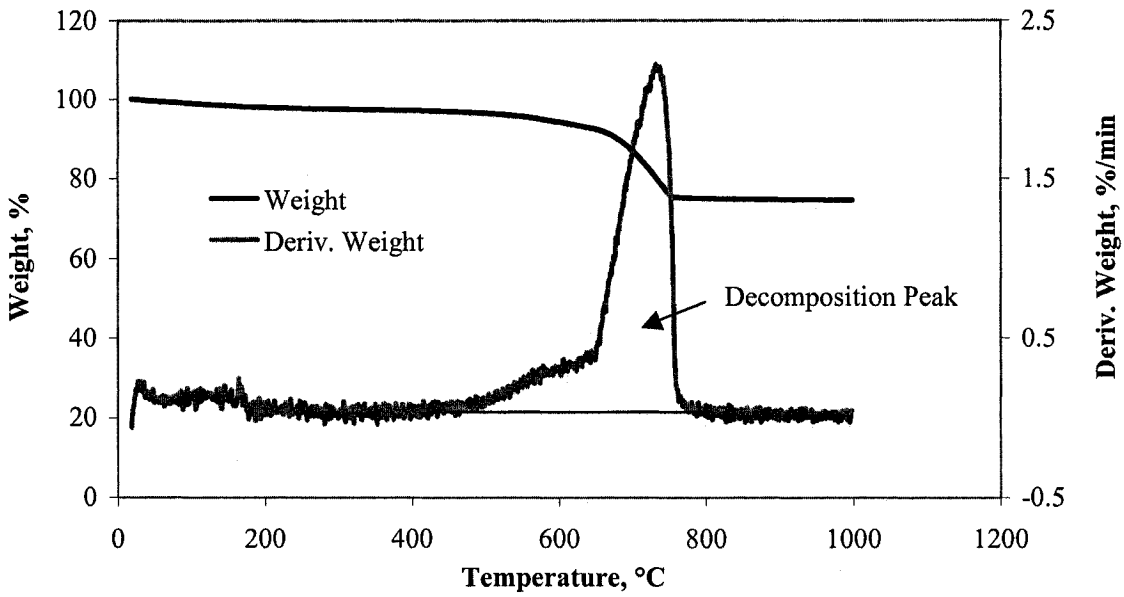

Fig. 5.3 The TGA result and its derivative curve for the synthesized β-C_2S calcined at 600°C for 6 hours

Although both TGA and XRD provided no direct confirmation of the existence of β-C_2S in the synthesized material, it can be achieved by the use of NMR. The NMR is an experimental technique that is not dependent on whether a material is crystalline or amorphous. The NMR used here is the ^{29}Si NMR that characterizes the molecular structure based on the silicon atoms. The ^{29}Si NMR analysis was conducted for the specimen calcined at 600°C for 6 hours to characterize the amorphous portion of the specimen that was not accomplished by the XRD. The ^{29}Si NMR pattern for the synthesized β-C_2S calcined at 600°C for 6 hours is shown in Fig. 5.5 along with that for the commercial β-C_2S. The β-C_2S, as one of the components in a cement clinker, generally has an NMR peak at –71 ppm, as shown in the figure. As mentioned in the section 2.4.2.1, there are five different phases of C_2S, α-, α'_H-, α'_L-, β- and γ-C_2S. The NMR peaks for those different phases are varied within ±3 ppm. It can be confirmed in Fig. 5.5 that the commercial β-C_2S is indeed β-C_2S with the peak at –71 ppm. The synthesized β-C_2S also has a peak at –71 ppm. The scale on the left hand side is for the commercial β-C_2S and that on the right hand side is for the synthesized β-C_2S. The peak of the synthesized β-C_2S is much weaker compared to that of the commercial β-C_2S. It is however clearly indicated in the figure that the amorphous portion of the synthesized product is β-C_2S.

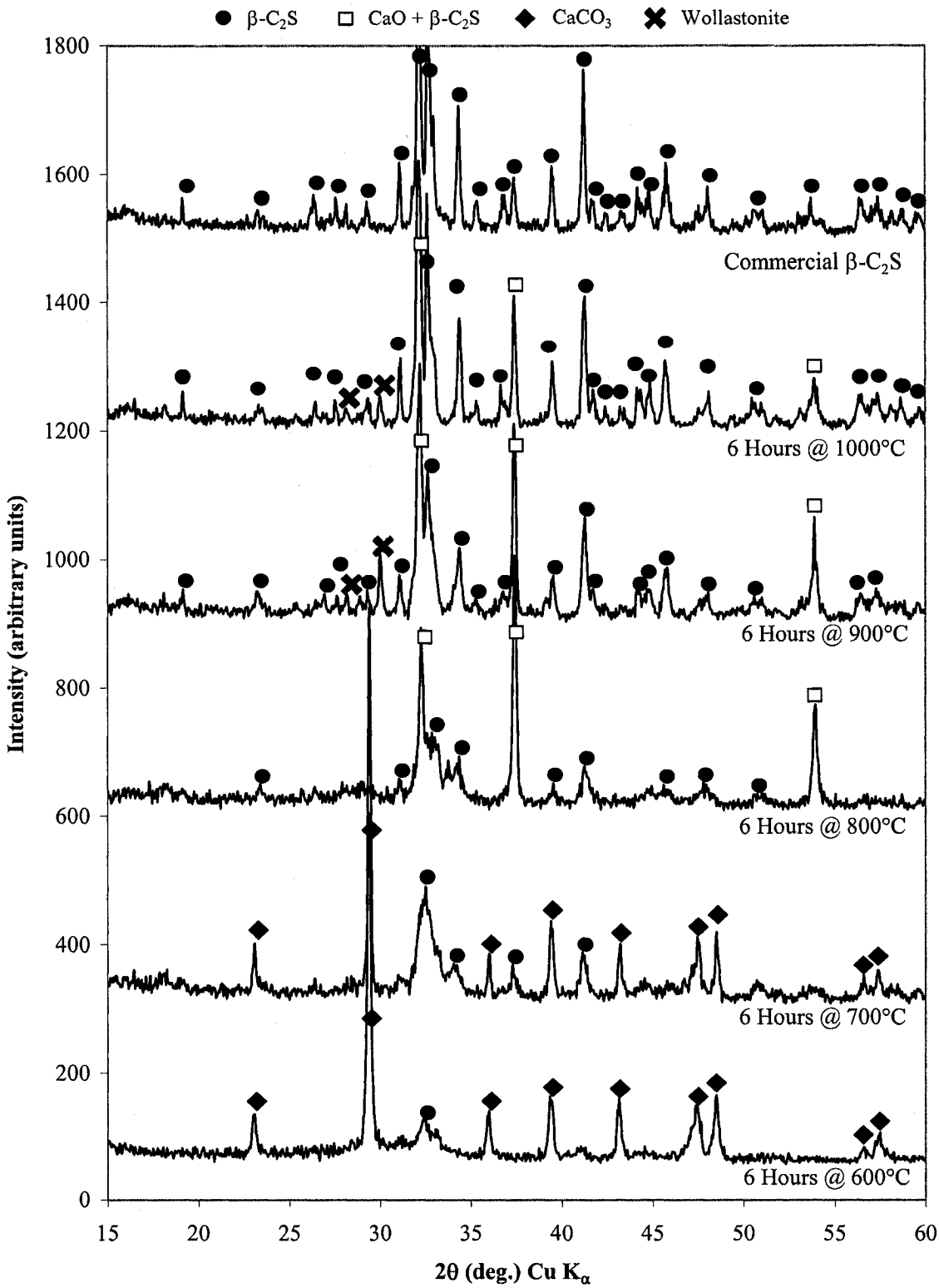

Fig. 5.4 The XRD patterns of the synthesized β-C_2S calcined at 600, 700, 800, 900 and 1000°C for 6 hours and that of commercial β-C_2S

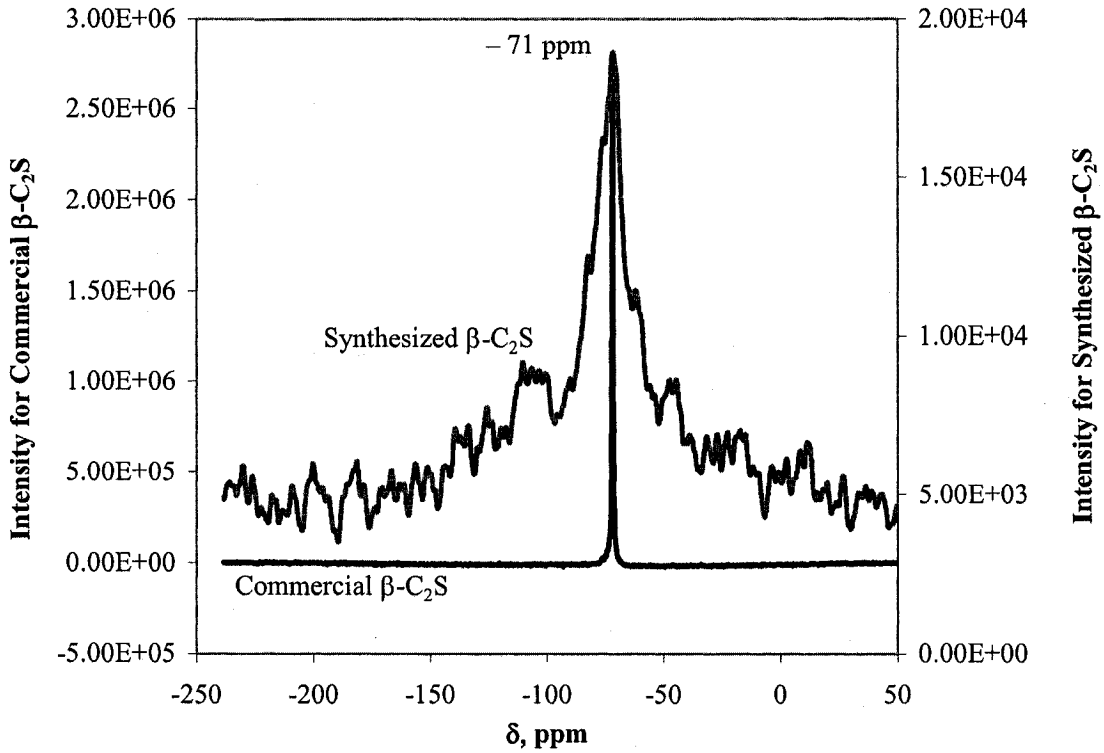

Fig. 5.5 The NMR patterns for the synthesized β-C_2S calcined at 600°C for 6 hours along with the commercial β-C_2S

The SEM analysis was conducted to observe the differences in morphology and particle size. The SEM images for the commercial β-C_2S and the synthesized β-C_2S calcined at 600°C for 6 hours are shown in Figs. 5.6 (a) and (b), respectively. The average particle size of the commercial β-C_2S is approximately 200 to 500 nm whereas the synthesized β-C_2S calcined at 600°C has a mixture of particles from 50 to 400 nm. The SEM image of the synthesized β-C_2S calcined at 600°C shown in Fig. 5.6 (b) indicates that the particles can be classified into two different groups in terms of the particle size range. One is the particle size range of 200 to 400 nm and the other is 50 to 100 nm. It can be suggested that the group of particle size range of 200 to 400 nm might be $CaCO_3$ and that of 50 to 100 nm might be the synthesized nano-sized β-C_2S.

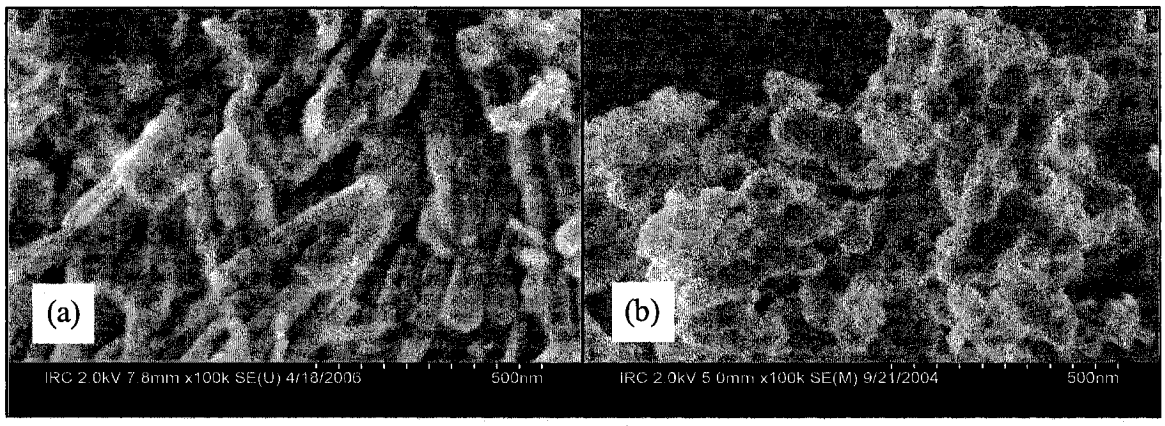

Fig. 5.6 SEM images of (a) Commercial β-C_2S and (b) Synthesized β-C_2S calcined at 600°C for 6 hours

5.3.2 Stage 2: Reactivity and Hydration of the Synthesized Highly Reactive Nano-sized β-C_2S

The synthesized β-C_2S specimens calcined at 600, 700, 800, 900 and 1000°C for 6 hours were mixed with deaerated water for w/c ratio 2.0. The conduction calorimetry results are shown in Fig. 5.7, along with those of the commercial β-C_2S and C_3S for w/c 0.5. The calorimetry curve for commercial C_3S is very remarkable owing to its rapid hydration rate, compared to the slow hydration rate of the commercial β-C_2S. The calorimetry curve for the commercial β-C_2S is shown at the bottom. The heat development of the commercial β-C_2S is too small to be detected by the conduction calorimetry. As shown by the XRD patterns in Fig. 5.4, the synthesized β-C_2S calcined at 1000°C is almost identical to the commercial β-C_2S. Also the BET surface area values of the synthesized β-C_2S calcined at 1000°C and the commercial β-C_2S are 2.9 m^2/g and 2.4 m^2/g, respectively. The effect of these low surface areas can be observed in the calorimetry results as well where the curve for the synthesized β-C_2S calcined at 1000°C overlaps the curve for the commercial β-C_2S. The synthesized β-C_2S calcined at 1000°C basically showed no development of heat of hydration within the 3 days hydration period. The curves for the synthesized β-C_2S calcined at 800°C and 900°C overlap the curve for the commercial β-C_2S as well. A slight development of heat of hydration can however be observed for the synthesized β-C_2S calcined at 700°C. The synthesized β-C_2S calcined at 600°C for 6 hours shows even more heat development. It is evident that the higher the surface area of the synthesized β-C_2S, the higher is the reactivity

and the faster is the hydration. The BET surface area results shown in Fig. 5.2 indicate that there is a subtle line distinguishing the characteristics of the synthesized β-C_2S between the calcination temperatures higher and lower than 800°C. For the calcination temperatures higher than 800°C, the surface area values remain relatively lower, whereas there is a sudden increase in surface area when the calcination temperature decreases to 700°C. The similar increase in surface area can be found from 700°C to 600°C as well. This could be related to the sudden increase in the reactivity as observed in Fig. 5.7. The synthesized β-C_2S calcined at higher than 800°C indicated little hydration similar to the commercial β-C_2S, whereas those calcined at 600°C and 700°C clearly indicated the development of heat of hydration. Especially the hydration of the β-C_2S calcined at 600°C is even faster than that of commercial C_3S in terms of the peak location. The synthesized nano-sized β-C_2S calcined at 600°C for 6 hours unintentionally contains 48% $CaCO_3$, determined from the TGA analysis, which indicates that calcination at 600°C for 6 hours is not sufficient enough to remove all the $CaCO_3$ from the system. At the same time, calcination at higher temperature than 600°C for longer period than 6 hours would lead to a larger particle size and less reactive β-C_2S. Therefore, the calcination at 600°C for 6 hours is considered to be the synthesizing process to optimize the reactivity of β-C_2S.

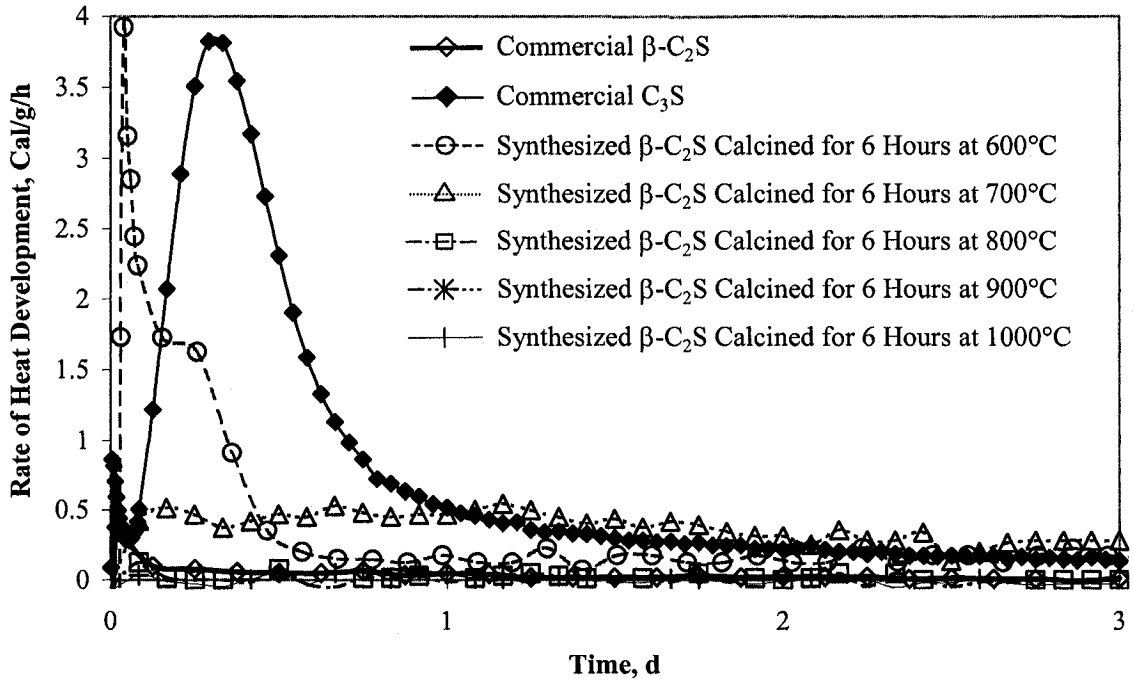

Fig. 5.7 Conduction calorimetry curves for the synthesized β-C_2S calcined at 600, 700, 800, 900 and 1000°C for 6 hours with w/c 2.0 and for those of the commercial β-C_2S and C_3S with w/c 0.5

The XRD was conducted for the synthesized β-C_2S calcined at 600°C and 1000°C for 6 hours hydrated for 3, 7, 14 and 28 days for w/c 2.0 to observe any hydration products associated with hydration of synthesized β-C_2S. The XRD patterns shown in Fig. 5.8 are the ones for the synthesized β-C_2S calcined at 600°C, synthesized β-C_2S calcined at 1000°C and control (anhydrous) commercial β-C_2S and for those hydrated for 28 days with w/c 2.0. The XRD patterns for both control and 28 days hydrated commercial β-C_2S are almost identical, indicating that the amount of $Ca(OH)_2$ produced by the hydration of commercial β-C_2S at 28 days is not sufficient enough to be detected by the XRD. This is not the case for the synthesized β-C_2S calcined at 1000°C. The XRD pattern of the synthesized β-C_2S calcined at 1000°C hydrated for 28 days has some peak development for $Ca(OH)_2$ although the XRD pattern of control commercial β-C_2S and that of synthesized β-C_2S calcined at 1000°C were very similar as compared in Fig. 5.4. This $Ca(OH)_2$ development may be a combination of $Ca(OH)_2$ produced by the hydration of synthesized β-C_2S and $Ca(OH)_2$ produced by the hydration of CaO remained in the synthesized β-C_2S. There were Ca^{2+} ions in the sucrose solution that did not react with SiO_4^{4-} and remained as CaO. The XRD pattern of control synthesized β-C_2S calcined at 1000°C indicates some CaO peaks as shown in Fig. 5.4. The unreacted CaO might have reacted with water and formed $Ca(OH)_2$. The commercial β-C_2S produced no $Ca(OH)_2$, at 28 days hydration, that can be detected by the XRD. The BET surface area value of the synthesized β-C_2S calcined at 1000°C was similar to that of commercial β-C_2S. A similar reactivity can therefore be expected. The formation of $Ca(OH)_2$ is however possible with the hydration of synthesized β-C_2S calcined at 1000°C and will be examined by the TGA. The XRD pattern of control synthesized β-C_2S calcined at 600°C, which consists of 48% $CaCO_3$, mainly shows $CaCO_3$ peaks and a very small β-C_2S peak. This implies that the 52% β-C_2S portion in the synthesized β-C_2S is amorphous as suggested earlier. The XRD pattern of the synthesized β-C_2S calcined at 600°C hydrated for 28 days has a very similar pattern with that of the control one, except that the small β-C_2S peak has diminished and the C-S-H amorphous humps can be observed. Both of these phenomena indicate that the synthesized β-C_2S has hydrated and formed the C-S-H. It is important to note that there are no $Ca(OH)_2$ peaks observed for the synthesized β-C_2S calcined at 600°C hydrated for 28 days. $Ca(OH)_2$ has always been a by-product and even more an indicator of hydration. When either C_3S or OPC hydrates, a large amount of $Ca(OH)_2$ is formed associated with the C-S-H formation. Even a commercial β-C_2S would produce a certain amount of $Ca(OH)_2$ with hydration in the long-term. The synthesized β-C_2S calcined at 600°C, however, produces no detectable $Ca(OH)_2$ associated with hydra-

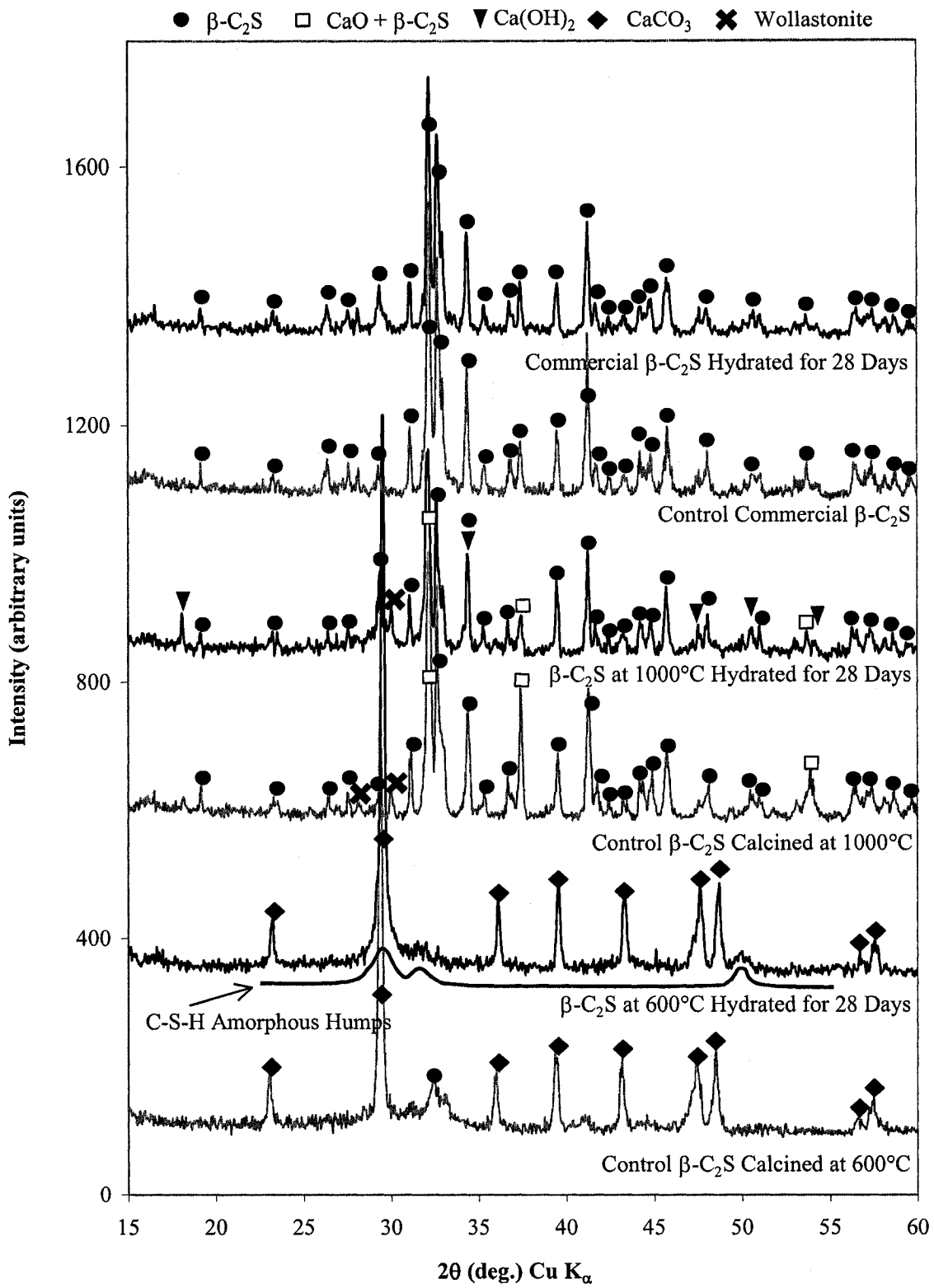

Fig. 5.8 The XRD patterns for the synthesized β-C_2S calcined at 600°C, synthesized β-C_2S calcined at 1000°C and control (anhydrous) commercial β-C_2S and for those hydrated for 28 days with w/c 2.0

tion. One possibility is that the $Ca(OH)_2$ itself is amorphous (Brunauer, 1957). The C/S ratio of the C-S-H formed by the hydration of synthesized β-C_2S may also be higher.

The amounts of $Ca(OH)_2$ in the hydrated specimens of the synthesized β-C_2S calcined at 1000°C at different periods of hydration for w/c 2.0 are shown in Fig. 5.9. The amount of $Ca(OH)_2$ increases as the hydration takes place up to 28 days. If this $Ca(OH)_2$ was solely from the hydration of unreacted CaO remained in the synthesized β-C_2S, it would not increase with hydration. At the same time, it is true that there is some portion of unreacted CaO in the system that would become $Ca(OH)_2$ when mixed with water. Therefore, the $Ca(OH)_2$ peak development in the 28 days hydrated synthesized β-C_2S calcined at 1000°C observed in Fig. 5.8 is owing to a combined effect of $Ca(OH)_2$ produced by the hydration of synthesized β-C_2S and $Ca(OH)_2$ produced by the hydration of CaO remained in the synthesized β-C_2S.

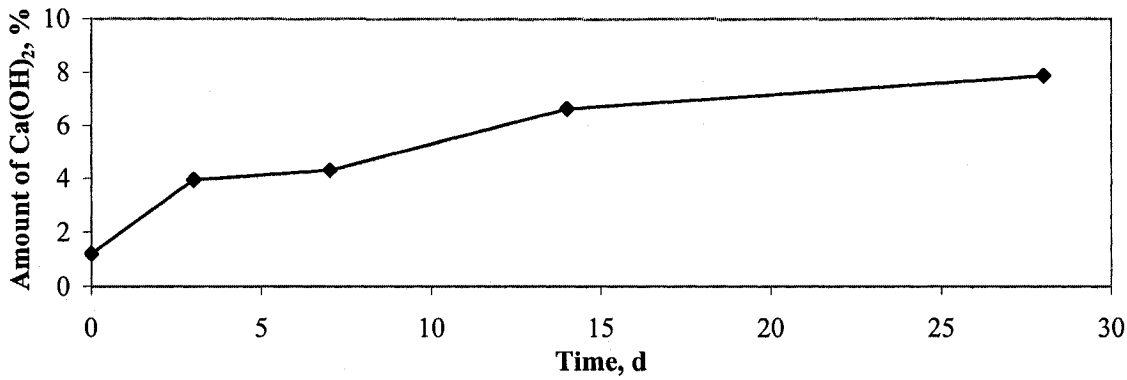

Fig. 5.9 The amounts of $Ca(OH)_2$ for the synthesized β-C_2S calcined at 1000°C at different periods of hydration for w/c 2.0, determined by TGA

The TGA was also conducted for the control synthesized β-C_2S calcined at 600°C and for the synthesized β-C_2S hydrated for 3, 14 and 28 days with w/c 2.0. The derivative curves of weight loss versus temperature are illustrated in Fig. 5.10. The curve for the control β-C_2S calcined at 600°C has a large peak from approximately 600°C to 800°C indicating the decomposition of $CaCO_3$. From the area under this peak, it was determined that the synthesized β-C_2S calcined at 600°C contained 48% nano-sized $CaCO_3$. This peak significantly decreases when it is hydrated for 3 days and continues to decrease as hydration takes place. Also another peak, which seems to consist of two peaks, develops at around 500°C to 700°C at 3 days hydration and continues to

increase as hydration takes place. These phenomena could be an evidence of the product that some portion of $CaCO_3$ in the synthesized β-C_2S has been incorporated in the C-S-H formed.

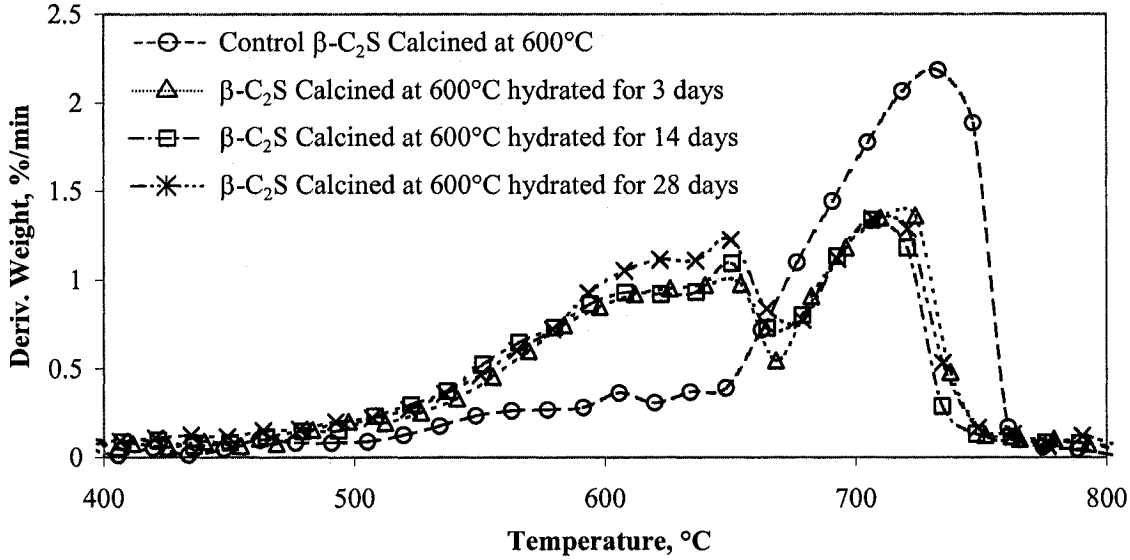

Fig. 5.10 The derivative curve of TGA for the control synthesized β-C_2S calcined at 600°C and for the synthesized β-C_2S hydrated for 3, 14 and 28 days with w/c 2.0

The determinations of microhardness were performed for the synthesized β-C_2S calcined at 600, 700, 800, 900 and 1000°C for 6 hours, to establish a link between the chemical synthesis and the mechanical property. The results are shown in Fig. 5.11 for the hydration of 3, 7, 14 and 28 days along with those for the commercial β-C_2S for w/c 2.0. The microhardness values for all of the synthesized β-C_2S increase as the hydration takes place up to 28 days, although the development of microhardness for the synthesized β-C_2S calcined at 900°C and 1000°C is very slight even after 28 days. The results indicate that lower the calcination temperature, the greater are the microhardness values at any period of hydration. At 3 days hydration, the microhardness values for the commercial β-C_2S is 2.5 MPa whereas that for the synthesized β-C_2S calcined at 600°C is 8.6 MPa. At 28 days hydration, the difference is not as significant as that at 3 days hydration, but the microhardness value for the synthesized β-C_2S calcined at 600°C is still significantly higher than that for the commercial β-C_2S. The reactivity of the β-C_2S was increased and the hydration was accelerated by synthesizing nano-sized particles of the β-C_2S as opposed to micro-sized particles of the commercial β-C_2S. As mentioned earlier, the long-term hydration is often de-pressed when the early hydration was accelerated. In this case, however, the microhardness value of the synthesized β-C_2S calcined at 600°C for the 28 days hydration is still significantly higher

than that of the commercial β-C_2S. This implies that the higher reactivity and accelerating effect in the early hydration did not adversely affect the development of mechanical property in the late hydration.

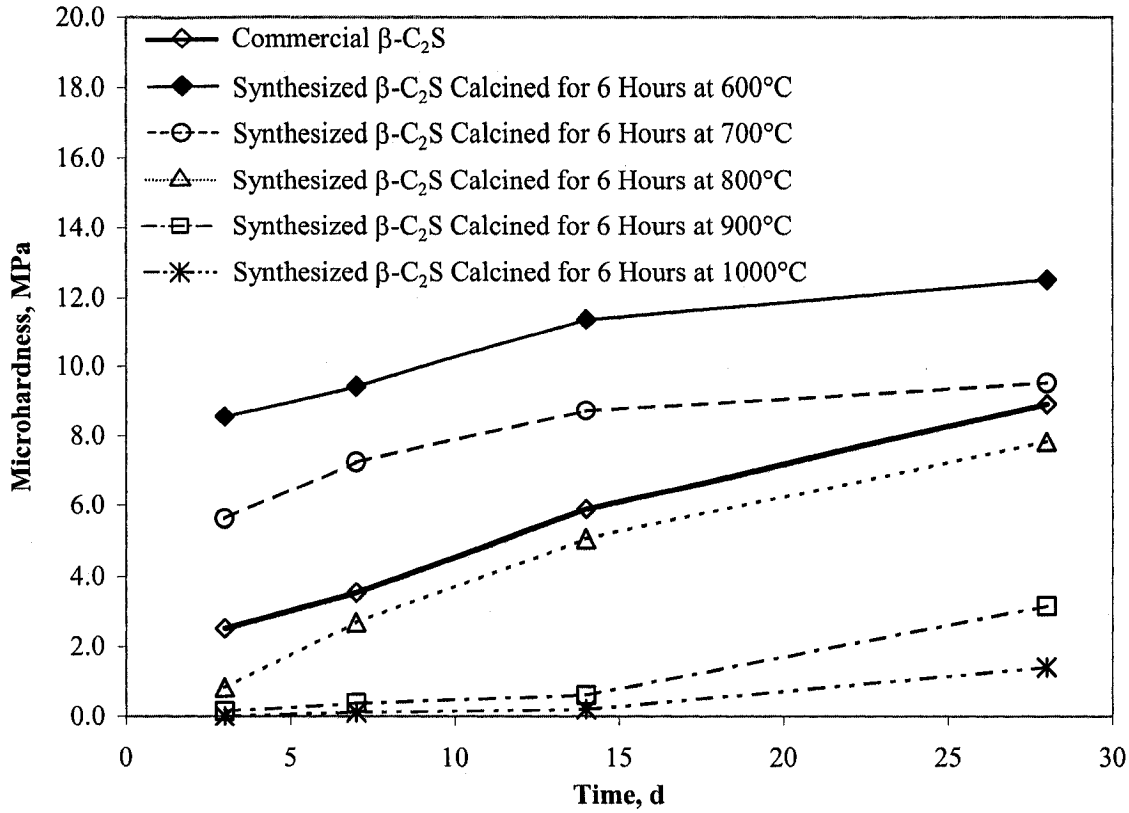

Fig. 5.11 Microhardness results for the synthesized β-C_2S calcined at 600, 700, 800, 900 and 1000°C for 6 hours along with commercial β-C_2S for w/c 2.0 hydrated for 3, 7, 14 and 28 days

There is no clear distinction in the mechanical property results between the synthesized β-C_2S calcined at temperatures lower and higher than 800°C, as shown in the BET surface area values and the calorimetry curves. The β-C_2S calcined at temperatures lower than 800°C had significantly higher BET surface area values than those calcined at temperatures higher than 800°C and the rates of heat development were greater for those calcined at lower than 800°C. The microhardness results, however, do not indicate any line distinguishing the characteristics of the synthesized β-C_2S between the calcination temperatures lower and higher than 800°C. The XRD pattern for the synthesized β-C_2S calcined at 1000°C indicated some $Ca(OH)_2$ peak development at 28 days hydration whereas the XRD pattern for the commercial β-C_2S showed none. This

$Ca(OH)_2$ peak development was confirmed by the TGA that it is owing to not only the hydration of unreacted CaO, but also the hydration of β-C_2S. A greater development of the mechanical properties for the synthesized β-C_2S calcined at 1000°C was therefore expected. The microhardness results, however, revealed that the strength development for the commercial β-C_2S was higher than that for the synthesized β-C_2S calcined at 1000°C. This underlies the importance of the determination of the mechanical properties to provide a link with the chemical synthesis.

5.3.3 Stage 3: Quantitative Variation of Ingredients for the Sucrose Method

Characterization of a series of synthesized β-C_2S calcined at various temperatures and durations in the previous section made it possible to optimize the fineness in terms of particle size and the reactivity of the synthesized β-C_2S. Determination of microhardness revealed that the synthesized β-C_2S calcined at 600°C for 6 hours developed much greater strength than the commercial β-C_2S. It is noted however that the synthesized β-C_2S consists of 48% $CaCO_3$ and that there is unreacted CaO remained in the synthesized β-C_2S system. These findings suggest that the stoichiometrically calculated amount of Ca^{2+} ions in the solution did not all react with the SiO_4^{4-} ions. There was also no evidence that some of the SiO_4^{4-} ions remained unreacted. This implies that a certain portion of Ca^{2+} ions did not react because there was not enough SiO_4^{4-} ions present in the solution. This resulted in the formation of CaO and $CaCO_3$. The ingredients of the Sucrose method were therefore modified by doubling the amount of amorphous silica (SiO_2) used as a reactant. The synthesis of highly reactive nano-sized β-C_2S was conducted calcining at 600°C for 6 hours with the excess amount of amorphous silica.

The TGA was conducted on the synthesized β-C_2S with the excess silica to determine the amount of $CaCO_3$ remained in the system. It was found that the β-C_2S with the excess silica consisted of 16% $CaCO_3$ as opposed to 48% $CaCO_3$ present in the synthesized β-C_2S without the excess silica. This significant decrease in the amount of $CaCO_3$ in the synthesized β-C_2S with the same temperature and the same duration of calcination implies that the Ca^{2+} ions which had interacted with carbon from the sucrose and formed $CaCO_3$ and the Ca^{2+} ions which were remained unreacted and formed CaO are reacting with the added excess silica to form less $CaCO_3$ and more β-C_2S in the system.

The XRD pattern of the synthesized β-C_2S calcined at 600°C with excess silica, shown in Fig. 5.12, is very similar to that of the β-C_2S calcined at 600°C without excess silica except the $CaCO_3$ peaks are weaker. This is associated with the decrease of the $CaCO_3$ content in the system as determined by the TGA. The XRD pattern in Fig. 5.12 implies that the rest of 84% of synthesized product is amorphous. It is necessary to conduct NMR to identify the product. The ^{29}Si NMR patterns for the synthesized β-C_2S calcined at 600°C for 6 hours with and without excess silica along with that of the commercial β-C_2S are shown in Fig. 5.13. The synthesized β-C_2S with excess silica has indeed a peak at –71 ppm that is a typical of the β-C_2S. The peak is however very weak compared to that of commercial β-C_2S and even that of synthesized β-C_2S without excess silica. Nevertheless, it is confirmed that the synthesized product with excess amount of amorphous silica calcined at 600°C for 6 hours is β-C_2S.

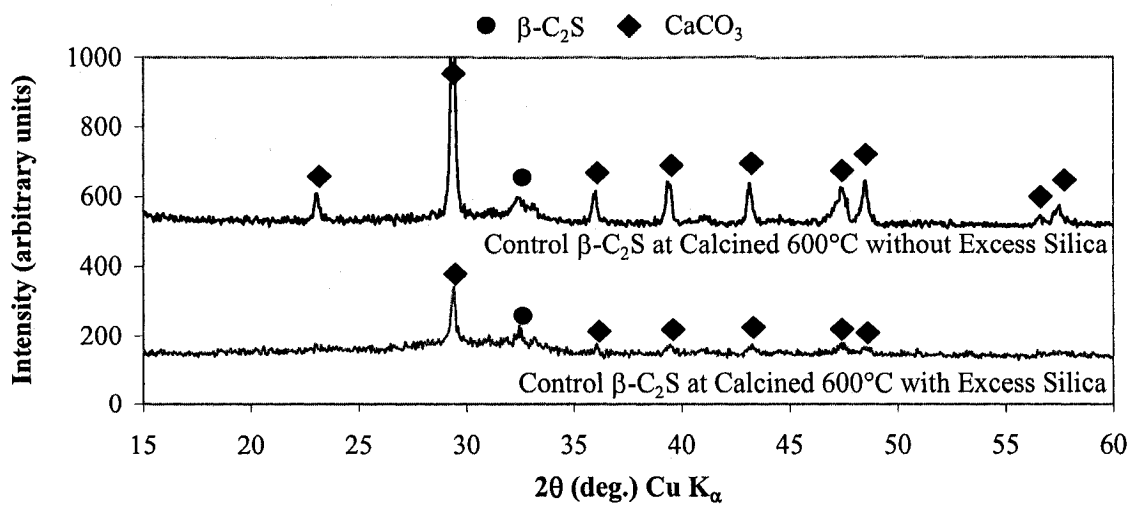

Fig. 5.12 The XRD patterns for the control β-C_2S calcined at 600°C with and without excess silica

The BET surface area value of the β-C_2S with excess silica was 70.9 m^2/g. This is significantly higher than those of the β-C_2S calcined 600°C without excess silica and the commercial β-C_2S, 47.3 m^2/g and 2.4 m^2/g, respectively. The smaller particle size can be expected from the higher surface area value. The SEM image for the synthesized β-C_2S with excess silica is shown in Fig. 5.14. The average particle size is approximately 20 to 50 nm, which is significantly smaller than the synthesized β-C_2S without excess silica shown in Fig. 5.6 (b). As previously observed in Fig 5.6 (b), two different groups in terms of the particle size range were observed in the synthesized β-C_2S without excess silica. The group of the particle size range of 200 to 400 nm, which was

suggested to be $CaCO_3$, however, cannot be observed in the synthesized β-C_2S with excess silica as shown in Fig. 5.14. This correlates with the significant decrease in the amount of $CaCO_3$ determined by the TGA.

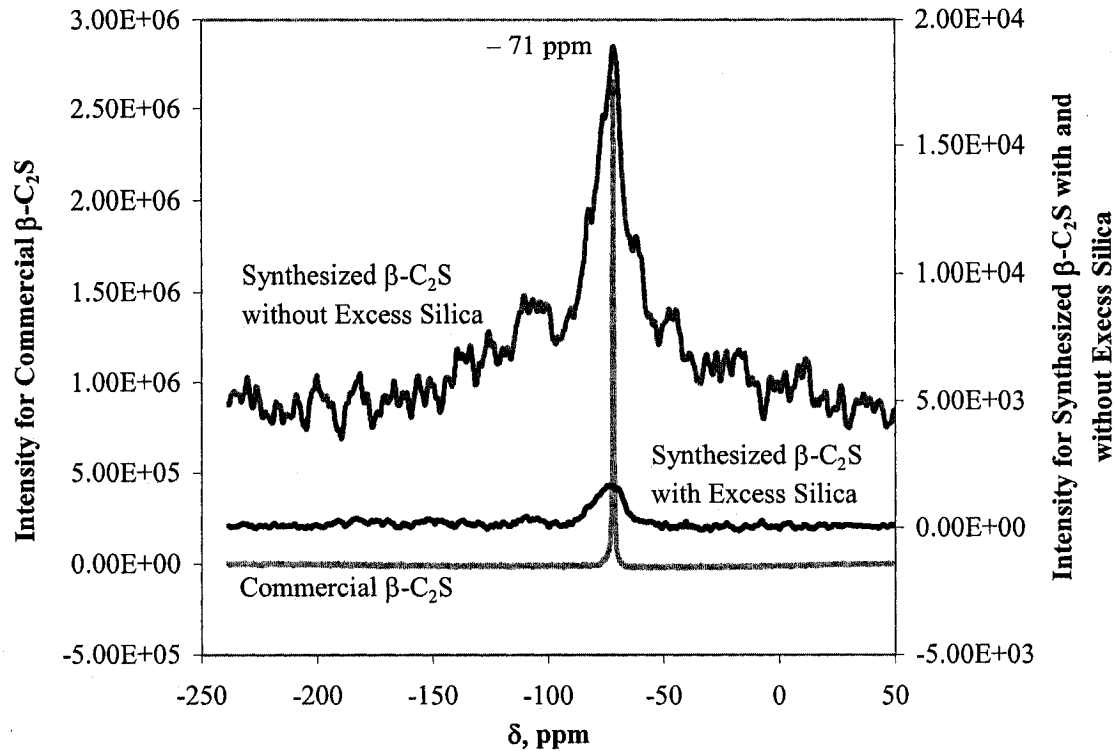

Fig. 5.13 The NMR patterns for the synthesized β-C_2S calcined at 600°C for 6 hours with and without excess silica along with that of the commercial β-C_2S

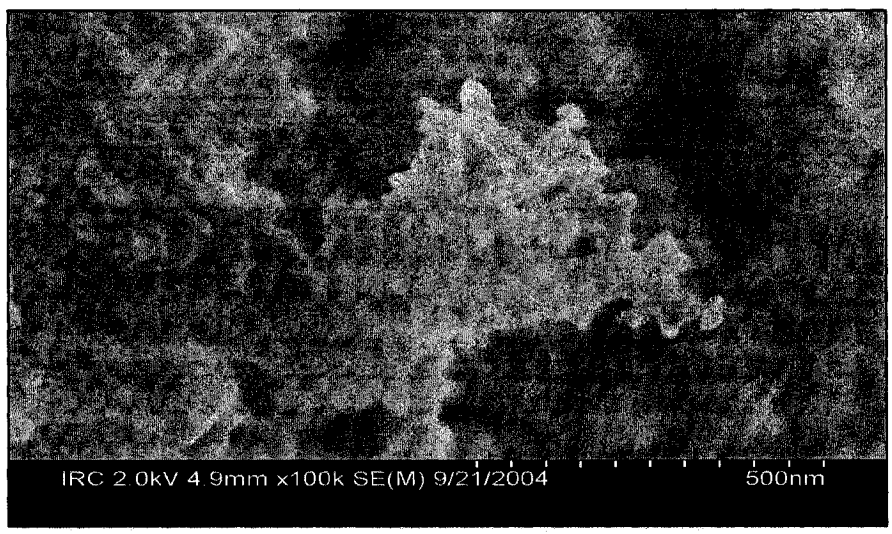

Fig. 5.14 SEM image of the synthesized β-C_2S calcined at 600°C for 6 hours with excess silica

The conduction calorimetry curves for the synthesized β-C_2S with and without excess silica for w/c 2.0 and for those of the commercial β-C_2S and C_3S for w/c 0.5 are shown in Fig. 5.15. The calorimetry curves of the synthesized β-C_2S without excess silica calcined for 6 hours at 600°C and those of the commercial β-C_2S and C_3S were already shown in Fig. 5.7. The calorimetry curve for the synthesized β-C_2S with excess silica indicates an extremely higher rate of heat development as shown in Fig. 5.15. This result correlates with the significant increase in the BET surface area value and the decrease in the particle size. The 48% $CaCO_3$ content in the synthesized β-C_2S calcined at 600°C for 6 hours without excess silica was suspected to be one of the reasons that the hydration of β-C_2S was significantly accelerated as shown in Fig. 5.7. This suggestion was based on the observation in the previous chapter, where the hydration of OPC was significantly accelerated by the addition of nano-sized $CaCO_3$. The result shown in Fig. 5.15, however, implies that this may not be the case. The $CaCO_3$ content was decreased from 48% to 16%, when the β-C_2S was synthesized with excess silica, however, the hydration of the synthesized β-C_2S with excess silica was remarkably accelerated. It is possible that the $CaCO_3$ in this material is much finer and that its interaction with the system composed results in greater reactivity. It is also possible that the synthesized β-C_2S itself is more highly reactive than in the previous case because of the smaller particle size of β-C_2S.

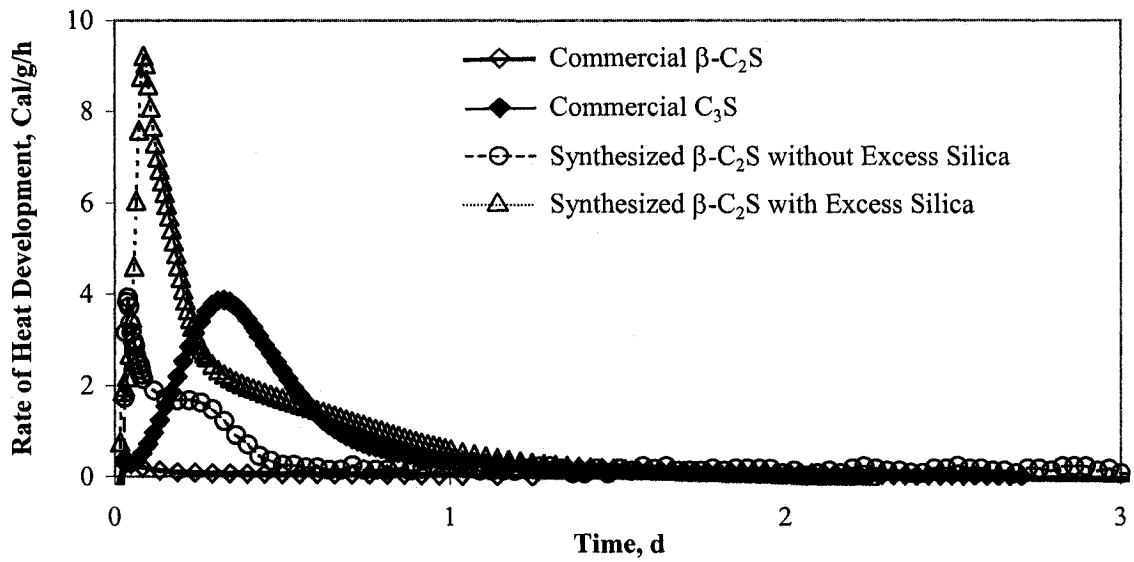

Fig. 5.15 Conduction calorimetry curves for the synthesized β-C_2S with and without excess silica for w/c 2.0 and for those of the commercial β-C_2S and C_3S for w/c 0.5

CHAPTER 6

THEME 3: THE SYNTHESIS OF THE NANO-SIZED $Ca(OH)_2$ AND ITS EFFECT ON THE POZZOLANIC REACTION WITH METAKAOLINITE

6.1 Introduction

Theme 3 of this thesis: The Synthesis of the Nano-sized $Ca(OH)_2$ and its Effect on the Pozzolanic Reaction with Metakaolinite, is described in Chapter 6 including the experimental and analytical approaches, materials, specimen preparation, results and discussion. In the first section, details of the experimental and analytical approaches are presented, followed by a description of the planetary-mill grinding method and vacuum-calcination method. In the following section, the results and discussion are presented. All the experimental techniques used to obtain the results are described in Chapter 3, unless otherwise stated.

6.2 Experimental

6.2.1 Experimental and Analytical Approaches

The objective of Theme 3 was to synthesize a nano-sized $Ca(OH)_2$ and study its effect on the pozzolanic reaction with metakaolinite. The synthesis of the nano-sized $Ca(OH)_2$ was conducted

by a physical process, the planetary-mill grinding method and a physico-chemical process, the vacuum-calcination method. This was in contrast to the synthesis of the highly reactive nano-sized β-C_2S which utilized a wet chemical process, the Sucrose method. The relative reactivity of the two synthesized $Ca(OH)_2$, compared to a reagent grade micro-sized $Ca(OH)_2$, was investigated by applying the Hedvall effect. The two synthesized $Ca(OH)_2$ were then reacted with metakaolinite to observe the effect of the size of $Ca(OH)_2$ on the pozzolanic reaction. Details of the experimental and analytical approaches are summarized in Table. 6.1. The results and discussion are presented in the same chronological manner as shown in the table. In Stage 1, the characterization of two types of the nano-sized $Ca(OH)_2$ was conducted. A material identification was first performed to confirm that the synthesized material was indeed $Ca(OH)_2$. The material identification of the nano-sized $Ca(OH)_2$ in this theme is not as critical as that of the nano-sized β-C_2S in the previous theme, since the synthesis by the physical process is less likely to change the chemical composition of the starting material than that by the chemical process. It is important that the purity of the synthesized material be verified. Following the material identification, the surface area and particle size of the synthesized nano-sized $Ca(OH)_2$ were compared with those of the reagent grade micro-sized $Ca(OH)_2$. In Stage 2, the Hedvall effect, a novel method developed at the Institute for Research in Construction (IRC), National Research Council Canada, was applied to examine the relative reactivity of the nano-sized $Ca(OH)_2$ as opposed to the micro-sized $Ca(OH)_2$. In Stage 3, the effect of the nano-sized $Ca(OH)_2$ on the pozzolanic reaction was investigated by the conduction calorimetry. In Stage 4, the study focused on the thermal decomposition of nano-sized $Ca(OH)_2$. The thermal decomposition of $Ca(OH)_2$ with a doublet characteristic has been observed by a number of studies in the past (Greene, 1960; Herrick et al., 1992). An understanding of the thermal decomposition of $Ca(OH)_2$ with two peaks (doublet) has been intensively attempted. The study of the thermal decomposition of nano-sized $Ca(OH)_2$ elucidated the nature of the doublet characteristic.

6.2.2 Materials

Reagent grade micro-sized $Ca(OH)_2$ was supplied by Anachemia Canada Inc., Montreal, Quebec, Canada. Its purity was higher than 95%. The BET surface area value was 16.6 m^2/g. Isopropyl alcohol was supplied by EMD Chemicals Inc., Gibbstown, New Jersey, USA. Silver nitrate used for the Hedvall effect experiments was supplied by Anachemia Canada Inc., Montreal, Quebec,

Canada. Its purity was higher than 99%. Metakaolinite, MetaMax, was supplied by Engelhard, Iselin, New Jersey, USA. Its chemical composition is shown in Table 6.2.

Table. 6.1 The experimental and analytical approaches for Theme 3

Stage 1	Synthesis and characterization of nano-sized $Ca(OH)_2$ by the planetary-mill grinding method and the vacuum-calcination method
	▪ Material identification by TGA and XRD ▪ Fineness by BET surface area determination ▪ Particle characterization by SEM
Stage 2	The determination of the reactivity of the synthesized nano-sized $Ca(OH)_2$ by the application of the Hedvall effect
	▪ Calibration of the exothermic peak for unreacted $AgNO_3$ ▪ Relative reactivity of the different types of $Ca(OH)_2$
Stage 3	Effect of the nano-sized $Ca(OH)_2$ on pozzolanic reaction with metakaolinite
	▪ Conduction calorimetry
Stage 4	Study of the thermal decomposition characteristics of $Ca(OH)_2$
	▪ 1st experiment ▪ 2nd experiment

Table. 6.2 Chemical composition of metakaolinite (wt. %)

SiO_2	Al_2O_3	Fe_2O_3
52.0	44.6	0.5

6.2.3 Specimen Preparation

6.2.3.1 Planetary-mill Grinding Method

Grinding is one of the most classic physical processes used to synthesize finer materials. The planetary-mill grinding is based on in-solution grinding as opposed to micronizing that is based on dry-grinding. Grinding was conducted by the Fritsch planetary mill grinder, shown in Fig. 6.1 (a). The planetary-mill grinder consists of two large and two small mortars, made of agate, on a

rotating circular plate. Those two large mortars were used in the synthesis process. Each mortar contains seven small agate grinding balls as shown in Fig. 6.1 (b). A 10g powder of reagent grade micro-sized $Ca(OH)_2$ and 3 ml of isopropyl alcohol were placed in the both mortars, as shown in Fig. 6.1 (c). A lid was tightly placed and grinding was continued for 3 days. The content was then dried in an 80°C oven to remove the isopropyl alcohol from the system.

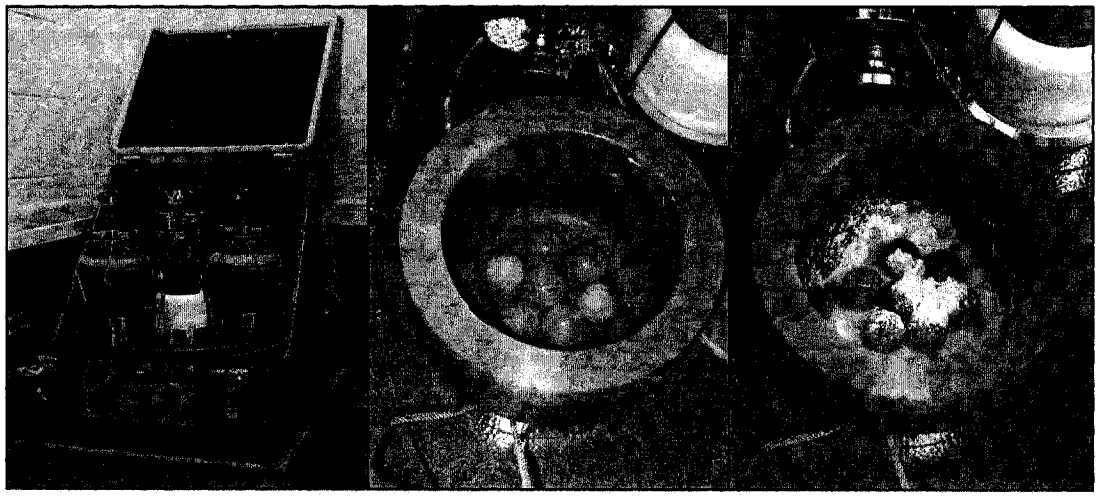

(a) (b) (c)

Fig. 6.1 (a) The planetary-mill grinder (b) An agate mortar and grinding balls and (c) $Ca(OH)_2$ powder and isopropyl alcohol in the mortar

6.2.3.2 Vacuum-calcination Method

The fundamental purpose of the vacuum-calcination method for the synthesis of a nano-sized $Ca(OH)_2$ is to prepare a nano-sized CaO by calcining a reagent grade micro-sized $Ca(OH)_2$ and to re-hydrate it to form the nano-sized $Ca(OH)_2$ as described in Section 2.5.3.2. A small device, shown in Fig. 6.2 (a), was designed and fabricated at the Institute for Research in Construction (IRC), National Research Council Canada, to perform the low temperature vacuum-supported calcination. The device contains a cylinder, 50 mm in diameter and 110 mm in height with an attached hollow rod 450 mm in length. A thermocouple was installed so that the temperature inside the cylinder could be measured. An aluminum crucible containing 5g of $Ca(OH)_2$ was placed inside the cylinder. Then a lid was put on top of the cylinder using a Teflon tape to seal the cylinder. The whole unit was placed into a muffle furnace with the rod extending to the outside through the furnace doors as shown in Fig. 6.2 (b). The rod was connected to the vacuum pump. The thermocouple was installed through the rod and taken out through a small hole between the rod and a vacuum tube to be connected to a digital thermometer. Following the calcination period, the whole unit was taken out of the muffle furnace and cooled to room temperature. The synthe-

sized nano-sized CaO powder was mixed with deaerated water for 1 minute in order to re-hydrate it to form $Ca(OH)_2$. The solution was then filtered and the solid was dried under vacuum for 1 day.

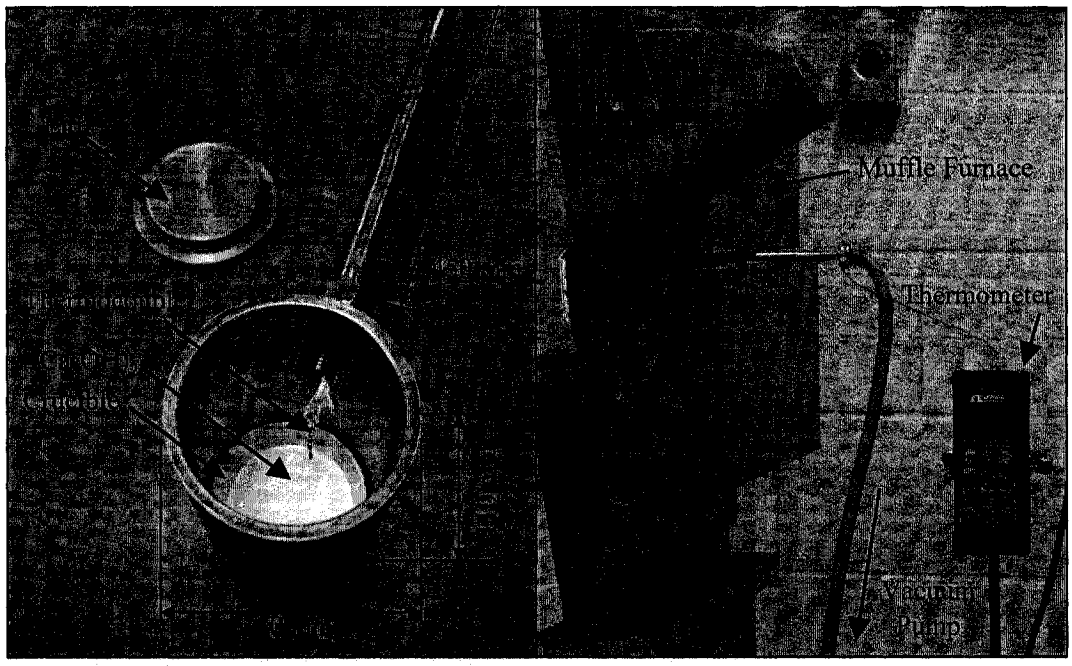

Fig. 6.2 (a) The device for synthesis of vacuum-calcination $Ca(OH)_2$ and (b) The setup with the muffle furnace

6.3 Results and Discussion

6.3.1 Stage 1: Synthesis and Characterization of Nano-sized $Ca(OH)_2$ by the Planetary-mill Grinding Method and the Vacuum-calcination Method

The TGA was conducted for the synthesized nano-sized $Ca(OH)_2$ both by the planetary-mill grinding and vacuum-calcination methods. Both TGA curves are shown in Fig. 6.3. From the calculation of the area under the peaks, the $Ca(OH)_2$ by the planetary-mill grinding method has about 81.8% $Ca(OH)_2$ and 18.2% $CaCO_3$, whereas that by the vacuum-calcination method has about 96.8% $Ca(OH)_2$ and 3.2% $CaCO_3$. A source of a relatively large amount of $CaCO_3$ in the $Ca(OH)_2$ synthesized by the planetary-mill grinding method is rather unclear. The chemical

reaction between the ground $Ca(OH)_2$ and isopropyl alcohol was suspected. The same amount of $CaCO_3$, however, was found in the synthesized $Ca(OH)_2$ ground in the lime water in lieu of isopropyl alcohol, indicating that the isopropyl alcohol was not the source of $CaCO_3$. The 3.2% $CaCO_3$ content in the $Ca(OH)_2$ synthesized by the vacuum-calcination method may be from the carbonation of nano-sized CaO before re-hydration, since the synthesized highly-reactive, high-surface area CaO is very sensitive to CO_2 in the air.

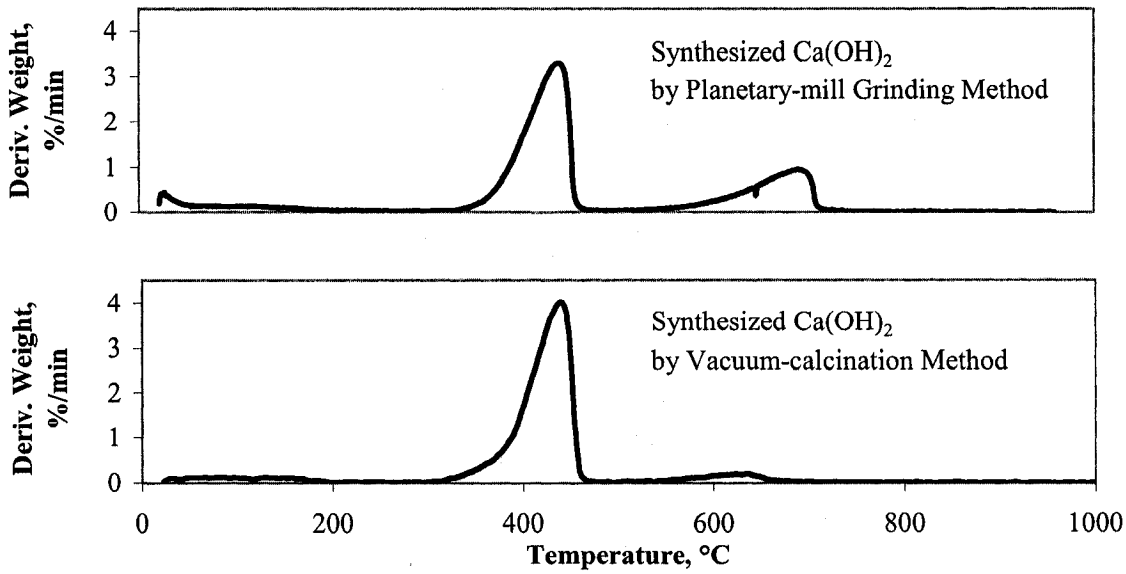

Fig. 6.3 TGA curves for synthesized $Ca(OH)_2$ by the planetary-mill grinding method and vacuum-calcination method

The BET surface area values for $Ca(OH)_2$ synthesized by the planetary-mill grinding and vacuum-calcination methods were 53.2 m^2/g and 38.1 m^2/g, respectively, whereas that for the reagent grade micro-sized $Ca(OH)_2$ was 16.1 m^2/g. A large decrease in the particle size of nano-sized $Ca(OH)_2$ can be expected. The SEM images for the micro-sized $Ca(OH)_2$, the nano-sized $Ca(OH)_2$ by the planetary-mill grinding method and that by the vacuum-calcination method are shown in Figs. 6.4 (a), (b) and (c), respectively. The particle size of the micro-sized $Ca(OH)_2$ can be as large as 1 μm, whereas the particles of the nano-sized $Ca(OH)_2$ synthesized by the planetary-mill grinding and the vacuum-calcination methods are approximately 50 to 400 nm. The particles of $Ca(OH)_2$ synthesized by the vacuum-calcination method seemed to be more crystalline whereas those by the planetary-mill grinding method are less structured and more amorphous. This observation can be confirmed by the XRD results where the height of the peaks indicates the degree of crystallinity.

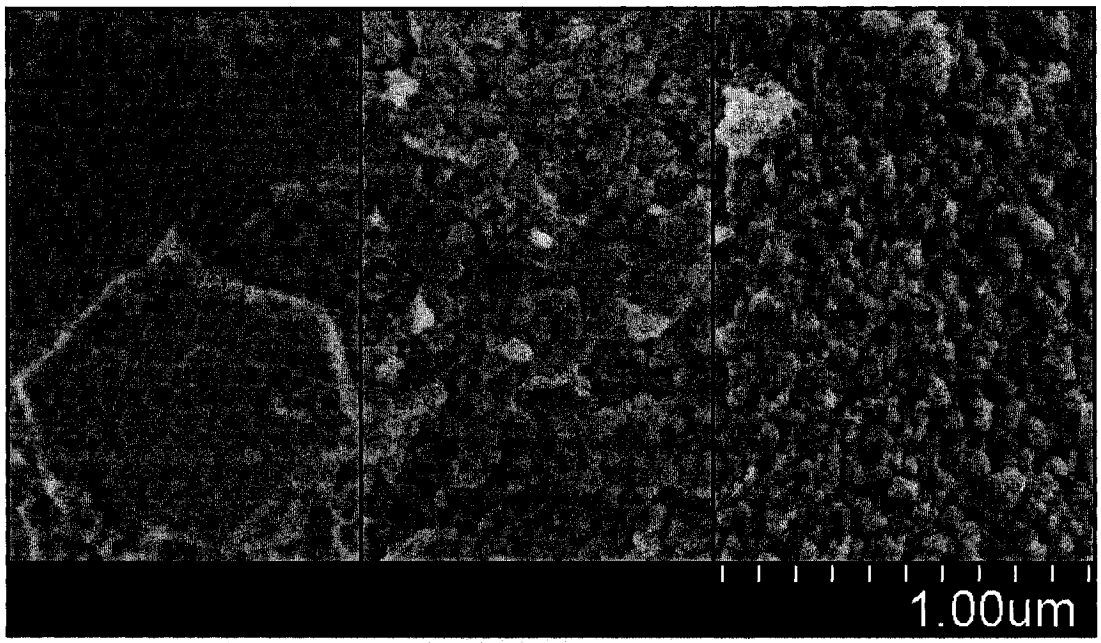

(a) (b) (c)

Fig. 6.4 SEM images of (a) reagent grade micro-sized $Ca(OH)_2$ (b) nano-sized $Ca(OH)_2$ synthesized by the planetary-mill grinding method and (c) nano-sized $Ca(OH)_2$ synthesized by vacuum-calcination method

The XRD patterns for the synthesized nano-sized $Ca(OH)_2$ both by the planetary-mill grinding and vacuum-calcination methods along with that of the micro-sized $Ca(OH)_2$ are shown in Fig. 6.5. All three specimens indicate that $Ca(OH)_2$ peaks. This confirms that the synthesized products are indeed $Ca(OH)_2$. The $CaCO_3$ content detected by TGA in $Ca(OH)_2$ synthesized by the planetary-mill grinding method is not detected by the XRD peaks, implying that this $CaCO_3$ might be amorphous. By comparing the height of the peaks, the micro-sized $Ca(OH)_2$ is approximately as crystalline as the $Ca(OH)_2$ synthesized by the vacuum-calcination method and is more crystalline than the $Ca(OH)_2$ synthesized by the planetary-mill grinding method. It is well known that a material with a lower surface area and larger particle size is generally more crystalline than a material with a higher surface area and smaller particle size. This applies to the case of the synthesized $Ca(OH)_2$ as well. The BET surface area values of the micro-sized $Ca(OH)_2$ and $Ca(OH)_2$ synthesized by the vacuum-calcination method are lower than that of nano-sized $Ca(OH)_2$ by the planetary-mill grinding method and therefore more crystalline as observed by the XRD.

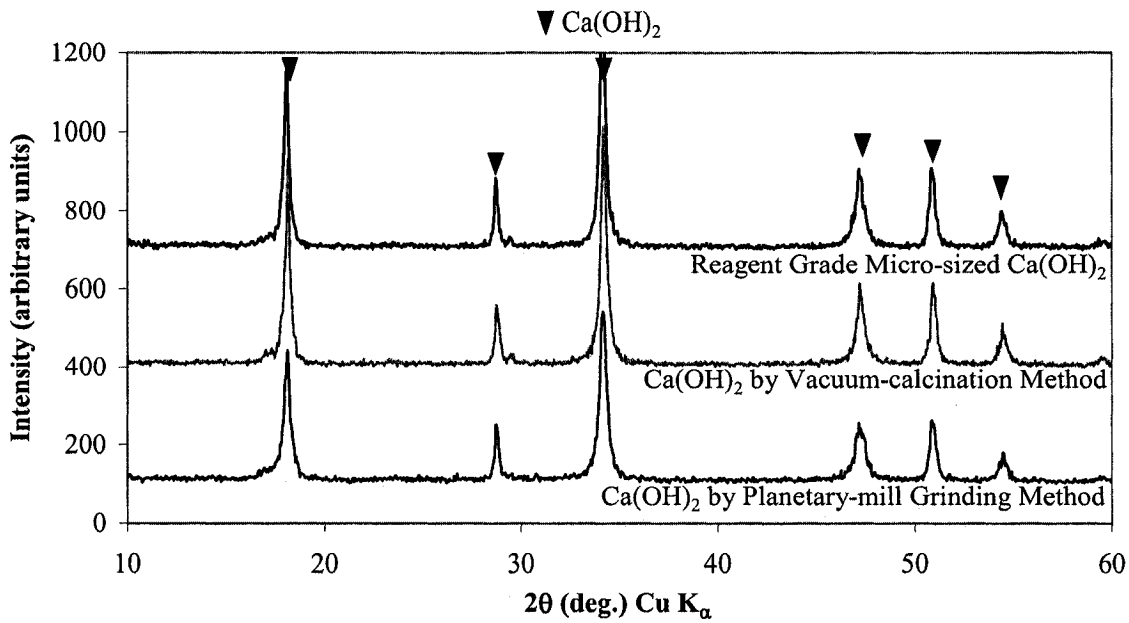

Fig. 6.5 The XRD patterns for the synthesized nano-sized $Ca(OH)_2$ both by the planetary-mill grinding and vacuum-calcination methods along with that of the micro-sized $Ca(OH)_2$

6.3.2 Stage 2: The Determination of the Reactivity of the Synthesized Nano-sized $Ca(OH)_2$ by the Application of the Hedvall Effect

6.3.2.1 Introduction

A change in the rate of chemical reaction of a solid during and as a consequence of a crystalline transformation is known as the Hedvall effect (Ramachandran and Sereda, 1971). The Hedvall effect was applied to investigate the relative reactivity of the synthesized $Ca(OH)_2$. The relative reactivity of different types of $Ca(OH)_2$ can be determined by the amount of $Ca(OH)_2$ that reacts with $AgNO_3$ when they are blended and heated by the DSC from room temperature to 250°C. The reaction between $Ca(OH)_2$ and $AgNO_3$ is as follows:

$$Ca(OH)_2 + 2AgNO_3 \rightarrow Ca(NO_3)_2 \cdot H_2O + Ag_2O \qquad (6.1)$$

Stoichiometrically, 1 mole of $Ca(OH)_2$ reacts with 2 moles of $Ag(NO)_3$. The basic theory of applying the Hedvall effect is to add an excess amount of $AgNO_3$ into a mix, that is more than the stoichiometric amount, and to determine the amount of unreacted $AgNO_3$. From the amount of

unreacted $AgNO_3$, the exact amount of $AgNO_3$ reacted with $Ca(OH)_2$ can be determined. Two materials were placed in a plastic cylindrical tube and shaken for 1 minute using a SPEX MIXER, to blend them well. The temperature of the DSC was ramped from room temperature to 250°C at 10°C/min, held isothermally at 250°C for 10 minutes and ramped down to 150°C at the same rate, with a 100 ml/min nitrogen gas flow. Heat flow measurements were made on both heating and cooling. The heat flow curve by the DSC for the specimen containing 90% $AgNO_3$ and 10% $Ca(OH)_2$ and that for the specimen containing 40% $AgNO_3$ and 60% $Ca(OH)_2$ are shown in Figs. 6.6 (a) and (b), respectively. Content percentages shown are based on the mass. The added amounts of $AgNO_3$ in the specimens shown in Figs. 6.6 (a) and (b) are, respectively, greater and less than the stoichiometric amount of $Ag(NO)_3$ that can react with $Ca(OH)_2$. The endothermic peak on heating shown in both Figs. 6.6 (a) and (b) consists of two peaks. The first smaller peak indicates the phase transition of $AgNO_3$ from α to β. The second larger peak indicates the phase transition of $AgNO_3$ from solid to liquid. The exothermic peak on cooling shown in Fig. 6.6 (a) is a re-crystallization of unreacted $AgNO_3$ (Ramachandran and Sereda, 1971). The added amount of $AgNO_3$ is much greater than the amount of $AgNO_3$ that could react with $Ca(OH)_2$. Therefore, the unreacted $AgNO_3$, which was liquefied on heating, re-crystallized on cooling. There is no exothermic peak on cooling in Fig. 6.6 (b). This is because the added amount of $AgNO_3$ is much less than the amount of $AgNO_3$ that could react with $Ca(OH)_2$. Therefore there was no unreacted $Ag(NO)_3$ to be re-crystallized on cooling. The DSC heat flow curve on cooling indicates the amount of unreacted $AgNO_3$ in the specimen, and therefore the amount of reacted $AgNO_3$ can be calculated.

6.3.2.2 Calibration of the Exothermic Peak for Unreacted $AgNO_3$

The amount of heat flow, represented by the height of exothermic peak detected by the DSC has to be calibrated in terms of an amount of unreacted $AgNO_3$ in a specimen. The DSC was conducted for a series of specimens containing SiO_2 (silica sand) and various amounts of $AgNO_3$. There would be no chemical reaction between $AgNO_3$ and SiO_2. The amount of $AgNO_3$ in the mix is therefore the amount of unreacted $AgNO_3$. The amounts of $AgNO_3$ used were 5%, 10%, 20%, 30%, 40%, 50%, 75% and 100%. The DSC curve shown in Fig. 6.7 is the heat flow curve on cooling for the specimen containing 20% $AgNO_3$ and 80% SiO_2. The peak height on cooling was measured as 0.156 W/g for 20% unreacted $AgNO_3$. The calibration curve for the peak height versus the various amounts of unreacted $AgNO_3$ is shown in Fig. 6.8, indicating a linear relationship.

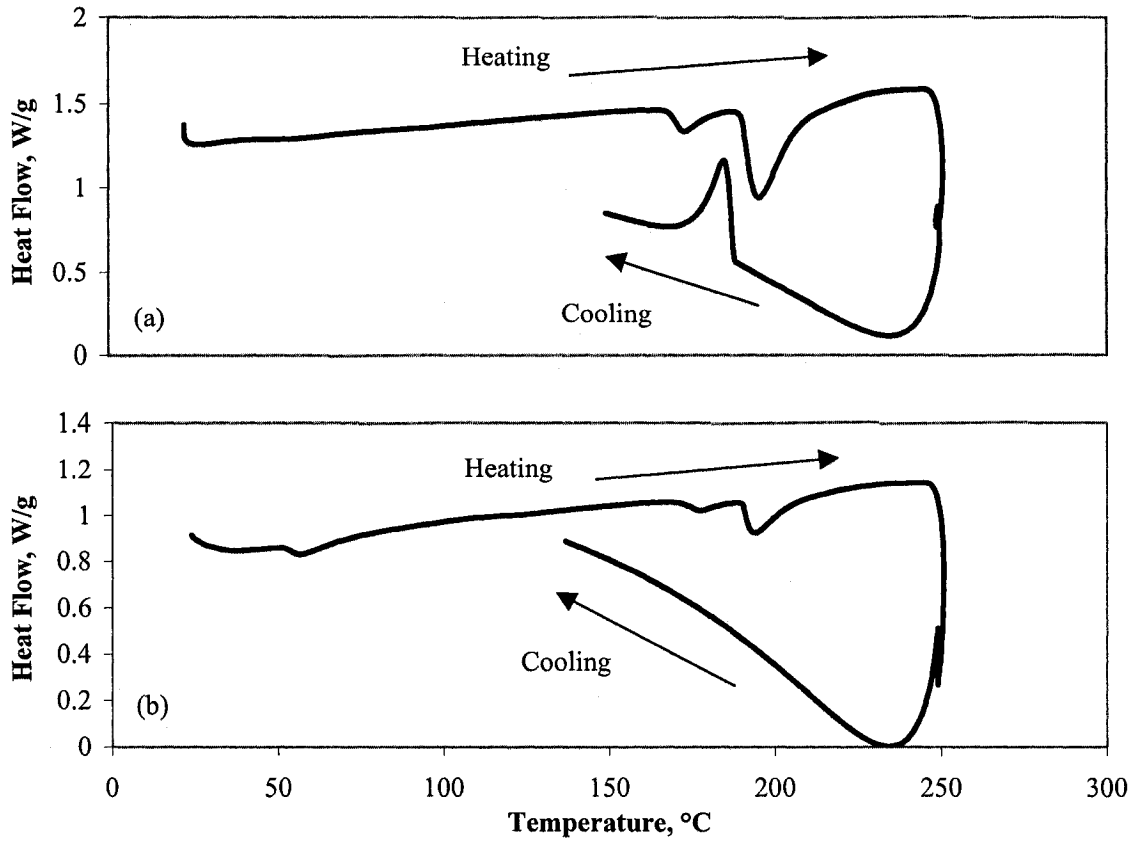

Fig. 6.6 The DSC heat flow curve for the specimens containing (a) 90% $AgNO_3$ and 10% $Ca(OH)_2$ and (b) 40% $AgNO_3$ and 60% $Ca(OH)_2$

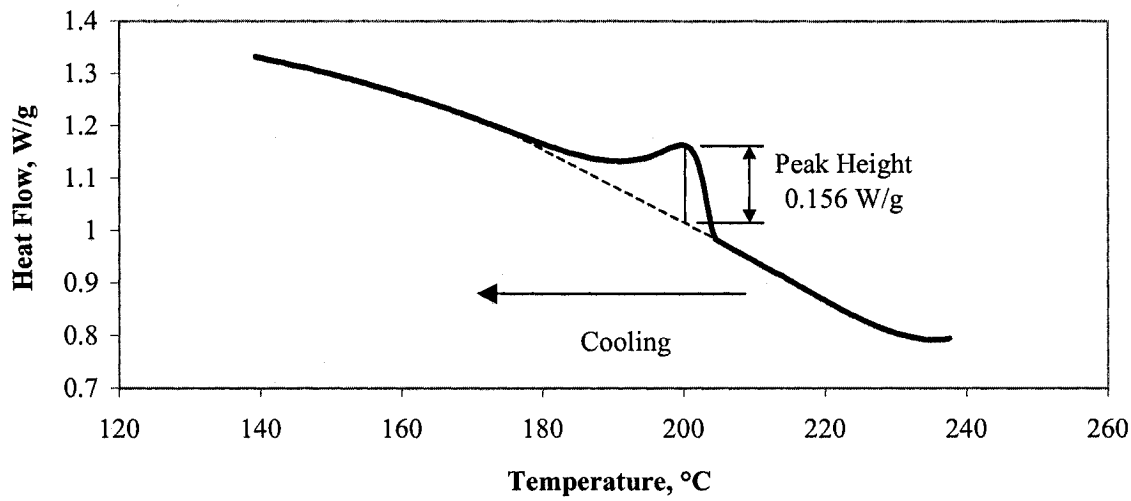

Fig. 6.7 The DSC heat flow curve on cooling for the specimen containing 20% $AgNO_3$ and 80% SiO_2

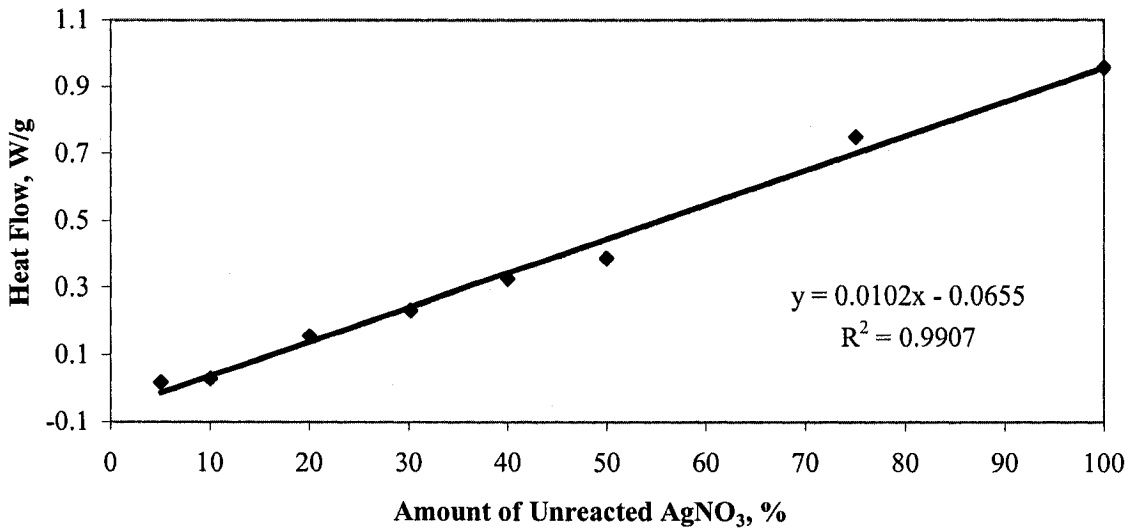

Fig. 6.8 The calibration curve for the heat flow versus the various amounts of unreacted $AgNO_3$

6.3.2.3 Relative Reactivity of the Different Types of $Ca(OH)_2$

The Hedvall effect was applied to the following three different types of $Ca(OH)_2$; the reagent grade micro-sized $Ca(OH)_2$ and the $Ca(OH)_2$ synthesized by the planetary-mill grinding and vacuum-calcination methods. The DSC heat flow curve on cooling for the specimen containing 90% $AgNO_3$ and 10% micro-sized $Ca(OH)_2$ is shown in Fig. 6.9. The values of mass of $AgNO_3$ and $Ca(OH)_2$ in the specimen are 0.901 g and 0.101 g, respectively. Since the amount of added $AgNO_3$ is much higher than stoichiometric amount that would react with the amount of added $Ca(OH)_2$, a high exothermic peak is expected. The exothermic peak height on cooling was 0.569 W/g as shown in Fig. 6.9. The amount of unreacted $AgNO_3$ in the system can be calculated from the calibration curve in Fig. 6.8 and is 62.2%. This indicates that 37.8% $AgNO_3$ in the specimen reacted with $Ca(OH)_2$. Since the total mass of $AgNO_3$ in the specimen was 0.901 g, 0.341 g of $AgNO_3$ was reacted with $Ca(OH)_2$. Two moles of $AgNO_3$ react with 1 mole of $Ca(OH)_2$ as shown in Eq. (6.1). The mass of $Ca(OH)_2$ reacted with $AgNO_3$ is therefore:

$$\frac{0.341\text{ g of } AgNO_3}{2\text{ moles} \times 169.9\text{ g/mol of } AgNO_3} \times 1\text{ mole} \times 74.1\text{ g/mol of } Ca(OH)_2 = 0.0742\text{ g of } Ca(OH)_2 \quad (6.2)$$

The total mass of $Ca(OH)_2$ in the specimen was 0.101 g, therefore 73.5% $Ca(OH)_2$ was reacted. Theoretically 100% $Ca(OH)_2$ should react with $AgNO_3$ since the amount of $AgNO_3$ was greater

than the stoichiometric amount. Approximately 26.5% $Ca(OH)_2$, however, did not react with $AgNO_3$. A possible reason might be that the heating rate, 10°C/min, from room temperature to 250°C was too fast for $Ca(OH)_2$ to fully react with $AgNO_3$. The reaction between $Ca(OH)_2$ and $AgNO_3$ might not be instantaneous. Nevertheless, the relative reactivity of different types of $Ca(OH)_2$ can still be determined if the same conditions, such as content percentages 90% $AgNO_3$ and 10% $Ca(OH)_2$ and the heating rate of 10°C/min, are used.

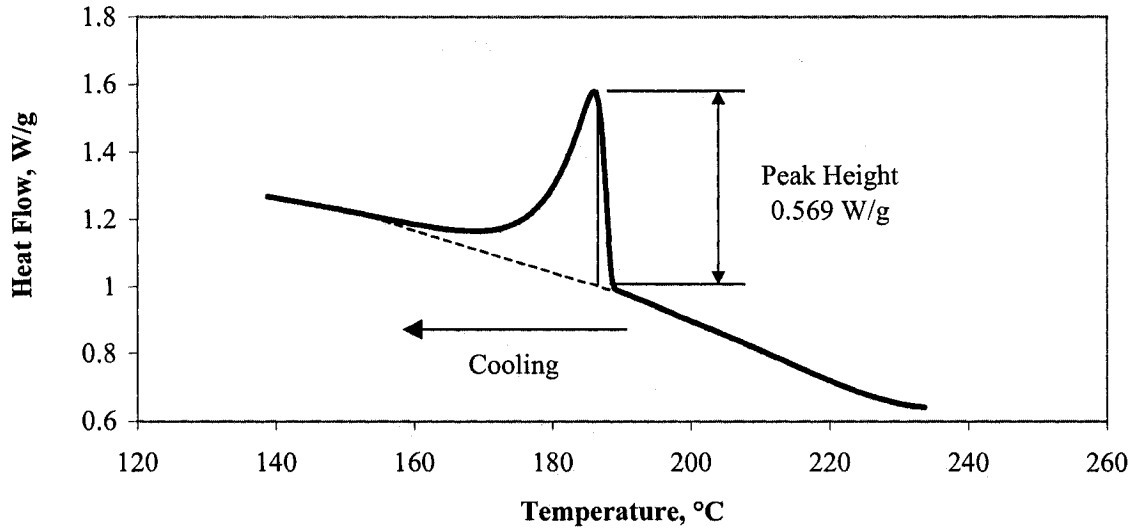

Fig. 6.9 The DSC heat flow curve on cooling for the specimen containing 90% $AgNO_3$ and 10% micro-sized $Ca(OH)_2$

The DSC measurements were conducted for a specimen containing 90% $AgNO_3$ and 10% nano-sized $Ca(OH)_2$ synthesized by the planetary-mill grinding method and for that containing 90% $AgNO_3$ and 10% nano-sized $Ca(OH)_2$ synthesized by the vacuum-calcination method. The results are shown in Table 6.3 along with the result for the micro-sized $Ca(OH)_2$. The reactivity of the nano-sized $Ca(OH)_2$ synthesized by the planetary-mill grinding method was very similar to that of the micro-sized $Ca(OH)_2$. A larger difference in the result was expected considering the difference in the BET surface area values. The reactivity of the nano-sized $Ca(OH)_2$ synthesized by the vacuum-calcination method was significantly higher than $Ca(OH)_2$ by the planetary-mill grinding. The BET surface area value of $Ca(OH)_2$ by the vacuum-calcination method was lower than that by the planetary-mill grinding method. The reactivity is, however, in the opposite order. This indicates that the crystallinity of $Ca(OH)_2$ significantly influences its reactivity. The results from the XRD and SEM indicated that the crystallinity of the $Ca(OH)_2$ synthesized by the vacuum-calcination method is greater than that by the planetary-mill grinding. At the same time, the particle size of the $Ca(OH)_2$ synthesized by the vacuum-calcination method is significantly

smaller than that of micro-sized $Ca(OH)_2$. The difference in reactivity determined by the application of the Hedvall effect might be owing to those two factors. In the next section, the reactivity of the different $Ca(OH)_2$ will be compared by the conduction calorimetry for the $Ca(OH)_2$ – metakaolinite reaction.

Table. 6.3 Relative reactivity of the different types of $Ca(OH)_2$ determined by the Hedvall effect

	Exothermic Peak on Cooling, W/g	Percentage of Unreacted $AgNO_3$, %	Percentage of Reacted $AgNO_3$, %	Percentage of Reacted $Ca(OH)_2$, %
Micro-sized $Ca(OH)_2$	0.5687	62.2	37.8	73.5
Nano-sized $Ca(OH)_2$ by Planetary-mill Grinding Method	0.5757	62.9	37.1	72.2
Nano-sized $Ca(OH)_2$ by Vacuum-calcination Method	0.4963	55.1	44.9	87.7

6.3.3 Stage 3: Effect of the Nano-sized $Ca(OH)_2$ on the Pozzolanic Reaction with Metakaolinite

The conduction calorimetry was performed to observe the effect of nano-sized $Ca(OH)_2$, as opposed to micro-sized $Ca(OH)_2$ on the pozzolanic reaction with metakaolinite. The 50% metakaolinite and 50% $Ca(OH)_2$ by total mass were mixed using w/c 1.0. The conduction calorimetry curves shown in Fig. 6.10 represent the reaction of metakaolinite with three different $Ca(OH)_2$ preparations; the reagent grade micro-sized $Ca(OH)_2$ and the $Ca(OH)_2$ synthesized by the planetary-mill grinding and vacuum-calcination methods. It is clearly indicated that the rate of heat development of the pozzolanic reaction between metakaolinite and the $Ca(OH)_2$ is significantly increased by the nano-sized $Ca(OH)_2$. The rate of heat development for the pozzolanic reaction of the metakaolinite with the $Ca(OH)_2$ synthesized by the planetary-mill grinding and vacuum-calcination methods are very similar. In terms of the peak positions, however, the pozzolanic reaction with the $Ca(OH)_2$ synthesized by the vacuum-calcination method occurs faster than that with the $Ca(OH)_2$ synthesized by the planetary-mill grinding method. This might be related to the difference in reactivity determined by the application of the Hedvall effect. The more crystalline $Ca(OH)_2$, synthesized by the vacuum-calcination method, might accelerate the pozzolanic reac-

tion more significantly than the more amorphous $Ca(OH)_2$, synthesized by the planetary-mill grinding method.

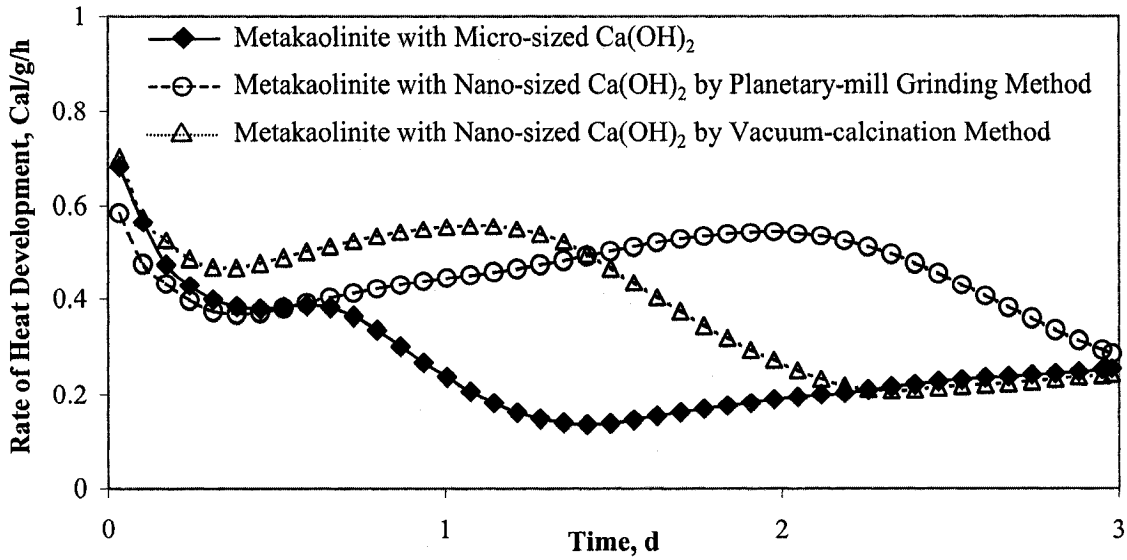

Fig. 6.10 Conduction calorimetry curves for the pozzolanic reaction of metakaolinite with the different $Ca(OH)_2$

6.3.4 Stage 4: Study of the Thermal Decomposition Characteristics of $Ca(OH)_2$

6.3.4.1 Introduction

During the process of establishing the method for the synthesis of the nano-sized $Ca(OH)_2$, it was found that the $Ca(OH)_2$ synthesized by a certain method decomposes at lower temperatures than a reagent grade micro-sized $Ca(OH)_2$. The decomposition of the reagent grade micro-sized $Ca(OH)_2$ typically starts at around 350°C, peaks out at 450°C and ends at 500°C. The decomposition of some of the synthesized $Ca(OH)_2$ had their peaks at around 425°C. These differences may be attributed to the effects of particle size, surface area, morphology and crystallinity of the synthesized $Ca(OH)_2$. It would be expected that two distinctively different types of $Ca(OH)_2$ in one system would result in decomposition peaks that have a doublet characteristic. As described in Section 2.5.5, an understanding of the thermal decomposition of $Ca(OH)_2$ with a doublet characteristic has been intensively attempted. A better understanding of the doublet characteristic of the $Ca(OH)_2$ decomposition, however, is required to characterize the role of the nano-sized $Ca(OH)_2$ in the pozzolanic reaction. Further clarification of previously observed doublet characteristics should result. Two different experiments were designed and conducted in order to study

the doublet characteristic associated with the thermal decomposition of $Ca(OH)_2$. The first experiment involved the preparation of three distinctively different types of $Ca(OH)_2$. Two of three were blended with each other and the characteristics of the thermal decomposition were studied. The second experiment involved the use of DSC apparatus with nitrogen gas preconditioned at different values of relative humidity (RH). A reagent grade $Ca(OH)_2$ was subjected to the cycles of heating and cooling in the various RH environments. The thermal decomposition of $Ca(OH)_2$ was studied analyzing the DSC heat flow curves.

6.3.4.2 Specimen Preparation and Experimental Procedure of the 1st Experiment

Three different types of $Ca(OH)_2$ were prepared by calcining reagent grade $Ca(OH)_2$ and $CaCO_3$ to form two different types of CaO and by re-hydrating them in two different ways to form $Ca(OH)_2$. It is summarized in Fig. 6.11. Reagent grade $Ca(OH)_2$ and $CaCO_3$ were both supplied by Anachemia Canada Inc., Montreal, Quebec, Canada. Reagent grade micro-sized $Ca(OH)_2$ was heated to 600°C in a muffle furnace at the rate of 10°C/min and held isothermally for 1 hour. At the end of the isothermal period, the calcined $Ca(OH)_2$, that is CaO-1, was cooled down to room temperature in a desiccator and purged with a nitrogen gas to prevent the CaO from carbonation. The BET surface area value of the CaO-1 was 31.2 m^2/g. The CaO-1 was then re-hydrated in an 11% RH environment for 7 days. The 11% RH environment was obtained using a saturated lithium chloride solution. The lithium chloride was supplied by Fisher Scientific, New Jersey, USA. The re-hydrated $Ca(OH)_2$, CH-1, has the BET surface area value of 20.1 m^2/g. The CaO-1 was also re-hydrated in deaerated water for 7 days. The CaO-1 was mixed with deaerated water in a plastic bottle which was rotated in a roller for a continuous stirring. After 7 days, the solution was then filtered and the remaining solid was dried under vacuum for 1 day. The re-hydrated $Ca(OH)_2$, CH-2, has a BET surface area value of 31.1 m^2/g. The reagent grade $CaCO_3$ was heated to 1050°C in the muffle furnace and held isothermally for 1 hour and cooled with the same process as CaO-1. The BET surface area value of the CaO-2 was 2.6 m^2/g. The CaO-2 was hydrated to form CH-3 with the same process as used to form CH-2. The CH-3 has the BET surface area value of 7.3 m^2/g.

The determination of the BET surface area was performed for the CH-1, CH-2 and CH-3 and the results were already shown with the specimen preparation. The XRD was also conducted for CH-1, CH-2 and CH-3 to characterize the materials. The TGA was conducted as well for CH-1, CH-2, CH-3, a mixture of CH-1 and CH-2 and a mixture of CH-1 and CH-3 with different proportions. The experimental procedures used in this experiment were described in Chapter 3.

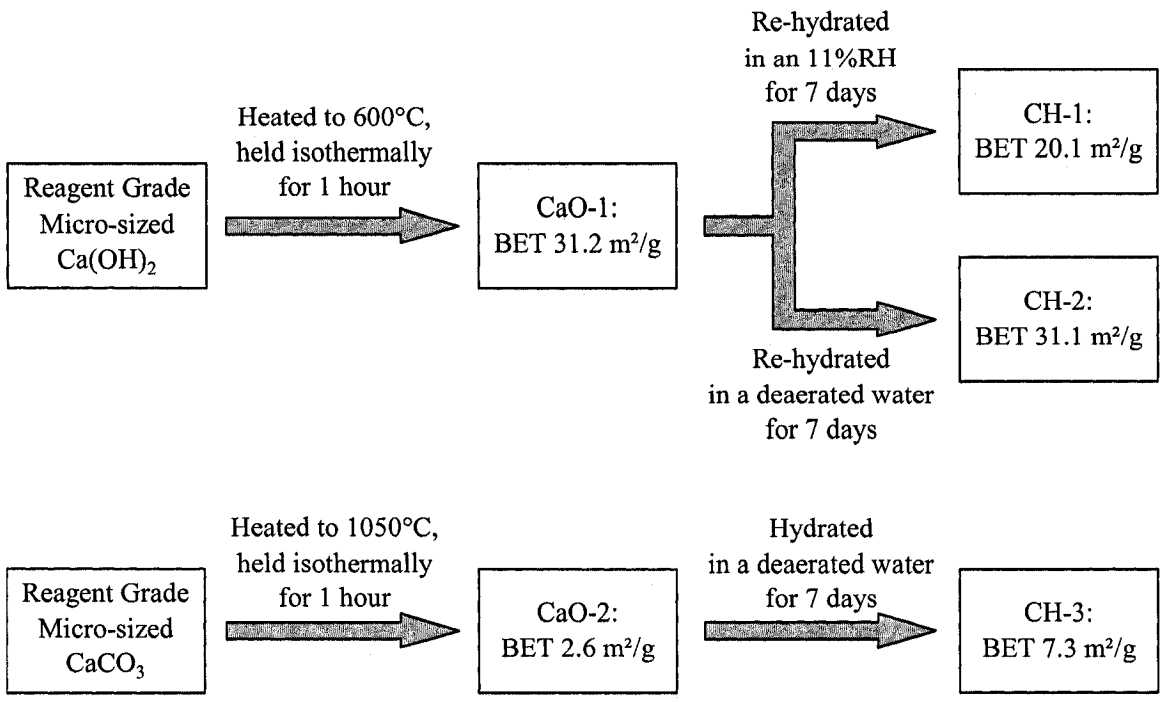

Fig. 6.11 Process of synthesis for three distinctively different types of $Ca(OH)_2$

6.3.4.3 Results and Discussion of the 1st Experiment

The XRD patterns of three different types of synthesized $Ca(OH)_2$ are shown in Fig. 6.12. The XRD results confirm that all the synthesized products are indeed $Ca(OH)_2$. Regarding the peak characteristics, the CH-3 has very intense peaks while the CH-1 has significantly less intensive peaks. The intensity of the peaks for CH-2 is between those for CH-3 and CH-1. The difference in the peak characteristics depends on the specimen preparation. The CH-1 and CH-2 were synthesized from the CaO calcined at 600°C whereas the CH-3 was synthesized from the CaO calcined at 1050°C. It is well known that, when a specimen is calcined at higher temperatures, the particles tend to agglomerate to form larger, more crystalline particles generally resulting in lower surface area value. This can be observed in the XRD patterns. The CH-3, calcined at 1050°C, has more intense and sharper peaks than the CH-1 and CH-2, calcined at 600°C, indicating that the CH-3 has a more crystalline structure than CH-1 and CH-2. The difference in the peak characteristics between CH-1 and CH-2 is not as distinct as that of CH-3. The peaks for CH-2 are however slightly more intense and shaper than those for CH-1. The CH-1 and CH-2 were both calcined at 600°C. The CH-1 however was re-hydrated in an 11% RH vapour environment whereas the CH-2 was re-hydrated in a liquid environment. The difference in the peak characteristics may imply that the $Ca(OH)_2$ hydrated in a liquid phase has a more crystalline structure than that hydrated in

a vapour phase. The SEM images for CH-1, CH-2 and CH-3 are shown in Figs. 6.13 (a), (b) and (c), respectively. The average particle size ranges of CH-1, CH-2 and CH-3 are approximately 100 to 300 nm, 100 to 500 nm and 0.5 to 2 μm, respectively. No crystalline $Ca(OH)_2$ can be observed in CH-1, while well-crystalline hexagonal $Ca(OH)_2$ is present in CH-2. Those crystals are significantly larger in CH-3. These observations in the SEM are well correlated to the XRD patterns. The peak characteristic for CH-3 was more intense and sharper indicating larger and more crystalline material. The peak characteristic of CH-1 was less intense and less sharp indicating the presence of smaller and less crystalline material.

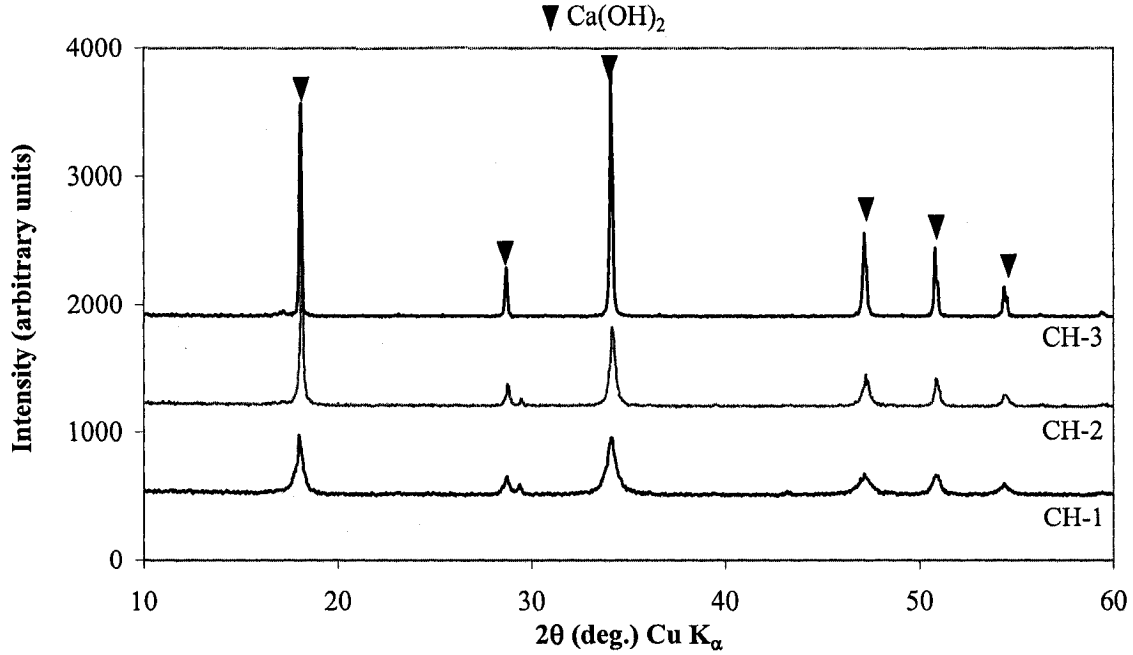

Fig. 6.12 The XRD patterns of three distinctively different types of $Ca(OH)_2$, CH-1, CH-2 and CH-3

The derivative curves of TGA for the CH-1, CH-2 and their mixtures with different proportions are illustrated in Fig. 6.14. The decomposition peak of curve 1, that represents 100% of CH-1, occurs at about 429°C whereas the decomposition peak of curve 5, that represents 100% of CH-2, occurs at about 456°C. The relatively large difference in decomposition peak temperature can be explained by differences in the surface area, morphology and crystallinity. As observed in Fig. 6.12, the CH-2, re-hydrated in the liquid phase, has more crystalline structure than the CH-1, re-hydrated in the vapour phase. This observation can be correlated to the decomposition temperature. The CH-2, re-hydrated in the liquid phase, decomposes at much higher temperature than the CH-1, re-hydrated in the vapour phase. It is clear that the decomposition temperature of a more crystalline material is higher than that of a less crystalline material. The CH-1 and CH-2 were

blended in different proportions and the TGA was conducted as shown in Fig. 6.14. The decomposition peaks of blended $Ca(OH)_2$ evidently have a doublet characteristic where the height of the doublet peaks changes depending on the proportion of each type of $Ca(OH)_2$. The doublet characteristics indicate that those two $Ca(OH)_2$, CH-1 and CH-2 are distinctively different types of $Ca(OH)_2$ as the two similar types of $Ca(OH)_2$ blended in one mixture tend to merge into one decomposition peak. The results shown in Fig. 6.14 imply that the doublet characteristics associated with the $Ca(OH)_2$ decomposition previously observed can systematically be re-produced and should help to elucidate the possible types of $Ca(OH)_2$ present in a hydrated cement paste. The results shown in Fig. 6.15 are the derivative curves of TGA for the CH-1, CH-3 and their mixtures with different proportions. More distinct doublet characteristics are observed. The CH-3 was re-hydrated in the liquid phase and the precursor CaO was calcined at a higher temperature, resulting in larger and more crystalline particles of $Ca(OH)_2$. The decomposition peak of curve 1, that represents 100% of CH-1, occurs at about 429°C whereas the decomposition peak of curve 5, that represents 100% of CH-3, occurs at about 458°C. The mixtures of CH-1 and CH-3 also clearly indicate the doublet characteristics where the height of the peaks changes depending on the proportions of each type of $Ca(OH)_2$.

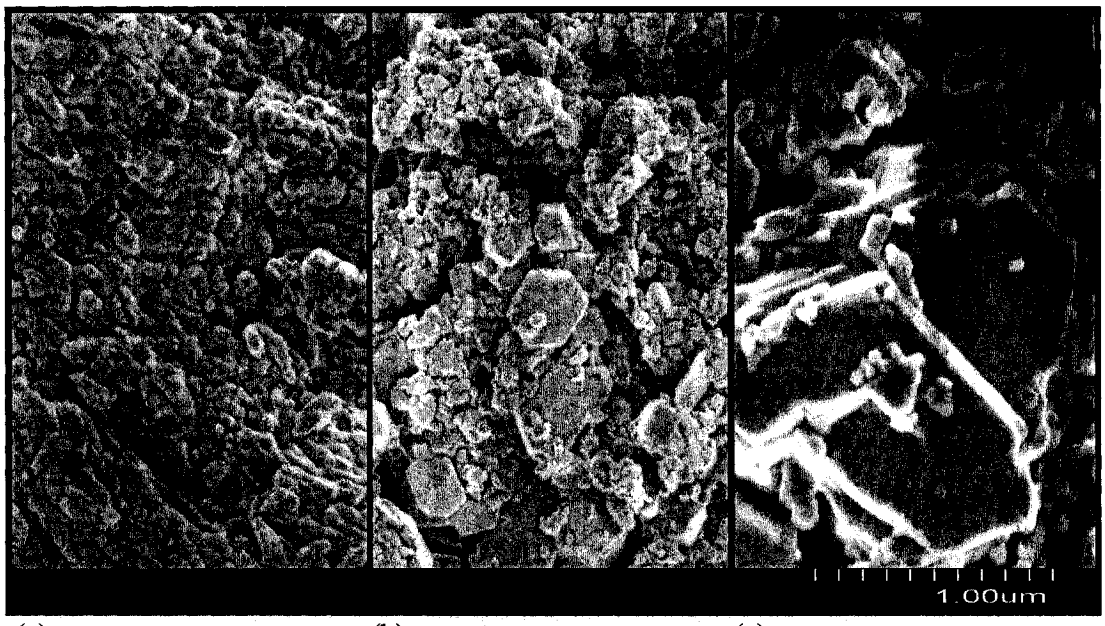

(a) (b) (c)

Fig. 6.13 SEM images of (a) CH-1, (b) CH-2 and (c) CH-3

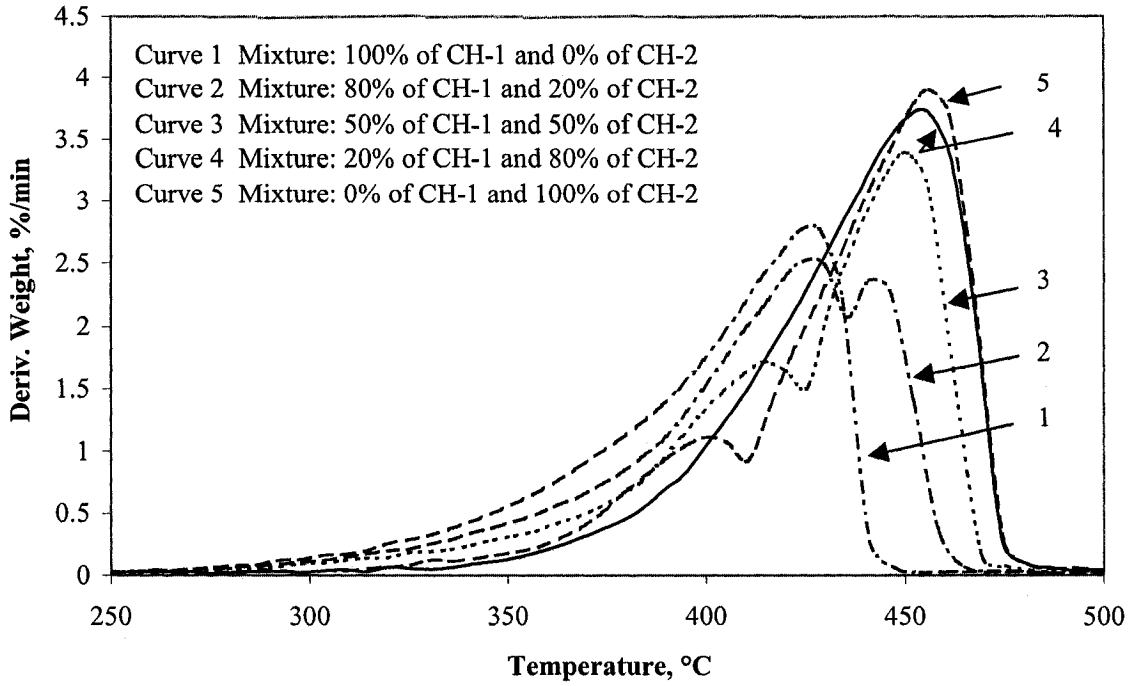

Fig. 6.14 The derivative curves of TGA for CH-1, CH-2 and their mixtures with different proportions

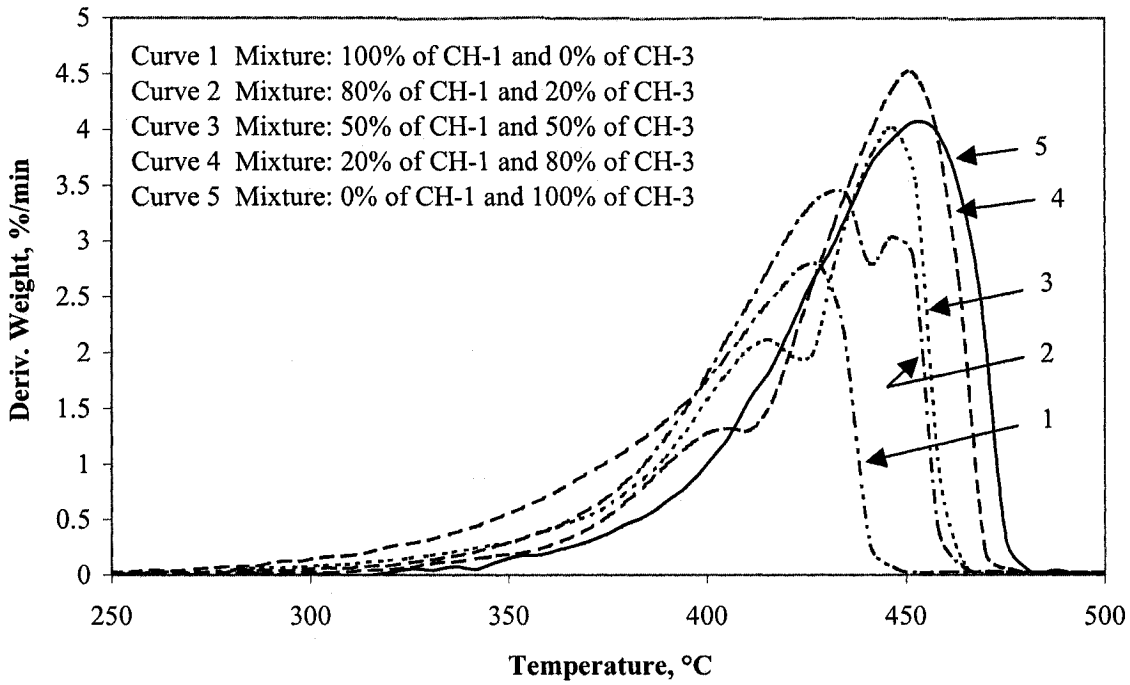

Fig. 6.15 The derivative curves of TGA for CH-1, CH-3 and their mixtures with different proportions

The results shown in Figs. 6.14 and 6.15 verified that the thermal decomposition temperature is largely dependent on the crystallinity of $Ca(OH)_2$. The relation between the thermal decomposition temperature and crystallinity of $Ca(OH)_2$ observed from the XRD peak characteristics was studied. Crystallinity determined by the XRD is mainly affected by crystallite size and strain. In addition, there is an instrumental error associated with the XRD peaks. Therefore, the XRD analysis only indicates crystallinity of material indirectly. However, in order to quantify the crystallinity from the XRD peak characteristics, the following method for the calculation of crystallinity index was conducted. The inverse of the peak width at half peak height (e.g. at 2θ = 34.09°) from the baseline was taken as an indicator of the crystallinity. The crystallinity index of the CH-1, for example, can be calculated as shown in Fig. 6.16. The values of crystallinity index of the CH-1, CH-2 and CH-3 along with the BET surface area values and the thermal decomposition temperatures are summarized in Table 6.4.

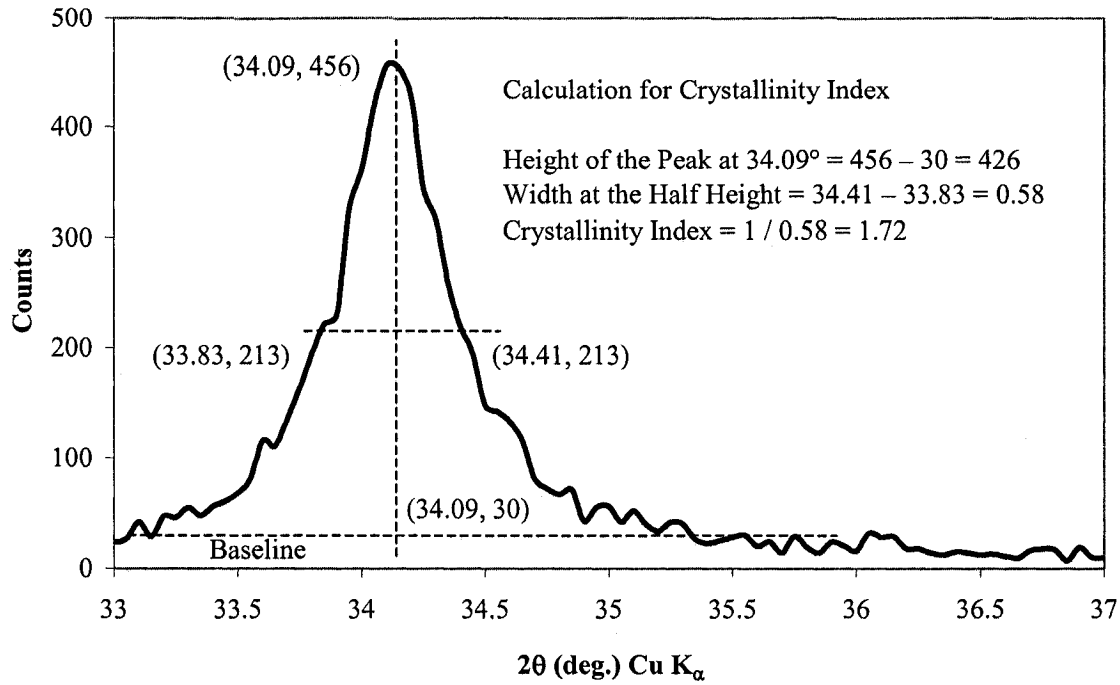

Fig. 6.16 Calculation of the crystallinity index for CH-1 at 34.09° (2θ)

Table 6.4 The values of crystallinity index for CH-1, CH-2 and CH-3 along with the BET surface area values and the thermal decomposition temperatures

$Ca(OH)_2$	BET, m^2/g	Crystallinity Index	Decomp. Onset, (1)	Decomp. Peak	Decomp. End, (2)	(2) – (1)
CH-1	20.1	1.72	231°C	426°C	467°C	236°C
CH-2	31.1	3.03	299°C	454°C	511°C	212°C
CH-3	7.3	5.26	308°C	452°C	512°C	204°C

The higher the value of the crystallinity index, the more crystalline is the $Ca(OH)_2$. The decomposition peak temperature of the CH-1 is lower than those of the CH-2 and CH-3, indicating that the $Ca(OH)_2$ re-hydrated in the vapour phase decomposes significantly lower than that re-hydrated in the liquid phase. It is also evidently indicated from the decomposition onset temperatures that the more amorphous the $Ca(OH)_2$, the lower is the decomposition onset temperature. The CH-3, which is the most crystalline $Ca(OH)_2$, starts to decompose latest. The temperature values shown in the last column imply the temperature duration of the decomposition. They were calculated by subtracting the decomposition onset temperature from the decomposition end temperature. It can be observed that the higher the crystalline index, the shorter is the decomposition temperature. It is noteworthy that BET surface area values and the particle size of the $Ca(OH)_2$ have only a slight influence on the decomposition temperatures. It can be concluded that the crystallinity of the material may have a greater influence on the decomposition temperature than the surface area and the particle size of the material.

6.3.4.4 Specimen Preparation and Experimental Procedure of the 2nd Experiment

The reagent grade $Ca(OH)_2$, supplied by Anachemia Canada Inc., Montreal, Quebec, Canada, was used in this experiment. The DSC was conducted as described in Chapter 3. The temperature was ramped from room temperature to 1050°C at 10°C/min with a 100 ml/min nitrogen gas flow. In this experiment, however, the nitrogen gas was preconditioned at different values of RH (12, 38, 60, 80 and 100%) using different salt solutions. The experimental setup used to condition the nitrogen gas for delivery to the DSC cell is shown in Fig. 6.17. The nitrogen is passed over a salt solution or water at a predetermined RH. This is followed by flow into a vessel equipped with an RH sensor to verify the RH of the carrier gas and through a flow meter into the DSC cell. It is important to note that in this experiments, the RH values refer to room temperature equilibrium conditions. As the temperature in the DSC cell increases, the saturation vapour pressure increases as well. The effective RH would therefore be less.

Two series of the experiments were conducted. The Series I procedure is as follows; the reagent grade $Ca(OH)_2$ was heated in the DSC cell from room temperature to 600°C at 10°C/min with a nitrogen flow of 100 ml/min preconditioned at different values of RH (12, 38, 60, 80 and 100%). Five continuous heating and cooling (to 100°C) cycles were performed. The Series II procedure is as follows; the reagent grade $Ca(OH)_2$ was subjected to heating and cooling cycles as for Series I with the exception that it was held isothermally for different periods (1 minute, 5 minutes, 5 hours

and 22 hours) at 600°C before cooling. All experiments were performed with the preconditioned environment at 100% RH.

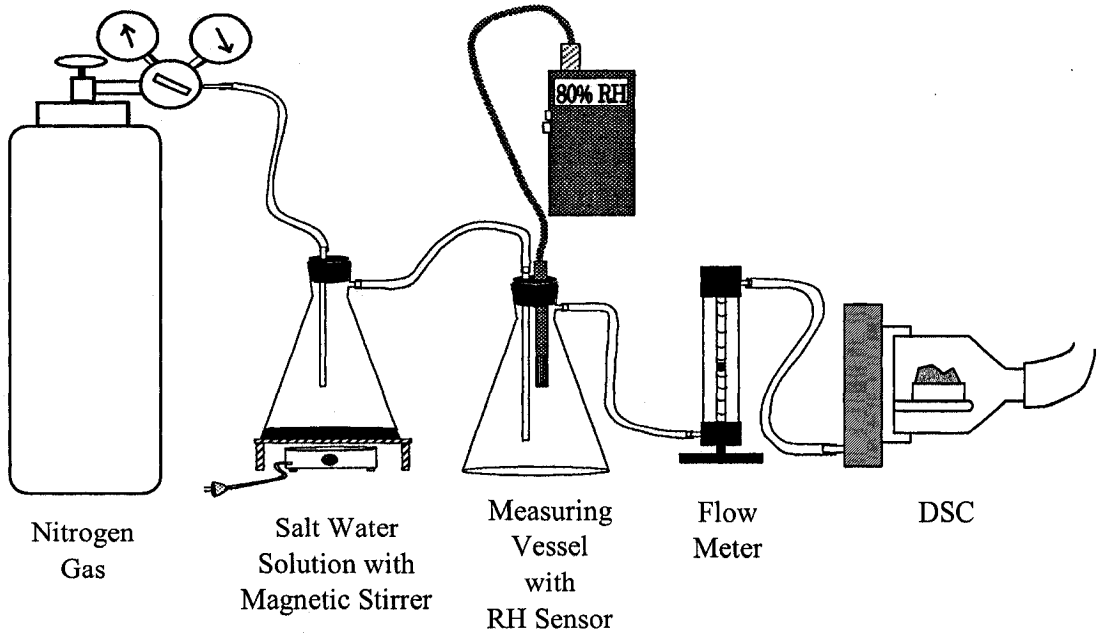

Fig. 6.17 The experimental setup to condition the nitrogen gas for delivery to the DSC cell

6.3.4.5 Results and Discussion of the 2nd Experiment

The results and discussion of the Series I are presented. The DSC heat flow curves for the 1st heating of $Ca(OH)_2$ in the various RH environments are shown Fig. 6.18. It is indicated in the figure that the decomposition of $Ca(OH)_2$ is represented by a single peak, in lieu of a doublet, for the 1st heating. As the RH increases, the $Ca(OH)_2$ decomposes at higher temperatures. It is apparent that the $Ca(OH)_2$ can decompose more readily in the lower RH environments. The liquid hydrated $Ca(OH)_2$ decomposes to CaO, when the temperature increases from room temperature to 600°C on heating. The CaO re-hydrates to form $Ca(OH)_2$, when the temperature decreases from 600°C to 100°C on cooling. The DSC heat flow curves for the 4th heating of $Ca(OH)_2$ in the various RH environments are typical and are illustrated in Fig. 6.19. The shift of the curves with the RH observed in Fig. 6.18 can also be observed in Fig. 6.19. More energy is required to decompose the $Ca(OH)_2$ in the higher RH environments. Well-defined doublets also appear in these higher RH environments. This can be explained by examining the 3rd cooling and 4th heating curves for the different RH environments. The DSC heat flow curves for the 3rd cooling and the 4th heating of $Ca(OH)_2$ in the 38% and 100% RH environments are shown in Fig. 6.20. The peaks on cooling and heating indicate the re-hydration and decomposition of the $Ca(OH)_2$, respectively.

The CaO starts re-hydrating on cooling at 285°C in the 100% RH environment whereas it starts re-hydrating only at 235°C in the 38% RH environment. As mentioned earlier, the RH values in this work refer to room temperature equilibrium conditions. The effective RH in the DSC cell constantly changes while the temperature decreases on cooling, that is, the CaO re-hydrates while the effective RH changes. The range of the effective RH variation with temperature in the 100% RH cell is much wider than that in the 38% RH cell. The CaO therefore re-hydrates in the wider range of effective RH in the 100% RH cell than the 38% RH cell. This might be the reason for the more distinct doublets in the 100% RH environment during decomposition in the 4th heating as opposed to those indicated in the 38% RH environment. The $Ca(OH)_2$ hydrated in the different RH environments would result in a difference in degree of crystallinity and therefore difference in a decomposition temperature.

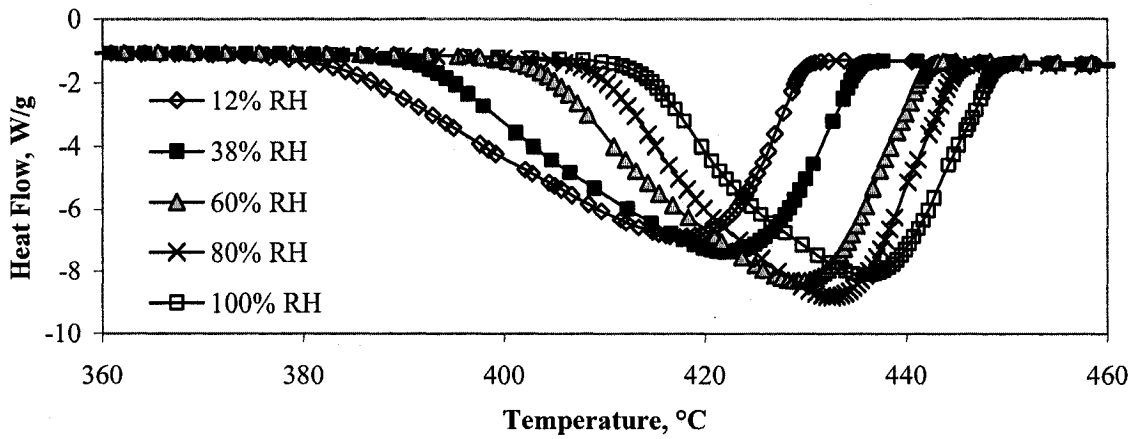

Fig. 6.18 The DSC heat flow curves for the 1st heating of $Ca(OH)_2$ in the various RH environments

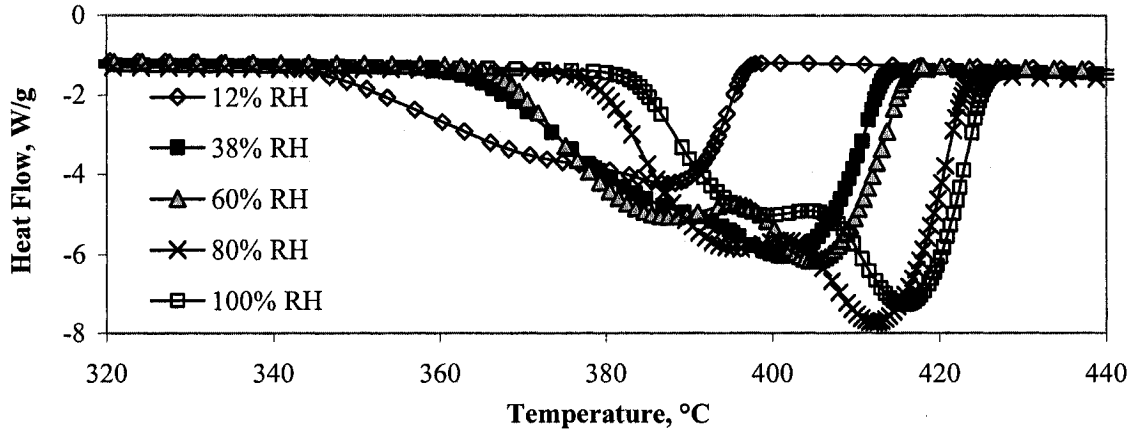

Fig. 6.19 The DSC heat flow curves for the 4th heating of $Ca(OH)_2$ in the various RH environments

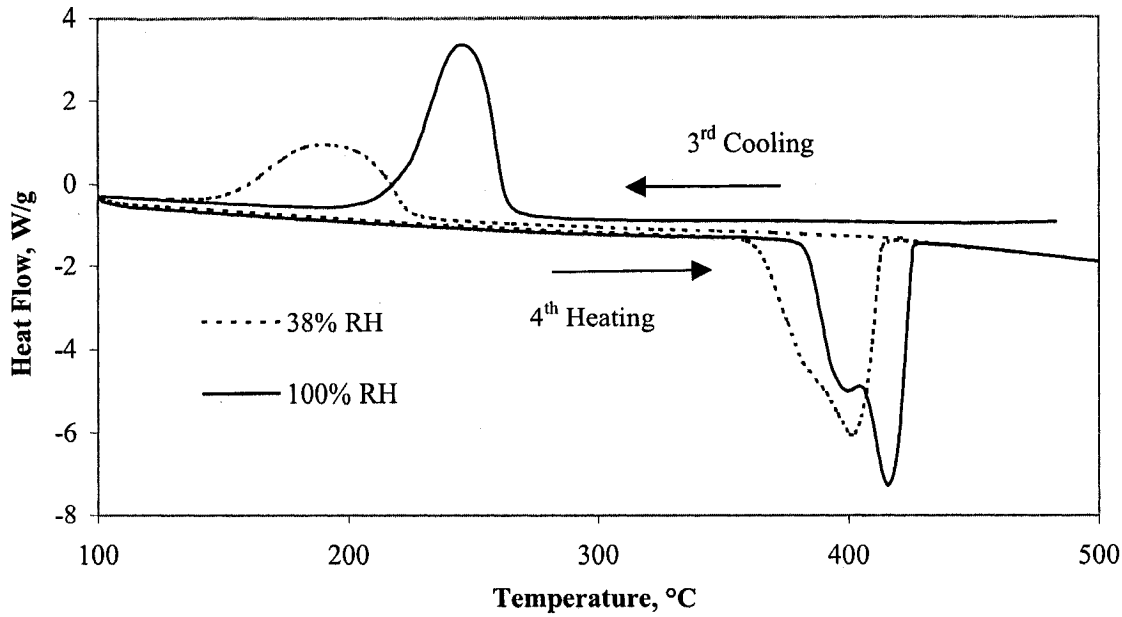

Fig. 6.20 The DSC heat flow curves for the 3rd cooling and the 4th heating of $Ca(OH)_2$ in 38% and 100% RH environments

The results and discussion of the Series II are presented. The effect of an isothermal hold after heating to 600°C followed by cooling to 100°C and re-heating to 600°C in a 100% RH environment was investigated. The DSC heat flow curves of $Ca(OH)_2$ held isothermally for 1 minute, 5 minutes, 5 hours and 22 hours at 600°C are shown in Fig. 6.21. The DSC curves for the 1st heating are shown to the right of the figure and illustrated by a single peak at about 435°C. To the left of the figure, the DSC curves for the 2nd heating are shown with much lower peak temperatures occurring than the 1st heating. The $Ca(OH)_2$ that decomposed on the 1st heating was initially hydrated in the liquid phase (reagent grade $Ca(OH)_2$) whereas the $Ca(OH)_2$ that decomposed on the 2nd heating was hydrated in the DSC cell on cooling, that is, the vapour phase. The resulting difference in the decomposition temperature between the $Ca(OH)_2$ hydrated in the liquid and vapour phases was observed in the 1st experiment. The DSC curves for the 2nd heating also indicate the well-defined doublets appearing for the longer isothermal hold. All display two endothermic peaks - low temperature peaks at about 402°C and high temperature peaks at 420°C. The low temperature peaks increase in magnitude with an isothermal period up to about 5 hours with a slight decrease occurring at 22 hours. The CaO is calcined while holding isothermally at 600°C. Depending on the isothermal holding period, the nature of the CaO is changed and therefore the characteristics of the $Ca(OH)_2$ on re-hydration and subsequent decomposition are also changed.

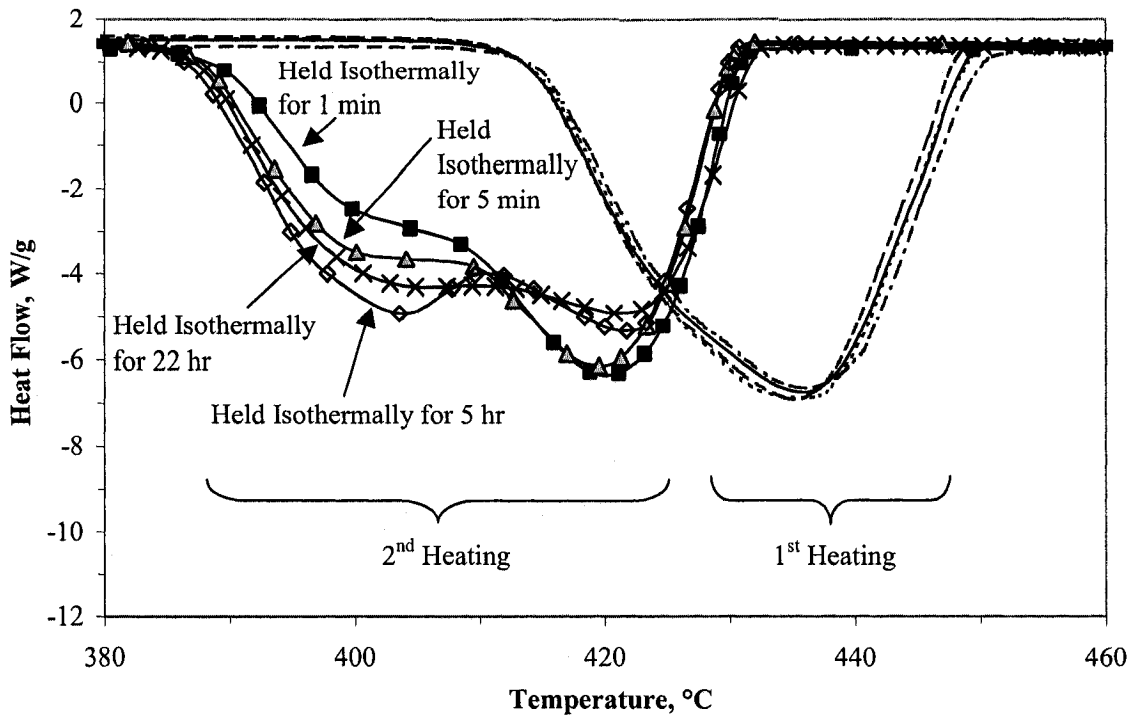

Fig. 6.21 The DSC heat flow curves of $Ca(OH)_2$ held isothermally for 1 minute, 5 minutes, 5 hours and 22 hours at 600°C

CHAPTER 7

CONCLUSIONS AND RECOMMENDATIONS FOR FUTURE RESEARCH

7.1 Introduction

Three themes were chosen for this thesis based on the application and potential of nanotechnology to enhance the use of the cement-based construction materials and optimize the gains made toward sustainable development. They are:

Theme 1: The use of nano-sized $CaCO_3$ addition to cement paste containing high volumes of supplementary cementing materials.

Theme 2: The synthesis and characterization of the highly reactive nano-sized β-C_2S by the Sucrose method.

Theme 3: The synthesis of the nano-sized $Ca(OH)_2$ and its effect on the pozzolanic reaction with metakaolinite.

The specific findings for each theme are first presented in this chapter. Within each theme, they are presented in the same chronological manner as the results and discussion. Secondly the overall conclusions for each theme are presented. Finally, the recommendations for future research are provided.

7.2 Specific Findings of Theme 1

7.2.1 Stage 1: Hydration Mechanism of Cement Paste Containing High Volumes of Fly Ash

The specific findings in the Stage 1 generally confirm previous work.

7.2.1.1 Early Hydration (0 ~ 3 Days)

1. The conduction calorimetry results indicated that the hydration of OPC paste was significantly delayed when 50% fly ash was added, owing mainly to the delayed hydration of C_3S in OPC by the addition of fly ash.
2. The delayed hydration of OPC containing 50% fly ash was not effectively observed by the XRD. The development of the $Ca(OH)_2$ peaks is affected by the pozzolanic reaction itself. The intensities would be higher as the OPC hydration takes place, and at the same time, they would be lower as the pozzolanic reaction takes place because of the consumption of $Ca(OH)_2$.
3. The amounts of $Ca(OH)_2$ in the OPC at 1 day and 3 days hydration, determined by the TGA, were significantly greater than those of OPC containing 50% fly ash owing to the consumption of $Ca(OH)_2$ by the pozzolanic reaction with fly ash.
4. The microhardness values at 1 day and 3 days hydration were significantly lower for the OPC containing 50% fly ash than those for the OPC itself.
5. The modulus of elasticity determination revealed very similar results to the microhardness determination.
6. The determinations of microhardness and modulus of elasticity unequivocally indicated that the early hydration of OPC paste was delayed by the addition of 50% fly ash.
7. It was suggested that the calcium ions saturated in the solution of OPC hydration were consumed by the pozzolanic reaction. The dilution effect and the requirement for calcium ions in the pozzolanic reaction can account for the delayed hydration of OPC paste when high volumes of fly ash were added.

7.2.1.2 Late Hydration (3 ~ 28 Days)

1. The amorphous humps associated with the formation of the C-S-H were observed with the XRD results for the OPC at 28 days hydration. It was however rather difficult to conclusively

identify the hydration products of OPC containing 50% fly ash by the XRD. It was suggested that some peaks might indicate the presence of calcium aluminate hydrates and/or calcium carboaluminate hydrates.

2. The amounts of $Ca(OH)_2$, determined by the TGA, in the hydrated OPC containing 50% fly ash at any time of the hydration up to 28 days were significantly lower than those in the OPC owing to the $Ca(OH)_2$ consumption by the pozzolanic reaction. The amount of $Ca(OH)_2$ in OPC containing 50% fly ash increased with hydration, however, it started decreasing at 7 days hydration. This indicated that the consumption of $Ca(OH)_2$ by the pozzolanic reaction became greater than the production of $Ca(OH)_2$ by the cement hydration at 7 days.
3. The microhardness values of the OPC containing 50% fly ash hydrated up to 28 days were significantly lower than those of the OPC, implying that the hydration of OPC paste containing 50% fly ash was delayed up to 28 days hydration compared to that of OPC owing to the addition of high volumes of fly ash.

7.2.2 Stage 2: Hydration Mechanism of Cement Paste with the Additions of Micro- and Nano-sized $CaCO_3$

Several new findings related to the hydration mechanism of cement paste with the additions of micro- and nano-sized $CaCO_3$ are described in the following sections.

7.2.2.1 Early Hydration (0 ~ 3 Days)

1. The conduction calorimetry results showed that the additions of micro-sized $CaCO_3$ had little or almost no effect on the hydration of OPC up to 3 days hydration in terms of the rate of heat development. It was, however, clear that both 10% and 20% additions of the nano-sized $CaCO_3$ significantly accelerated the early hydration of OPC. It was also evident that the greater the amount of $CaCO_3$ addition, the greater was the accelerating effect.
2. At 10 hours hydration, both 10% and 20% additions of micro-sized $CaCO_3$ increased the amount of $Ca(OH)_2$ produced only slightly greater than the OPC, whereas the additions of the nano-sized $CaCO_3$ significantly increased the amount of $Ca(OH)_2$ produced.
3. The amounts of $CaCO_3$ in the specimens hydrated up to 3 days, determined by the TGA, decreased as the hydration took place. This phenomenon was more remarkable for the nano-sized $CaCO_3$ addition compared to the micro-sized $CaCO_3$ addition. It implied that some portion of added $CaCO_3$ was chemically reacted in the hydration process.

4. The SEM images revealed the presence of the needle-like characteristics in the OPC containing 20% nano-sized $CaCO_3$, hydrated for 10 hours. This could be a mixture of ettringite and $3CaO{\cdot}Al_2O_3{\cdot}3CaCO_3{\cdot}32H_2O$. The reaction between C_3A and gypsum could be accelerated by the nano-sized $CaCO_3$ addition and/or there could be a reaction between C_3A and the added nano-sized $CaCO_3$, itself.
5. The XRD peaks for anhydrous C_3S detected in OPC at 10 hours hydration were more intense than those in OPC with the 20% nano-sized $CaCO_3$ addition, indicating that the hydration of OPC was accelerated by the 20% nano-sized $CaCO_3$ addition.

7.2.2.2 Late Hydration (3 ~ 28 Days)

1. The amounts of $CaCO_3$ in the specimens hydrated up to 28 days, determined by the TGA, decreased as the hydration took place. It was suggested by Ramachandran and Zhang (1986) that some portion of added $CaCO_3$ was chemisorbed or even incorporated into the interlayer region of the C-S-H structure.
2. The XRD pattern of OPC with the 20% nano-sized $CaCO_3$ addition at 28 days hydration indicated that the presence of the two peaks at 9.2° and 11.7° (2θ) might be attributed to the calcium carboaluminate hydrate which is the possible reaction product caused by the addition of $CaCO_3$.

7.2.3 Stage 3: Hydration Mechanism of Cement Paste Containing High Volumes of Fly Ash with the Additions of Micro- and Nano-sized $CaCO_3$ Hydrated at 23°C and 5°C

Several new findings related to the hydration mechanism of cement paste containing high volumes of fly ash with the additions of micro- and nano-sized $CaCO_3$ are described in the following sections.

7.2.3.1 Early Hydration (0 ~ 3 Days)

1. The conduction calorimetry results showed that the additions of micro-sized $CaCO_3$ had little or almost no effect on the hydration of OPC containing 50% fly ash up to 3 days hydration in terms of the rate of heat development. It was clear, however, that both 10% and 20% additions of the nano-sized $CaCO_3$ significantly accelerated the delayed early hydration of OPC

paste containing 50% fly ash. It was also evident that the greater the amount of $CaCO_3$ addition, the greater was the accelerating effect.

2. The amounts of $CaCO_3$ in the specimens hydrated up to 3 days, determined by the TGA, continued to decrease up to 3 days. It was indicated that the existence of fly ash in the specimens had a very little effect on the reduced amounts of $CaCO_3$. The added $CaCO_3$ might have interacted during the hydration of the control OPC itself.
3. It was evident that the additions of the nano-sized $CaCO_3$ significantly improved the microhardness of the OPC containing 50% fly ash. At 1 day hydration, the microhardness value of OPC, 56.3 MPa, was reduced to 15.4 MPa when 50% fly ash was added. It was however increased to 34.6 MPa when 20% nano-sized $CaCO_3$ was added to the OPC containing 50% fly ash.
4. The modulus of elasticity of the OPC containing 50% fly ash was also significantly improved by the additions of the nano-sized $CaCO_3$. At 3 days hydration, the modulus of elasticity value of OPC, 9.9 GPa, was reduced to 2.5 GPa when 50% fly ash was added. It was however increased to 7.0 GPa when 20% nano-sized $CaCO_3$ was added.
5. One possibility for accelerating the hydration of OPC and for the significant strength development by the addition of the nano-sized $CaCO_3$ is that the nano-sized $CaCO_3$ particles act as nucleation sites to accelerate the cement hydration process. This could explain the lower efficacy of the micro-sized $CaCO_3$ addition, as opposed to the nano-sized $CaCO_3$ addition on the accelerating effect and the strength development. The micro-sized $CaCO_3$ would be too large to function as effective nucleation sites.
6. The microhardness and modulus of elasticity were both improved by the addition of the 20% nano-sized $CaCO_3$ even when the specimens were cured in a 100% RH environment at 5°C, instead of 23°C. The 5°C curing temperature was used to observe the effect of low temperature curing condition.

7.2.3.2 Late Hydration (3 ~ 28 Days)

1. The amounts of $Ca(OH)_2$, determined by TGA, for OPC containing 50% fly ash and those with the additions of micro- and nano-sized $CaCO_3$ hydrated up to 28 days, were all decreased up to 28 days, indicating that 50% fly ash has a significant influence on the amounts of $Ca(OH)_2$ produced with or without the accelerating effect of the nano-sized $CaCO_3$ addition. The addition of nano-sized $CaCO_3$ might even accelerate the pozzolanic reaction.
2. The microhardness values were significantly increased by the additions of the nano-sized $CaCO_3$ up to 28 days hydration. The microhardness value for OPC at 28 days hydration was

163.9 MPa, whereas that for OPC containing 50% fly ash and that for OPC containing 50% fly ash with 20% nano-sized $CaCO_3$ were 45.7 MPa and 94.4 MPa, respectively.

3. The accelerated reaction in the early hydration often decelerates the long-term strength development. The microhardness and modulus of elasticity were not decelerated, however, for a long-term hydration, even though the early hydration of OPC paste containing 50% fly ash with the additions of the nano-sized $CaCO_3$ was significantly accelerated.
4. The investigation of microhardness and modulus of elasticity in terms of porosity provided the valuable information on the relation between the mechanical properties and pore structure. The plot of logarithm microhardness values versus porosity clearly indicated that the microhardness values were in the following order, OPC, OPC containing 50% fly ash with 20% nano-sized $CaCO_3$ > 10% nano-sized $CaCO_3$ > 20% micro-sized $CaCO_3$ and 10% micro-sized $CaCO_3$ > OPC containing 50% fly ash without the additions of $CaCO_3$.

7.2.4 Stage 4: Repeating Experiments with High Volumes of Ground Granulated Blast -furnace Slag

Several new findings related to the hydration mechanism of cement paste containing high volumes of GGBFS with the additions of micro- and nano-sized $CaCO_3$ are described in the following stage.

7.2.4.1 Early Hydration (0 ~ 3 Days)

1. The conduction calorimetry results showed that the addition of the nano-sized $CaCO_3$ significantly accelerated the early hydration of OPC paste containing high volumes of not only fly ash but also ground granulated blast-furnace slag (GGBFS). This confirmed that the efficacy of the nano-sized $CaCO_3$ addition as an accelerating additive on GGBFS, which is gaining wider use.
2. The microhardness was significantly improved when the nano-sized $CaCO_3$ was added to the OPC containing high volumes of GGBFS. The microhardness values at 1 day hydration for the control OPC and that containing 50% GGBFS were 48.2 MPa and 12.0 MPa, respectively. The microhardness value, however, became 29.0 MPa when the 20% nano-sized $CaCO_3$ was added.
3. The additions of micro-sized $CaCO_3$ resulted in only a modest effect on the rate of heat development. The improvement of strength development by the additions of micro-sized

$CaCO_3$, however, could be observed from the results of microhardness and modulus of elasticity. A small difference observed in terms of rate of heat development resulted in a large difference in terms of mechanical properties. This underlies the importance of the determination of mechanical properties to provide a link with cement chemistry.

7.2.4.2 Late Hydration (3 ~ 28 Days)

1. The microhardness of the OPC containing 50% GGBFS was significantly lower than that of the control OPC at 28 days hydration. It was however increased when the nano-sized $CaCO_3$ was added. The microhardness value for the control OPC was 145.7 MPa whereas that for OPC containing 50% GGBFS and that for OPC containing 50% GGBFS with the addition of the nano-sized $CaCO_3$ were 28.7 MPa and 143.1 MPa, respectively.
2. The results of microhardness and modulus of elasticity at 28 days indicated that the accelerated early hydration did not decelerate but contributed to the strength development in the long-term hydration.

7.3 Specific Findings of Theme 2

7.3.1 Stage 1: Synthesis and Characterization of the Highly Reactive Nano-sized β-C_2S by the Sucrose Method

1. The calcination of the synthesized β-C_2S was conducted at 600, 700, 800, 900 and 1000°C for 6 and 9 hours and it was concluded that the BET surface area of the synthesized β-C_2S could be optimized when the specimen was calcined at 600°C for 6 hours. The BET surface area value of the synthesized β-C_2S calcined for 6 hours at 600°C was 47.3 m^2/g.
2. It was determined by the TGA that the synthesized β-C_2S calcined at 600°C for 6 hours contained 48% $CaCO_3$. It could be owing to the decomposition of leftover sucrose that was not completely calcined at 600°C for 6 hours and the decomposition of $CaCO_3$ that was formed by the Ca^{2+} ions.

3. The XRD pattern of the synthesized β-C_2S calcined at 600°C for 6 hours only indicated the $CaCO_3$ peaks, which was 48% of the synthesized β-C_2S content. The remainder would be amorphous materials; it was suggested that it was β-C_2S.
4. The ^{29}Si NMR pattern verified that the synthesized β-C_2S calcined at 600°C for 6 hours had a peak at –71 ppm, the main peak for the typical β-C_2S. It confirmed that the amorphous portion of the synthesized product was β-C_2S
5. The SEM analysis revealed that the particles of the synthesized β-C_2S calcined at 600°C for 6 hours could be classified into two different groups in terms of the particle size range; one is the particle size range of 200 to 400 nm and the other is 50 to 100 nm. It was suggested that the group of particle size range of 200 to 400 nm might be $CaCO_3$ and that of 50 to 100 nm might be the synthesized nano-sized β-C_2S.

7.3.2 Stage 2: Reactivity and Hydration of the Synthesized Highly Reactive Nano-sized β-C_2S

1. The conduction calorimetry results showed no development of heat of hydration for the synthesized β-C_2S calcined at 800°C, 900°C and 1000°C. A slight development of heat of hydration was observed for the synthesized β-C_2S calcined at 700°C. A significant amount of heat of hydration was produced by the synthesized β-C_2S calcined at 600°C. Its hydration was even faster than that of commercial C_3S in terms of the peak location.
2. The XRD pattern of the synthesized β-C_2S calcined at 600°C hydrated for 28 days had a very similar pattern with that of the control one, except that the small β-C_2S peak had diminished and the C-S-H amorphous humps could be observed. Both of these phenomena indicated that the synthesized β-C_2S had hydrated and formed the C-S-H.
3. There were no $Ca(OH)_2$ peaks observed for the synthesized β-C_2S calcined at 600°C hydrated for 28 days. One possibility was that the produced $Ca(OH)_2$ is amorphous. The C/S ratio of the C-S-H formed by the hydration of synthesized β-C_2S might also be higher.
4. The TGA result showed that the control β-C_2S calcined at 600°C had a large peak from approximately 600°C to 800°C indicating the decomposition of $CaCO_3$. This peak significantly decreased when it was hydrated for 3 days and continued to decrease as hydration took place. Also other peaks developed at around 500°C to 700°C at 3 days hydration and contin-

ued to increase as hydration took place. The peak could be evidence that some portion of $CaCO_3$ in the synthesized β-C_2S reacted with the hydration product of β-C_2S.

5. The microhardness values for all of the synthesized β-C_2S increased as the hydration took place up to 28 days. The results indicated that lower the calcination temperature, the greater were the microhardness values at any period of hydration.
6. The microhardness values for the synthesized β-C_2S calcined at 600°C and 700°C were greater than those for the commercial β-C_2S at any time of the hydration up to 28 days. The strength development of the synthesized β-C_2S calcined at 600°C was considered remarkable. At 3 days hydration, the microhardness value for the commercial β-C_2S was 2.5 MPa whereas that for the synthesized β-C_2S calcined at 600°C was 8.6 MPa.

7.3.3 Stage 3: Quantitative Variation of Ingredients for the Sucrose Method

1. The ingredients used in the application of the Sucrose method were modified by doubling the amount of amorphous silica (SiO_2) to prevent a certain portion of Ca^{2+} ions from remaining unreacted.
2. The TGA result indicated that the β-C_2S with excess silica consisted of 16% $CaCO_3$ as opposed to 48% $CaCO_3$ present in the synthesized β-C_2S without excess silica.
3. The XRD pattern of the synthesized β-C_2S with excess silica was very similar to that of the β-C_2S without excess silica except the $CaCO_3$ peaks were weaker. It was implied that the rest of the synthesized product was 84% amorphous.
4. The ^{29}Si NMR pattern verified that the synthesized β-C_2S with excess silica had a peak at –71 ppm, the main peak for the typical β-C_2S. It confirmed that the amorphous portion of the synthesized product was β-C_2S.
5. The BET surface area value of the β-C_2S produced with excess silica was 70.9 m^2/g. This was significantly higher than the values for the β-C_2S produced without excess silica and the commercial β-C_2S, 47.3 m^2/g and 2.4 m^2/g, respectively.
6. The SEM image for the synthesized β-C_2S with excess silica showed that the average particle size was approximately 20 to 50 nm, which was significantly smaller than the synthesized β-C_2S without excess silica.
7. The conduction calorimetry results showed the extremely higher rate of heat development for the synthesized β-C_2S with excess silica than that without excess silica. This result correlates

with the significant increase in the BET surface area value and the significant decrease in the particle size.

7.4 Specific Findings of Theme 3

7.4.1 Stage 1: Synthesis and Characterization of Nano-sized $Ca(OH)_2$ by the Planetary-mill Grinding Method and the Vacuum-calcination Method

1. The TGA results indicated that the $Ca(OH)_2$ synthesized by the planetary-mill grinding method contained about 81.8% $Ca(OH)_2$ and 18.2% $CaCO_3$, whereas that by the vacuum-calcination method contained about 96.8% $Ca(OH)_2$ and 3.2% $CaCO_3$. A source of 18.2% $CaCO_3$ in the $Ca(OH)_2$ synthesized by the planetary-mill grinding method was not determined. A source of 3.2% $CaCO_3$ in the $Ca(OH)_2$ by the vacuum-calcination method might be from the carbonation of nano-sized CaO before re-hydration.
2. The BET surface area values for $Ca(OH)_2$ synthesized by the planetary-mill grinding and vacuum-calcination methods were 53.2 m^2/g and 38.1 m^2/g, respectively, whereas that for the reagent grade micro-sized $Ca(OH)_2$ was 16.1 m^2/g.
3. The SEM analysis revealed that the particle size of the micro-sized $Ca(OH)_2$ was as large as 1 μm, whereas the particles of the nano-sized $Ca(OH)_2$ synthesized by the planetary-mill grinding and the vacuum-calcination methods were approximately 50 to 400 nm.
4. The XRD patterns confirmed that the synthesized products were indeed $Ca(OH)_2$.

7.4.2 Stage 2: The Determination of the Reactivity of the Synthesized Nano-sized $Ca(OH)_2$ by the Application of the Hedvall Effect

1. The amount of heat flow, represented by the height of the exothermic peak detected by the DSC was calibrated in terms of an amount of unreacted $AgNO_3$ in a specimen. The calibration curve for the peak height versus the various amounts of unreacted $AgNO_3$ was determined. A linear relationship was confirmed.

2. The application of the Hedvall effect revealed that the reactivity of the nano-sized $Ca(OH)_2$ synthesized by the vacuum-calcination method was significantly higher than that of $Ca(OH)_2$ by the planetary-mill grinding method.
3. The BET surface area value of $Ca(OH)_2$ by the vacuum-calcination method was lower than that by the planetary-mill grinding method. The reactivity was however, in the opposite order. This indicated that the crystallinity of $Ca(OH)_2$ significantly influenced its reactivity.

7.4.3 Stage 3: Effect of the Nano-sized $Ca(OH)_2$ on the Pozzolanic Reaction with Meta-kaolinite

1. The conduction calorimetry results clearly indicated that the rate of heat development of the pozzolanic reaction between metakaolinite and the $Ca(OH)_2$ was significantly increased by the nano-sized $Ca(OH)_2$.
2. In terms of the peak positions, the pozzolanic reaction with the $Ca(OH)_2$ synthesized by the vacuum-calcination method occurs faster than that with the $Ca(OH)_2$ by the planetary-mill grinding method. The more crystalline $Ca(OH)_2$, synthesized by the vacuum-calcination method, might accelerate the pozzolanic reaction more significantly than the more amorphous $Ca(OH)_2$, synthesized by the planetary-mill grinding method.

7.4.4 Stage 4: Study of the Thermal Decomposition Characteristics of $Ca(OH)_2$

1. The thermal decomposition temperature of $Ca(OH)_2$ is largely dependent on the crystallinity. The more crystalline the $Ca(OH)_2$, the higher is the decomposition temperature.
2. The $Ca(OH)_2$, re-hydrated in a liquid phase, had a more crystalline structure than the $Ca(OH)_2$, re-hydrated in a vapour phase. It therefore decomposed at higher temperatures.
3. The TGA, XRD and SEM results implied that the thermal decomposition of $Ca(OH)_2$ was influenced not mainly by the particle size but by the crystallinity of the $Ca(OH)_2$.
4. It was possible to synthesize the doublet characteristic associated with the decomposition of $Ca(OH)_2$ by decomposing and re-hydrating in the various RH environments.

7.5 Overall Conclusions

Summarizing the specific findings previously presented, the overall conclusion for each theme can be given as follows;

Theme 1: One of the major disadvantages of OPC paste containing high volumes of SCMs was often the slower initial setting and rate of early strength development. The addition of nano-sized $CaCO_3$, however, counteracted the delayed hydration of OPC paste containing high volumes of SCMs. The long-term strength development was also improved by the addition of nano-sized $CaCO_3$. The efficacy of the use of the nano-sized $CaCO_3$ addition as an accelerating additive was confirmed.

Theme 2: The highly reactive nano-sized β-C_2S was successfully synthesized at 600°C applying the Sucrose method for the first time in the field of civil engineering. The hydration of the highly reactive nano-sized β-C_2S was significantly faster than that of the commercial β-C_2S. It was also revealed that the microhardness value of the highly reactive nano-sized β-C_2S hydrated at 28 days was significantly higher than that of the commercial β-C_2S. A link between the chemical synthesis and the mechanical property was established.

Theme 3: The nano-sized $Ca(OH)_2$ was successfully synthesized by the planetary-mill grinding method and vacuum-calcination method. The Hedvall effect was applied to determine the relative reactivity of the synthesized $Ca(OH)_2$. The efficacy of the use of the nano-sized $Ca(OH)_2$ to enhance the pozzolanic reaction with metakaolinite was confirmed. The effect of crystallinity on the thermal decomposition of $Ca(OH)_2$ was also elucidated.

7.6 Recommendations for Future Research

The overall objectives of this thesis were accomplished; however, future research will be required to improve the current study and to lead to the practical application of each theme in the thesis.

The recommendations for future research are presented for each theme.

7.6.1 Theme 1: The use of nano-sized $CaCO_3$ addition to cement paste containing high volumes of supplementary cementing materials

1. Extend the determinations of microhardness and modulus of elasticity for the OPC containing high volumes of SCMs with the addition of the nano-sized $CaCO_3$ hydrated for longer than 28 days.
2. Focus more on the formation of carboaluminate hydrate, the reaction product between the OPC and $CaCO_3$.
3. Synthesize a nano-sized $CaCO_3$ which would have a greater efficacy as an accelerating additive to compensate for the delayed hydration of OPC containing high volumes of SCMs.
4. Investigate the possibility of a replacement for gypsum in OPC using nano-sized $CaCO_3$ in order to control the rapid reaction of C_3A and to provide functionality as an accelerating additive at the same time.
5. Determine the effects of the nano-sized $CaCO_3$ addition on the OPC – carbonates related issues, such as sulphate resistance, efflorescence and carbonation.
6. Extend studies of the influence of the nano-sized $CaCO_3$ addition on mechanical properties, including compressive strength with larger scale specimens for mortar and concrete.
7. Standardize the addition of high volumes of the nano-sized $CaCO_3$ through submission to appropriate CSA committees.

7.6.2 Theme 2: The synthesis and characterization of the highly reactive nano-sized β-C_2S by the Sucrose method

1. Characterize and determine the mechanical properties for the synthesized β-C_2S with excess silica.
2. Synthesize a highly reactive nano-sized C_3S at low temperatures by the Sucrose method.
3. Investigate the efficacy of an addition of nano-sized $CaCO_3$ on the hydration of highly reactive nano-sized β-C_2S.

4. Conduct a rheological study on high-surface area cementitious materials, such as the highly reactive nano-sized β-C_2S to observe the effect of w/c ratio on their hydration.

7.6.3 Theme 3: The synthesis of the nano-sized $Ca(OH)_2$ and its effect on the pozzolanic reaction with metakaolinite

1. Improve the quality control of $Ca(OH)_2$ synthesized by the planetary-mill grinding method and the vacuum-calcination method.
2. Apply the Hedvall effect with a slower ramping rate, < 10°C/min to maximize the stoichiometric amount of $Ca(OH)_2$ that would react with $AgNO_3$.
3. Conduct SEM analysis on the pozzolanic reaction of the nano-sized $Ca(OH)_2$ and metakaolinite to characterize the formation of C-S-H.
4. Determine the mechanical properties for the hydrated specimens of the nano-sized $Ca(OH)_2$ and metakaolinite.

REFERENCES

Anson M. (1964), "An Investigation into a Hypothetical Deformation and Failure Mechanism for Concrete," *Magazine of Concrete Research*, Vol. 16, No. 47, pp. 73-82.

ASTM (1992) "C150: Standard Specification for Portland Cement," Annual Book of ASTM Standards, Vol. 4, Cement; Lime; Gypsum, pp.132-136.

ASTM (1999) "E384: Standard Test Method for Microhardness of Materials," Annual Book of ASTM Standards, Vol. 3, Metals – Mechanical Testing; Elevated and Low Temperature Tests; Metallography, pp.400-405.

Beaudoin, J.J. (1979), "Porosity Measurement of Some Hydrated Cementitious Systems By High Pressure Mercury Intrusion-Microstructural Limitations," *Cement and Concrete Research*, Vol. 9, Issue 6, pp.771-781.

Beaudoin, J.J. (1982), "Effect of Humidity and Porosity on Fracture of Hardened Portland Cement," *Cement and Concrete Research*, Vol. 12, Issue 6, pp.705-716.

Beaudoin, J.J. (1983), "Comparison of Mechanical Properties of Compacted Calcium Hydroxide and Portland Cement Paste Systems," *Cement and Concrete Research*, Vol. 13, Issue 3, pp.319-324.

Beaudoin, J.J. and Feldman, R.F. (1975), "A Study of Mechanical Properties of Autoclaved Calcium Silicate Systems," *Cement and Concrete Research*, Vol. 5, Issue 2, pp.103-118.

Beaudoin, J.J. and Ramachandran, V.S. (1975), "Strength Development in Magnesium Oxychloride and Other Cements," *Cement and Concrete Research*, Vol. 8, Issue 1, pp.103-112.

Beaudoin, J.J. and Ramachandran, V.S. (1978), "Strength Development in Magnesium Oxychloride," *Cement and Concrete Research*, Vol. 5, Issue 6, pp.617-630.

Beaudoin, J.J. and Ramachandran, V.S. (1992), "A New Perspective on the Hydration Characteristics of Cement Phases," *Cement and Concrete Research*, Vol. 22, Issue 4, pp.689-694.

Bensted, J. (1980), "Some Hydration Investigations Involving Portland Cement – Effect of Calcium Carbonate Substitution of Gypsum," World Cement Technology, Vol. 11, No. 8, pp.395-406.

Bensted, J. and Barnes, P. (2002), *Structure and Performance of Cements*, Spon Press, New York, USA.

Bernard, O., Ulm, F.J. and Lemarchand, E. (2003), "A Multiscale Micromechanics-Hydration Model for the Early-Age Elastic Properties of Cement-Based Materials," *Cement and Concrete Research,* Vol. 33, Issue 9, pp.1293-1309.

Berry, E.E., Hemmings, R.T. and Langley, W.S. (1989), "Beneficiated Fly Ash: Hydration, Microstructure and Strength Development in Portland Cement Systems," *Fly ash, silica fume, slag, and natural pozzolans in concrete: proceedings, third international conference,* Trondheim, Norway, American Concrete Institute, SP 114-11, pp.241-273.

Borchardt, H.J. and Thompson, B.A. (1959), "Reactions of Alkaline Earth Oxides. III. A Re-examination of the Hedvall Effect," *Journal of the American Chemical Society*, Vol. 82, pp. 5630-5632.

Bouzoubaâ, N. and Fournier, B. (2003), "Current Situation of SCMs in Canada," Material Technology Laboratory Report MTL 2003-04(TR), CANMET Energy Technology Centre, Natural Resources Canada.

Boyer, H.E. and Gall, T.L. (1985), *Metals Handbook Desk Edition*, American Society for Metals, Ohio, USA.

Bredig, M.A. (1950), "Polymorphism of Calcium Orthosilicate," *Journal of the American Ceramic Society,* Vol. 33, No. 6, pp.188-192.

Brunauer, S., Emmett, P.H. and Teller, E. (1938), "Adsorption of Gases in Multimolecular Layers," *Journal of the American Chemical Society*, Vol.60, pp.309-319.

Brunauer, S., Kantro, D.K. and Copeland, L.E. (1957), "The Stoichiometry of the Hydration of β-Dicalcium Silicate and Tricalcium Silicate at Room Temperature," *Journal of the American Chemical Society,* Vol. 80, No. 4, pp.761-767.

Campillo, I., Dolado, J.S. and Porro, A. (2003), "High-Performance Nanostructured Materials For Construction," *1st International Symposium on Nanotechnology in Construction,* The Advanced Concrete and Masonry Centre and The Scottish Centre for Nanotechnology in Construction Materials (NANOCOM), Paisley, Scotland, pp.110-121.

Carleson, E.T. and Berman, H.A. (1960), "Some Observations on the Calcium Aluminate Carbonate Hydrates," *Journal of Research of the National Bureau of Standards – A. Physics and Chemistry,* Vol. 64A, No.4, pp.333-341.

Crennan, J.M., El-Hemaly, S.A.S. and Taylor, H.F.W. (1977), "Autoclaved Lime-quarts Materials, I. Factors Influencing Strength," *Cement and Concrete Research,* Vol. 7, Issue 5, pp.493-502.

Cuberes, M.T. (2005), "Ultrasonic Force Microscopy: A Technique for Mapping Materials Properties at a Nanometer Scale with Potential Applications to Building Materials," *2nd International Symposium on Nanotechnology in Construction,* The Centre for Nanomaterials Applications in Construction (NANOC), LABIEN-Tecnalia, Bilbao, Spain.

CSA Standard A3000-03 (2003), "Cementitious Material Compendium", Canadian Standard Association

CSA Standard A23.5-86, "Supplemental Cementing Materials," Canadian Standard Association

CSA Standard A23.5-97, "Canadian Specification for Supplementary Cementing Materials (includes fly ash)," Canadian Standard Association.

CSA Standard A362-98, "Blended Hydraulic Cement," Canadian Standard Association.

Das, R.N. (2001), "Nanocrystalline Ceramics From Sucrose Process," *Materials Letters*, Vol. 47, Issue. 6, pp.344-350.

Das, R.N., Bandyopadhyay, A and Bose, S. (2001), "Nanocrystalline a-Al_2O_3 Using Sucrose," *Journal of the American Ceramic Society*, Vol. 84, Issue 10, pp.2421-2423.

Davis, H.E., Troxell, G.E. and Hauck, G.F. (1982), *The Testing of Engineering Materials*, 4th Edition, McGraw-Hill, Inc., New York, USA.

De Miguel, Y. (2004), "Silicate Chain Formation in C-S-H Gel," Presented at Nanotechnology at the Construction Materials Workshop, Institute for Research in Construction, National Research Council, September, 2004, Ottawa, Canada.

Detwiler, R.J. and Tennis, P.D. (1996), "The Use of Limestone in Portland Cement: A State-of-the-Art Review," Portland Cement Association.

Feldman, R.F. and Beaudoin, J.J. (1976), "Microstructure and Strength of Hydrated Cement," *Cement and Concrete Research*, Vol. 6, Issue 3, pp.389-400.

Feldman, R.F., Ramachandran, V.S. and Sereda, P.J. (1965), "Influence of $CaCO_3$ on the hydration of $3CaO{\cdot}Al_2O_3$," *Journal of the American Ceramic Society*, Vol. 48, pp.25-30.

Gawlicki, M. and Nocun-Wczelik, W. (1980), "Influence of Thermal Treatment on the Transition $\beta \rightarrow \gamma$-C_2S," *7th International Congress on the Chemistry of Cement, Paris,* Vol. 2, I-161-165.

Garboczi, E.J. and Neumann, D.A. (2003), "Virtual Concrete: Working at the Nanometer Scale," *1st International Symposium on Nanotechnology in Construction,* The Advanced Concrete and Masonry Centre and The Scottish Centre for Nanotechnology in Construction Materials (NANOCOM), Paisley, Scotland, pp.96-98.

Gerry, W.J. and Seabrook, P.T. (2000), "Early Strength Properties: HVFA Concrete Mixes for High-Rise Construction, Preliminary Report," *Case Study Report, Knowledge Base, EcoSmart Concrete*, www.ecosmart.ca.

Gillies, V. (2001), "The EcoSmart Concrete Project: The Results from the Case Studies," *Case Study Report, Knowledge Base, EcoSmart Concrete*, www.ecosmart.ca.

Glasson, D.R. (1956), "The Production of Active Solids by Thermal Decomposition. Part VIII. Calcination of Calcium Hydroxide," *Journal of the Chemical Society*, pp.1506-1510.

Glasson, D.R. (1958), "Reactivity of Lime and Related Oxides. II. Sorption of Water Vapour On Calcium Oxide," *Journal of Applied Chemistry*, Vol. 8, pp.798-803.

Goldstein, J.I., Newbury, D.E., Echlin, P., Joy, D.C., Romig, A.D., Lyman, C.E., Fiori, C. and Lifshin, E. (1992), *Scanning Electron Microscopy and X-ray Microanalysis*, 2nd Edition, Plenum Press, New York, USA.

Greene, K.T. (1960), "Early hydration reactions of Portland cement," *Chemistry of Cement: Proceedings of the Fourth International Symposium, Washington DC,* Vol. I, Session IV, Paper IV-1, pp.359-374.

Herrick, J., Scrivener, K. and Pratt, P. (1992) "The development of microstructure in calcium sulphoaluminate expansive cement, *Materials Research Society Symposia Proceedings*, Vol. 245, pp.277-282.

Hong, S.H. and Young, J.F. (1999), "Hydration Kinetics and Phase Stability of Dicalcium Silicate Synthesized by the Pechini Process," *Journal of the American Ceramic Society*, Vol. 82, No. 7, pp. 1681-1686.

Hughes, J.J. and Trtik, P. (2003), "Micro-Mechanical Properties of Cement Paste Measured By Depth Sensing Nano-Indentation: Correlation of Physical Properties With Phase Type," *1st International Symposium on Nanotechnology in Construction,* The Advanced Concrete and Masonry Centre and The Scottish Centre for Nanotechnology in Construction Materials (NANOCOM), Paisley, Scotland, pp.42.

Ingram, K., Poslusny, M., Daugherty, K. and Rowe, W. (1990), "Carboaluminate Reactions as Influenced by Limestone Additions," *Carbonate Additions to Cement,* ASTM STP 1064, Klieger, O. and Hooton, R. D., Eds., ASTM International, Philadelphia, pp.14-23.

Ingram, K.D. and Daugherty, K.E. (1991), "A Review of Limestone Additions to Portland Cement and Concrete," *Cement and Concrete Composites,* Vol. 13, No. 3, pp.165-170.

Ishida, H., Mabuchi, K., Sasaki, K. and Mitsuda, T. (1992), "Low-Temperature Synthesis of β-Ca_2SiO_4 from Hillebrandite," *Journal of the American Ceramic Society*, Vol. 75, No. 9, pp.2427-2432.

Ishida, H., Okada, Y. and Mitsuda, T. (1992), "Highly Reactive β-Dicalcium Silicate: II, Hydration Behaviour at 25°C Followed by ^{29}Si Nuclear Magnetic Resonance," *Journal of the American Ceramic Society*, Vol. 75, No. 2, pp.359-363.

Ishida, H., Sasaki, K. and Mitsuda, T. (1992), "Highly Reactive β-Dicalcium Silicate: I, Hydration Behaviour at Room Temperature," *Journal of the American Ceramic Society*, Vol. 75, No. 2, pp.353-358.

Ishida, H., Sasaki, K., Mizuno, A., Okada, Y. and Mitsuda, T. (1992), "Highly Reactive β-Dicalcium Silicate: IV, Ball-Milling and Static Hydration at Room Temperature," *Journal of the American Ceramic Society*, Vol. 75, No. 10, pp.2779-2784.

Ishida, H., Sasaki, K., Okada, Y. and Mitsuda, T. (1992), "Highly Reactive β-Dicalcium Silicate: III, Hydration Behaviour at 40-80°C," *Journal of the American Ceramic Society*, Vol. 75, No. 9, pp.2541-2546.

Ishida, H., Yamazaki, S., Sasaki, K., Okada, Y. and Mitsuda, T. (1993), "α-Dicalcium Silicate Hydrate: Preparation, Decomposed Phase and its Hydration," *Journal of the American Ceramic Society*, Vol. 76, No. 7, pp.1707-1712.

Jack, J.C. and Kennedy, T. (1970), "The Thermal Analysis of Argentic Oxynitrate and Silver Oxide," *Journal of Thermal Analysis*, Vol. 3, pp.25-35.

Jenkins, R. and Snyder, R.L. (1996), *Introduction to X-ray Powder Diffractometry*, John Wiley & Sons, Inc., New York, USA.

Juenger, M.C.G., Monteiro, P.J.M., Lamour, V.H.R., Gartner E.M., Denbeaux, G.P. and Attwood, D.T. (2003), "Observation of the Nanostructure of Cement Hydration by Soft X-ray Transmission Microscopy," *1st International Symposium on Nanotechnology in Construction,* The Advanced Concrete and Masonry Centre and The Scottish Centre for Nanotechnology in Construction Materials (NANOCOM), Paisley, Scotland, pp.104-106.

Kim, Y.J, Kriven, W.M. and Mitsuda, T. (1993), "TEM Study of Synthetic Hillebrandite ($Ca_2SiO_4 \cdot H_2O$)," *Journal of Material Research*, Vol. 8, No. 11, pp.2948-2953.

Kirkpatrick, R.J. (2005), "Molecular Dynamics Modeling of the Structure of Water on Solid Surfaces," Presented at the 107th Annual Meeting, Exposition & Technology Fair, The American Ceramic Society, April, 2005, Baltimore, USA.

Klemm, W.A. and Adams, L.D. (1990), "An Investigation of the Formation of Carboaluminates," *Carbonate Additions to Cement,* ASTM STP 1064, Klieger, O. and Hooton, R. D., Eds., ASTM International, Philadelphia, pp.60-72.

Kantro, D.L. and Weise, C.H. (1979), "Hydration of Various Beta-Dicalcium Silicate Preparations," *Journal of the American Ceramic Society*, Vol. 62, No. 8, C-170-C-172.

Kralj, D., Matkovic, B., Trojko, R., Young, J.F., Chan, C.J. (1986), "Preparations of Dicalcium Silicate at 950°C," *Journal of the American Ceramic Society*, Vol. 69, No. 8, pp.C-170 – C-172.

Kurtis, K.E., Monteiro, P.J.M., Brown, J.T. and Meyer-Ilse, W. (1998), "Imaging of ASR gel by Soft X-ray Microscopy," *Cement and Concrete Research*, Vol. 28, Issue 3, pp.411-421.

Lafayette, W. (2002), "Lasers Coax Large Molecules To Change Their Shape," *Tech Space, Spacedaily*, http://www.spacedaily.com/news/materials-02m.html.

Larsen-Basse, J. and Chong, K.P. (2005), "Nanomaterials in Construction and Rehabilitation: Contributions and Perspectives of the US National Science Foundation," *2nd International Symposium on Nanotechnology in Construction,* The Centre for Nanomaterials Applications in Construction (NANOC), LABIEN-Tecnalia, Bilbao, Spain.

Lea, F.M. (1970), *The Chemistry of Cement and Concrete,* Third Edition, Edward Arnold Ltd., London, England.

Liu, J., Duan, C., Ossowski, M.M., Mei, W.N., Smith, R.W. and Hardy J.R. (2002), "Molecular Dynamics Simulation of Phase Transition in $AgNO_3$," *Journal of Physics and Chemistry of Solids*, Vol. 63, pp.409-414.

Livingston, R.A. (2005), "Neutron Scanning Methods for Concrete Nanostructure Characterization," *2nd International Symposium on Nanotechnology in Construction,* The

Centre for Nanomaterials Applications in Construction (NANOC), LABIEN-Tecnalia, Bilbao, Spain.

Makar, J.M. (2004), "Reinforcement Mechanisms in Carbon Nanotube/Cement Composites," Presented at Nanotechnology at the Construction Materials Workshop, Institute for Research in Construction, National Research Council, September, 2004, Ottawa, Canada.

Makar, J.M. (2005), "Cement Paste/Carbon Nanotube Composites - Early Results," Presented at Institute for Research in Construction Seminar, Institute for Research in Construction, National Research Council, May, 2005, Ottawa, Canada.

Makar, J.M. and Beaudoin, J.J. (2003), "Carbon Nanotubes and Their Application in the Construction Industry," *Proceedings, 1st International Symposium on Nanotechnology in Construction*, Paisley, Scotland.

Mehta, P.K. (1999), "Concrete Technology for Sustainable Development," *Concrete International*, Vol. 21, Issue 11, pp. 47-53.

Mehta, P.K. and Monteiro, P.J.M. (2006), *Concrete: Microstructure, Properties and Materials*, 3rd Edition, McGraw-Hill, Inc., New York, USA.

Meyer, C. (2002), "Concrete and Sustainable Development," Concrete Materials Science to Application – A Tribute to Surendra P. Shah, *American Concrete Institute,* Special Publication ACI 206.

Mitchell, L.D., Margeson, J. and Beaudoin, J.J. (2003), "Synthesis and Characterization of Nanoparticulate Calcium Aluminates," *1st International Symposium on Nanotechnology in Construction,* The Advanced Concrete and Masonry Centre and The Scottish Centre for Nanotechnology in Construction Materials (NANOCOM), Paisley, Scotland, pp.122-134.

Mitchell, L.D., Whitfield, P.S., Margeson, J., and Beaudoin, J.J. (2002), "Sucrose Synthesis of Nanoparticulate Alumina," *Journal of Materials Science Letters 21,* pp.1773-1775.

Muller, C., Hardtl, R. and Shielbl, P. (1997), "High Performance Concrete with Fly Ash," *3rd International Symposium on Advances in Concrete Technology*, SP-171, pp.171-200.

National Resources Canada (2002), "Supplementary Cementing Material Program," *News Release 2002/128d*, http://www.nrcan.gc.ca/media/archives/newsreleases/2002/2002128d_e.htm

Nettleship, I., Shull, J.L. Jr., Waltraud, M.K. (1993), "Chemical Preparation and Phase Stability of Ca_2SiO_4 and Sr_2SiO_4 Powders," *Journal of the European Ceramic Society,* Vol. 11, pp.291-298.

Niesel, N. (1972), "The Importance of the $\alpha'_L - \alpha'_H$ Transition in the Polymorphism of Dicalcium Silicate," *Silicates Industriels*, Vol. 37, pp.136-138.

Partl, M.N., Gubler, R. and Hugener, M. (2003), "Nano-Science and -Technology Asphalt Pavements," *1st International Symposium on Nanotechnology in Construction,* The

Advanced Concrete and Masonry Centre and The Scottish Centre for Nanotechnology in Construction Materials (NANOCOM), Paisley, Scotland, pp.259-271.

Péra, J., Husson, S. and Guilhot, B. (1999), "Influence of Finely Ground Limestone on Cement Hydration," *Cement and Concrete Composites*, Vol. 21, Issue 2, pp.99-105.

Péro, H. (2003), "The Nanotechnology to New Production Systems: The EU Perspective," *1st International Symposium on Nanotechnology in Construction,* The Advanced Concrete and Masonry Centre and The Scottish Centre for Nanotechnology in Construction Materials (NANOCOM), Paisley, Scotland, pp.8.

Pignat, C., Navi, P. and Scrivener, K.L. (2003), "Nanoscale Characterisation of Simulated Cement Paste Pore Space," *1st International Symposium on Nanotechnology in Construction,* The Advanced Concrete and Masonry Centre and The Scottish Centre for Nanotechnology in Construction Materials (NANOCOM), Paisley, Scotland, pp.205.

Portland Cement Association (2002), *Design and Control of Concrete Mixtures*, 7th Canadian Edition, Cement Association of Canada, Ottawa, Canada.

Pratt, P.L. and Ghose, A. (1983), "Electron Microscope Studies of Portland Cement Microstructures During Setting and Hardening," *Philosophical Transactions of the Royal Society of London*, A310, pp. 93-103.

Raki, L. (2004), "Cement-Based Nanocomposites for Controlled Release of Admixtures," Presented at Nanotechnology at the Construction Materials Workshop, Institute for Research in Construction, National Research Council, September, 2004, Ottawa, Canada.

Raki, L., Beaudoin, J.J. and Mitchell L. (2004), "Layered Double Hydroxide-Like Materials: Nanocomposites for Use in Concrete," *Cement and Concrete Research*, Vol. 34, Issue 9, pp.1717–1721.

Raki, L. and Mojumdar S.C. (2005), "Preparation and Properties of Calcium Silicate Hydrates Nanocomposites," Presented at the 107th Annual Meeting, Exposition & Technology Fair, The American Ceramic Society, April, 2005, Baltimore, USA.

Ramachandran, V.S. (1988), "Thermal Analysis of Cement Components Hydrated in the Presence of Calcium Carbonate," *Thermochimica Acta*, 127, pp.385-394.

Ramachandran, V.S., Feldman, R.F. and Beaudoin, J.J. (1981), *Concrete Science*, Heyden & Son Ltd., London, UK.

Ramachandran, V.S., Malhotra, V.M., Jolicoeur, C. and Spiritos, N. (1998), *Superplasticizer: Properties and Applications in Concrete*, Materials Technology Laboratory, CANMET, Ottawa, Canada.

Ramachandran, V.S., Paroli, R.M., Beaudoin, J.J. and Delgado, A.H. (2003), *Thermal Analysis of Construction Materials*, Noyes Publications, Norwich, USA.

Ramachandran, V.S. and Sereda, P.J. (1971), "Hedvall Effect in Cement Chemistry," *Nature Physical Science*, Vol. 233, No. 42, pp.134-135.

Ramachandran, V.S. and Zhang, C. (1986), "Dependence of Fineness of Calcium Carbonate on the Hydration Behavior of Tricalcium Silicate," *Durability of Building Materials*, 4, pp.45-66.

Ramachandran, V.S. and Zhang, C. (1986), "Influence of $CaCO_3$ on Hydration and Microstructural Characteristics of Tricalcium Silicate," *II Cemento*, Vol. 3, pp.129-152.

Richardson, I.G. (2004), "Tobermorite/jennite- and tobermorite/calcium hydroxide-based models for the structure of C-S-H: applicability to hardened pastes of tricalcium silicate, h-dicalcium silicate, Portland cement, and blends of Portland cement with blast-furnace slag, metakaolin, or silica fume," *Cement and Concrete Research*, Vol. 34, Issue 9, pp.1733–1777.

Richardson, I., Love, C., Dyson, H., Brough, A. and Brydson, R.M. (2005), "Composition, Morphology and Nanostructure of C-S-H in a Range of Systems and the Location of Mg in Slag Cement," Presented at the 107th Annual Meeting, Exposition & Technology Fair, The American Ceramic Society, April, 2005, Baltimore, USA.

Rock Products (2003), "Greener Cement to Use More Limestone," *PREMEDIA Business Magazines & Media Inc.*, http://rockproducts.com/mag/rock_greener_cement_limestone/

Roy, D.M. (1989), "Fly Ash and Silica Fume Chemistry and Hydration," *Fly ash, silica fume, slag, and natural pozzolans in concrete: proceedings, third international conference,* Trondheim, Norway, American Concrete Institute, SP 114-5, pp.117-137.

Roy, D.M., O'Holleran, T.P. and Neurgaonkar, R.R. (1978), "Preparation and Hydration Studies of Reactive β-Ca_2SiO_4 Prepared by the EDS Technique," *Cemento*, Vol. 75, No. 3, pp.337-342.

Roy, D.M. and Oyefesobi, S.O. (1977), "Preparation of Very Reactive Ca_2SiO_4 Powder," *Journal of the American Ceramic Society*, Vol. 60, No. 3-4, pp.178-180.

Salamanca-Buentello, F., Persad, D.L., Court, E.B., Martin, D.K., Daar, A.S. and Singer, P.A. (2005), "Global Experts Rank Top 10 Nanotechnology Applications to Aid Poor," *Joint Centre for Bioethics, University of Toronto*, http://www.utoronto.ca/jcb/home/news_nano_dev_countries.htm

Sasaki, K., Ishida, H., Okada, Y. and Mitsuda, T. (1993), "Highly Reactive β-Dicalcium Silicate: V, Specific Surface Area on Hydration," *Journal of the American Ceramic Society*, Vol. 76, No. 4, pp.870-874.

Scrivener, K.L., Touzo, B. and Glotter, A. (2003), "Nanostructure of Calcium Aluminate Cement Clinker," *1st International Symposium on Nanotechnology in Construction,* The Advanced Concrete and Masonry Centre and The Scottish Centre for Nanotechnology in Construction Materials (NANOCOM), Paisley, Scotland, pp.44.

Sereda, P.J. (1972), "Significance of Microhardness Porous Inorganic Materials," *Cement and Concrete Research*, Vol. 2, Issue 6, pp.717-729.

Sereda, P.J., Feldman, R.F. and Swenson, E.G. (1966), "Effect of Sorbed Water on Some Mechanical Properties of Hydrated Portland Cement Pastes and Compacts," *Symposium*

on Structure of Portland Cement Paste and Concrete, Special Report 90, Highway Research Board, Washington D.C.

Shell, S. (2001), "High Volume Flyash: A Concrete Solution," Environmental Design + Construction, http://www.edcmag.com.

Skalny, J. and Young, J.F. (1980), "Mechanism of Portland Cement Hydration," *7th International Congress on the Chemistry of Cement*, Paris, Volume I, II-1/3 – II-1/44.

Skibsted, J., Jacobsen, H. and Anderson, M.D. (2005), "Characterization of the Nanostructure of the C-S-H Phase by Solid State 27Al and 29 Si MAS NMR Spectroscopy," Presented at the 107th Annual Meeting, Exposition & Technology Fair, The American Ceramic Society, April, 2005, Baltimore, USA.

Soroka, I. and Sereda, P.J. (1968), "The Structure of Cement-Stone and the Use of Compacts as Structural Models," *5th International Congress on the Chemistry of Cement, Tokyo,* Vol. 3, pp.67-73.

Soroka, I. and Setter, N. (1977), "The Effect of Fillers on Strength of Cement Mortars," *Cement and Concrete Research*, Vol. 7, Issue 4, pp.449-456.

Soroka, I. and Stern, N. (1976), "Calcareous Fillers and the Compressive Strength of Portland Cement," *Cement and Concrete Research*, Vol. 6, Issue 3, pp.367-376.

Takemoto, K. and Uchiyama, H. (1980), "Hydration of Pozzolanic Cement," *7th International Congress on the Chemistry of Cement*, Paris, Volume I, IV-2/1 – IV-2/29.

Taylor, H.F.W. (1964), *The Chemistry of Cements*, Academic Press Inc. Ltd., London, UK.

Taylor, H.F.W. (1964), *The Chemistry of Cements: Volume 2*, Academic Press Inc. Ltd., London, UK.

Taylor, H.F.W. (1977), "Discussion of the Paper: Microstructure and Strength of Hydrated Cements by R.F. Feldman and J.J. Beaudoin," *Cement and Concrete Research*, Vol. 7, Issue 4, pp.465-468.

Timoshenko, S.P. and Woinowsky-Krieger, S. (1959), *Theory of Plates and Shells*, McGraw-hill Book Company, New York, USA.

Uchikawa, H. and Uchida, S. (1981), "Influence of Pozzolana on the Hydration of C_3A," *7th International Congress on the Chemistry of Cement*, Volume III, IV-24 – IV-29.

Wansom, S., Kidner, N.J., Woo, L.Y. and Mason, T.O. (2006), "AC-impedance response of multi-walled carbon nanotube/cement composites," *Cement and Concrete Composites*, Vol. 28, Issue 6, pp.509-519.

Wilson, A. (1993), "Cement And Concrete: Environmental Considerations," *Environmental Building News*, Volume 2, No. 2, http://www.BuildingGreen.com.

Yang, N. and Zhong, B. (1982), "A Study on Active β-Dicalcium Silicate," *Journal of the Chinese Silicate Society*, Vol. 10 No. 2, pp.161-166.